USGS
science for a changing world

Prepared in cooperation with the U.S. Department of Transportation, Pipeline Research Council International, and DGH Consulting Inc.

Landslide and Land Subsidence Hazards to Pipelines

By Rex L. Baum, Devin L. Galloway, and Edwin L. Harp

Open-File Report 2008–1164

U.S. Department of the Interior
U.S. Geological Survey

COVER NOTE. Natural gas pipeline crossing an active landslide in Archuleta County, Colorado. The 10-cm diameter, flexible steel pipeline is a temporary replacement for a 20-cm diameter pipeline that ruptured on May 2, 2008, when the landslide reactivated as a result of snowmelt.

Landslide and Land Subsidence Hazards to Pipelines

By Rex L. Baum, Devin L. Galloway, and Edwin L. Harp

Prepared in cooperation with the U.S. Department of Transportation, Pipeline Research Council International, and DGH Consulting Inc.

This report consists of three chapters:
1. Landslide hazards to pipelines—Regional hazard mapping
2. Land subsidence hazards
3. Landslide investigation methods

Open-File Report 2008–1164

U.S. Department of the Interior
U.S. Geological Survey

U.S. Department of the Interior
DIRK KEMPTHORNE, Secretary

U.S. Geological Survey
Mark D. Myers, Director

U.S. Geological Survey, Reston, Virginia: 2008

For product and ordering information:
World Wide Web: http://www.usgs.gov/pubprod
Telephone: 1-888-ASK-USGS

For more information on the USGS—the Federal source for science about the Earth, its natural and living resources, natural hazards, and the environment:
World Wide Web: http://www.usgs.gov
Telephone: 1-888-ASK-USGS

Suggested citation:
Baum, R.L., Galloway, D.L., and Harp, E.L., 2008, Landslide and land subsidence hazards to pipelines: U.S. Geological Survey Open-File Report 2008-1164, 192 p.

Contents

Prepared in cooperation with the U.S. Department of Transportation, Pipeline Research Council International, and DGH Consulting Inc.

Landslide Hazards to Pipelines–Regional Hazard Mapping

By Edwin L. Harp

Chapter 1 of
Landslide and Land Subsidence Hazards to Pipelines

Open-File Report 2008–1164

U.S. Department of the Interior
U.S. Geological Survey

Contents

Figures

Tables

Conversion Factors

Inch/Pound to SI

Multiply	By	To obtain
	Length	
foot (ft)	0.3048	meter (m)
mile (mi)	1.609	kilometer (km)
	Volume	
cubic foot (ft^3)	0.02832	cubic meter (m^3)
cubic yard (yd^3)	0.7646	cubic meter (m^3)
	Hydraulic conductivity	
foot per second (ft/s)	0.3048	meter per second (m/s)

SI to Inch/Pound

Multiply	By	To obtain
	Length	
meter (m)	3.281	foot (ft)
kilometer (km)	0.6214	mile (mi)
	Volume	
cubic meter (m^3)	35.31	cubic foot (ft^3)
cubic meter (m^3)	1.308	cubic yard (yd^3)
	Hydraulic conductivity	
meter per second (m/s)	3.281	foot per second (ft/s)

Landslide Hazards to Pipelines–Regional Hazard Mapping

By Edwin L. Harp

Abstract

Because of the long, linear nature of pipeline corridors, they often cross areas that are highly susceptible to landslides. Techniques to assess the hazard posed by the presence of landslides can be applied to these corridors provided certain minimum data requirements, such as slope and material properties, can be met within these areas. The level and sophistication of maps designed to portray landslide hazard or attributes that relate to landslide hazard vary widely. They range from maps that depict the qualitative judgment of the geologist, technician, or engineer to maps that display the percent chance (probability) of a landslide occurring in the future with respect to time, area, or both. Quantitative methods of depicting probability of landslides vary from the purely statistical correlation of various factors to physical process-based models that attempt to replicate the failure and, in some cases, the movement of slope materials. Depending on the type of landslides being considered, the type of analysis employed, and the accuracy of the data available, landslide-hazard maps are subject to considerable variation in their uncertainty. Due to the fact that datasets of the variables required for hazard assessments are often incomplete and include approximations, it is often difficult to quantify the uncertainty that exists in estimates of hazard levels.

Introduction

In addition to earthquake shaking, ground displacement, construction disturbance, ground settlement, and movement due to freeze and thaw processes, pipelines often are threatened by impact and displacement from landslides. Landslides that can affect pipeline corridors vary widely in type and in size. Landslide material ranging from bedrock with high intact compressive and shear strengths to soil with low cohesion, and failures ranging from a few cubic meters to millions of cubic meters volume can and have occurred in pipeline corridors throughout the world (Schuster and others, 1998; Porter and others, 2006; Çevik and Topal, 2003). Much of the hazard to pipelines from landslides derives from the long, linear nature of the corridors. With widths of up to one kilometer, pipeline corridors extend great distances through topography with wide varieties of susceptibility to landslides. Almost every pipeline that traverses areas in mountainous terrain has some vulnerability to landslide hazards (fig. 1-1).

Fortunately, not all cases of high landslide susceptibility translate into high hazard to the pipeline. Except for some surface pipelines, most pipelines are buried to depths of about one meter, only those landslides that penetrate to those depths, or induce damaging stresses at those depths, will pose a real hazard to the pipe. Therefore, those failures that tend to be shallow and non-eroding to the surrounding terrain pose little hazard to pipelines. In fact, a large portion of commonly occurring landslides (falls and slides in soil and rock and debris flows) that tend to be triggered in great numbers in seismic or extreme precipitation events are negligible threats to

pipelines except in cases where (1) large enough rock fragments from rock falls and rock slides exist to penetrate or transmit damaging stresses to pipeline-burial depths, (2) established rock-fall and rock-slide chutes erode to such depths, or (3) debris flows commonly scour deep enough to affect the pipeline integrity. Otherwise the problem of defining landslide hazards to pipelines reduces to documenting and analyzing the hazard posed by the various types of deep-seated landslides, that is landslides that penetrate to pipeline-burial depths.

It also follows that there is a size, or volume limit of landslides that would result in damage to a pipeline. Those landslide masses that are below a certain limit may not generate sufficient stress upon failure to deform a pipeline to rupture. Such landslide volume limits would depend upon the size and strength of the particular pipe used in a given corridor.

Regional Landslide Hazard Analysis

The common types of landslides whose distributions can be estimated using regional hazard analysis techniques are those whose failure depths are relatively shallow, for example average depths of no more than a few meters. These types of failures are falls and slides in rock and soil caused by earthquakes and severe precipitation events, and slumps and translational slides in soil and weathered bedrock that can form debris flows, usually triggered by intense rainfall (infrequently caused by seismic or volcanic events).

Documentation

The accurate documentation of landslides is a key element of any analysis. A landslide inventory map at scales of 1:24,000 or larger (1:12,000 scale is larger than 1:24,000 scale) is necessary to accurately conduct a landslide-hazard analysis using slope, material properties (such as shear strength), and hydrologic data as input. Such an inventory is compiled most effectively by the combination of field investigation and aerial photography at scales of 1:20,000 or larger (fig. 1-2).

Satellite imagery is increasingly available for many parts of the Earth and at larger scales. However, most satellite imagery still has a resolution of 30 m or greater. Some of the more recent satellites offer resolutions of less than one meter. The larger landslides (those with long dimensions of greater than approximately 100 m) could be mapped at the scales of 30-meter resolution, but many of the landslides triggered by an event (severe rainfall or earthquake shaking) would be too small to be seen at these scales. Even though some imagery is of sufficiently large scale to detect failures of one meter or less, satellite imagery is rarely acquired with the necessary overlap so that three-dimensional viewing can be achieved. This makes it extremely difficult to interpret and map slope failures in their correct (that is within approximately 30 m) locations. In remote areas where pipeline corridors are often located, imagery is often sparse or nonexistent. Without suitable imagery to construct a representative and accurate landslide inventory, a landslide hazard analysis and/or map cannot be constructed.

Methods of Analysis

Methods to assess the susceptibility or hazard posed by landslides fall into two general categories: qualitative and quantitative. The qualitative methods can be separated into two subcategories: (1) those that evolve from field and/or aerial photographic investigations based largely on experience and judgement, and (2) those that are determined based on comparisons of index factors or weighted parameters, such as slope aspect, vegetation type, geology, or soil type. Quantitative methods can also be separated into two general categories: (1) statistical methods and

(2) methods that rely on geotechnical probabilistic models to evaluate susceptibility or hazard (Aleotti and Chowdury, 1999). The above categories are extremely broad. A great degree of variation exists in both qualitative and quantitative methods, and, in many instances, qualitative and quantitative methods have been merged to introduce a significant degree of judgment and intuition into numerical categorization.

Methods that involve the use of neural networks fall into the category of non-physically based methods where a computer algorithm compares assigned weights for selected parameters with an expert pre-evaluation of the hazard. The comparisons and weight adjustment continue until a certain level of convergence is attained (Aleotti and Chowdury, 1999). In a general sense, the automated adjustments of neural networks are similar to the adjustments of parameters in statistical or deterministic methods made by the investigator to obtain a better fit to the data.

Qualitative Methods

Geomorphic Analysis

The first of the qualitative methods base landslide susceptibility or hazard on implicit determinations made by field observation or by use of aerial-based imagery. The assessment of susceptibility or hazard is derived from the evaluator's experience and recognition of morphological patterns that are similar to other situations (Aleotti and Chowdury, 1999). Hazard criteria are generally implicit rather than explicit (that is, susceptibility or hazard levels are specified but not the criteria by which they were assigned), and assessments produced by this process, although relatively rapid and including a large number of factors, are difficult to compare with those generated by other investigators (fig. 1-3).

Weighted Parameter Analysis

A second general type of qualitative analysis is that based on a combination of weighted parameter maps. The evaluator selects and maps parameters (such as slope, geology, and drainage density) that influence the stability of slopes based on personal experience and assigns a weight to each parameter in accordance with its relative contribution to slope failure. The weighted parameter maps are overlain on one another to generate the final hazard map. This type of analysis has the advantage of specifying the parameters affecting slope instability and their relative contributions. It also allows automation of the process with the use of a Geographic Information Systems (GIS) platform. However, it still retains subjectivity in establishing relative weights to assign to the various parameters.

An example of a weighted parameter criteria is that used by Harp and Noble (1993) to assign numerical scores to various fracture characteristics of rock slopes to assess rock-fall susceptibility and to use the criteria as a means to estimate hazard. The method has since been employed to assess susceptibility along corridors (Wieczorek and Harp, 2000) and in subregional areas (Harp and Jibson, 2002; Coe and others, 2005). Coe and others (2007; 2005) have used the rock-mass-quality criteria from Harp and Noble (1993) in combination with other weighted parameters such as distance from base of slope and active talus deposits to construct a hazard map for Little Mill Campground (U.S. Forest Service) in American Fork Canyon near Provo, Utah (fig. 1-4).

Quantitative Methods

Statistical Analyses

The main limitation of the above methods is the subjective weighting of various parameters that influence the landslide process. The advantages of statistical techniques are that they allow the weights of the different mapped geological and topographical parameters to be determined by direct comparison with a landslide map. This allows the determination of landslide density captured by each parameter. This process can be accomplished with a bivariate analysis where each parameter is compared separately to a landslide distribution or by multivariate analyses where the various parameters are evaluated simultaneously to determine coefficients of regression. A bivariate analysis by Coe and others (2004) was used to evaluate the influence of terrain parameters (slope and elevation) in triggering landslides from Hurricane Mitch (October 1998) in Guatemala. On a GIS platform, ratios of slope and elevation for landslide sources versus slope and elevation for nonlandslide sources were computed and used to prepare a susceptibility map for the area affected (fig. 1-5). After obtaining the numerical ratios (percentages of slope and elevation parameters with respect to landslide locations versus percentages of these parameters with respect to the total area), numbers from 1 to 5 were assigned to reflect the relative susceptibilities.

Multivariate analysis methods determine parameter weights or parameter coefficients that numerically describe their respective influences on, or correlations with, the landslide distribution or density (Gartner and others, 2007; Cannon and others, 2007; DeGraff and others, 2007; fig. 1-6). The main advantage of these methods is that the weights or coefficients are now mathematically calculated by a multivariate or step-wise regression instead of being assigned by subjective judgment or experience. Correlation coefficients are then statistically evaluated to determine the degree of significance of each of the various factors considered in the analysis.

Geotechnical Models

The deterministic analysis method refers to standard engineering slope-stability analyses that are done for specific sites. Physical properties of materials are quantified and serve as input in specific mathematical models, and factor of safety (FS) is calculated. FS is the ratio of the forces resisting slope movement to the forces driving it. Thus, FS values greater than 1.0 indicate stability while those less than 1.0 indicate instability. Therefore, the greater the FS value the more stable the slope. These methods are discussed in a later section of this paper.

Probabilistic geotechnical models refer to models that use standard geotechnical analyses that are coupled with a probabilistic evaluation, usually on a GIS platform, to estimate FS or a similar index of performance over a regional area. Most geotechnical models adapted to a GIS employ some form of probabilistic input in the calculation of FS (El-Ramly and others, 2002; Miller and Sias, 1998; Aleotti and Chowdury, 1999; Xie and others, 2004; Franciss, 2004) or in a comparison of FS values with a landslide distribution to estimate probability of failure (fig.7; Harp and others, 2006; Harp and others, 2004; Harp and others, 2002; Montgomery and Dietrich, 1994; Montgomery and others, 2001).

Models that employ probabilistic input do so for variables in the FS equation for cohesion and internal angle of friction (shear-strength parameters), pore pressure or degree of saturation or water-table depth, and unit weight of soil or weathered bedrock. The ideal is to have enough measured data for these variables to know their respective value ranges and statistical distributions. Most often this is not the case, and a Poisson or normal distribution for each of these variables is assumed. Sometimes some other distribution (triangular or uniform) is assumed (Aleotti and Chowdury, 1999). The output from the FS calculations using randomly selected values for these

variables is a distribution of FS values that serves as a probability density function in terms of FS. This function estimates the probability (percent chance) that FS • 1.0. An additional approximation for these models includes the geometry of the failure surface (usually a simple shape such as planar, spherical, or elliptical).

The use of probabilistic models usually employs the assumption that FS values are normally or lognormally distributed. This allows the estimation of the standard deviation and the coefficient of variation of FS or the individual variables that go into the FS calculation. Most engineers have a reasonably good idea of average values of parameters such as shear strength, unit weights, and other standard geotechnical properties. If a highest and lowest conceivable value (HCV, LCV) of these parameters can be reliably estimated, the "Three-Sigma Rule" can then be invoked to estimate the standard deviation of the parameter (Duncan, 2000). Since 99.73 percent of all values of a normally distributed parameter fall within three standard deviations of the average value, the standard deviation can then be estimated by the formula: $\sigma =$ (HCV-LCV)/6. The coefficient of variation (V) is then V = σ/average value of parameter. Duncan (2000) states that although most geotechnical engineers are good at estimating average values of parameters, they have a tendency to estimate a range of values between HCV and LCV that is too small. (Duncan, 2000, p. 308) also comments that "There is no proof that factors of safety are lognormally distributed, but the writer believes that it is a reasonable approximation."

Models that employ discrete values (point estimates) as input, calculate FS values and compare the resulting spatial FS values on a GIS layer with the landslide distribution to determine the probability or percent chance of a landslide occurring at a particular FS value. This method is used with a landslide inventory map to allow the input variables to be adjusted to obtain the best fit, or "back calculation," with respect to the landslide data. Such a process estimates a spatial probability of landslide occurrence or conditional probability that, given the occurrence of a triggering event of some level of rainfall or seismic shaking, the model predicts the probabilities of landslides for different FS values and then apportions them into different hazard categories (fig 7B).

The methods described above are used for both shallow and deep-seated landslides. While there is no reason that regional models cannot conceptually describe deep-seated landslide hazard, there are several practical reasons (greater uncertainties of depth, geometry, hydrologic factors, etc.) why hazard analyses that employ geotechnical models over a regional scale are not nearly as reliable on a regional basis as geotechnical models used for shallow landslides.

Shallow Landslide Analyses

Numerous similar methods to estimate shallow landslide hazard exist that include the hazard posed by falls and slides in rock and soil and the shallow slumps and translational failures that form debris flows. All of these methods employ the infinite slope analysis that models slope segments as rigid friction blocks that are considered to be infinitely long in all directions.

There are a number of methods commonly used in GIS analyses to estimate the stability of slopes that are divided into grid cells. Many of these methods calculate the FS of each cell. SINMAP (Pack and others, 1999) and SHALSTAB (Montgomery and Dietrich, 1994) are two similar analyses that predict slope stability using an infinite-slope analysis. SINMAP uses ranges of rainfall and material properties expressed as uniform probability distributions. Both models use the same equation to calculate the factor of safety (FS) for each grid cell in a GIS layer:

$$FS = \frac{C_r + C_s + \cos^2\alpha\left[\gamma_s\left(D - D_w\right) + \left(\gamma_s - \gamma_w\right)D_w\right]\tan\phi}{\sin\alpha\cos\alpha\left(\gamma_s D\right)} \quad (1)$$

Where C_r and C_s are root strength and soil cohesion, respectively, D is the vertical soil-depth thickness, D_w is the vertical thickness of the saturated layer, and γ is the unit weight of soil (*s*) and water (*w*). Both methods assume ground-water flow parallel to existing slopes. The variables α and ϕ are the slope and friction angles, respectively.

Level I Stability Analysis (LISA; Hammond and others, 1992) is another infinite slope analysis developed by the USDA Forest Service that calculates a probability for failure of slope cells from different combinations of variables within the infinite-slope equation, each with their own probability distribution. This analysis was one of several models used by Morrissey and others (2001) to predict debris flows in Madison County, Virginia. This model uses essentially the same equation for factor-of-safety as SINMAP and SHALSTAB except that a term for tree surcharge (weight) is introduced.

Yet another method is Iverson's transient-response model (Iverson, 2000), which links a pore-pressure response function with the governing factor-of-safety equation. The pore-pressure response function is determined by applying a fixed rainfall intensity for a specified period of time into a one-dimensional infiltration equation using an estimate of soil hydraulic diffusivity. A modification of this method (TRIGRS) has been produced by Baum and others (2002) for tension-saturated soils using varying rainfall intensities (for example, real storm rainfall intensities and durations) and by Savage and others (2004) for soils having partially saturated zones. These models allow calculation of factor-of-safety at different depths in the soil column and at different times in the rainfall period. These models require an estimate of the hydraulic properties of the existing soils (which can vary three to four orders of magnitude even within materials of uniform texture; Reid, 1997; Freeze and Cherry, 1979) and the initial pore-pressure distribution, parameters that are not commonly available for most slopes. The uncertainties related to properties such as hydraulic conductivity introduce uncertainties into both the FS of a given slope segment and to the timing of the FS response to the infiltrating rainfall. For example, a silty sand can commonly vary from 10^{-7} to 10^{-3} m/s (Freeze and Cherry, 1979). This leads to standard deviations (estimated by the "three sigma rule" above; Duncan, 2000) in the hydraulic conductivity of 1.7 x 10^{-4} m/s and coefficients of variation of 17. As some hydraulic conductivities will be lower than the intensities of rainfall, surface runoff may occur that is not predicted with the result of FS remaining higher than predicted as well as decreases of FS with rainfall being delayed from that predicted. So, in some cases, models that require material properties whose actual values are highly uncertain, may produce FS values that have such large degrees of uncertainty that they are not useful. However, calibration against a landslide dataset can greatly reduce the uncertainties.

Harp and others (2006) have used a simpler version of the infinite slope equation to construct a shallow landslide hazard map for the city of Seattle, Washington (fig. 1-7 A and B). This version assigns each geologic unit an average shear strength in terms of cohesion (c') and internal angle of friction (φ') based on actual test data. This equation takes the form:

$$FS = \frac{c'}{\gamma t \sin\alpha} + \frac{\tan\varphi'}{\tan\alpha} - \frac{m\gamma_w \tan\varphi'}{\gamma\tan\alpha} \quad (2)$$

where FS, α, and γ_w, are the same as in eq. 1, γ is the unit weight of slope material, c' is the effective cohesion of the slope material, ϕ' is the effective friction angle of the slope material, t is the slope-normal thickness of the potential landslide block, and m is the proportion of the slope thickness that is saturated (Jibson and others, 2000; Harp and others, 2002; Harp and others, 2004). This analysis assumes that ground-water flow is parallel to the ground surface and that the stability of each cell is independent of the cells surrounding it. This model was used in conjunction with a dataset of landslide locations within the city for over 100 years to compare with the FS values and compile a hazard map based on correlations with the dataset.

The above model has also been used in areas of the world where little test data are available. A landslide hazard map was constructed for the city of Tegucigalpa, Honduras, based on the landslides triggered by Hurricane Mitch in October 1998 (Harp and others, 2002; fig. 1-8) and for the islands of Chuuk State, Federated states of Micronesia based on landslides triggered by Typhoon Chata'an in July 2002 (Harp and others, 2004; fig. 1-9). The TRIGRS model has recently been used by Salciarini and others (2006) in the Umbria region of central Italy where landslide inventories allowed calibration of the model. In all these applications, estimated shear-strengths have been calibrated to ensure that no cells fail under dry conditions.

The above methods of regional analysis have been applied to most common types of shallow landslides (falls, slides, and slumps in rock and soil). They have been successfully used to portray landslide hazard to communities where these types of failures have caused considerable damage to people and property. As mentioned above, the shallow landslide types pose minimum hazard to pipelines that are buried unless their movement results in penetration or erosion to pipeline-burial depths. Some pipelines, however, are not buried but are carried above ground on supports and bridges, and buried pipelines have locations where there are pumping stations, valves, and connections above ground and would therefore be vulnerable to shallow-landslide movement or impact.

Deep-Seated Landslide Analyses

The primary threat to pipelines from slope failures arise from the movement of landslides whose failure surface or surfaces are several meters or greater in depth. Landslides with rotational and/or translational movement, and in rock or soil, all pose potential threats to pipeline integrity from displacements large enough to damage or rupture the pipe.

As for the shallow landslides discussed above, both qualitative and quantitative methods of hazard analysis are used for deep-seated landslides. The field geomorphic, weighted parameters, and statistical methods described in an earlier section are applied to deep-seated landslide susceptibility or hazard in the same manner as shallow landslide susceptibility or hazard. Deterministic geotechnical analyses coupled with a GIS on a regional scale are necessarily different than those used for shallow landslides. First, the use of the infinite slope analysis is not appropriate for most deeper landslides. Secondly, there are more differences, structurally and geometrically, between one deep-seated landslide and another than between shallow landslides. And finally, deep-seated landslides tend to be less related to a single triggering event or group of events than populations of shallow landslides. Deep-seated landslides are more spread out over time than shallow failures, and their populations are generally not as high density as shallow landslides leaving them less robust for statistical or probabilistic analysis.

Methods to evaluate the stability of specific deep-seated landslides are numerous and rely on adequate sampling and testing of the material properties of the landslide material to formulate a reliable estimate of the stability of the landslide usually described as FS. These methods applied to individual landslides are discussed and evaluated in a later section. Here, we will examine the

methods of coupling slope-stability analysis for deep-seated landslide with GIS techniques to evaluate slope stability on a regional basis.

Despite the tendency of deep-seated landslides to have much greater differences in geometries and mechanisms of failure than shallow landslides, methods to merge GIS analyses and slope-stability calculations for deep-seated landslides have begun to be employed on a regional basis. Miller (1995) and Miller and Sias (1997) have used conventional two-dimensional (2-D) moment equilibrium analyses coupled with ground-water models to estimate factor-of safety (FS) throughout landslide terrain in watersheds in northwestern Washington. For these analyses, circular or elliptical slip surfaces along a regional grid parallel to slope were analyzed to select circles with minimum FS for each grid point.

Other investigators such as El-Ramly and others (2002) have employed similar 2-D conventional stability analyses coupled with statistical techniques to evaluate and minimize the variance of the various input parameters (such as shear strength, unit weight, and pore pressure) so that probabilities of failure or "unsatisfactory performance" could be quantified. With these methods, results are highly dependent on the degree to which the input parameters can be specified and the variance-reduction techniques achieve effective averaging. In fact Aleotti and Chowdury (1999, p.34) indicate that when FS is determined as a probability density function based on input parameters which are themselves probability distributions, …"the data must be more detailed or numerous than those for deterministic analyses."

In addition to deficiencies in data for input parameters, the lack of accounting for three-dimensional (3-D) effects on slope stability often introduces errors and hampers 2-D analytical accuracy. For this reason, many scientists have chosen to evaluate regional hazards from deep-seated landslides by 3-D analyses. Xie and others (2004) and Franciss (2004) have used 3-D slope-stability analyses coupled with ground-water models to assess FS on a regional basis for slopes in Japan and Brazil respectively. One of the most commonly used models to assess 3-D stability employs the method of columns in which a surface grid element and its underlying column is examined together with adjacent columns within a slope/drainage area for all the possible combinations of columns to determine the least stable of these combinations. Usually a basal failure surface of spherical or elliptical shape is adopted for the analysis. Brien and Reid (2007) have constructed a deterministic deep-seated landslide-hazard analysis for part of the city of Seattle using a hydrologic model and a method of columns to calculate most likely failure surfaces (fig. 1-10). In some cases, other geometries such as wedges have been employed to match known geometries of local failure (Franciss, 2004).

Input for the various mathematical models in the above deterministic methods are acquired from actual measured data where possible and estimated where not. Most geotechnical data gathered even from a site-specific slope-stability investigation would still be insufficient to use for application to evaluating slope stability over a much wider area. For this purpose, the most common techniques of estimating the distributions of properties such as shear-strength parameters (c' and $'$), unit weight ( ), and pore pressure, are assumed to have a normal distribution about an expected mean value. In most cases, the ranges of values and the mean are selected from existing data and from judgment based on experience. With these selected estimates, the distribution (probability density function (PDF)) is then approximated by first order second moment (FOSM) methods (Wu and others, 1996) to determine the mean and variance of the parameter data. Using these estimates a probability density function of a performance indicator, in many cases, FS is calculated. The PDF of FS is then another distribution of FS values with its own mean and variance. This PDF describes the probability of FS values being • 1.0.

Utility of the Various Susceptibility or Hazard Assessment Methods

Qualitative Methods

The main advantages of the methods of qualitative hazard assessment are that they are relatively rapid. The susceptibility or hazard is assigned based solely on the investigator's judgment and is either unspecified or is based on a weighting of specified factors that affect slope stability. In either case, the assignment of weights or simply hazard itself is based on judgment of the investigator and cannot be replicated by others. Although subjective, once the weights have been established, the process of overlapping weighted maps and developing a hazard map can be automated and performed on a GIS platform.

Quantitative Methods

Statistical

Of the statistical methods of assessing landslide susceptibility and hazard, bivariate methods are the most straightforward. Simply comparing sets of mapped factors to a landslide map and determining the weight factors based on the density of landslides captured by the separate factors is reproducible, especially if the weighting factors are directly proportional to the densities of landslides for the respective factors. The final overlay of factor maps to calculate the resulting hazard or susceptibility is easily accomplished within a GIS.

Multivariate methods of modeling landslide hazards gained popularity from their ability to assess the effect of numerous factors on the susceptibility of slopes to landslides either simultaneously or stepwise. All considered factors could be regressed against a mapped landslide distribution and correlation coefficients could be determined and susceptibility assigned based on the individual correlations. Carrera (1983) did much of the early work in using these methods to compare with landslide distributions in various drainage basins in Italy in which landslides and all considered factors had been carefully mapped and quantified. Carrera and others (1991) used 15 slope-related variables to regress against mapped landslides in the Tescia Basin in Umbria, Italy, and was able to predict both stable and unstable slopes with approximately 80 percent accuracy.

The advantage of the various statistical methods is that they are extremely systematic and reproducible once the different slope-related stability factors are defined and the data collected. The actual mapping of these factors and analysis of the data concerning the factors is often time-consuming and cumbersome (Aleotti and Chowdury, 1999). Carrera and others (1991) remarked that the gathering of data and encoding of the various factors for a multivariate statistical study of a basin in Calabria, Italy (Carrera, 1983, 1989), required a great deal of time. They also stated that "black box" models such as their discriminant analysis of the Tescia Basin "do not unravel the internal structure of the process involved," because even with all of the variables included, the analysis is too simple. It also is basin specific and cannot be transferred to other basins with different geology and morphology (Carrera and others, 1991, p. 443). Use of these methods requires that there is a reliable landslide inventory for comparison with the various factors.

Deterministic/Probabilistic

The main advantage of these types of analyses is that uncertainties in the variables that affect slope stability can be taken into consideration. These analyses can incorporate modifications of slope geometry or other changes that affect the stability of the slopes due to construction activities that might occur in the development of a pipeline corridor. If sets of comprehensive data exist for variables such as shear strength, material unit weights, and levels of pore pressure, then a

distribution of performance factors such as FS can be reliably estimated. If not, which is usually the case, values of the means and variances of these variables are estimated as previously discussed in the section on shallow landslide analyses. Variables such as shear strength may not be normally or lognormally distributed, especially when considering formations that have interbedded layers of differing properties. They may be bimodal or multimodal in their distribution. So, when normal distributions are assumed for variables that may not have normal distributions, the results, although having what seem to be sophisticated estimates of mean, variance, and numerical probabilities, in reality may have no more basis than the hazard map based solely on the implicit judgment and experience of the investigator. The results can be misleading and give a false sense of quantitative assessment. This is especially true for the analysis of slopes with deep-seated landslides. Not only are material properties poorly known for most of these cases, but the failure geometries are also poorly known and are highly variable from one to another and are difficult, if not impossible, to generalize. Therefore, landslide hazard analyses for deep-seated landslides are inherently fraught with high (and often unknown) degrees of uncertainty and are of limited use. A summary of advantages and disadvantages of the various methods of landslide hazard analysis is presented by Aleotti and Chowdury (1999; reproduced here in modified form as table 1-1). Baum and others (2005) review the application of several different methods of hazard and susceptibility assessment in Seattle, Washington, and provide insight into some of the relative advantages and disadvantages of the different methods.

Estimation of Displacement or Runout

Precise prediction or estimation of displacement of coherent landslides or the runout of mobilized fluid landslides is not within the current capabilities of modeling methods. Models of granular or particle flow have been used to attempt to match the distances and paths of debris flows (Hungr and Morgenstern, 1984; Denlinger and Iverson, 2004; Iverson and others, 2004). However, no current models accurately model runout distances except in uniform materials that contain few irregular particles. Trees and other types of vegetation that commonly become incorporated in debris flows are irregularities that cannot be modeled successfully by these methods but can impart considerable influence on runout distances and flow paths. The three-dimensional modeling of the movement of large landslide masses and mixtures of water and earth materials is useful however, to obtain order-of-magnitude estimates of displacement and runout for risk assessment considerations (Denlinger and others, 2006).

Despite the advances being made in the modeling of landslide displacement and runout, it is still beyond reliable modeling capabilities to precisely estimate the velocity or the total displacement of dislocated earth materials. The most reliable methods of estimating runout still rely on the presence of previous deposits. Preexisting debris flows, rock falls, rock slides, slumps, and other types of landslides provide "ground-truth" data (Baum and others, 2000) from which estimates of average, maximum, and minimum future landslide runouts can be based with the confidence that these estimates included in-place conditions and irregularities of the real slopes under consideration.

Table 1-1. Advantages and disadvantages of different methods of landslide hazard assessment (after Aleotti and Chowdury, 1999).

Methods	Advantage	Disadvantage	Role of GIS
Field geomorphic analyses	Allow a rapid assessment taking into account a large number of factors.	Totally subjective; methodology uses implicit rules that hinder the critical analysis of the results.	Only as a drawing tool
Combination of index maps	Solves the problem of hidden rules. Total automation of steps. Standardization of data management.	Subjective in attributing weighted values to each parameter.	Overlay of different maps
Statistical analyses (bivariate, multivariate, etc.)	Objective in methodology. Total automation of steps. Standardization of data management.	Systematic collection and analysis of data regarding different factors is cumbersome.	Analysis and map overlay
Probabilistic approaches	Allows consideration of different uncertainties. Quantitative in scope. Objective in scope and methodology. Provides insight not possible in deterministic methods.	Requires comprehensive data. Otherwise subjective probabilities required. Probability distributions difficult, especially for low level of hazard.	Analysis and map overlay

References Cited

Aleotti, P., and Chowdury, R., 1999, Landslide hazard assessment: summary review and new perspectives: Bulletin of Engineering Geology and the Environment, v. 58, p. 21–44.

Baum, R.L., Coe, J.A., Godt, J.W., Harp, E.L., Reid, M.E., Savage, W.Z., Schulz, W.H., Brien, D.L., Chleborad, A.F., McKenna, J.P., and Michael, J.A., 2005, Regional landslide-hazard assessment for Seattle, Washington, USA: Landslides, v. 2, no. 4, p. 266–279.

Baum, R.L., Savage, W.Z., and Godt, J.W., 2002, TRIGRS–A Fortran program for transient rainfall infiltration and grid-based regional slope-stability analysis: U.S. Geological Survey Open-File Report 02-0424, 27 p., 2 appendixes. *http://pubs.usgs.gov/of/2002/ofr-02-424/*

Baum, R.L., Harp, E.L., and Hultman, W.A., 2000, Map showing recent and historic landslide activity on coastal bluffs of Puget sound between Shilshole Bay and Everett, Washington: U.S. Geological Survey Miscellaneous Field Studies Map, MF–2346, scale 1:24,000.

Blaikie, P., Cannon, T., Davis, I., and Wisner, B., 1994, At risk: Routledge, 190 p.

Brien, D.L., and Reid, M.E., 2007, Modeling 3-D slope stability of coastal bluffs using 3-D ground-water flow, southwestern Seattle, Washington: U.S. Geological Survey Scientific Investigations Report 2007-5092, 54 p.

Cannon, S.H., Gartner, J.E., Michael, J.A., Bauer, M.A., Stitt, S.C., Knifong, D.L., McNamara, B.J., and Roque, Y.M., 2007, Emergency assessment of debris-flow hazards from basins burned by the 2007 Witch Fire, San Diego County, southern California: U.S. Geological Survey Open-File Report 2007-1420, 1 sheet.

Carrera, A., Cardinali, M., Detti, R., Guzzetti, F., Pasqui, V., and Reichenbach, P., 1991, GIS techniques and statistical models in evaluating landslide hazard: Earth Surface Processes and Landforms, v. 16, p. 427–445.

Carrera, A., 1989, Landslide hazard mapping by statistical methods: a “black-box” model approach, *in* Siccardi, F., and Bras, R.L., eds., Proceedings Natural Disasters in European-Mediterranean Countries, Perugia 27 June–1 July, CNR-U.S.N.S.F., p. 205–224.

Carrera, A., 1983, Multivariate models for landslide hazard evaluation: Mathematical Geology, v. 15, no. 3, p. 403–426.

Çevik, E., and Topal, T., 2003, GIS-based landslide susceptibility mapping for a problematic segment of the natural gas pipeline, Hendek, Turkey: Environmental Geology, v. 44, p. 949–962.

Coe, J.A., Godt, J.W., Baum, R.L., Buckram, R.C., and Michael, J.A., 2004, Landslide susceptibility from topography in Guatemala, *in* Lacerda, W.A., Erlich, M., Fonterra, S.A.B., and Sayao, A.S.F., eds., Landslides—evaluation and stabilization, Proceedings of the 9th International Symposium on Landslides: London, A.A. Balkema Publishers, v. 1, p. 69–78.

Coe, J.A., Harp, E.L., Tarr, A.T., and Michael, J.A., 2005, Rock-fall hazard assessment of Little Mill Campground, American Fork Canyon, Uinta National Forest, Utah: U.S. Geological Survey Open-File Report 2005-1229, 48 p., 2 pls.

Coe, J.A., Harp, E.L., Tarr, A.T., and Michael, J.A., 2007, Rockfall hazard at Little Mill Campground, Uinta National Forest: Part 1. Geologic hazard assessment: *in* Schaefer, V.R., Schuster, R.L., and Turner, A.K., eds., Conference Presentations: 1st North American Landslide Conference, Vail, Colorado, AEG Special Publication 23, Association of Environmental & Engineering Geologists, CD-ROM, 14 p.

DeGraff, J.V., Cannon, S.H., Gartner, J.E., and Gallegos, A.J., 2007, Reducing post-wildfire debris flow risk through the burned area emergency response (BAER) process, *in* Schaefer, V.R., Schuster, R.L., and Turner, A.K., eds., Conference Presentations: 1st North American Landslide

Conference, Vail, Colorado, AEG Special Publication 23, Association of Environmental & Engineering Geologists, CD-ROM, 10 p.
Denlinger, R.P., O'Connell, R.H., and Jones, M., 2006, Summary of preliminary 2-D inundation modeling for three Hattian landslide dam breaches: U.S. Geological Survey Open-File Report 2006-1094, 47 p.
Denlinger, R.P., and Iverson, R.M., 2004, Granular avalanches across irregular three-dimensional terrain: 1. Theory and computation: Journal of Geophysical Research, v. 109, F01014.
Duncan, J.M., 2000, Factors of safety and reliability in geotechnical engineering: Journal of Geotechnical and Geoenvironmental Engineering, p. 307–316.
El-Ramly, H., Morgenstern, N.R., and Cruden, D.M., 2002, Probabilistic slope stability analysis for practice: Canadian Geotechnical Journal, p. 665–683.
Franciss, F.O., 2004, Landslide hazard assessment on hilly terrain, *in* Lacerda, W.A., Ehrlich, M., Fontoura, S.A.B., and Sayão, A.S.F., eds., Landslides–evaluation and stabilization: Proceedings of the 9th International Symposium on Landslides, Rio de Janeiro, Brazil, v. 1, p. 143–150.
Freeze, R.A., and Cherry, J.A., 1979, Groundwater: Englewood Cliffs, N.J.,Prentice-Hall, Inc., 604 p.
Gartner, J.E., Cannon, S.H., Santi, P.M., and Dewolfe, V.G., in press, Empirical models to predict the volumes of debris flows generated by recently burned basins in the Western U.S.: Geomorphology.
Godt, J.W., Schulz, W.H., Baum, R.L., and Savage, W.Z., in press, Modeling rainfall conditions for shallow landsliding in Seattle , Washington, *in* Baum, R.L., Godt, J. W., and Highland, L.M., eds., Landslide and engineering geology of the Seattle, Washington area: Boulder, Colo., Geological Society of America, Reviews in Engineering Geology:
Hamlin, S.N., and Takasaki, K.J., 1984–85, Water-quality reconnaissance of ground water in the inhabited outer atoll islands of Chuuk State, Federated States of Micronesia: U.S. Geological Survey Water-Resources Investigations Report 96-4180, 77 p.
Hammond, C., Hall, D., Miller, S., and Swetik, P., 1992, Level I stability analysis (LISA) documentation for version 2: USDA Forest Service Intermountain Research Station, General Technical Report INT-285, 121 p.
Harding–Lawson Associates, 1979, Seismically induced ground-failure susceptibility, Anchorage, Alaska: Miscellaneous Publication 32, Digitally recompiled by Weems, S.M., and Combellick, R.A., 1997, Alaska Division of Geological and Geophysical Surveys.
Harp, E.L, Michael, J.A., and Laprade, W.T., 2006, Shallow landslide hazard map of Seattle, Washington: U.S. Geological Survey Open-File Report 2006-1139, 20 p., 2 pls.
Harp, E.L., Reid, M.E., and Michael, J.A., 2004, Hazard analysis of landslides triggered by Typhoon Chata'an on July 2, 2002, in Chuuk State, Federated States of Micronesia: U.S. Geological Survey Open-File Report 2004-1348, 24 p., 2 pls.
Harp, E.L., and Jibson, R.W., 2002, Anomalous concentrations of seismically triggered rock falls in Pacoima Canyon: are they caused by highly susceptible slopes or local amplification of seismic shaking: Bulletin of the Seismological Society of America, v. 92, no. 8, p. 3,180–3,189.
Harp, E.L., and Jibson, R.W., 1995, Inventory of landslides triggered by the 1994 Northridge, California, earthquake: U.S. Geological Survey Open-File Report 95-213, 17 p., 2 pls.
Harp, E.L., Held, M.D., Castañeda, M.R., McKenna, J.P., and Jibson. R.W., 2002, Landslide hazard map of Tegucigalpa, Honduras: U.S. Geological Survey Open-File Report 2002-219, 9 p., 2 pls.
Harp, E.L., and Noble, M.A., 1993, An engineering rock classification to evaluate seismic rock-fall susceptibility and its application to the Wasatch Front: Bulletin of the Association of Engineering Geologists, v. 30, p. 293–319.

Hungr, O., and Morgenstern, N.R., 1984, High velocity ring shear tests on sand: Geotechnique, v. 34, p. 415–421.
Iverson, R.M., Logan, M., and Denlinger, R.P., 2004, Granular avalanches across irregular three-dimensional terrain: 2. Experimental tests: Jornal of Geophysical Research, v. 109, F01015.
Iverson, R.M., 2000, Landslide triggering by rain infiltration: Water Resources Research, v. 36, no. 7, p. 1,897–1,910.
Jibson, R.W., Harp, E.L., and Michael, J.A., 2000, A method for producing digital probabilistic seismic landslide hazard maps: Engineering Geology, v. 58, p. 271–289.
Miller, D.J., and Sias, J., 1998, Deciphering large landslides: linking hydrological groundwater and slope stability models: Hydrological Processes, v. 12, p. 923–941.
Miller, D.J., 1995, Coupling GIS with physical models to assess deep-seated landslide hazards: Environmental and Engineering Geoscience, v.1, no. 3, p. 263–276.
Montgomery, D.R., and Dietrich, W.E., 1994, A physically based model for the topographic control on shallow landsliding: Water Resources Research, v. 30, no. 4, p. 1,153–1,171.
Montgomery, D.R., Greenberg, H.M, Laprade, W.T., and Nashem, W.D., 2001, Sliding in Seattle: Test of a model of shallow landsliding potential in an urban environment, *in* Wigmosta, M.S. and Burges, S.J., eds., Land use and watersheds: Human influence on hydrology and geomorphology in urban and forest areas, Water Science and Application 2, American Geophysical Union, p. 59–73.
Morrissey, M.M., Wieczorek, G.F., and Morgan, B.A., 2001, A comparative analysis of hazard models for predicting debris flows in Madison County, Virginia: U.S. Geological Survey Open-File Report 01-67, 27 p.
Pack, R.T., Tarboton, D.G., and Goodwin, C.N., 1999, GIS-based landslide susceptibility mapping with SINMAP, *in* Bay, J.A., ed.: Proceedings of the 34th Symposium on Engineering Geology and Geotechnical Engineering, p. 210–231.
Porter, M., Marcuz, G., Reale, R., and Savigny, K.W., 2006, Geohazard risk management for the Nor Andino gas pipeline: Proceedings of the 6th International Pipeline Conference, Calgary, Alberta, Canada, p. 1–9.
Reid, M.E., 1997, Slope instability caused by small variations in hydraulic conductivity: Journal of Geotechnical and Geoenvironmental Engineering, v. 123, no. 8, p. 717–725.
Salciarini, D., Godt, J.W., Savage, W.Z., Conversini, P., Baum, R.L., and Michael, J.A., 2006, Modeling regional initiation of rainfall-induced shallow landslides in the eastern Umbria Region of central Italy: Landslides, v. 3, p. 181–194.
Savage, W.Z., Godt, J.W., and Baum, R.L., 2004, Modeling time-dependent areal slope stability, *in* Lacerda, W.A., Ehrlich, M., Fontoura, S.A.B., and Sayão, A.S.F., eds., Landslides–evaluation and stabilization: Proceedings of the 9th International Symposium on Landslides, Rio de Janeiro, Brazil, v. 1, p. 23–36.
Schuster, R.L., Baum, R.L., and Highland, L.M., 1998, The April 1998 El Niño-triggered Anzar road landslide, San Benito County, California: Association of Engineering Geologists News, v. 41, no. 4, p. 5–7.
van Westen, C.J., van Asch, T.W.J., and Soeters, R., 2006, Landslide hazard and risk zonation–why is it still so difficult?: Bulletin of Engineering Geology and the Environment, v. 65, p. 167–184.
Wieczorek, G.F., and Harp, E.L., 2000, Rock-fall hazard assessment of the Aspen Forest Trail, Navajo National Monument, Arizona: U.S. Geological Survey Open-File Report 2000-305, 11p.
Wu, T.H., Tang, W.H., and Einstein, H.H., 1996, Landslide hazard and risk assessment, *in* Turner, A.K., and Schuster, R.L., eds., Landslides–investigation and mitigation: Transportation Research Board, National Research Council Special Report 247, p. 106–118.

Xie, M., Esaki, T., Mitani, Y., and Cai, M., 2004, A 3-D deterministic approach for mapping landslide hazards using GIS, *in* Lacerda, W.A., Ehrlich, M., Fontoura, S.A.B., and Sayão, A.S.F., eds., Landslides–evaluation and stabilization: Proceedings of the 9th International Symposium on Landslides, Rio de Janeiro, Brazil, v. 1, p. 97–102.

Glossary of Terms

Hazard-Probability of occurrence within a reference period (van Westen and others, 2006).

Susceptibility (of slopes)-Tendency to fail. Often expressed as factor-of-safety.

Vulnerability-The characteristics of a person or group in terms of their capacity to anticipate, cope with, resist, and recover from the impact of a natural hazard (Blaikie and others, 1994).

Figure 1A. Deep-seated rotational slump in San Benito County, California, that has broken a natural gas pipeline. Landslide was triggered by rainfall from El Niño conditions April 22, 1998 (Photo by Robert Schuster, USGS).

Figure 1B. Toe of landslide in figure 1A showing broken pipeline (brown-colored pipe) and the temporary replacement (white-colored pipe; photo by Lynn Highland, USGS).

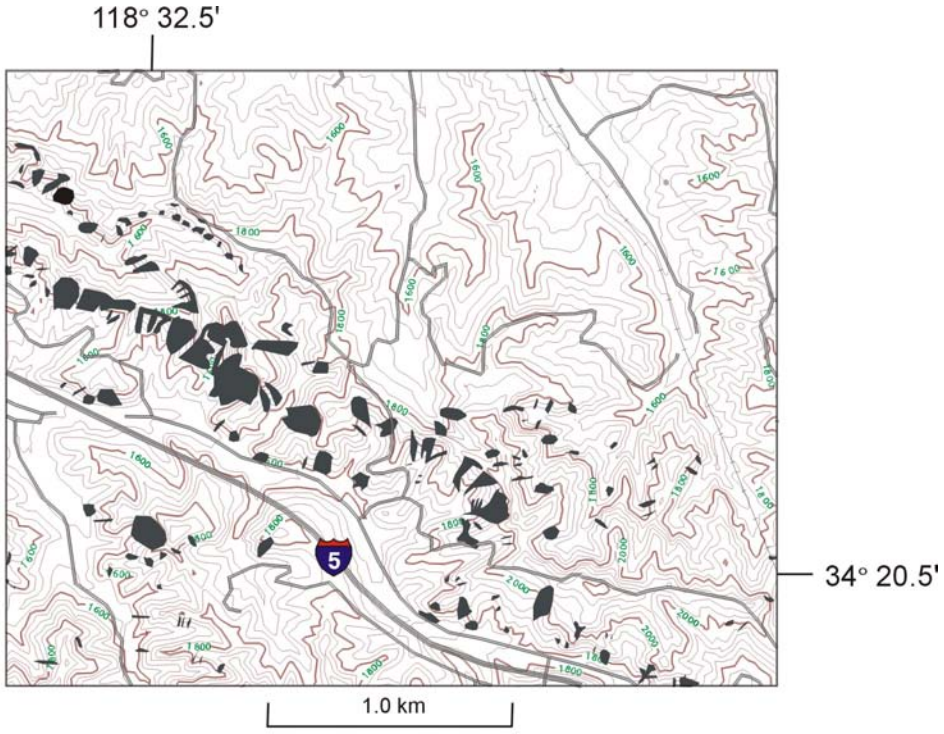

Figure 2. Portion of landslide inventory map for landslides triggered by the 1994 Northridge, California, earthquake (after Jibson and others, 2000).

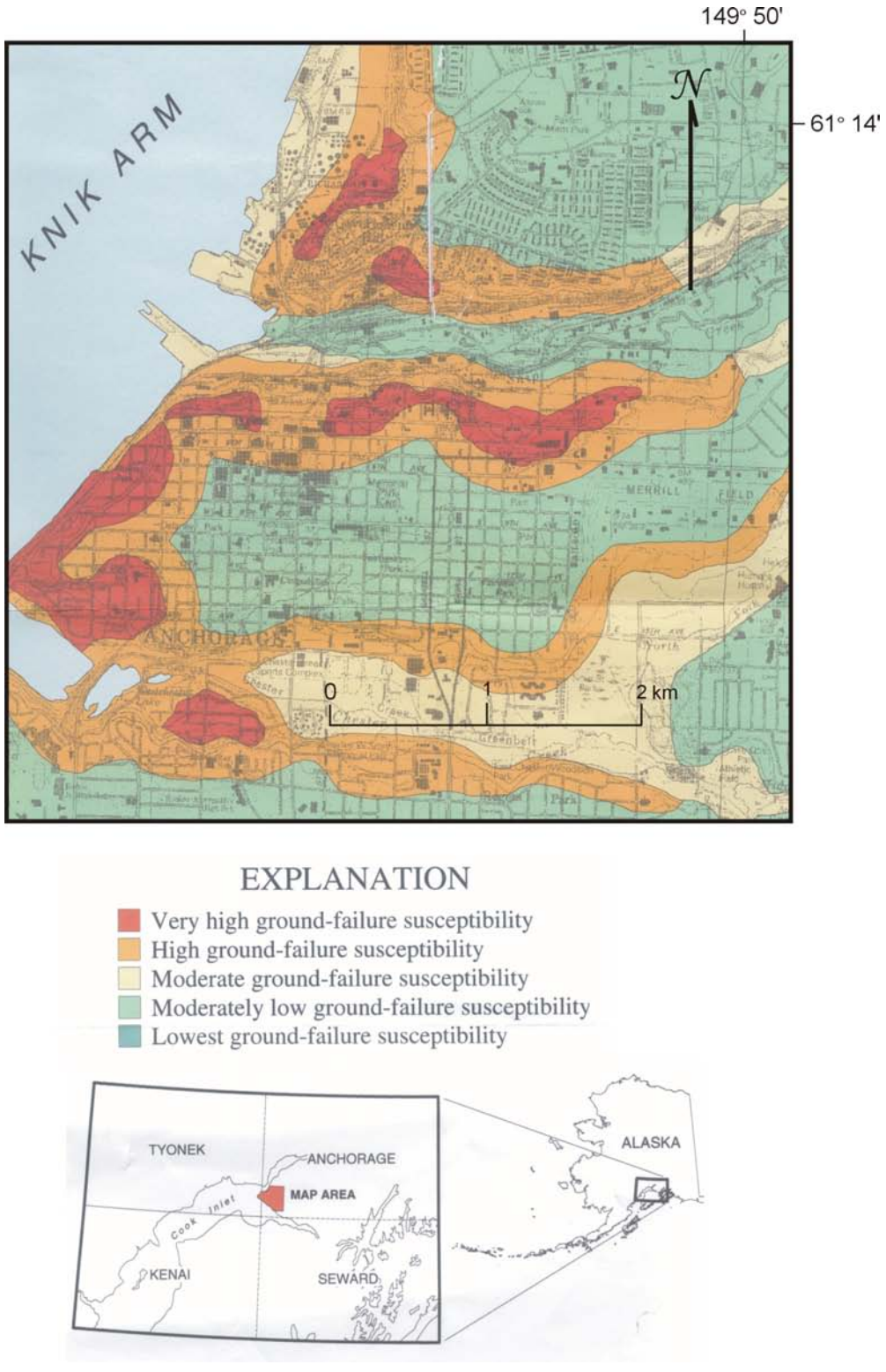

Figure 3. Map of Anchorage, Alaska, depicting qualitative relative seismic susceptibility based on judgment of authors (from Harding and Lawson, 1979; Weems and Combellick, 1997).

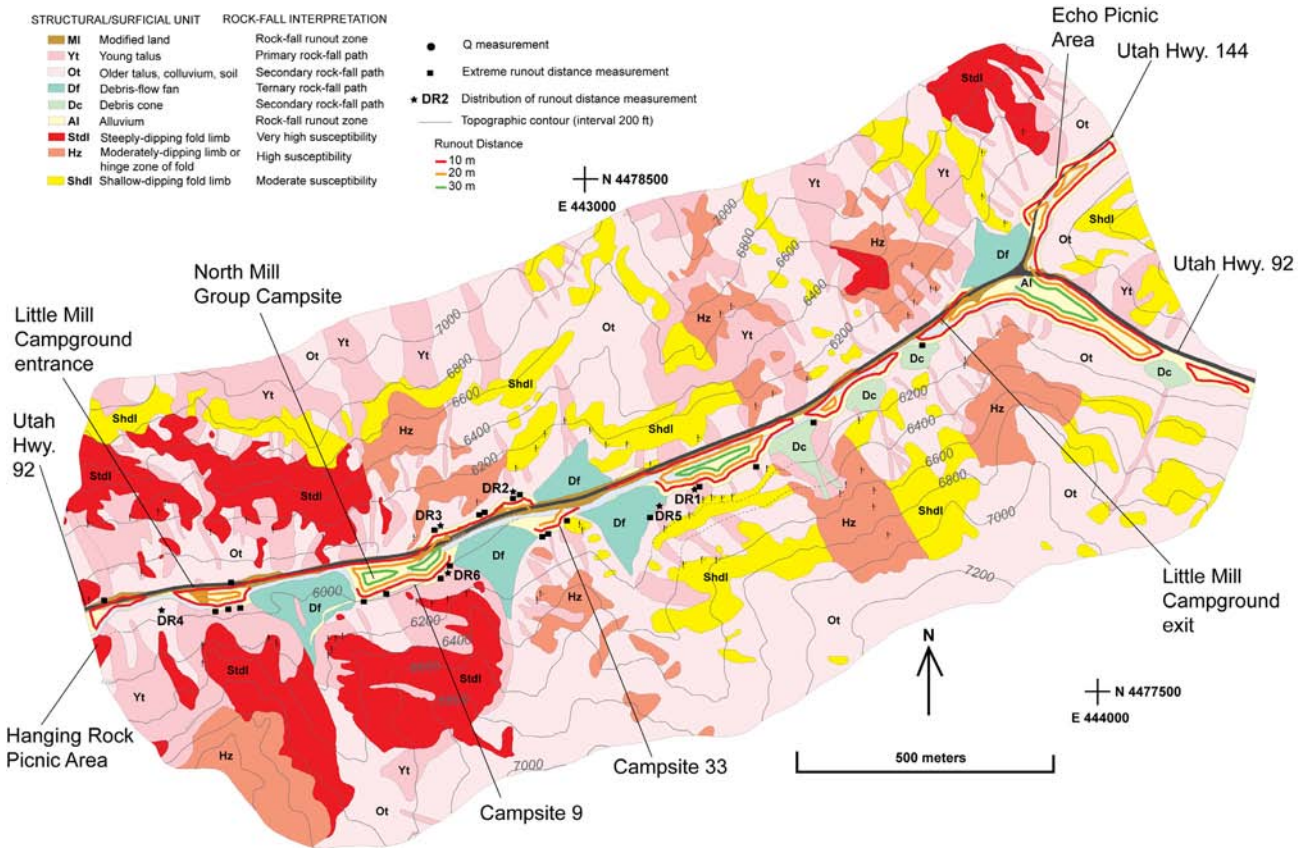

Figure 4. Rock-fall hazard map of Little Mill Campground, American Fork Canyon, Utah (from Coe and others, 2007).

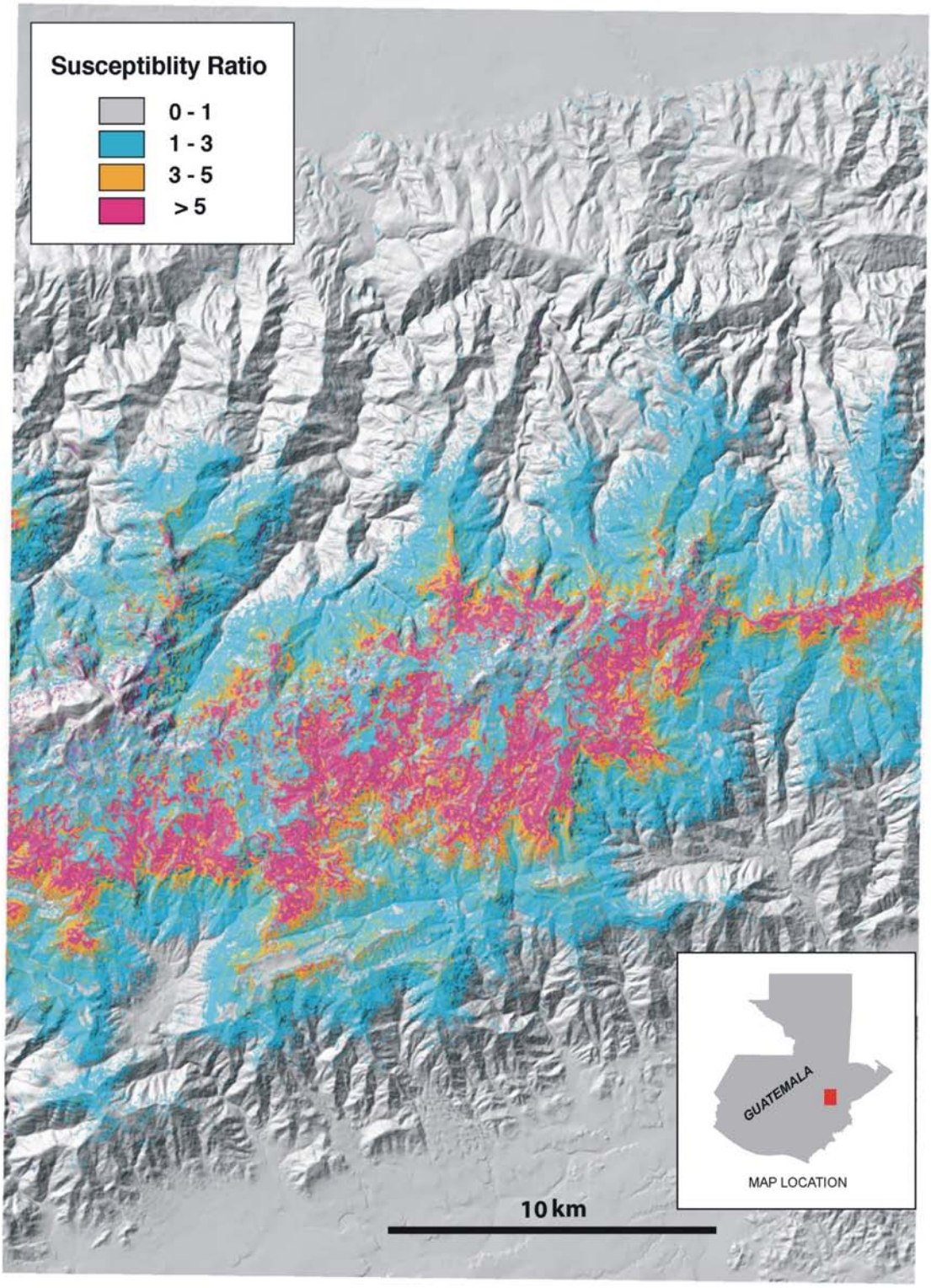

Figure 5. Landslide susceptibility map produced from ratio grid based on elevation and slope (from Coe and others, 2004).

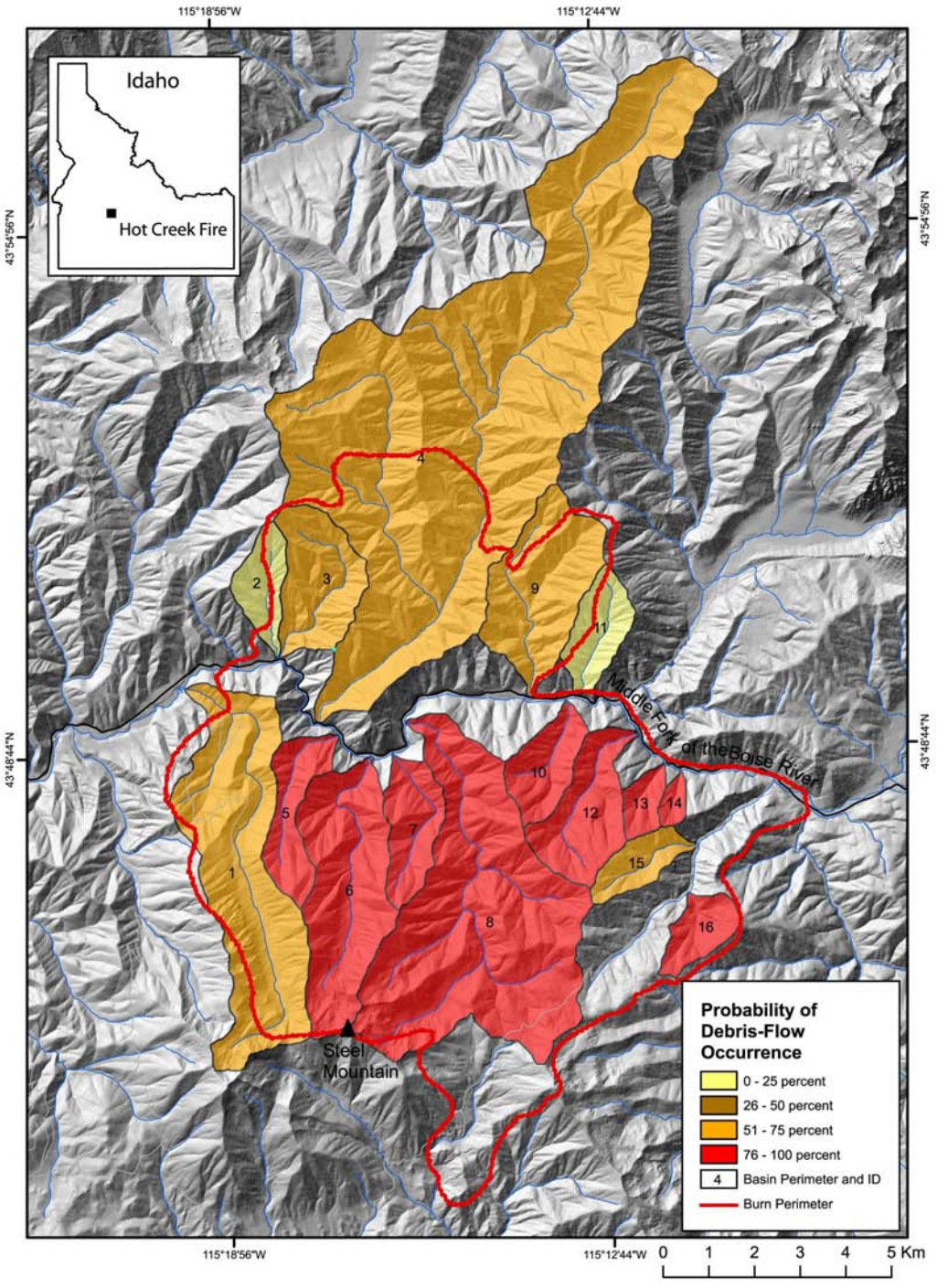

Figure 6. Map of probability of debris flow occurrence for basins burned by the Hot Creek Fire, Idaho, in response to a 1-hour, 10-year recurrence storm (from DeGraff and others, 2007).

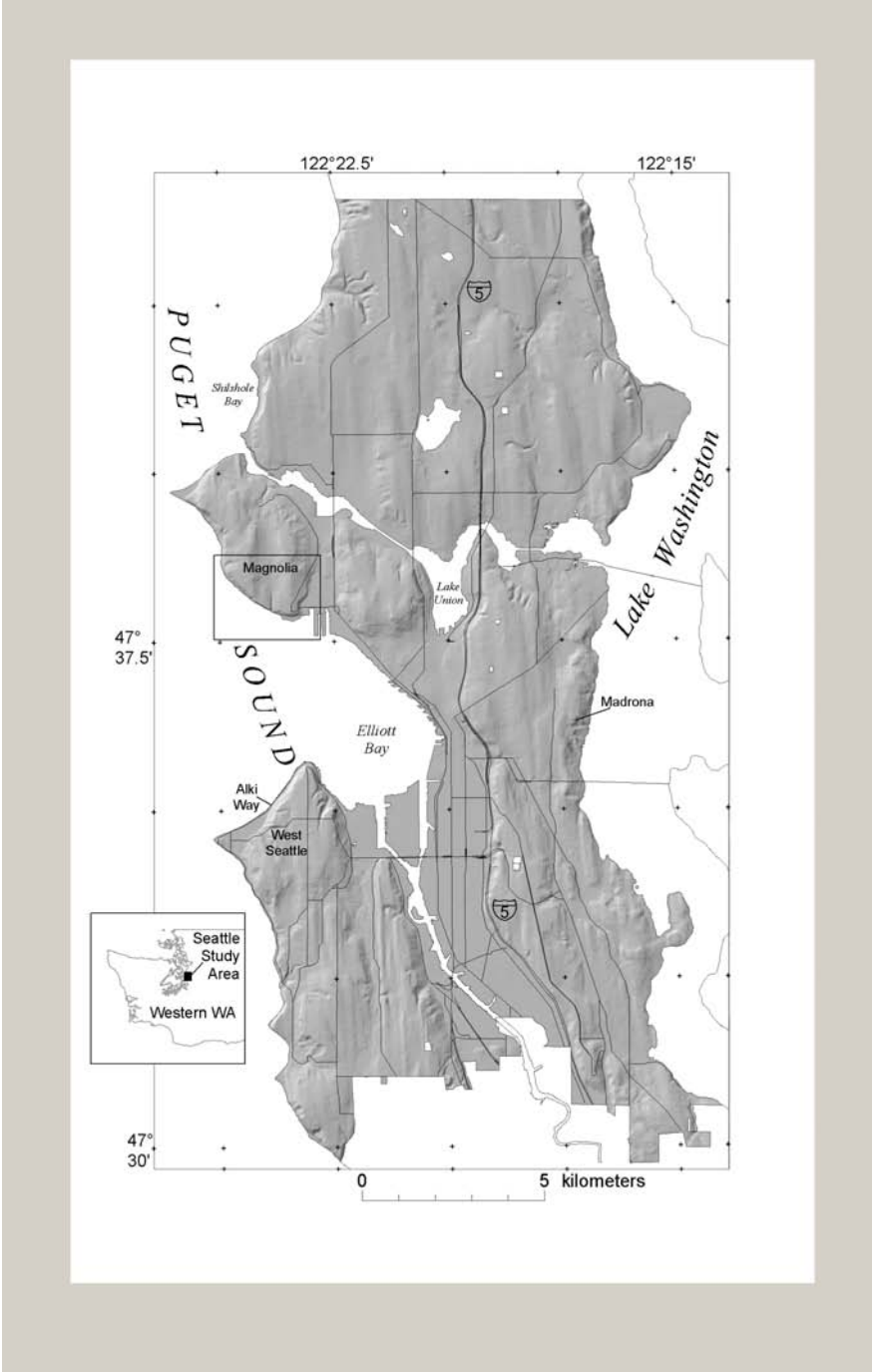

Figure 7A. Shaded relief map of Seattle, Washington, study area and location of area shown in figure 7B.

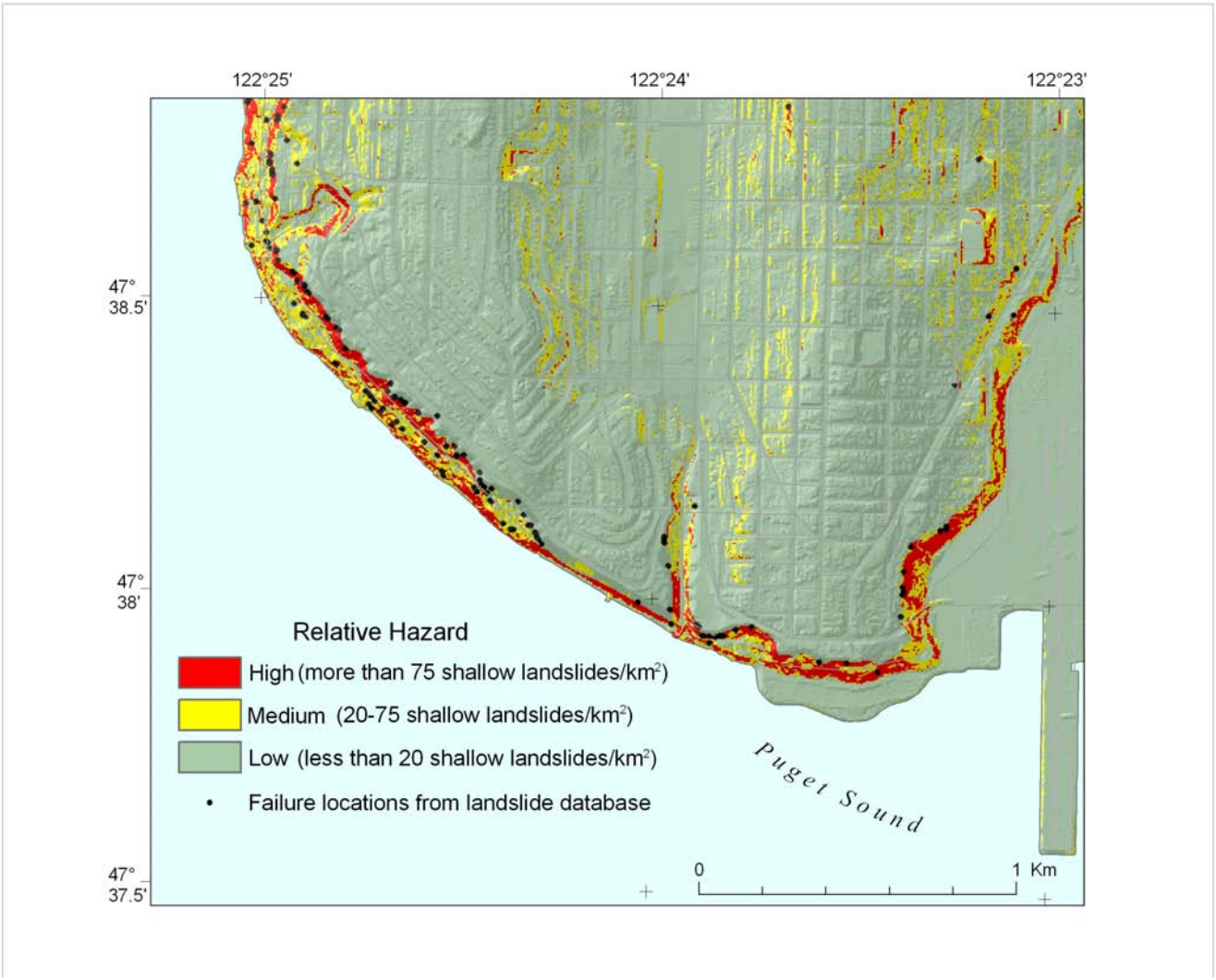

Figure 7B. Shallow landslide hazard map of portion of Seattle, Washington (from Harp and others, 2006).

Figure 8A. Location of metropolitan area of Tegucigalpa, Honduras.

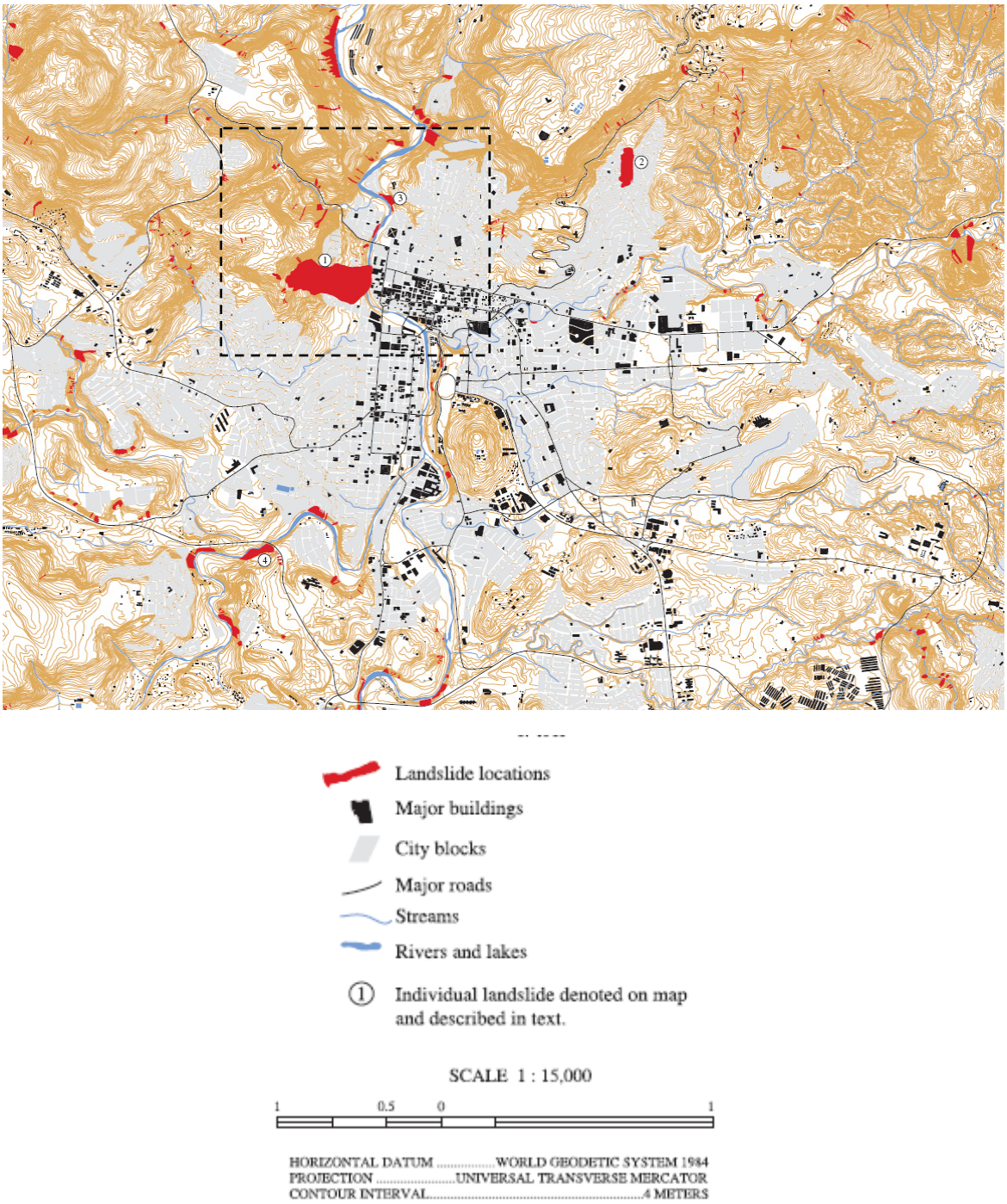

Figure 8B. Inventory of landslides triggered by Hurricane Mitch in Tegucigalpa, Honduras (from Harp and others, 2002). Dashed rectangle denotes area shown in figure 8C.

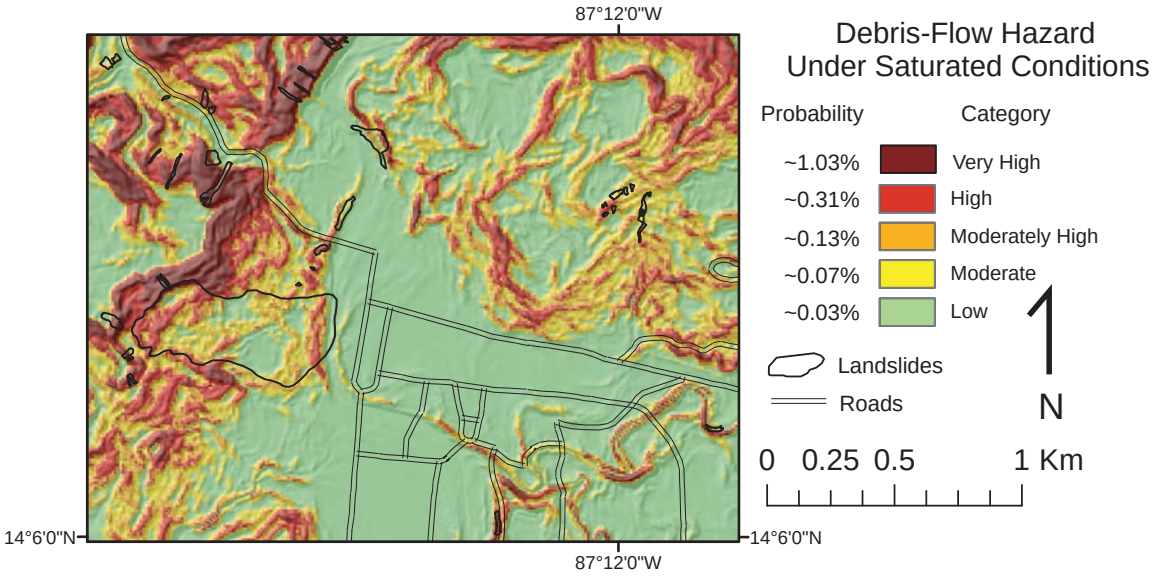

Figure 8C. Landslide hazard map for central part of Tegucigalpa, Honduras (from Harp and others, 2002).

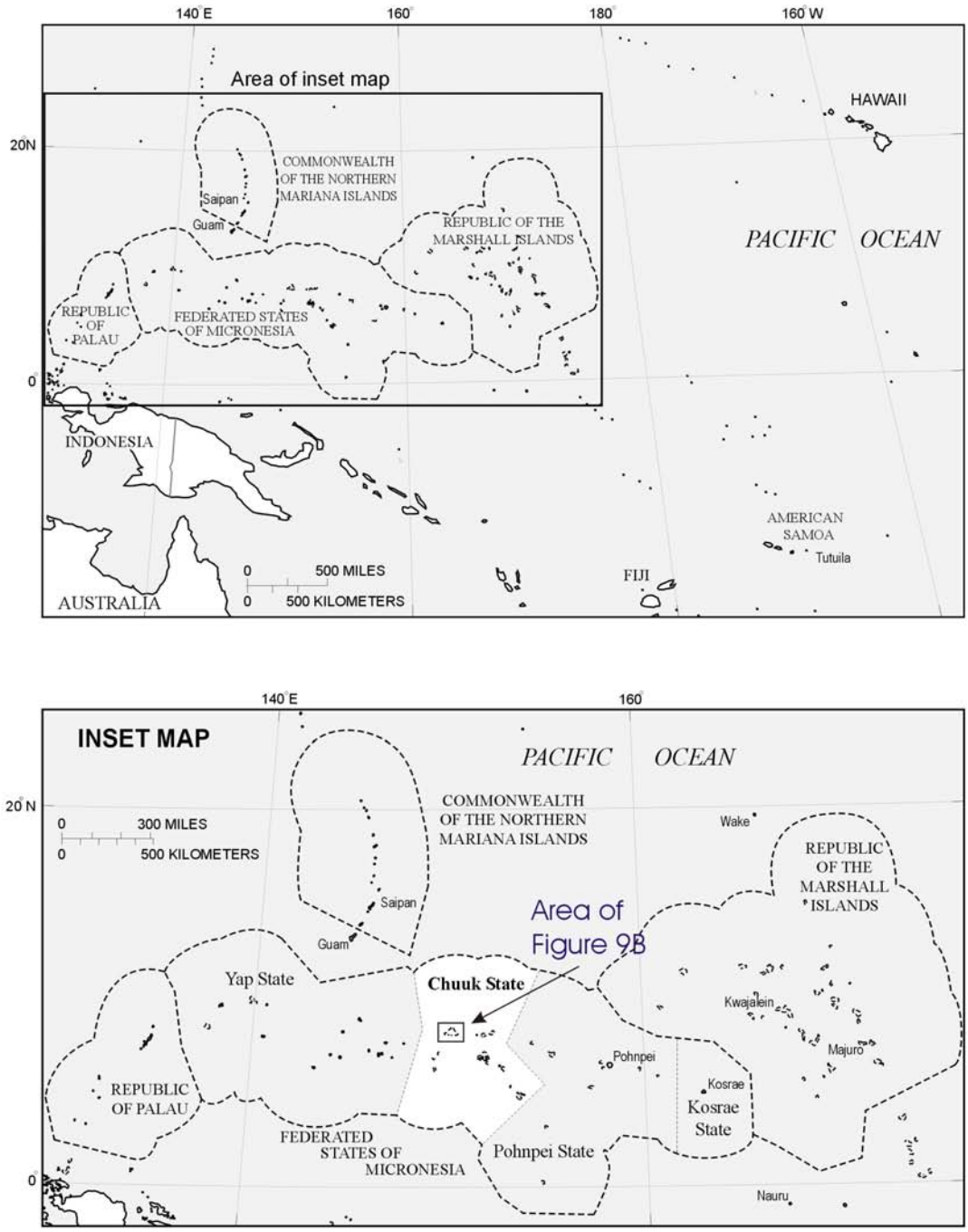

Figure 9A. Location maps of Chuuk State in the Federated States of Micronesia (from Harp and others, 2004).

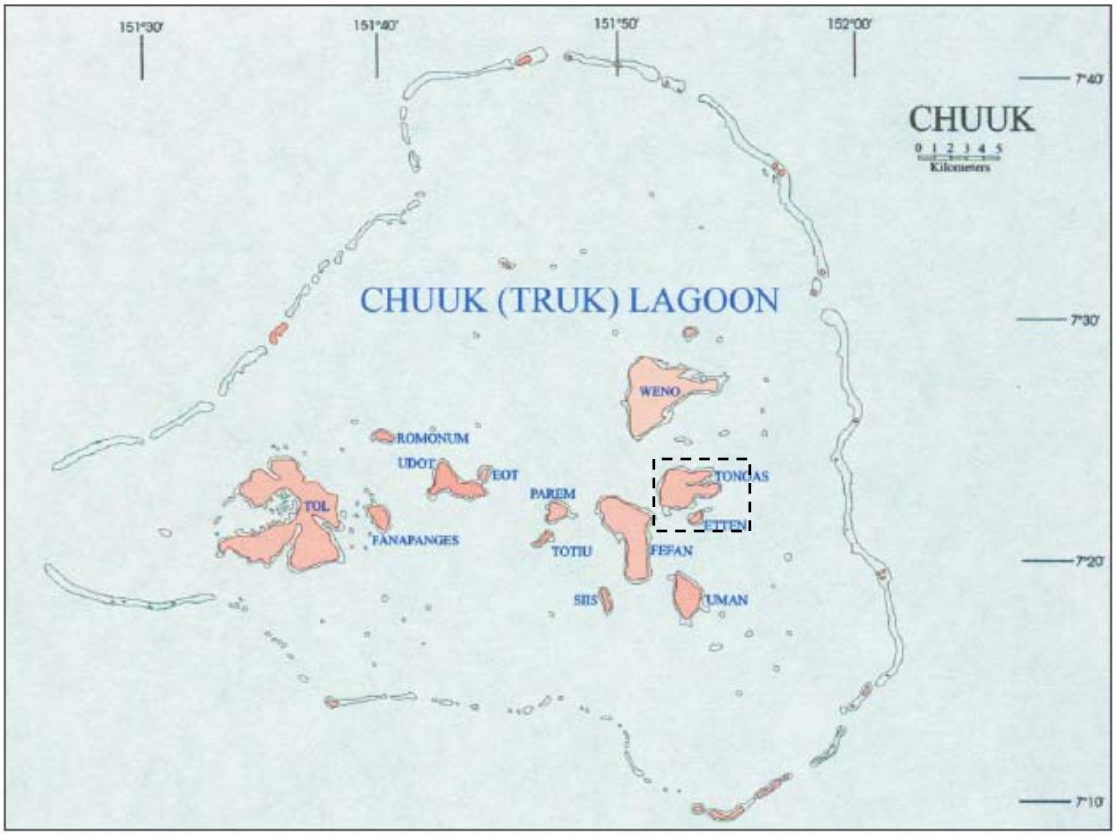

Figure 9B. Map of Chuuk islands within Chuuk (Truk) Lagoon (after Hamlin and Takasaki, 1984-85). Dashed rectangle denotes area shown in figure 9C.

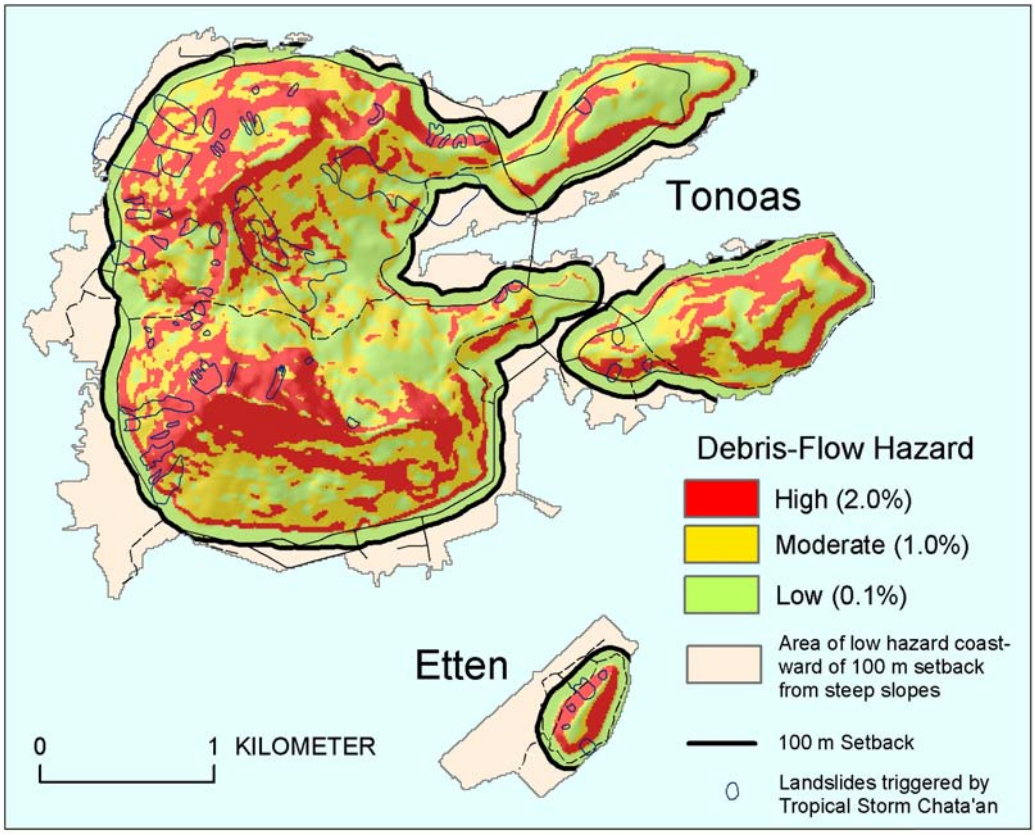

Figure 9C. Debris-flow hazard map of islands of Tonoas and Etten based on landslides triggered by Typhoon Chata'an (from Harp and others, 2004).

Prepared in cooperation with the U.S. Department of Transportation, Pipeline Research Council International, and DGH Consulting, Inc.

Land Subsidence Hazards

By D.L. Galloway, G.W. Bawden, S.A. Leake, and D.G. Honegger

Chapter 2 of
Landslide and Land Subsidence Hazards to Pipelines

Open-File Report 2008–1164

U.S. Department of the Interior
U.S. Geological Survey

Contents

List of Figures

List of Tables

Conversion Factors

SI to Inch/Pound

Multiply	By	To obtain
	Length	
centimeter (cm)	0.3937	inch (in.)
millimeter (mm)	0.03937	inch (in.)
meter (m)	3.281	foot (ft)
kilometer (km)	0.6214	mile (mi)
	Area	
square meter (m^2)	0.0002471	acre
square kilometer (km^2)	247.1	acre
square meter (m^2)	10.76	square foot (ft^2)
square kilometer (km^2)	0.3861	square mile (mi^2)
	Volume	
cubic meter (m^3)	264.2	gallon (gal)
cubic meter (m^3)	0.0002642	million gallons (Mgal)
cubic meter (m^3)	35.31	cubic foot (ft^3)
cubic meter (m^3)	0.0008107	acre-foot (acre-ft)
	Flow rate	
meter per year (m/yr)	3.281	foot per year (ft/yr)
centimeter per year (cm/yr)	0.3937	inch per year (in/yr)
millimeter per year (mm/yr)	0.03937	inch per year (in/yr)
	Density	
gram per cubic centimeter (g/cm^3)	62.4220	pound per cubic foot (lb/ft^3)

Temperature in degrees Celsius (°C) may be converted to degrees Fahrenheit (°F) as follows:
°F=(1.8×°C)+32

Temperature in degrees Fahrenheit (°F) may be converted to degrees Celsius (°C) as follows:
°C=(°F-32)/1.8
Vertical coordinate information is referenced to the North American Vertical Datum of 1988 (NAVD 88)
Horizontal coordinate information is referenced to the North American Datum of 1983 (NAD 83)
Altitude, as used in this report, refers to distance above the vertical datum.
*Transmissivity: The standard unit for transmissivity is cubic foot per day per square foot times foot of aquifer thickness [$(ft^3/d)/ft^2$]ft. In this report, the mathematically reduced form, foot squared per day (ft^2/d), is used for convenience.
Specific conductance is given in microsiemens per centimeter at 25 degrees Celsius (µS/cm at 25°C).
Concentrations of chemical constituents in water are given either in milligrams per liter (mg/L) or micrograms per liter (µg/L).

Land Subsidence Hazards

By D.L. Galloway, G.W. Bawden, S.A. Leake, and D.G. Honegger

Abstract

Land subsidence poses a hazard to pipelines. The information presented in this chapter is intended to aid recognition and assessment of the principal land subsidence hazards to pipelines. Subsidence is a global problem and, in the United States, more than 44,000 km^2 in 45 States have been directly affected by subsidence. The principal causes are subsurface fluid withdrawal, drainage of organic soils, sinkholes, underground mining, hydrocompaction, thawing permafrost, and natural consolidation. Many subsidence areas have been identified, mapped, and documented. Most anthropogenic land subsidence in the United States is caused by the withdrawal of subsurface fluids from porous granular media; humans also have caused widespread and significant subsidence by other processes. Mining of coal and minerals, and drainage of organic soils are the most significant of these as measured by area affected. Various ancillary and anecdotal factors aid identifying unrecognized, actively subsiding regions and other regions prone to subsidence, such as increased incidences of damaged or protruding wells, a history of adjustments to local geodetic controls, increasing incidences of coastal or riverine flooding, local conveyance and drainage problems, and ground failures—surface faulting and earth fissuring. Measuring, mapping and monitoring subsidence are necessary to assess subsidence hazards. Analysis and simulation of subsidence processes, constrained by the available data, often are used to assess present and potential future hazards.

Introduction

Land subsidence is a gradual settling or sudden sinking of the Earth's surface owing to subsurface movement of earth materials. Subsidence is a global problem and, in the United States, more than 44,000 km^2 in 45 States, an area roughly the size of New Hampshire and Vermont combined, have been directly affected by subsidence. The principal causes are subsurface fluid withdrawal, drainage of organic soils, sinkholes, underground mining, hydrocompaction, thawing permafrost, and natural consolidation (National Research Council, 1991). More than 80 percent of the identified subsidence in the Nation is a consequence of our exploitation of underground water, and the increasing development of land and water resources threatens to exacerbate existing land subsidence problems and initiate new ones (Galloway and others, 1999). In many areas of the arid Southwest, and in more humid areas underlain by soluble rocks such as limestone, gypsum, or salt, land subsidence is an often-overlooked consequence of our land- and water-use practices. Some subsidence also is associated with tectonic and volcanic processes; however this type of subsidence is beyond the scope of this report.

Subsidence contributes to permanent inundation of coastal lands as the land settles with respect to sea level, aggravates riverine flooding, alters topographic gradients, and ruptures the land surface in addition to causing other hazards related to deterioration of land and water resources, and to disruption of cultural infrastructure. The National Research Council (1991) estimated that annual costs in the United States from flooding and structural damage caused by land subsidence exceeded $125 million. The assessment of other costs related to land subsidence is complicated by difficulties in identifying and mapping the affected areas, establishing cause-and-effect relations,

assigning economic value to environmental resources, and by inherent conflicts in the legal system regarding the recovery of damages under established land and water rights. Thus, the total cost of subsidence is probably significantly larger than the current best estimate.

Purpose

The information presented in this chapter is intended to aid recognition and assessment of the principal land subsidence hazards to pipelines. Though subsidence generally refers to the downward motion of land surface, lateral ground movements accompany the subsidence. Both kinds of surface displacement affect pipelines to varying degrees. The lateral movements at land surface can be attributed to relatively deep-seated poroelastic deformation, to flexures or bending of the land surface and to ground failures such as those associated with the collapse of surficial material into underground voids (for example, sinkholes) and with differential subsidence and (or) tensional stresses in the subsurface materials (for example, earth fissures).

Regional subsidence features (such as aquifer-system or reservoir compaction accompanying ground-water and (or) oil and gas extraction) generally create relatively small lateral (sub-horizontal) strains[1] at the land surface owing in part to poroelastic deformation of the aquifer system, and in part to the flexure of land surface. Poroelastic deformation refers to the coupled interaction between fluid flow and deformation of the skeletal-matrix of the host rock (Biot, 1941; Verruijt, 1969; Detournay and Cheng, 1993; Wang, 2000). Poroelastic deformation is relevant to subsidence caused by the extraction of subsurface fluids and is discussed further in the *Analysis and Simulation* section of this report. Flexure characterizes the motion of the land surface subjected to the relative vertical displacement of some portion of the surface, such as the small component of lateral movement associated with the rotation or tilt (slope) of the land surface between two sites with differing amounts of subsidence.

Meters of vertical displacement may occur locally regardless of the type of process causing the subsidence. Figures 2.1 and 2.2 illustrate various deformation factors important to pipelines traversing subsidence features. Consider a hypothetical pipeline mechanically coupled to the land surface and originally laid on a flat surface. Figure 2.1 shows the computed axial (approximately horizontal) displacements and strains (0.125 ppm, extension) resolved (a) in the axis of a hypothetical pipeline traversing the center of an idealized linear subsidence feature with a maximum 50-mm vertical displacement in a radial displacement field with linear displacement to 0 mm at a radius of 100 m; and (b) perpendicular to the axis of a hypothetical pipeline traversing a chord $\overline{AB}$ of the circle defined by the same subsidence pattern. In this example, the axial strain results from the flexure of the pipeline owing to differential subsidence. Figure 2.2 illustrates an idealized nonlinear radial subsidence surface and selected deformation profiles computed using $S = -3\times10^{-4}e^{r^2}$ where S is subsidence and r is the radius from the center of the feature. The maximum subsidence is 1 m at the center and approaches zero at a radius of 100 m. Consider the 200-m-long cross section A-A′ (fig. 2.2*A*), and profiles of deformation features derived from the trace of cross section A-A′ through the center of the subsidence feature (fig. 2.2*B*). The slope of the surface is a maximum of about 0.85° at a radius of about 41 m. At this point, curvature is zero and defines the inflection point on the surface. Curvature is approximated as the second derivative of the subsidence surface and reaches a maximum of about 6 x 10^{-4} at the center of the feature. Axial displacement computed at 1-m intervals over the profile reaches a maximum value of about 1.1 x

[1] The strains referred to here are computed as the dimensionless ratio of the relative component displacement measured in an interval, area or volume and the original length, area or volume, respectively. A uniaxial strain of 1 part per million (ppm) is 1 x 10^{-6} strain, and is equivalent to a change in length of 1 mm over a linear length of 1 km.

10^{-4} m extension at the inflection point. The cumulative axial displacement (extension) along the profile from the end, up to the inflection point, is about 3.2 x 10^{-3} m, which represents a lengthening or extensional strain of about 54 ppm. Between the inflection point and the center of subsidence, the profile lengthens an additional about 2.3 x 10^{-3} m. Accounting for the remaining distance from the center of subsidence to the other end of the profile, the profile lengthens about 1.1 x 10^{-2} m over its original 200-m length for a cumulative axial strain of about 54 ppm. The profile lengthens unevenly over its extent because of curvature. The inflection points on the profile define a transition from relative extension to relative compression along the profile.

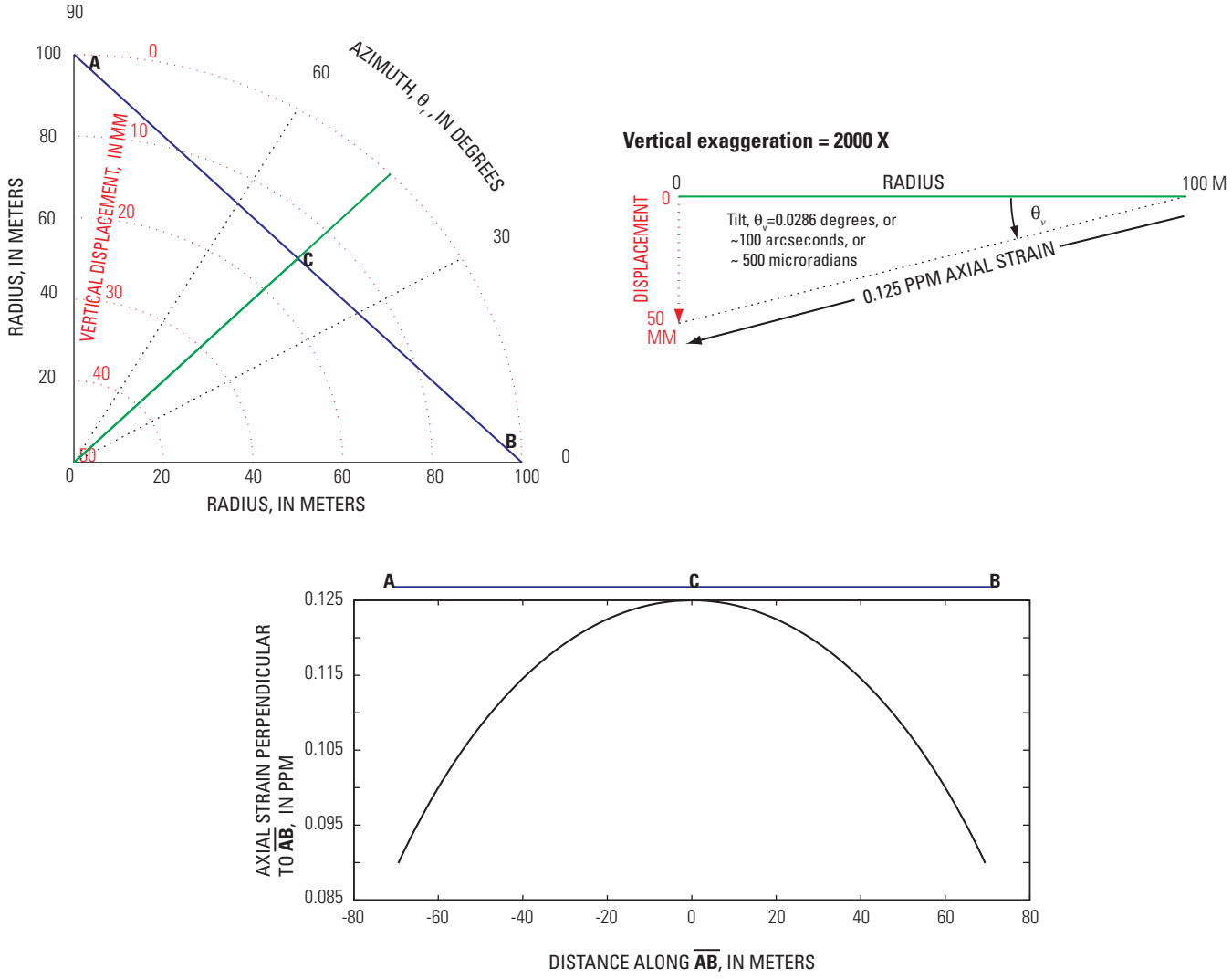

Figure 2.1. Selected deformation factors (vertical displacement, slope [tilt] and axial strain) for hypothetical pipelines traversing an idealized linear subsidence feature.

The strains illustrated in figures 2.1 and 2.2 may not be large enough to cause failure of most pipelines, but could cause problems in gravity-driven flow in a pipeline or other conveyance constructed on the land surface. Pressurized pipelines are less susceptible to flow impedance owing to small changes in the vertical gradient of the pipeline. Large local subsidence features (ground

failures such as sinkholes and earth fissures) can be associated with large near-field lateral strains (>100 ppm) and can cause structural failure of a nearby pipeline.

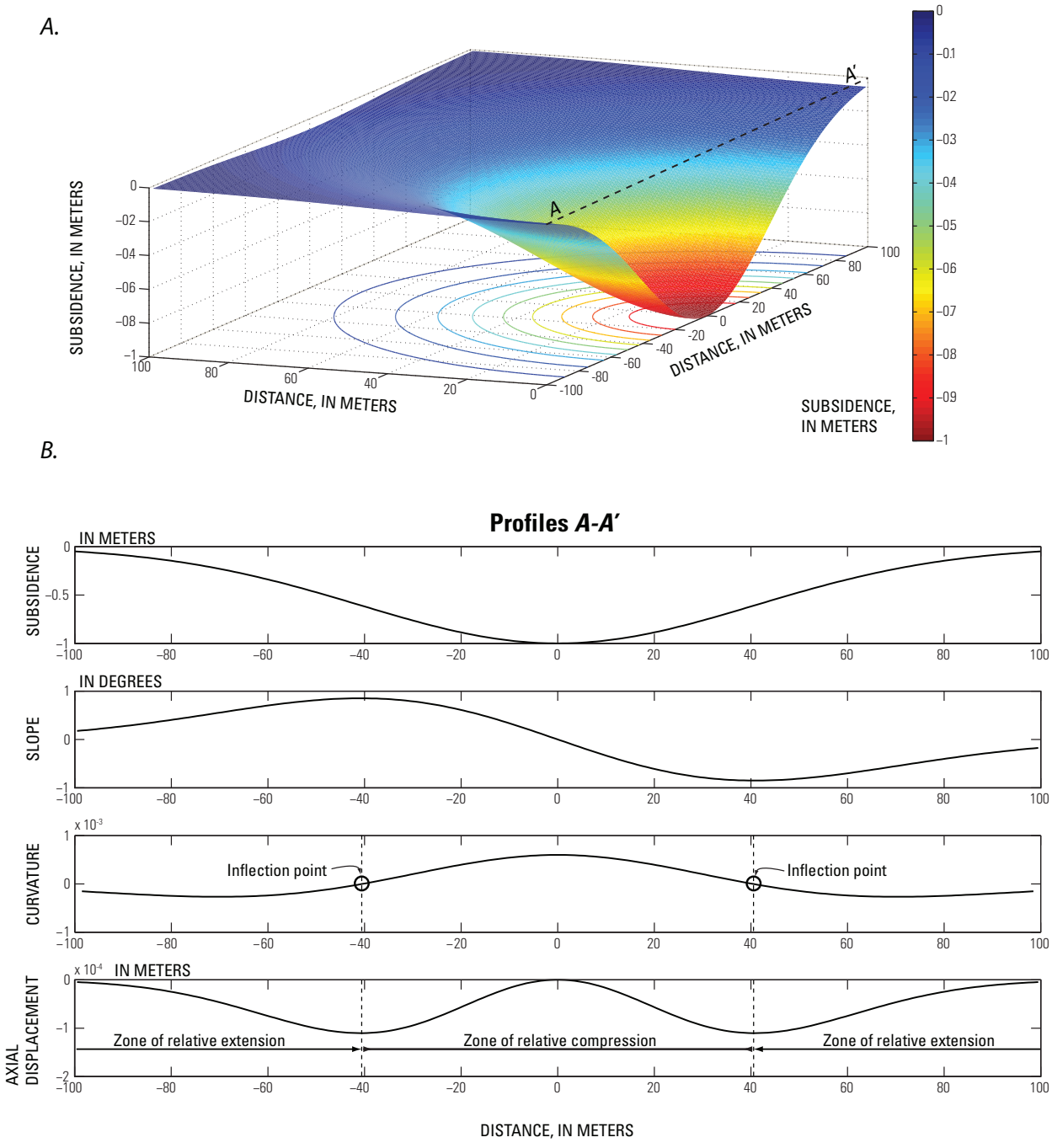

Figure 2.2. Selected deformation features for an idealized nonlinear subsidence feature. *A*. Subsidence surface. *B*. Deformation profiles.

Scope

For practical applications, means to identify locations of future subsidence hazards relies upon identifying (a) areas that have subsided recently, (b) areas that are actively subsiding, (c) areas where activities leading to subsidence will occur, or (d) areas that are very similar in terms of topography, geomorphology, hydrology, and soil properties to areas where evidence of past subsidence and subsidence-related hazards are observed.

This chapter of the report focuses on the means listed above to recognize and assess land subsidence hazards and covers the following types of subsidence hazards:

1. Subsurface fluid withdrawal: Deep-seated deformation of the porous skeletal matrix of the saturated rocks, owing to fluid-pressure declines principally caused by ground-water and hydrocarbon discharge and recharge. Two types of ground motion are discussed:
    a. Aquifer-system compaction—principal hazard associated with ground-water mining in susceptible alluvial, basin-fill deposits;
    b. Ground failures—earth fissures and surface faults associated with areas of differential ground displacements.
2. Drainage of organic soils: Primarily oxidation of peat, muck, bog, fen, moor, and muskeg deposits associated with desiccation after water tables have been lowered to enable agricultural and other land uses.
3. Sinkholes: Typically localized collapse of the overburden into underlying cavities that form in relatively soluble deposits such as salt, gypsum, and carbonate rocks (for example, limestone and dolomite). Two general types of sinkholes are discussed:
    a. Natural—karst terrain;
    b. Anthropogenic—accelerated dissolution and collapse related to water-use, petroleum extraction and mining practices.
4. Underground mining: Often gradual downwarping, sometime sudden collapse over mine footprints; typically associated with coal mines.
5. Hydrocompaction: Shallow subsidence associated with rewetting of dry, low-density sediments.
6. Thawing permafrost: Subsidence associated with the development of thermokarst terrain.
7. Natural consolidation: Gradual reduction in volume and increase in density of a soil mass in response to increased depositional load.

Piping and internal erosion is often associated with wetting or modification of natural or prior drainage conditions within erodible sediments such as loess, fine sands and silts, and plays a role in exposing earth fissures through erosion to fissure gulleys. Piping and internal erosion within erodible sediments is not covered in this document. Earth fissures are covered in this document as indicated in item 1b above.

Acknowledgments

Robert Butler (Golder Associates Ltd.), Thomas Holzer and Keith Prince (both U.S. Geological Survey), and Moness Rizkalla (Visitless Integrity Assessment Ltd.) provided valuable review comments and suggestions that improved this manuscript.

Recognition

The occurrence of land subsidence is most obvious in the case of catastrophic sinkholes such as those in the mantled karst of Winter Park, Florida (fig. 2.3*A*). Where ground-water mining or drainage of organic soils is involved, the subsidence is typically gradual and widespread, and its discovery usually follows increased flooding. Gazing out over the San Joaquin Valley, California, one would be hard-pressed to recognize that more than 9 m of subsidence has occurred in some locations as a result of ground-water pumping in the valley (fig. 2.3*B*). However, the discovery of land subsidence in the southern San Joaquin Valley has been attributed to a visual observation in which a farmer reported that the mail truck traversing his mile-long driveway began to fade from view (Thomas Holzer, USGS, written commun., 2007). In the absence of obvious clues such as protruding wells, failed well casings, broken pipelines, drainage reversals, and reduced freeboard in canals and aqueducts, repeat measurements of land-surface elevation are needed to reveal the subsidence.

A *B*

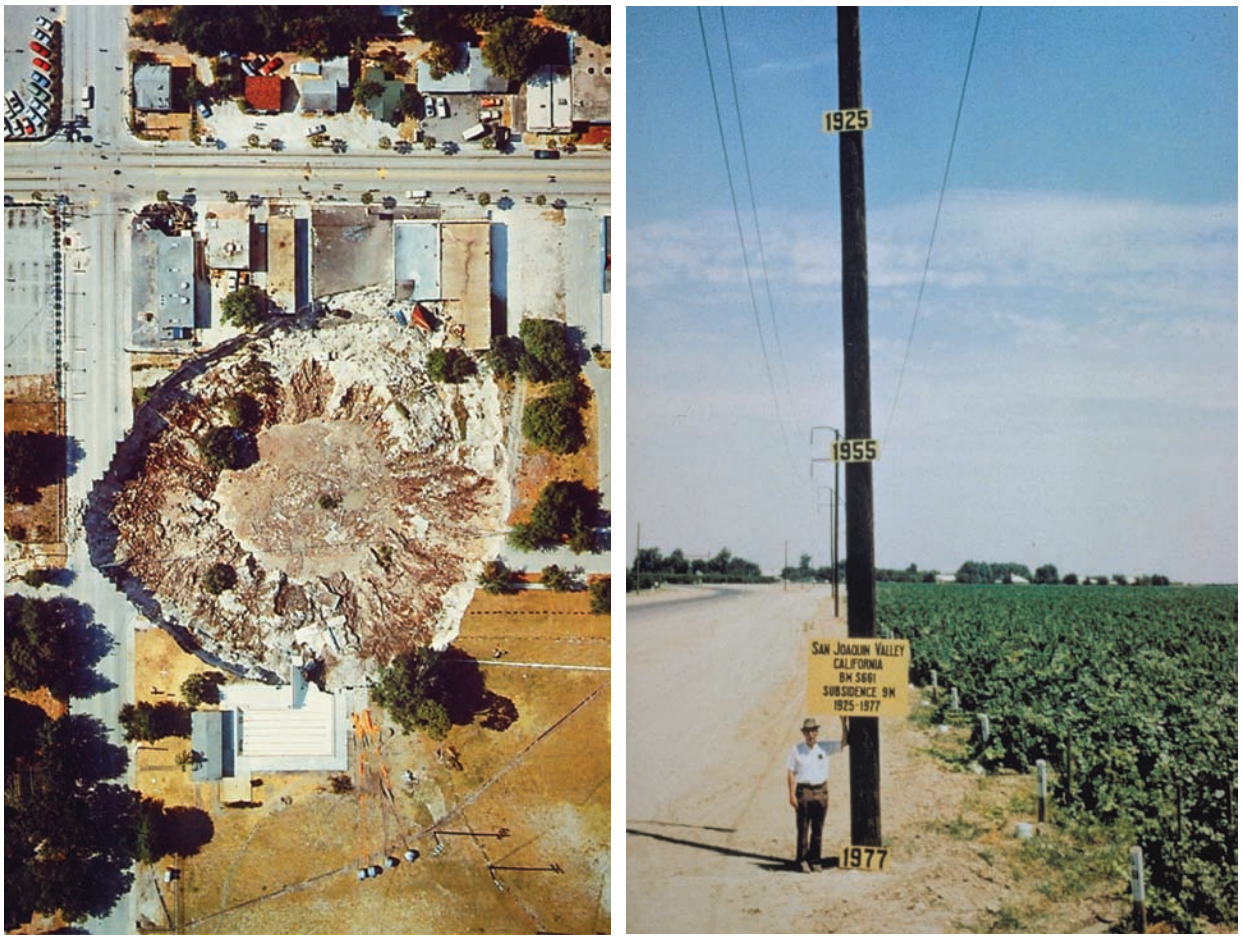

Figure 2.3. *A.* Cover-collapse sinkhole, Winter Park, Florida (1981). *B.* Approximate location of maximum subsidence measured in the San Joaquin Valley, California (1977).

The problem of detection in regional land subsidence is compounded by the large areal scale of the elevation changes and the requirement for vertically stable reference marks—bench marks—located outside the area affected by subsidence. Where stable bench marks exist and repeat surveys are made, subsidence is easily measured using professional surveying instruments and methods.

Known Subsidence Areas

Many subsidence areas have been identified, mapped, and documented. Most anthropogenic land subsidence in the United States is caused by the withdrawal of subsurface fluids from porous granular media; humans also have caused widespread and significant subsidence by other processes. Underground mining of coal and minerals, and drainage of organic soils are the most significant of the other processes as measured by area affected. Collectively, the impacts from these processes rival those from withdrawal of subsurface fluids. The National Research Council (1991) estimates that about 8,000 and 9,400 km^2 of land, respectively, have subsided because of mining and drainage of organic soils. Though mining subsidence is widespread and mostly associated with coal extraction, organic soil subsidence is concentrated in two areas, the Florida Everglades and the San Joaquin–Sacramento River Delta, California (National Research Council, 1991; Galloway and others, 1999).

Subsurface Fluid Withdrawal

Withdrawal of subsurface fluids from clastic sediments has permanently lowered the elevation of about 26,000 km^2 of land in the 48 conterminous United States (fig. 2.4, table 2.1)—an area of similar extent to the State of Massachusetts (Holzer and Galloway, 2005). Permanent subsidence can occur when fluids (primarily water and hydrocarbons) stored beneath the Earth's surface are removed by pumpage or drainage. The reduction of fluid pressure in the pores and cracks of aquifer systems and petroleum reservoirs, especially in unconsolidated clastic rocks, is inevitably accompanied by some deformation of the aquifer system or reservoir. Because the granular structure—the "skeleton"—of the fluid-bearing and -storing rocks is not rigid, but more or less compliant, a shift in the balance of support for the overlying material causes the skeleton to deform slightly. Both the aquifers and aquitards that constitute the aquifer systems, and their equivalents in petroleum reservoirs, undergo deformation, but to different degrees. Almost all the permanent subsidence in aquifer systems is attributable to the compaction[2] of aquitards during the typically slow process of aquitard drainage (Tolman and Poland, 1940). Because most of the subsidence attributed to subsurface fluid withdrawal is caused by ground-water extractions the following discussions will focus on the development of ground-water resources in aquifer systems, though the subsidence process is similar for hydrothermal and hydrocarbon resource development.

In alluvial aquifer systems, especially those that include semiconsolidated, low-permeability silt and clay layers (aquitards) of sufficient aggregate thickness, long-term ground-water-level declines can result in a vast one-time release of "water of compaction" from compacting aquitards, which manifests itself as land subsidence. Accompanying this release of water is a largely nonrecoverable reduction in the pore volume of the compacted aquitards, and thus an overall reduction in the total storage capacity of the aquifer system. This "water of compaction" cannot be reinstated by allowing water levels to recover to their predevelopment status. The extraction of this resource for economic gain constitutes ground-water mining in the truest sense of the term.

[2] In this report, the term "compaction" refers to a decrease in thickness of sediments as a result of increase in vertical compressive stress. The identical physical process is referred to as "consolidation" by soils engineers.

In compacting aquifer systems, the subsidence is generally regional and spread over a large area so that regional-scale lateral (sub-horizontal) strains are rarely as large as 2 ppm and resulting regional-scale tilts are < 240 arcseconds. Locally, however, lateral strains may be large, such as near pumping wells where hydraulic gradients are large, where the aquifer system thins abruptly above inflections in the basement topography of the aquifer system, and near the boundaries of hydrogeologic units with contrasting hydraulic and (or) mechanical properties.

The extraction of oil, gas, and associated water from petroleum reservoirs also causes subsidence. Land subsidence caused by hydrocarbon production has been documented in many basins of the world (Poland and Davis, 1969; Yerkes and Castle, 1969; Martin and Serdengecti, 1984; Van Hasselt, 1992; Chilingarian and others, 1995; Nagel, 2001). Subsidence of the Goose Creek oil field on Galveston Bay near Houston, Texas was the first subsidence attributed to subsurface-fluid withdrawal to be described in the literature (Pratt and Johnson, 1926). The subsided volume amounted to about 20 percent of the produced volume of oil, gas, water, and sand. Subsidence at the Wilmington (California, USA) and Ekofisk (North Sea, Norwegian sector) oil fields are well known examples due both to the magnitude of subsidence as well as the cost of remediation.

Parts of the city and port of Long Beach, California, suffered major problems owing to rapid (as much as 0.75 m/yr) land subsidence during 1937–62 related to extraction of oil, gas, and associated water from the underlying Wilmington oil field (Harris and Harlow, 1947; Gilluly and Grant, 1949; Mayuga and Allen, 1969; Poland and Davis, 1969). Problems principally were caused by flooding, but also were caused by structural damages to infrastructure, including pipelines, attributed to horizontal strains on the sides of the subsidence bowl. Total subsidence in Long Beach reached as much as 9 m before the land surface was stabilized by an integrated program of fluid injection to balance the extraction. The amount of subsidence at Long Beach was nearly proportional to (about 39 percent) the amount of oil and associated water extracted (Poland and Davis, 1969).

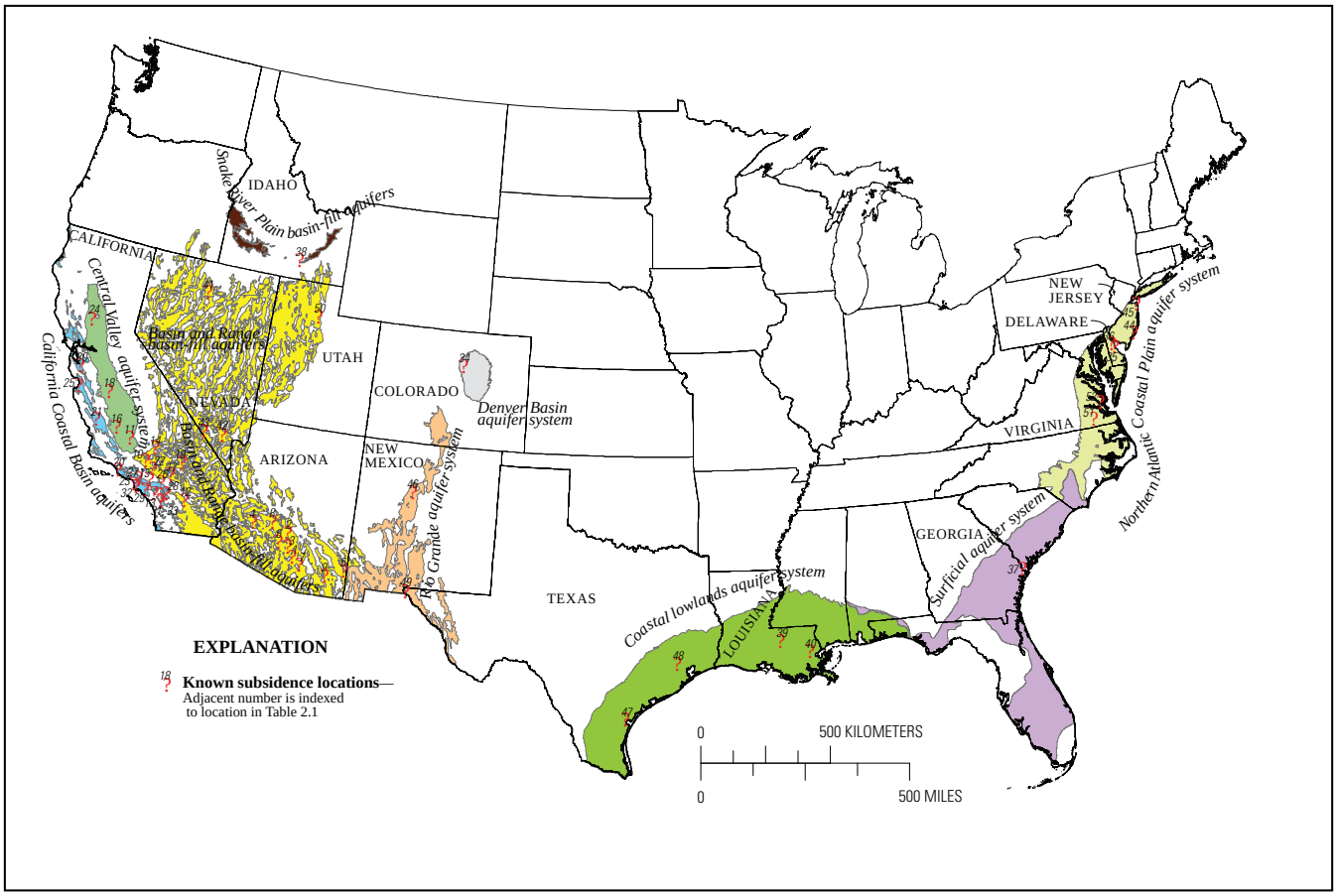

Figure 2.4. Selected, known areas of permanent land subsidence owing principally or secondarily to ground-water or oil and gas extractions (see table 2.1) in the 48 conterminous United States and associated aquifer systems (modified from Galloway and others, 1999).

Table 2.1 Locations of selected known subsidence in the USA attributed to ground-water and oil-and-gas extractions.

[Map ID—Map identification number on figure 2.4; Latitude-Longitude—approximate in decimal degrees, reference datum is NAD83; Fluid—W is ground water, O&G is oil and gas; Aquifer Name (U.S. Geological Survey, 2003)—na is not applicable]

Map ID	State	Location Name	Latitude	Longitude	Fluid	Aquifer Name
1	Arizona	Avra Valley	32.4372	-111.3158	W	Basin and Range basin-fill aquifers
2	Arizona	East Salt River Basin	33.2525	-111.6461	W	Basin and Range basin-fill aquifers
3	Arizona	Eloy, Picacho Basin	32.7525	-111.5556	W	Basin and Range basin-fill aquifers
4	Arizona	Harquahala Plain	33.4147	-113.1558	W	Basin and Range basin-fill aquifers
5	Arizona	San Simon Basin	32.2344	-109.1475	W	Basin and Range basin-fill aquifers
6	Arizona	Stanfield Basin	32.8786	-111.9636	W	Basin and Range basin-fill aquifers
7	Arizona	Tucson Basin	32.2217	-110.9697	W	Basin and Range basin-fill aquifers
8	Arizona	West Salt River Basin	33.5422	-112.3733	W	Basin and Range basin-fill aquifers
9	Arizona	Wilcox Basin	31.9814	-109.8814	W	Basin and Range basin-fill aquifers
10	California	Antelope Valley	34.7344	-118.1333	W	Basin and Range basin-fill aquifers
11	California	Bakersfield (San Joaquin Valley)	35.3669	-119.0189	W, O&G	Central Valley aquifer system
12	California	Coachella Valley	33.6858	-116.1833	W	Basin and Range basin-fill aquifers
13	California	Elsinore Valley	33.6919	-117.4646	W	Other rocks
14	California	Fremont Valley	35.2172	-117.8494	W	Basin and Range basin-fill aquifers
15	California	La Verne	34.1133	-117.765	W	California Coastal Basin aquifers
16	California	Lost Hills (San Joaquin Valley)	35.6161	-119.6603	O&G	na
17	California	Lucerne Valley	34.4444	-116.95	W	Basin and Range basin-fill aquifers
18	California	Mendota (San Joaquin Valley)	36.7539	-120.3783	W	Central Valley aquifer system
19	California	Mojave River Basin	34.9381	-116.6114	W	Basin and Range basin-fill aquifers
20	California	Oxnard Plain	34.1919	-119.1769	W	California Coastal Basin aquifers
21	California	Paso Robles	35.6978	-120.6217	W	California Coastal Basin aquifers
22	California	Pomona	34.5186	-117.75	W	Basin and Range basin-fill aquifers
23	California	Redondo Beach	33.8444	-118.3881	W	California Coastal Basin aquifers
24	California	Sacramento Valley	39.0233	-121.9581	W	Central Valley aquifer system
25	California	Salinas Valley	36.6933	-121.7156	W	California Coastal Basin aquifers
26	California	San Bernardino	34.1053	-117.2942	W	Basin and Range basin-fill aquifers
27	California	San Gabriel Valley	34.0522	-118.2433	W	California Coastal Basin aquifers
28	California	San Jacinto Basin	33.7839	-116.9572	W	California Coastal Basin aquifers
29	California	Santa Ana Basin	33.7481	-117.8744	W	California Coastal Basin aquifers
30	California	Santa Clara Valley	37.3531	-121.9047	W	California Coastal Basin aquifers
31	California	Temecula	33.4906	-117.1494	W	California Coastal Basin aquifers
32	California	Wilmington	33.7892	-118.2632	O&G	na
33	California	Wolf Valley	33.4647	-117.1025	W	California Coastal Basin aquifers
34	Colorado	Denver Area	39.74	-104.9922	W	Denver Basin aquifer system
35	Delaware	Bowers Area	39.0594	-75.4022	W	Northern Atlantic Coastal Plain aquifer system
36	Delaware	Dover Area	39.1561	-75.5264	W	Northern Atlantic Coastal Plain aquifer system
37	Georgia	Savannah Area	32.0808	-81.0908	W	Surficial aquifer system
38	Idaho	Raft River Area	42.5989	-113.2292	W	Snake River Plain basin-fill aquifers
39	Louisiana	Baton Rouge	30.4436	-91.1869	W	Central lowlands aquifer system
40	Louisiana	New Orleans	30.0346	-90.0249	W, O&G	Central lowlands aquifer system
41	Nevada	Humboldt Valley	40.8589	-117.1175	W	Basin and Range basin-fill aquifers
42	Nevada	Las Vegas Valley	36.1719	-115.1397	W	Basin and Range basin-fill aquifers
43	Nevada	Pahrump Valley	36.1583	-115.9633	W	Basin and Range basin-fill aquifers
44	New Jersey	Atlantic City-Oceanside	39.3808	-74.4514	W	Northern Atlantic Coastal Plain aquifer system
45	New Jersey	Baranagat Bay-New York Coastal Area	40.3108	-74.035	W	Northern Atlantic Coastal Plain aquifer system
46	New Mexico	Rio Rancho, Albuquerque Basin	35.2417	-106.66	W	Rio Grande aquifer system
47	Texas	Corpus Christi	27.7964	-97.4036	O&G	na
48	Texas	Houston-Galveston Area	29.7606	-95.37	W, O&G	Central lowlands aquifer system
49	Texas	Hueco-Bolson, El Paso	31.7664	-106.4961	W	Rio Grande aquifer system
50	Utah	Salt Lake City	40.7596	-111.8883	W	Basin and Range basin-fill aquifers
51	Virginia	Franklin-Suffolk	36.7367	-76.9769	W	Northern Atlantic Coastal Plain aquifer system
52	Virginia	Williamsburg-West Point Area	37.2753	-76.5392	W	Northern Atlantic Coastal Plain aquifer system

Subsidence is a challenge for a number of other petroleum and natural gas reservoirs. In Venezuela, subsidence due to reservoir depletion has led to severe flooding along the coast of Lake Maracaibo. In the Netherlands, subsidence at the large Groningen gas field, though only on the order of tens of centimeters, poses significant challenges because large portions of the Netherlands are below sea level and protected by dikes. The Lost Hills and Belridge oil fields in the San Joaquin Valley, California subsided about 400 mm/yr during 1995–96 attributed to compaction of the

petroleum reservoirs (Fielding and others, 1998). Some of the subsidence contributing to relative sea-level rise and loss of wetlands along the Texas and Louisiana Gulf Coast has been attributed to hydrocarbon production (Morton and others, 2006).

Drainage of Organic Soils

In the U.S. system of soil taxonomy, organic soils or histosols are 1 of 10 soil orders. They are formally defined as having more than 50 percent organic matter in the upper 12 cm, but may be of lesser thickness if they overlie fragmental rock permeated by organic remains. Organic soil is commonly termed "peat," if fibrous plant remains are still visible, or "muck" where plant remains are more fully decomposed. Other common names for areas with accumulations of organic soil include "bog," "fen," "moor," and "muskeg." Organic soils form in wetlands where plant litter (roots, stems, leaves) accumulates faster than it can fully decompose. Fibrous peats typically include the remains of sedges and reeds that grew in shallow water. "Woody" peats form in swamp forests. In northerly latitudes with cool, moist climates, many peats comprise chiefly sphagnum moss and associated species. The total area of organic soils in the United States is about 210,000 km^2, about half of which is "moss peat" located in Alaska (Lucas, 1982; fig. 2.5). About 70 percent of the organic-soil area in the contiguous 48 States occurs in northern, formerly glaciated areas, where moss peats also are common (Stephens and others, 1984). In Canada, the term "muskeg" (MacFarlane, 1969) is typically used to describe highly organic soils, which are often subdivided into fibrous peat, amorphous peat, silty peat, and organic silt to differentiate the sequence of decreasing organic and intact fiber content, natural water content, and compressibility of these materials. Similar descriptive terms and ranges of properties of the various organic or peat soils are presented in U.S. Department of the Navy (1982, p. 7.1-20–21, table 5).

Figure 2.5. Locations of organic-soil areas in the U.S. (from Galloway and others, 1999).

Land subsidence invariably occurs when organic soils are drained for agriculture or other purposes. Causes include compaction, desiccation, erosion by wind and water, and, in some cases, prescribed or accidental burning. The effects of compaction and desiccation after initial draining

can be dramatic, because organic soils have very low density caused by their water content (as much as 80–90 percent).

The most prevalent mechanism of organic-soil subsidence, however, is oxidation. The balance between accumulation and decomposition of organic material shifts dramatically where peat wetlands are drained. Under undrained conditions, anaerobic microbial decomposition of plant litter cannot keep pace with the rate of accumulation. Lignin, an important cell-wall component of all vascular plants, is much more vulnerable to decomposition under aerobic conditions. Oxidation under aerobic conditions converts the organic carbon in the plant tissue to carbon dioxide gas and water.

The biochemical origin of much organic-soil subsidence was established through laboratory experiments with Florida peat in the early 20th century (Waksman and Stevens, 1929; Waksman and Purvis, 1932) that balanced the loss of dry soil weight with rates of carbon dioxide production (CO_2). This early laboratory work also suggested optimal temperature ranges and moisture contents for microbial decomposition. Later field studies and observations have confirmed oxidation as the dominant subsidence process in many instances. For example, in the Florida Everglades, sod fields, and residential areas—where causal mechanisms such as erosion, burning, and compaction are minimized or absent—have sunk as rapidly as the cultivated land (Stephens and others, 1984). It is believed that oxidation-related soil loss can be halted only by complete resaturation of the soil or complete consumption of its organic carbon content (Wosten and others, 1997).

Whereas natural rates of accumulation of organic soil are on the order of 10 cm per 100 years, the rate of loss of drained organic soil can be 100 times greater, as much as 10 cm/yr in extreme cases. Thus, deposits that have accumulated over many millennia can disappear over time scales that are very relevant to human activity.

Human experience with subsiding organic soils dates back nearly 1,000 years in The Netherlands and several hundred years in the English fen country. The old polders in the western Netherlands were reclaimed for agriculture between the 9th and 14th centuries, and by the 16th century the land had subsided to such an extent that windmills were needed to discharge water artificially to the sea (Schothorst, 1977). Because ground-water levels beneath the polders were still relatively high, the rate of subsidence was relatively low—about 1.52 mm/yr, over a roughly 1,000-year period in which progressively more sophisticated drainage systems were developed (Nieuwenhuis and Schokking, 1997). Greatly improved drainage in the 20th century increased the thickness of the drained zone above the water table. As a result, subsidence rates rose to about 5 mm/yr between the late 1920s and late 1960s, and current rates are more than 7.5 mm/yr.

The organic-soil subsidence rates in the Netherlands are still unusually low in a global context. This is due in part to the relatively cool climate, where temperatures are generally below the optimal range for microbial decomposition, and in part to a thin layer of marine clay that caps much of the peat. Larger average rates have been observed elsewhere: up to 100 mm/yr over the last 100 years in the Sacramento-San Joaquin Delta, California (slowing over time to as much as 10–30 mm/yr in the early 1990s [Rojstaczer and Deverel, 1993; Deverel and Rojstaczer, 1996]); about 20–30 mm/yr over the past 100 years in the English fens and the past 70 years in the Florida Everglades (about 14 mm/yr during the 1980s and 90s near Belle Glade, Florida [Shih and others, 1998]).

In the English fens and the Everglades, long-term subsidence rates have been monitored using stone or concrete columns driven into the underlying solid substrate (fig. 2.6). The history of both areas has been marked by alternate cycles of improved drainage followed by accelerated subsidence and, consequently, inadequate drainage (Stephens and others, 1984), so that the achievements of one generation become the problems of the next (Darby, 1956).

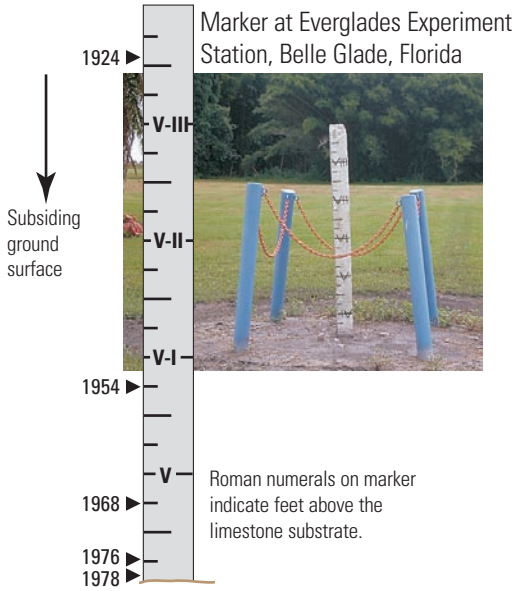

Figure 2.6. Subsidence in the Florida Everglades measured on a concrete marker shown in 1998 photograph (from Galloway and others, 1999).

Sinkholes

A sinkhole is a closed depression in a karst or pseudokarst area, commonly with a circular or ellipsoidal pattern. Its size generally is measured in meters or tens of meters, rarely in hundreds of meters; and it is commonly funnel-shaped and associated with subsurface drainage (fig. 2.7). Sudden and unexpected collapse of the land surface into subsurface cavities is arguably the most hazardous type of subsidence. The typically localized collapse features form naturally in relatively soluble evaporite (salt and gypsum) deposits and carbonate (limestone and dolomite) rocks. Human activities often facilitate the formation of sinkholes in these susceptible materials and trigger their collapse, as well as the collapse of preexisting subsurface cavities. Such catastrophic subsidence is commonly triggered by ground-water-level declines caused by pumping and (or) by purposeful or inadvertent diversion of surface runoff enhancing ground-water flow through susceptible rocks.

Salt and gypsum are, respectively, almost 7,500 and 150 times more soluble in water than limestone, underlie about 35–40 percent of the contiguous United States (fig. 2.8). Bedded or domal salt deposits underlie 25 States and constitute about one-half of the area underlain by salt and gypsum. Natural solution-related subsidence has occurred in each of the major salt basins (Ege, 1984; Johnson, 2005). Although evaporites underlie most of the Michigan-Appalachian and Gulf Coast basins, naturally forming collapse features are much less common in these areas. Human-induced collapse cavities are relatively uncommon in gypsum deposits, and more likely to develop above salt deposits, where they primarily are associated with purposeful and accidental dissolution through mining, or drilling into, salt deposits.

Figure 2.7. Sinkholes: *A*. The Meade sink overlying gypsum and salt beds in western Kansas (Photo from Kansas Geological Survey); *B*. Drilling induced sinkhole in carbonates near Tampa, Florida (Photo by Tom Scott). *C*. Cover-collapse sinkhole in mantled carbonate karst near Ocala, Florida (Photo by Tom Scott).

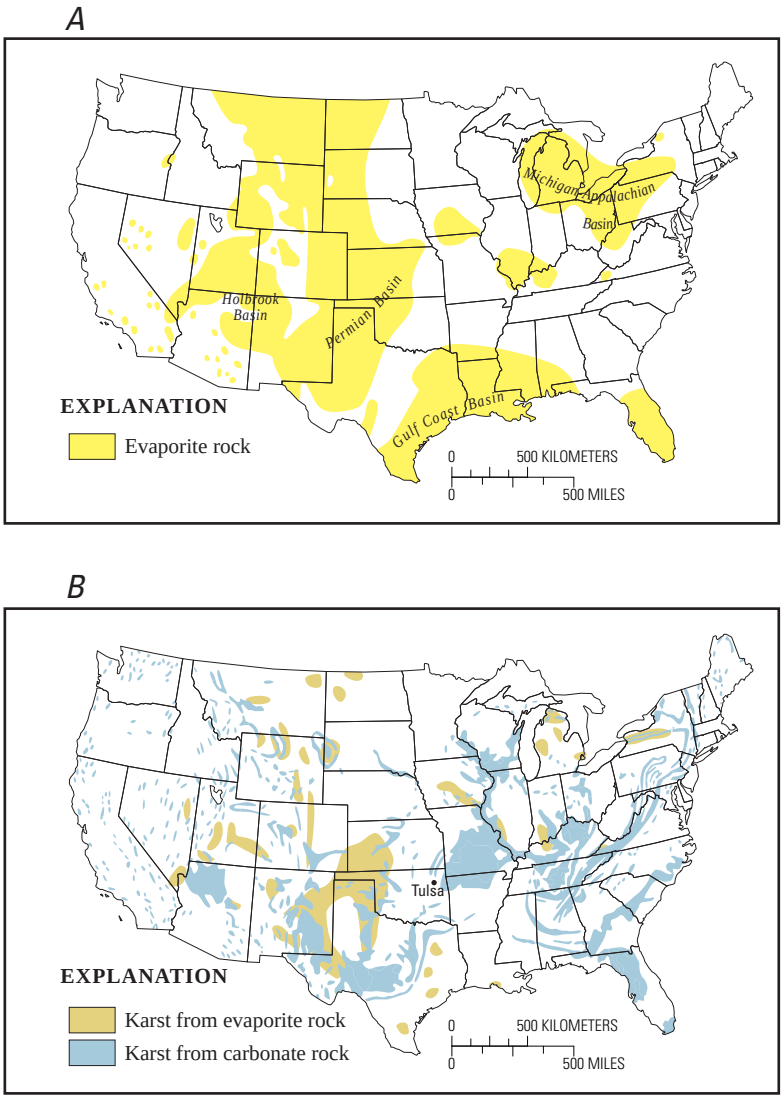

Figure 2.8. General locations of *A*. salt and gypsum (evaporite) deposits (from Martinez and others, 1998), and *B*. karst from evaporite and carbonate rocks (from Davies and LeGrand, 1972) in the 48 conterminous United States.

The high solubilities of salt and gypsum permit cavities to form in days to years, whereas cavity formation in carbonate rocks is a relatively slow process that generally occurs over centuries to millennia. The slow dissolution of carbonate rocks favors the stability and persistence of the distinctively weathered landforms known as karst. Both dissolution and erosional processes play roles in the maturation of karst in carbonates; if not for a balance between mechanical erosion and dissolution, the distinctive landscapes could not persist. The potential for dissolution is controlled by the amount of water available and also by the level of saturation of that water with respect to calcium carbonate. Where the potential for dissolution is low, mechanical erosion dominates the morphology of carbonates. For example, in the arid Southwest, carbonate exposures tend to erode as cliffs rather than form karst.

Carbonate karst landscapes constitute about 40 percent of the contiguous United States east of the longitude of Tulsa, Oklahoma (White and others, 1995; fig. 2.8*B*). In these more humid

landscapes, surface and subsurface drainage pathways converge in discrete conduits formed in the carbonate bedrock. Sinkholes, swallows (where streams disappear into the subsurface), and springs are linked to form an interconnected surface and subsurface drainage network. Thus, karst aquifer systems are directly affected by variability in timing and magnitude of surface runoff.

Underground Mining

In terms of land area affected, underground mining accounts for about 20 percent of the total land subsidence in the United States, and most of this fraction is associated with underground mining for coal (National Research Council, 1991). Subsidence attributed to underground coal mining, generally classified as pit subsidence or sag/trough subsidence, had affected about one quarter of the area undermined or 2 million acres in the United States by the 1970s with the eventual area undermined projected to increase 5-fold in the future (HRB Singer, Inc., 1977; Johnson and Miller, 1979). Most of the mining and subsidence has taken place in the eastern half (east of 100°W longitude) of the United States, mostly in Pennsylvania, Illinois and West Virginia (Gray and Bruhn, 1984). In the western half of the United States in the 1980s, underground coal mines occupied about 0.28 percent of the 15-percent portion of western land area underlain by coal deposits, and subsidence has occurred locally above many of these mined areas (Dunrud, 1984). The subsidence is time-dependent with vertical (generally largest) and horizontal components of movement, depending on the type and extent of mining. Early underground mining was less efficient than more recent underground mining. Subsidence over early mines can occur tens to hundreds of years after mining has ceased, whereas subsidence over more recent mines where virtually total extraction is practiced tends to occur contemporaneously with mining. Subsidence over underground coal workings develops as a gradual downwarping of the overburden into mine voids and is generally unrelated to subsurface water conditions. Mine voids and other subsurface voids can be discovered or located using gravimetric or ground-penetrating radar surveys.

Abandoned tunnels and underground mining for metallic ores, limestone, gypsum, and salt contribute a small percentage of the subsidence attributed to underground mining. These mined areas are subject to downwarping of the overburden, but limestone, salt and gypsum whether undermined or not are susceptible to extensive dissolution by water, frequently leading to sinkholes and in some cases catastrophic collapses (Galloway and others, 1999, p. 107-140).

Hydrocompaction

Preceding construction of the California Aqueduct in the San Joaquin Valley, California, combined field and laboratory studies of the mechanisms and requisite conditions for hydrocompaction, also known as hydroconsolidation and “near-surface subsidence,” were done (Bull, 1964; California Department of Water Resources, 1964). By means of laboratory tests on soil cores from depths to 30 or more meters, and by continuously flooded test plots equipped with subsurface benchmarks at various depths and, in some cases, with soil-moisture probes, these studies demonstrated that hydrocompaction occurred in the alluvial-fan sediments above the highest prehistoric water table and in areas where sparse rainfall and ephemeral runoff had never penetrated below the zone subject to summer desiccation by evaporation and transpiration. Under these circumstances the initial high porosity of the sediments (often enhanced by numerous bubble cavities and desiccation cracks) is sun-baked into the deposits and preserved by their high dry strength, even as they are subjected to the increasing load of 30 or more meters of accumulating overburden. In the San Joaquin Valley, such conditions are associated with areas of very low average rainfall and infrequent, flashy, sediment-laden runoff from small, relatively steep upland watersheds that are underlain by easily eroded shales and mudstones. The resulting muddy debris

flows and poorly sorted stream sediments typically contain montmorillonite clay in proportions that cause it to act, when dry, as a strong interparticulate bonding agent. Eolian soils or loess deposits within arid or semiarid terrain also frequently have low in-place densities as a result of cementation and (or) negative pore-suction particle bonding. Similarly, there are numerous cases in which fine-grained soils have been placed under dry conditions and without effective watering during compaction, producing settlement or collapse of susceptible fills of as much as 30 m thickness.

These natural soils or fills are often described as being metastable. When water is first applied in quantities sufficient to penetrate below the root zone the clay bonds are drastically weakened by wetting, and the weight of the overburden crushes out the excess porosity. The process of densifying to achieve the strength required to support the existing overburden may reduce the bulk volume by as much as 10 percent, the amounts increasing with increasing depth and overburden load.

Localized compaction beneath a water-filled pond or ditch often leads to vertical shear failure at depth between the water-weakened sediments and the surrounding dry material. At the surface this process surrounds the subsiding flooded area with an expanding series of concentric tensional fissures having considerable vertical offset—a severely destructive event when it occurs beneath an engineered structure.

Most of the potential hydrocompaction latent in anomalously dry, low-density sediments is realized as rapidly as the sediments are thoroughly wetted. The process goes rapidly to completion with the initial thorough wetting, and is not subject to reactivation through subsequent cycles of decreasing and increasing moisture content. However, an increase in the surface load such as a bridge footing or a canal full of water can cause additional compaction in prewetted sediments. Thus the progression of a hydrocompaction event is controlled largely by the rate at which the wetting front of percolating water can move downward through the sediments. A site underlain by a thick sequence of poorly permeable sediments may continue to subside for months or years as the slowly descending wetting front weakens progressively deeper deposits. If the surface-water source is seasonal or intermittent, the progression is further delayed.

Studies undertaken in the mid-1950s led to a better understanding of hydrocompaction and to the identification of long reaches of the California Aqueduct route through the San Joaquin Valley, California that were underlain by deposits susceptible to hydrocompaction. Construction of the aqueduct through these reaches was preceded by prewetting the full thickness of susceptible deposits beneath the aqueduct alignment, and thus compacting deposits to a nearly stable state. These measures added more than two years and millions of dollars to the cost of the project.

Thawing Permafrost

Thawing of permafrost is one of the key issues identified as potential consequences of climate variability and change for Alaska (Parson and others, 2001). Permafrost underlies about 85 percent of Alaska and varies widely in depth, continuity, and ice content (fig. 2.9). About 50 percent of Canada's land surface lies in the permafrost region, either in the continuous zone where permafrost extends to great depths or in the discontinuous zone where the permafrost is thinner and there are areas of unfrozen ground (Canadian Geotechnical Society, 2006). Thawing permafrost creates thermokarst terrain—uneven surface topography that includes pits, troughs, mounds, and depressions, which can fill with water.

Particular care often is required in the design and construction of pipelines or other infrastructure to prevent changes to the natural site cover and drainage conditions that increase the rate of thermal degradation and (or) the depth and extent of the active zone. Stripping of highly organic muskeg or tundra surficial soils, which provide a natural insulation layer, and placement of granular roadbed or trench backfill materials to facilitate access and construction can result in a

significant increase in the seasonal active zone, and resulting subsidence or instability. Thawing will speed organic-decomposition reactions, increase ground-water mobility, increase susceptibility to erosion and landslides, and can lead to further subsidence owing to the oxidation of drained, exposed organic material.

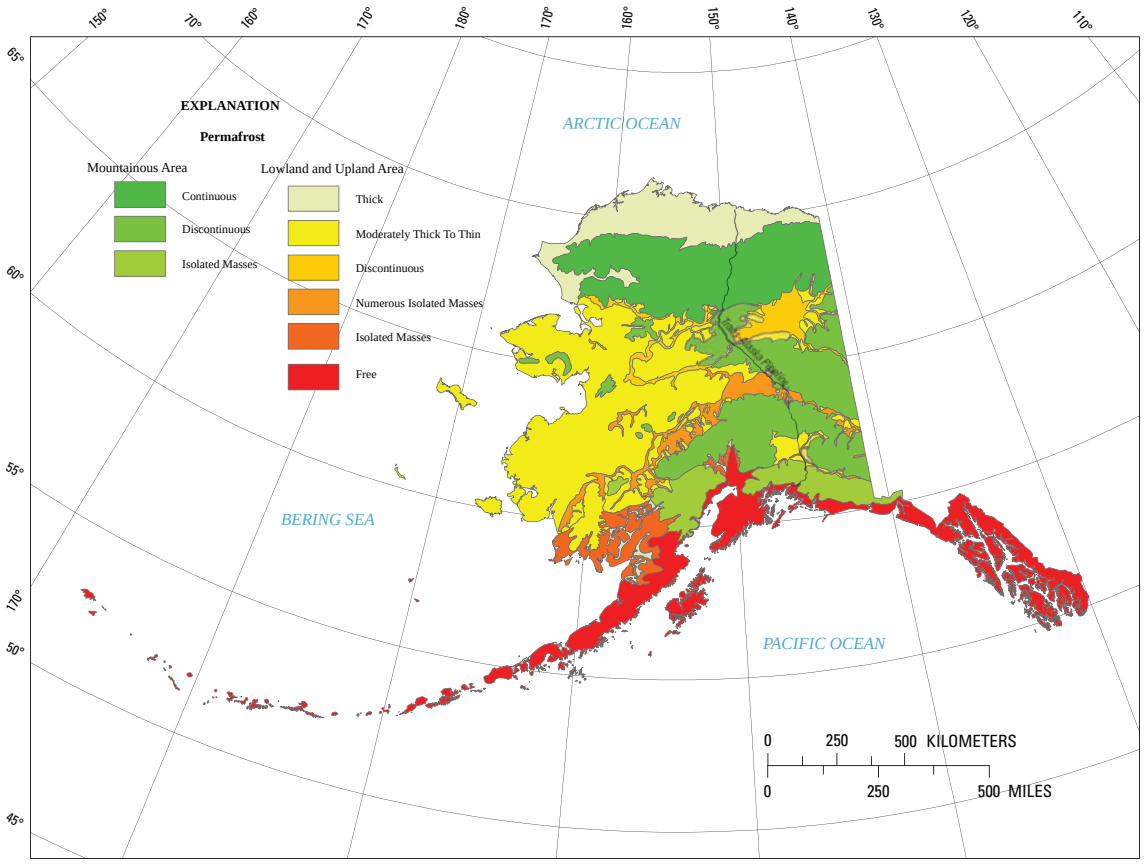

Figure 2.9. Map showing distribution of permafrost in Alaska (modified from U.S. Geological Survey, 1996).

Continuous permafrost on the North Slope of Alaska has warmed 2–4 °C since the late 1800s and more rapidly over the past couple of decades (Osterkamp and Romanovsky, 1996; Hinzman and others, 2005). Because temperatures at the upper surface of continuous permafrost are still low, no significant loss of continuous permafrost is projected over the 21st century. The discontinuous permafrost to the south is warmer, and increased warming suggests that much of the discontinuous permafrost south of the Yukon River and on the south side of the Seward Peninsula could be thawing.

Building on permafrost requires that structures be stabilized in permanently frozen ground below the active layer, and that they limit their heat transfer to the ground, usually by elevating them on piles. For example, to prevent thawing of permafrost from transport of heated oil in the

Trans-Alaska Pipeline, about 640 km of pipeline were elevated on thermosyphon piles (fig. 2.10), at an additional cost of $800 million. The pipeline was completed at a cost of $8 billion in 1977, about eight times the estimated cost of installing the conventional in-ground pipeline.

Figure 2.10. Trans-Alaska Pipeline near Glennallen, Alaska (July 2007) showing thermal syphons on vertical support members and adjustable “shoes” to accommodate horizontal and vertical movements. (Photos by Devin Galloway, USGS).

The near-term risk of disruption to operations of the Trans-Alaska pipeline owing to thawing permafrost is judged to be small. Breaks in the pipeline and other repair costs caused by melting permafrost could become significant in the future. The pipeline's support structures are designed for specific ranges of ground temperatures, and heaving or collapse if the permafrost thaws. Replacing them, if required, would cost about $1.25 million/km.

Where permafrost has high ice content, typically in about half the area of discontinuous permafrost, thawing can lead to the development of thermokarst terrain with subsidence, observed in some cases to exceed 4.8 m. Thawing of ice-rich discontinuous permafrost has damaged houses, roads, airports, pipelines, military installations, and railroad tracks (fig. 2.11); required costly road replacements and increased maintenance expenditures for pipelines and other infrastructure; and increased landscape erosion, slope instabilities, and landslides. Present costs of thaw-related damage to structures and infrastructure in Alaska have been estimated at about $35 million per

year, of which repair of permafrost-damaged roads is the largest component. Longer seasonal thaw of the active layer could disrupt petroleum exploration and extraction and increase associated environmental damage in the tundra, by shortening the season for minimal-impact operations on ice roads and drilling pads.

Figure 2.11. Abandoned railroad tracks warped by thermokarst near Valdez, Alaska. During construction of the roadbed the thermal equilibrium of the permafrost was disrupted causing differential thawing.

Natural Consolidation

Rates of natural consolidation generally are low and not likely to pose hazards to pipelines during their operational lifetime. The process of natural consolidation is included here in part for completeness, but also in part owing to the problem of differentiating the various regional and local processes that contribute to the total subsidence in an area. Soils engineers and geologists define consolidation in different terms. Geologic consolidation is the process whereby loosely aggregated, soft or liquid earth materials become firm and coherent rock—for example, the lithification of loose sediment to form sedimentary rock. This process largely is driven by diagenesis accompanying the aggradation of sediment over geologic time that successively buries older sediment under increasing loads of more recent deposits. Diagenesis refers to the chemical, physical, and biological changes undergone by sediment after its initial deposition and during and after lithification, exclusive of weathering and metamorphism (Neuendorf and others, 2005). Soils engineers refer to consolidation as the gradual reduction in volume and increase in density of a soil mass in response to increased load or effective compressive stress; for example, the squeezing of fluids from pore spaces. This report refers to “natural consolidation” in accordance with the soils engineer’s definition of consolidation. In areas of rapid sedimentary deposition, such as the deltas of large river systems or in topographic basins adjacent to zones of rapid tectonic uplift, long-term average deposition rates may be as large as 1 mm/yr (Ingebritsen and others, 2006, p. 357). Fluid pressures

greater than hydrostatic (geopressures or overpressures) are associated with areas of active deposition, and occur when fluid cannot drain rapidly enough to keep pace with increasing overburden loads caused by deposition—a condition known as compaction disequilibrium. Sediments that drain freely during deposition maintain fluid pressures near hydrostatic. In the Gulf of Mexico basin, overpressures largely have been attributed to compaction disequilibrium (Bredehoeft and Hanshaw, 1968; Sharp and Domenico, 1976; Harrison and Summa, 1991; Hart and others, 1995), and compressional strain is almost certainly the dominant process contributing to overpressures in most active basins (Ingebritsen and others, 2006).

Subsidence rates of geologically young deposits are expected to be high initially and decline exponentially or logarithmically with burial (Magara, 1978) as pore water is expelled as the sediments compact under increasing loads. As expected, regional subsidence rates attributed to natural consolidation are higher in the Louisiana coastal plain where Holocene sediments derived from the Mississippi flood plain and delta are relatively thick as compared to the Texas coastal plain where the Holocene sediments are relatively thin. However, anthropogenic factors in the developed coastal plains also contribute to subsidence and complicate the determination of natural consolidation rates.

For the Mississippi Delta estimated average subsidence rates vary widely and are confounded by estimates of the relative (subsidence and uplift) contributions from natural consolidation, from eustasy (global change in sea level), from tectonic uplift and downwarping, and glacio-isostasy (continental rebound from glacial retreats), and from local and regional land subsidence caused by anthropogenic factors (for example, see González and Törnqvist, 2006): subsurface fluid extraction (oil, gas, and ground water), oxidation of artificially drained organic soils, and reduced sediment deposition owing to diversion of sediments that would have compensated for some of the subsidence. During the latter part of the 20th century much of the deltaic plain has subsided more than 10 mm/yr relative to sea level (Penland and Ramsey, 1990). Estimates of eustasy range from a rise of 1 to 2 mm/yr (IPCC, 2001). Estimates of natural consolidation rates in the Mississippi Delta over the past few thousand years range from 2 to 4 mm/yr (Penland and others, 1988; Roberts and others, 1994). By contrast, in the Copano Bay area of the Texas coastal plain estimated rates of natural consolidation over the past 100,000 years are about two orders of magnitude smaller, 0.02-0.05 mm/yr (Paine, 1993).

Subsidence Susceptible Areas

The soils characteristics and the geology of the surficial and subsurface rocks can be used to help identify subsidence prone areas for each of the types of subsidence listed above. Where this information is unavailable, some reconnaissance soils and (or) geologic mapping may be needed. In the absence of other obvious features, such as sinkholes (karst terrane) and pit or sag/trough subsidence (associated with underground coal mines), other ancillary or anecdotal information that suggests subsidence may be occurring is often useful. Ancillary information is pertinent to regional-scale subsidence processes where the subsidence may be subtle and difficult to detect, therefore much of the emphasis in the following section is on those processes, such as subsidence accompanying the withdrawal of subsurface fluids.

Ancillary/Anecdotal Information

Increased incidence of damaged wells: Protruding well casings are common in agricultural areas and some urban areas where ground water has been extracted from alluvial aquifer systems (fig. 2.12). The land surface and aquifer system are displaced downward relative to the well casing, which is generally anchored at a depth where there is less compaction. Generally,

for shallow wells, casings protrude because the friction created between the casing and the compacting earth materials is small and the casing is not compressed. For deep wells the friction is high and the stressed casings are subject to failure through collapse and dislocation. Submersible pumps, pump columns, and the well itself may be damaged or require rehabilitation. Deep wells are most vulnerable and also are the most expensive to repair and replace. Where the frequency of well-casing failures is high, land subsidence is often suspected and is often the cause. For example, when drought conditions during 1976–77 in the Sacramento Valley, California, led to decreased surface-water deliveries and increased ground-water pumping for agricultural irrigation many wells were damaged by vertical compression of the casing attributed to compaction of the aquifer system (Borchers and others, 1998).

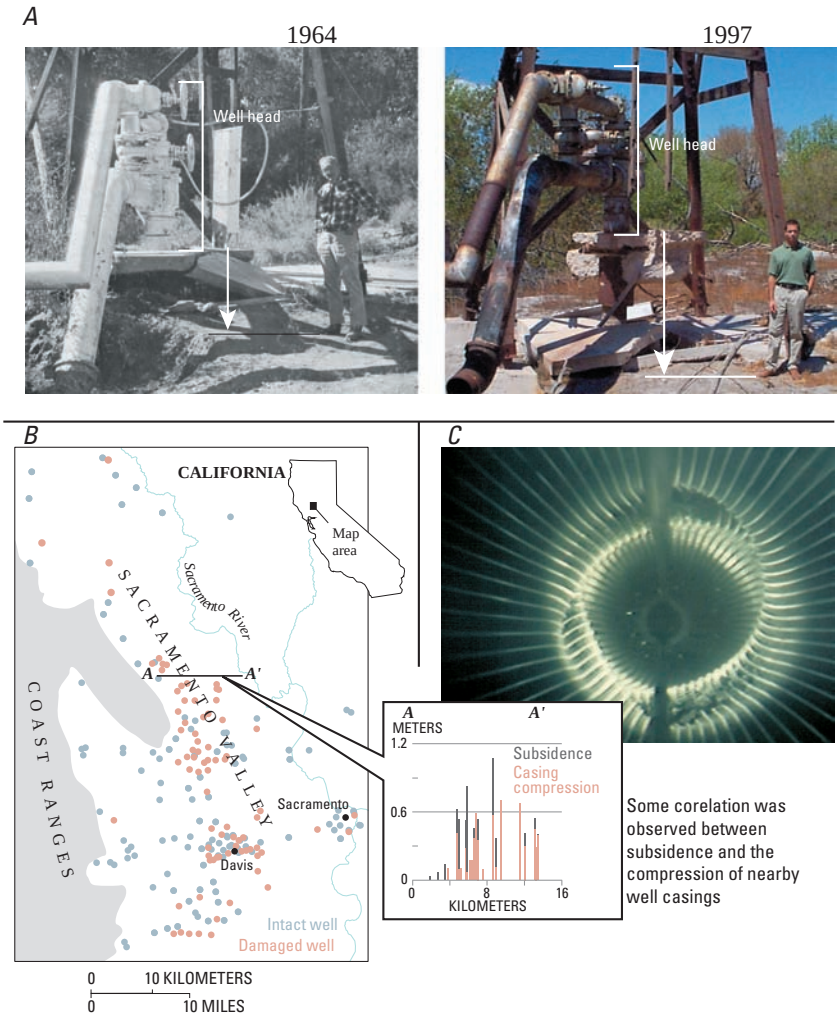

Figure 2.12. Damaged wells: *A*. Photographs showing progressively protruding well in Las Vegas, Nevada, in 1964 and 1997; *B*. Map showing distribution of damaged wells in Sacramento Valley, California, and correlation to subsidence along section A-A′ (modified from Borchers and others, 1998); *C*. Photograph from borehole camera showing collapsed, spiraled well screen in damaged well.

History of repeated adjustments to local geodetic controls: Detection of regional land subsidence may be thwarted by the assumption that the reference marks—bench marks—used to establish local geodetic control are stable, that is, located outside the area affected by subsidence. Often, public agencies or private contractors discover that key local bench marks have moved only after repeat surveys that span several years or longer. Prior to the discovery, when the cumulative subsidence magnitude is small, the apparent errors in the surveys may be adjusted throughout the geodetic network under the assumption that the discrepancies reflect random errors of the particular survey. The subsidence may then go undetected until later routine surveys, or until suspicions arise and steps are taken to confirm the current elevations of the affected bench marks. For example, comparison of repeat leveling surveys led to the confirmed discovery of land subsidence in Antelope Valley (Mojave Desert), California (McMillan, 1973), Las Vegas, Nevada (Maxey and Jameson, 1948), the San Joaquin Valley, California (Ingerson, 1941), and south-central Arizona (Robinson and Peterson, 1962).

Increasing incidence of local riverine or coastal flooding: Flooding caused by loss of elevation and changes of topographic gradients are the most costly impacts of land subsidence (Holzer and Galloway, 2005). Flooding is most severe where land subsides adjacent to water bodies, particularly in coastal regions subject to tidal surges. This causes either permanent submergence or more frequent flooding. Some of the more conspicuous examples of subsidence-related coastal flooding are in the greater Houston, Texas metropolitan area (fig. 2.13), Long Beach and Santa Clara Valley, California, New Orleans, Louisiana, and Venice, Italy. Approximately 4,900 km^2 of coastal lands, mostly tidal wetlands, have been lost from the 25,000 km^2 Mississippi deltaic plain due to water-logging since the 1930s (Barras and others, 2003). In New Orleans and Santa Clara Valley, riverine-flood-control levees have been built in subsidence-affected areas. In the land below high-tide level, local storm discharge must be captured and pumped over the levees to prevent widespread flooding.

Local conveyance and drainage problems: Changes of topographic gradients occur where loss of elevation is not uniform. This may result in stagnation or reversals of streams, aqueducts, storm drainages, or sewer lines; failure, overtopping or reduction in freeboard along reaches of levees, canals, and flood-conveyance structures; and, more generally, cracks and (or) changes in the gradient of linear engineered structures such as pipelines and roadways. Differential subsidence contributes to local flood hazards at Luke Air Force Base, Arizona (Schumann, 1995), and to conveyance losses in the California Aqueduct (Swanson, 1998) and the Central Arizona Project (*http://www.cap-az.com/static/index.cfm?contentID=90*, accessed September 14, 2007).

Ground failures: Two types of ground failures—earth fissure formation and movement on pre-existing surface faults—commonly are recognized in association with surface deformation caused by the extraction of subsurface fluids (fig. 2.14). Ground-water pumping in the greater Houston area has caused offsets on more than 86 faults at the land surface with a cumulative length of more than 240 km. These faults, which grow by aseismic creep, have wracked and destroyed many houses, buildings, and buried utilities. Today, surface faults are associated with land subsidence in at least five areas in the United States (south-central Arizona; Fremont Valley, California; Houston-Galveston area, Texas; Las Vegas Valley, Nevada; San Joaquin Valley, California). The density of faults varies greatly from area to area, but perhaps is highest in the greater Houston, Texas, and Fremont Valley, California, subsidence areas (for example, see Holzer, 1984).

A

B

Figure 2.13. Flooding in subsidence affected areas near Houston, Texas: *A*. Permanently submerged lands at the San Jacinto Battleground State Historical Park near the shores of Galveston Bay; *B*. Homes near Greens Bayou flooded during a storm in June 1989 (Photograph courtesy of Harris-Galveston Subsidence District).

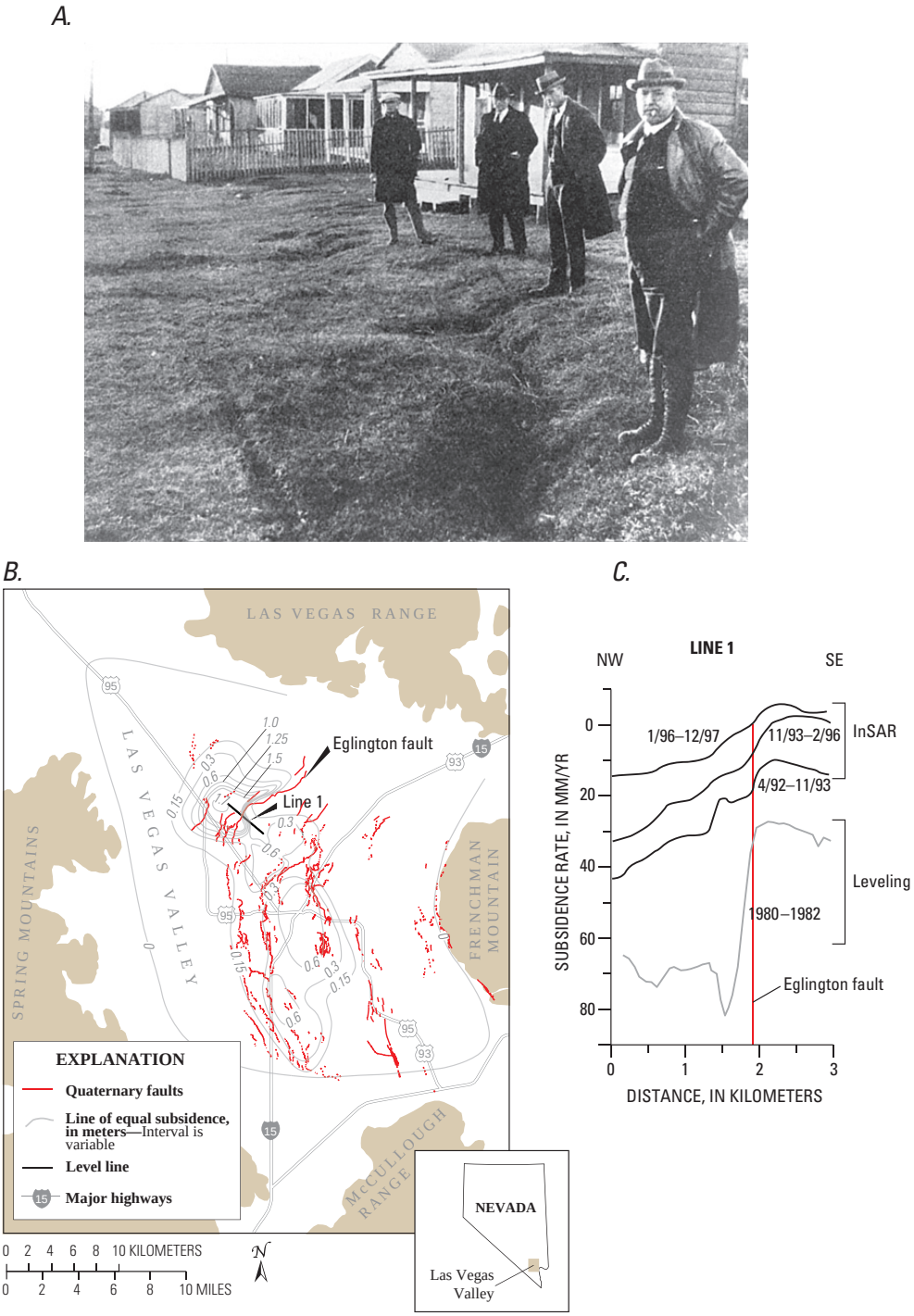

Figure 2.14. Surface faults associated with extraction of subsurface fluids: *A*. Photograph (circa 1926) of surface fault near Houston, Texas, about one-half mile north of the Goose Creek oil field; *B*. Surface faults in Las Vegas Valley, Nevada, shown in relation to measured subsidence caused by ground-water pumping, 1963–2000 (modified from Bell and others, 2002); *C*. Subsidence rates measured along Line 1 (shown in *B*.) showing differential subsidence across the Eglington fault (modified from Amelung and others, 1999).

Scarps formed by these faults resemble those caused by tectonism, and the two can be confused, particularly because both typically form along preexisting geologic faults. Scarps commonly are more than 1 km long and 0.5 m high. The longest reported scarp is 16.7 km (Verbeek and others, 1979). Scarps range from discrete shear failures to narrow, visually detectable flexures. They grow in height by creep. Observed creep rates in the Houston area range from 4 to 27 mm/yr, which is typical of these faults. The fastest observed creep rate is 60 mm/yr on the Picacho fault in central Arizona (Holzer, 1984). Neither sudden offset nor seismicity is observed on these faults. Detailed monitoring of differential vertical displacements across a few faults reveals that creep rates of individual faults vary with seasonal fluctuations of ground-water level. In addition, long-term changes in creep rate, including its cessation when water-level declines stop, have been reported (Holzer and Gabrysch, 1987). Only dip-slip displacements have been observed. The sense of faulting is high-angle and normal on the basis of measured ratios of horizontal to vertical displacement and field evidence.

Earth fissures occur in at least 18 unconsolidated sedimentary basins in 12 areas in the western United States (Holzer and Galloway, 2005). The density of fissures varies greatly between areas. In some places only a few isolated fissures have formed, whereas elsewhere, many fissures occur. Four distinct hazards are posed by fissures: (1) ground displacements associated with their formation, (2) deep, steep-walled gullies caused by post-fissure erosion, (3) interception of surface runoff, and (4) erosion of land near the fissure. Although horizontal displacements across fissures during their formation are small, they are sufficient to damage rigid engineered structures. In addition, differential vertical displacements in narrow zones near fissures may affect structures sensitive to small tilts. Gullies associated with fissures are commonly large enough to trap and injure livestock and other animals as well as pose a potential hazard to people. Fissures also serve as conduits for large quantities of water. Consequently, they are potential hazards to water-conveyance structures such as canals (fig. 2.15). Because of their depth, fissures also can serve as conduits or preferential flow paths for contaminants from the surface into shallow aquifers. Fissures can be sinks for a large volume of sediments. Their formation may locally trigger severe erosion and create badlands topography near the fissure.

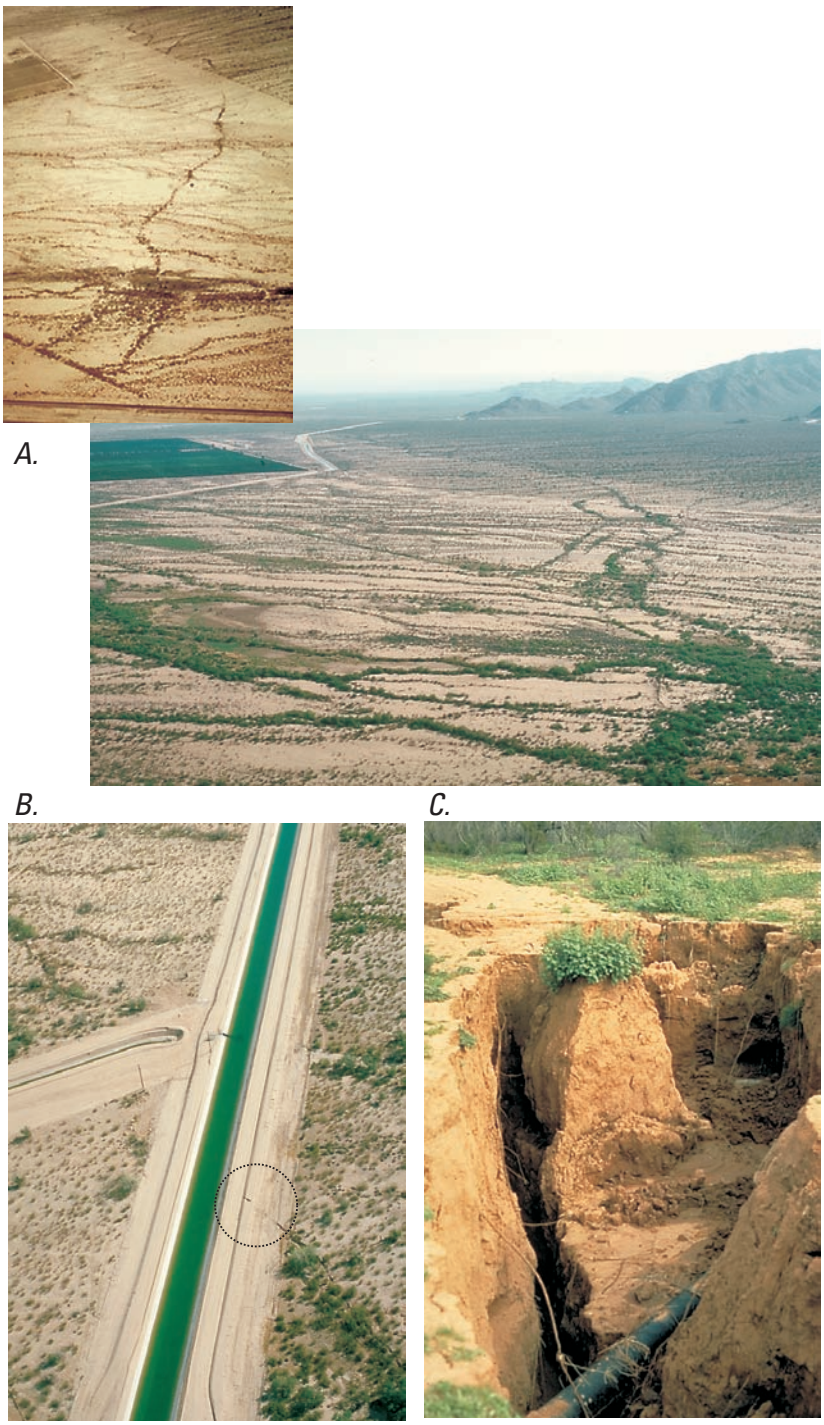

Figure 2.15. Earth fissures, south-central Arizona (modified from Carpenter, 1999): *A*. Picacho earth fissure, pictured in October 1967 (inset) and June 1989. By 1989 the fissure had developed into a system of multiple parallel cracks with a scarp of as much as 0.6 m of vertical offset. *B*. The Central Main Lateral Canal, part of the Central Arizona Project, (also pictured in *A*., upper left of 1989 photo) was damaged by a fissure (circled) where it crosses the Picacho earth fissure. *C*. Natural-gas pipeline undercut by erosional opening of an earth fissure near the Picacho Mountains.

Perhaps the most spectacular and costly single incident associated with the extraction of subsurface fluids was caused by petroleum production from the Inglewood oil field. On December 14, 1963, the dam of the Baldwin Hills Reservoir in Los Angeles, California, failed by piping along a fault on which movement had been induced by high-pressure fluid injection associated with the secondary recovery of petroleum. The catastrophic release of about 900,000 m^3 of water took 5 lives, damaged or destroyed 277 homes, and caused property damage of $12 million in addition to the loss of the reservoir (Hamilton and Meehan, 1971).

Preliminary Mapping

Compilations of the available geodetic, geologic, hydrogeologic, mining, and cultural information are useful. This information may be available from a variety of sources. Sources of geodetic information and data include local land surveyors, and municipal, State, such as State Transportation Departments, and Federal agencies such as the National Geodetic Survey (National Oceanic and Atmospheric Administration). Sources of geologic, hydrogeologic, and mining information pertinent to subsidence hazards may include local well drillers, hydrologic and engineering consulting firms, State agencies responsible for natural, geologic and water resources, and regulating mining activities, and Federal agencies such as the Office of Surface Mining (responsible for regulating the surface impacts of underground mining), and the USGS. For abandoned mines, maps and other information on subsurface conditions frequently are unavailable. The Association of American State Geologists (*http://www.stategeologists.org/*) is a good place to find information on how to access information resources for each of the State Geological Surveys or their equivalents.

Geologic maps may be obtained to assess geologic attributes associated with the various types of subsidence. Ground-water levels are available online from many States (such as Departments of Natural Resources, Environmental Quality, and Water Resources), and the USGS National Water Information System ground-water database (*http://waterdata.usgs.gov/nwis/gw*). Soils maps and other general soils information and specific information pertinent to organic soils and soils susceptible to hydrocompaction can be obtained from the U.S. Department of Agriculture, Natural Resources Conservation Service (*http://soils.usda.gov/*). Historical conditions may be evaluated using available aerial photography and satellite remote sensing data. Baseline geodetic monitoring may be needed to establish current conditions. Interferometric Synthetic Aperture Radar (InSAR) displacement maps may be generated to detect land-surface deformation since 1992.

Assessment

Subsidence assessments typically address the spatial (magnitude and direction) and temporal changes in the position of land surface, and the process causing the subsidence. Measuring and monitoring subsidence is critical to constrain analyses of the causative mechanisms and forecasts of future subsidence. Computer models of the particular subsidence process, constrained by the available data, often are used to assess present and potential future hazards.

Measurement, Mapping, and Monitoring

Various methods are used for measuring and mapping spatial gradients and temporal rates of regional and local subsidence and horizontal ground motion (table 2.2). The methods generally measure relative changes in the position of the land surface. The observable position typically is a geodetic reference mark that has been established so that any movement can be attributed to deep-seated ground movement and not to surficial effects such as frost heave. Any vertical or horizontal movement of a reference mark is measured in relation to other observation points or tied to a global

reference frame. When the reference mark can be assumed to be stable or its movement is otherwise known and measurable, it can be used as a control point, and the absolute position of the observation point can be determined. By this method, land subsidence has been measured using repeat surveys of bench marks referenced to some known, and presumed stable, reference frame. Access to a stable reference frame is essential for the measurements needed to map land subsidence. In many areas where subsidence has been recognized, and other areas where subsidence has not yet been well documented, accurate assessment has been hindered or delayed by the lack of a sufficiently stable vertical reference frame (control).

Table 2.2. Select methods of measuring aquifer-system compaction and land subsidence (modified from Galloway and others, 2000).

[GPS—Global Positioning System; InSAR—Interferometric Synthetic Aperture Radar; LiDAR—Light Detection and Ranging; PSI—Permanent Scatterer Interferometry; SAR—Synthetic Aperture Radar]

Method	Component displacement	Resolution[1] (mm)	Spatial density[2] (samples/survey)	Spatial scale
Spirit level	vertical	0.1-1	10-100	line-network
Geodimeter	horizontal	1	10-100	line-network
Borehole extensometer[3]	vertical	0.01-0.1	1-3	point
Horizontal extensometer				
Tape	horizontal	0.3	1-10	line-array
Invar wire	horizontal	10^{-4}	1	line
Quartz tube	horizontal	10^{-5}	1	line
GPS	vertical horizontal	20 5	10-100	network
Satellite SAR interferometry				
InSAR	range	1-10	10^5-10^7	map pixel[5]
PSI	range	1	variable[4]	map pixel[5]
LiDAR				
Tripod	vertical horizontal	10 10	10^6-10^8	3D point cloud
Airborne	vertical horizontal	300 360	variable	map pixel[6]

[1]Measurement resolution obtained under optimum conditions. [2]Number of measurements generally necessary to define the distribution and magnitude of land subsidence at the scale of the survey. [3]Counter-weighted pipe extensometer (Riley, 1969). [4]Depends on presence of permanent scatterers. [5]A pixel (picture element) on an InSAR/PSI displacement map based on existing spaceborne sensors is typically 40-80 meters resolution. [6]A pixel on an airborne LiDAR image typically varies from 0.25 to 2m.

"Sufficiently stable" is a somewhat relative term that has meaning in the context of a particular time-frame of interest and magnitude of differential movement. Because of continuous and episodic crustal motions caused mostly by postglacial rebound, tectonism, volcanism, and anthropogenic alteration of the Earth's surface, it is occasionally necessary to remeasure geodetic control on a national scale. Networks of geodetic control consist of known positions that are determined relative to a horizontal or vertical datum or both.

Two reference networks are used for horizontal and vertical geodetic control for the United States, the North American Datum of 1983 (NAD83) and the North American Vertical Datum of 1988 (NAVD88). NAD83 replaces the older North American Datum of 1927 (NAD27) and is the current geodetic reference system for horizontal control in the United States, Canada, Mexico, and Central America. It is the legally recognized horizontal control datum for the Federal government of the United States and for 44 of the 50 individual States. NAVD88 replaces the National Geodetic Vertical Datum of 1929 (NGVD 1929), which was based on local mean sea levels determined at 26 tidal gages. NAVD88 is based on the Earth's geoid—a measurable and calculable surface that is equivalent to mean sea level.

In partnership with other public and private parties, the National Geodetic Survey (NGS) has implemented High Accuracy Reference Networks (HARNs) in every State. HARN observation campaigns resulted in the establishment of some 16,000 survey stations. These updated reference networks facilitate the early and accurate detection and measurement of land subsidence.

Ground-Based Geodetic Surveys

Before the advent of the satellite-based Global Positioning System (GPS) in the 1980s, the most common means of conducting land surveys involved either the theodolite or, since the 1950s, the geodimeter (an electronic distance measuring device, or EDM). If only vertical position were sought, the spirit level has been the instrument of choice. The technique of differential leveling allows the surveyor to carry an elevation from a known reference point to other points by use of a precisely leveled telescope and graduated or bar-coded vertical rods. Despite its simplicity, this method can be very accurate. When surveying to meet the standards set for even the lower orders of accuracy in geodetic leveling, 10–15 mm changes in elevation can be routinely measured over distances of kilometers and 1–2 mm of elevation change over a few kilometers can be obtained with the highest quality (order) of leveling. Over long distances leveling and EDM measurement errors increase. When the length of the survey is small (on the order of 10 km or less) spirit leveling is still commonly used because it is accurate and relatively inexpensive. Large regional networks may warrant use of more efficient airborne, and space-based geodetic surveys. If more precise and accurate measurements of change are needed on a local scale, extensometers may be used, or if more spatial detail is required over short distances, tripod-mounted LiDAR (Light Detection and Ranging) may be used.

Extensometry

Vertical borehole extensometers can be used to measure the continuous change in vertical distance between the land surface and a reference point or "subsurface bench mark" at the bottom of a deep borehole (Riley, 1986). If the subsurface bench mark is established below the base of the compacting aquifer system or beneath an oxidizing or compaction organic soil, the extensometer can be used as the stable reference or starting point for local geodetic surveys. Designs that incorporate multiple-stage borehole extensometers in a single instrument are being used to measure aquifer-system compaction simultaneously in different depth intervals (figs. 2.16*A*,*B*).

When used in conjunction with good well logs and water-level data, the deformation history generated by an extensometer can provide the basis for stress-strain analysis (Riley, 1969) and modeling that constrains the average compressibility and vertical hydraulic conductivity of the aquitards (Helm, 1975; Sneed and Galloway, 2000; Pavelko, 2003). This capability derives from the fact that the compaction measured by the extensometer is directly related to the volume of water produced by the aquitards. Reliable estimates of aquitard properties are necessary for constraining predictive modeling, whether the objective is the prevention or mitigation of land subsidence or simply the optimal use of the storage capacity of the aquifer system.

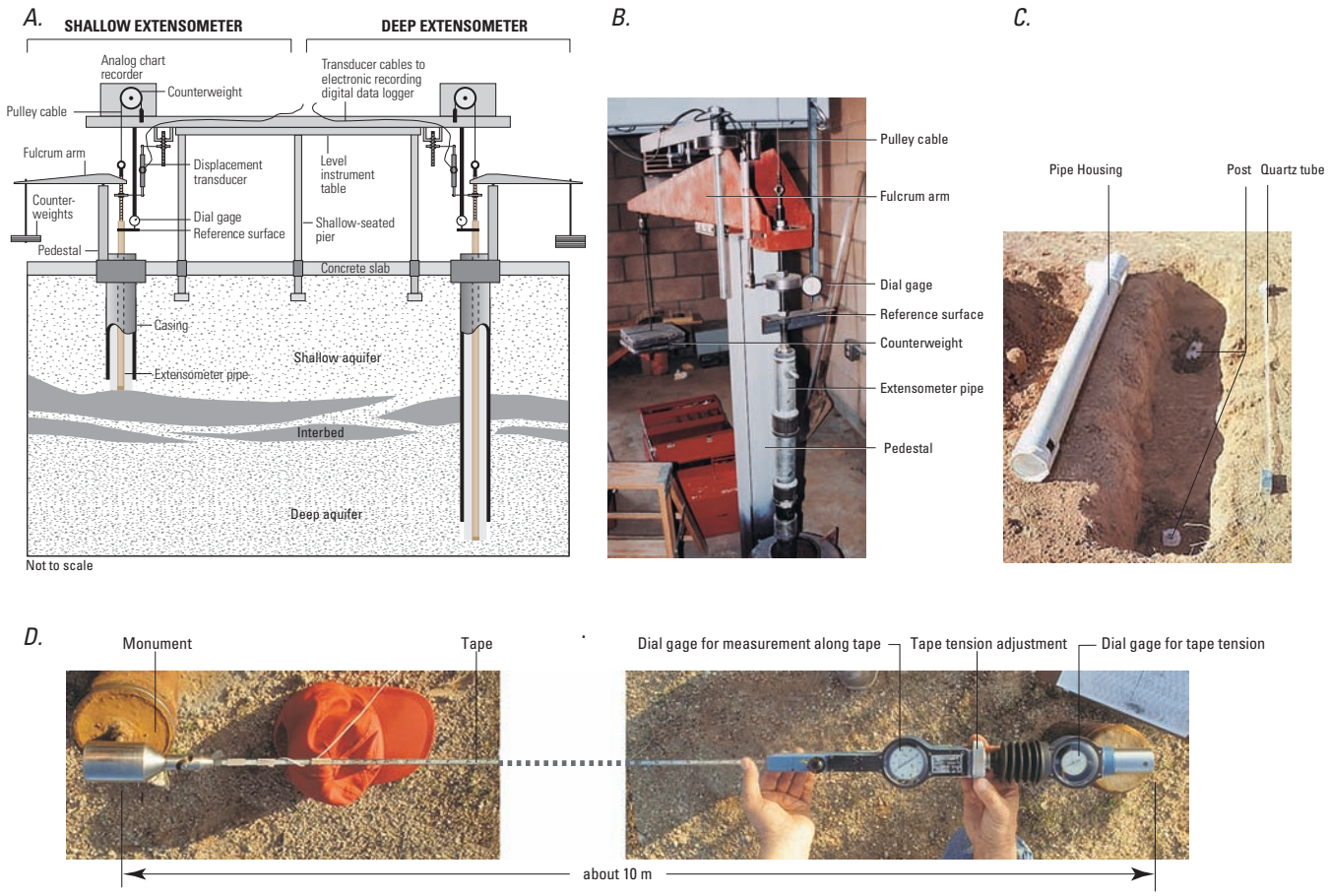

Figure 2.16. Extensometers: *A*. Schematic, and *B*. photo of counter-weighted, two-stage, borehole pipe extensometer, Lancaster, California. The extensometer measures compaction simultaneously in two depth intervals in the aquifer system. The compaction (vertical displacement) is measured as movement of the pipe relative to the reference table and reflects shortening (subsidence) or lengthening (uplift) of the distance between the shallow-seated piers and the anchor depths of the pipe extensometers. *C*. Buried horizontal quartz-tube extensometer, near Apache Junction, Arizona. A displacement sensor is placed between a post and the quartz tube to measure small displacements in the interval spanned by the coupled post-sensor tube post-instrument configuration. *D*. Tape extensometer, near Apache Junction, Arizona. The tape is attached at both ends to a specially equipped geodetic monument.

Several kinds of horizontal extensometers are used to measure differential horizontal ground motion at earth fissures caused by changes in ground-water levels (Carpenter, 1993). Buried horizontal extensometers constructed of quartz tubes (fig. 2.16*C*) or invar wires are useful when precise, continuous measurements are required on a scale of 3–30 m. Tape extensometers (fig. 2.16*D*) measure changes across intermonument distances up to 30 m with repeatability of approximately 0.3 mm. The tape extensometer is used in conjunction with geodetic monuments specially equipped with ball-bearing instrument mounts, which can serve as both horizontal and vertical control points. Arrays or lines of monuments can be extended for arbitrary distances, usually in the range of 60–180 m.

Tripod LiDAR

Ground-based tripod (terrestrial) LiDAR (shortened to T-LiDAR) is a portable remote sensing instrument that uses an infrared laser to scan the landscape and generate very detailed (centimeter to subcentimeter) and accurate (±4 mm) digital models of the scanned target at distances from 3 to 800 m (fig. 2.17). A three-dimensional image of a scanned target is obtained by measuring the two-way travel time of each laser pulse for distance and the look angle for angular positioning with respect to the center of the instrument, and by measuring the intensity of the reflected signal. The point positions are combined to generate a comprehensive image map of the target. More than 7 million point-position measurements per hour can be made depending upon the particular T-LiDAR system; scan rates, data densities, and point positional errors vary among the different systems. T-LiDAR is an active source technology that collects measurements independent of most weather conditions, sky view, and time of day, but is limited to line of sight measurements. A full three-dimensional image is obtained by scanning a target from multiple directions to characterize all sides of the target and to minimize shadowing. T-LiDAR scans obtained from different vantage points are aligned and combined through an algorithm that computes a best-fit surface through the individual points in each scan and then minimizes the misfit between common surfaces in each scan.

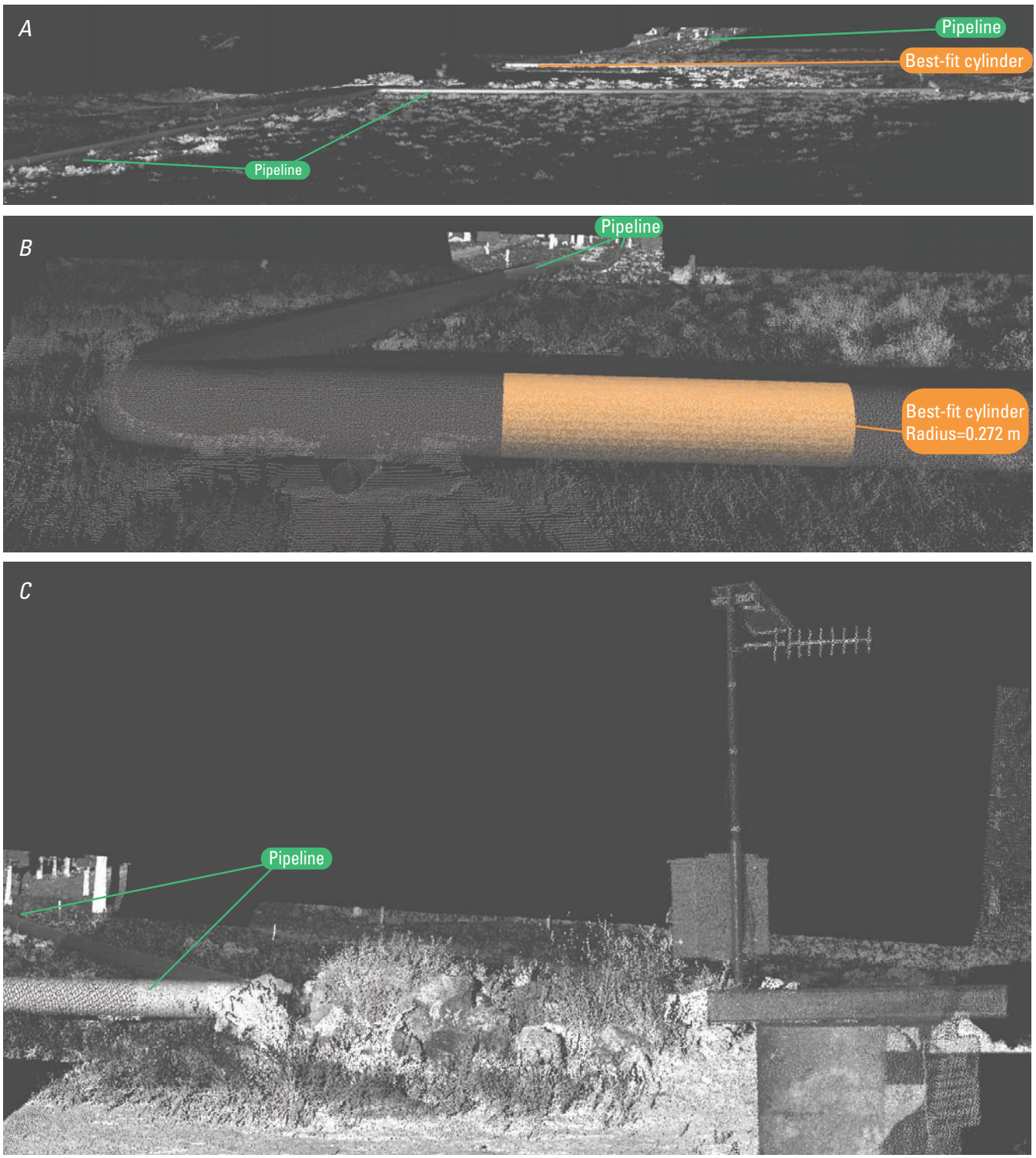

Figure 2.17. T-LiDAR imagery of a geothermal transmission line, Mammoth Lakes, Calif. *A*. One T-LiDAR setup imaged about 500 m of continuous pipeline. *B*. Best-fit primitives (idealized geometries) can be fit to the data to simulate the pipeline, as well as, measure sub-centimeter displacements. *C*. Detailed imagery shows a telemetered USGS well and adjacent pipeline.

Changes in the position of the land surface or structural features such as exposed pipelines can be obtained through differencing of precisely aligned T-LiDAR images collected at different times, known as Differential LiDAR (Dif-LiDAR). There are two approaches for Dif-LiDAR analysis: absolute and relative. Absolute Dif-LiDAR measures land-surface change by differencing two LiDAR datasets that are georeferenced with GPS. This approach is ideal for resolving very detailed spatial changes within a larger deformation field. Examples of absolute Dif-LiDAR include imaging land-surface change associated with earthquakes, volcanic activity, fluid extraction induced land subsidence, large-scale landslides, and areas that have undergone a significant change to their geomorphology. Technically, this approach produces the best information of land-surface change, but requires additional field equipment and time for GPS data collection and processing and may be unnecessary for all scientific applications. Alternatively, relative Dif-LiDAR applies the same best-fit surface-matching algorithm used in the alignment of an individual scan to common 'stable' regions outside of the area of interest that is changing. This approach is ideal for resolving very detailed spatial changes within a well-defined deformation zone or imaging change in a subset of a larger dataset where absolute positioning is not required. A few examples of relative Dif-LiDAR include measuring hill-slope change on moderate and small landslides, measuring three-dimensional movement of infrastructure across deforming boundaries, calculating volume change associated with debris flows and engineering projects, and characterizing how streams respond to floods. Dif-LiDAR can resolve the relative three-dimensional displacement field, rotation, localized tilt, and translation within the scanned region, but requires GPS ground control to uniquely measure these parameters for the data block as a whole and to reference the measurements to a global reference frame.

To further measure subtle displacement patterns across an actively deforming pipeline, individual objects such as poles, support structures, and exposed pipeline can be individually selected and mathematically fit to best-fit primitives (idealized geometric shapes) and tracked with time to image temporal deformation patterns. Primitive fitting takes advantage of the thousands of point measurements and the small (±4 mm) measurement error (random scatter) to fit a mathematically defined surface of the feature. For instance, vectors fit to fence posts on an active landslide can be used to monitor the change in the intersection of the fence post vector with the ground plane measured from one time period to the next and thereby track the movement of the individual post in space and time. Similarly, primitives can be fit to signs (planes), bridge support pillars (cylinders) and building (planes, polygons) and used to generate a detailed displacement map of the deformation or a time series of deformation maps. Because pipelines have artificial features with a number of surfaces that can be described mathematically, T-LiDAR is an ideal technique for measuring spatial and temporal changes in regions that are actively deforming, but the technique may be too labor intensive for characterizing pipelines at linear scales greater than about 5 km.

Airborne Geodetic Surveys

Airborne LiDAR is capable of rapidly and accurately collecting high-resolution elevation data along an infrastructure corridor with 15-cm vertical and 20-cm horizontal uncertainties (one standard deviation) for most commercial grade, and with 30 percent lower uncertainties for research-grade airborne LiDAR data. The LiDAR imagery can be used to map the pre- and post-emplacement topography of a pipeline corridor, to map the three-dimensional character of the pipeline, to assess possible hazards along the pipeline, to produce digital blueprints of older pipelines through primitive fitting (see Tripod LiDAR section above), and to develop large-scale deformation maps using repeat airborne LiDAR imagery. Movements greater than 0.6 m are needed between LiDAR surveys to resolve land-surface motion with most commercial grade

airborne LiDAR. There are four primary factors to consider for airborne-LiDAR mapping and monitoring of pipeline subsidence hazards: (1) ground sample distance (data density), (2) geodetic control, (3) vendor qualifications, and (4) data quality assurance/quality control (QA/QC):

Data Density: Ground sample distance is the average number of laser shots per square meter and controls the spatial resolution of the imagery. A general rule of thumb is that the ground sample distance should be a minimum of one-twelfth to one-eighth of the effective length of the smallest feature to be resolved. Lower resolution imagery may not have the data density necessary for characterizing the infrastructure or target area. One of the primary applications of airborne LiDAR is the generation of bare earth Digital Elevation Models (DEMs). DEMS are produced from the LiDAR point cloud by digitally removing vegetation and artificial structures (such as buildings, bridges, and dams) from the imagery. The resulting product is a bare earth representation of the land surface free of vegetation and structures. In regions with heavy vegetation, if the ground sample distance is too coarse, then the resulting DEM will lack the desired data density.

Geodetic Control: Currently, the largest error source in airborne LiDAR is uncertainty in the position of the aircraft in flight. The position of the aircraft needs to be determined or estimated at the same rate as the laser scanner; a rate of 10,000 samples per second is common for many laser scanners. The aircraft position is obtained through GPS positioning measurements on the ground and aircraft at 5–10 samples per second and interpolated with an onboard Inertial Measurement Unit (IMU) to match the laser scanner rate. Ground-based GPS base stations at known locations (controls) are combined with the onboard aircraft GPS to calculate the exact latitude, longitude, and elevation of the aircraft and then are transferred to each of the laser returns through the angular relationship of the scan angle and the aircraft and the two-way travel time of the laser pulse. Error in the GPS position of the aircraft is propagated to the land-surface measurements. Increasing the number of ground-based GPS control base stations minimizes the aircraft-position error, and a higher quality airborne LiDAR dataset. GPS surveys are discussed in more detail below in the *Global Positioning System* section of this chapter.

Vendor Qualifications: The capability and (or) experience to collect airborne LiDAR imagery with high measurement resolution using accurate and precise geodetic control varies widely. Most vendors can produce quality 2-m products, but the quality of the imagery for sub-meter LiDAR imagery varies among vendors.

QA/QC: Quality assurance and quality control procedures are necessary to verify that the dataset collected meets or exceeds the agreed specifications. The QA/QC component of the LiDAR survey is acquired by survey grade ground-based GPS systems (typically Real Time Kinematic rovers) collecting hundreds of point positions in a variety of characteristic geologic environments, ecosystems, and urban settings. Because the GPS measurements will have a lower uncertainty (typically about 1 cm horizontal and 3 cm vertical) than the airborne LiDAR measurements, they are considered the ground truth. By collecting QA/QC points in a variety of settings, it is possible to evaluate systematic biases in the dataset for a given rock unit, vegetation type, or adjacent laser swaths.

Space-based Geodetic Surveys

Space-based geodetic techniques that can measure changes in the land-surface position have significantly advanced over the past two decades with the development of GPS and interferometric synthetic aperture radar (InSAR). Continuously operating reference GPS sites or CORS can automatically determine three-dimensional ground position multiple times a second, and averaged over a day can be used to obtain long-term time series with millimeter-level resolution of horizontal position and sub-centimeter level resolution of vertical positioning at the CORS site. The InSAR techniques can measure sub-centimeter ground displacements at high spatial detail (10–100 m

resolution) over regions spanning 100 by 100 km, but are limited to measuring changes in the line-of-sight distance between the ground and satellite, which are most sensitive to vertical motion.

Global Positioning System

A revolution in surveying and measurement of crustal motion occurred in the early 1980s when tests of the satellite-based NAVSTAR GPS showed that it was possible to obtain 1 part in 1 million precision between points spaced from 8 to more than 40 km apart. GPS uses Earth-orbiting satellites to trilaterate positions based on the time required for radio signals transmitted from satellites to reach a receiving antenna. An accurate three-dimensional position can be determined from trilateration of the range distances between the receiver and at least four satellites. Since July 17, 1995, NAVSTAR has been operational with a full constellation of 24 satellites, and in North America provides essentially continuous coverage with nominally at least 6 satellites in view at all times. Guidelines have been formulated for establishing GPS-derived ellipsoid heights with accuracy standards at either the 20-mm or the 50-mm level (Zilkoski and others, 1997).

In land-subsidence and other crustal-motion surveys, the relative and absolute three-dimensional positions of two points can be determined when two GPS receivers, one at each observation point, receive signals simultaneously from the same set of four or more satellites. When the same points are reoccupied following some time interval, any motion between the points that occurred during the time interval can be measured. Geodetic networks of points can be surveyed in this fashion. Such a network, one of the first of its kind designed specifically to monitor land subsidence, was established in the Antelope Valley, Mojave Desert, California in 1992 (Ikehara and Phillips, 1994). It was designed to determine the subsidence of previously leveled benchmarks and enable precise measurement of points separated by tens of kilometers for future subsidence monitoring. Other large GPS-based geodetic networks for subsidence monitoring have been established in Albuquerque, New Mexico; the Avra Valley, Arizona; Houston-Galveston area, Texas; Las Vegas, Nevada; the Lower Coachella Valley, California; the Sacramento-San Joaquin Delta, California; and the Tucson basin, Arizona. GPS surveying also is a versatile exploratory tool that can be used in a rapid mode (kinematic or rapid static) to quickly (on the order of minutes to tens of minutes observation time per baseline) but coarsely (network of stations and baselines) define subsidence regions, in order to site more precise, site-specific and time-continuous measurement devices such as recording extensometers and tiltmeters, and real-time GPS stations.

One of the strengths of GPS is the ability to measure the three-dimensional deformation field—both horizontal and vertical movements. Uplift and subsidence associated with managed subsurface fluid production (injection and extraction) is accompanied by measurable horizontal movements in the Earth's crust. As the land surface subsides, points around the subsidence feature are pulled inward towards the region with the greatest subsidence and conversely, as a region inflates, points will move upward and away from the region of maximum inflation. If the points are directly on the margin of the subsidence/uplift feature, then the ratio of vertical to horizontal motion may be nearly 1:1 (Bawden and others, 2001). For example, in the San Gabriel Valley in southern California, ongoing ground-water pumping pulled nearby continuous GPS stations inward toward the region of maximum drawdown (fig. 2.18*A*). Record rainfall in the same region in the winter-spring 2005 produced more than 4 cm of uplift with greater than 1 cm of radial outward motion of the nearby GPS sites (fig. 2.18*B*).

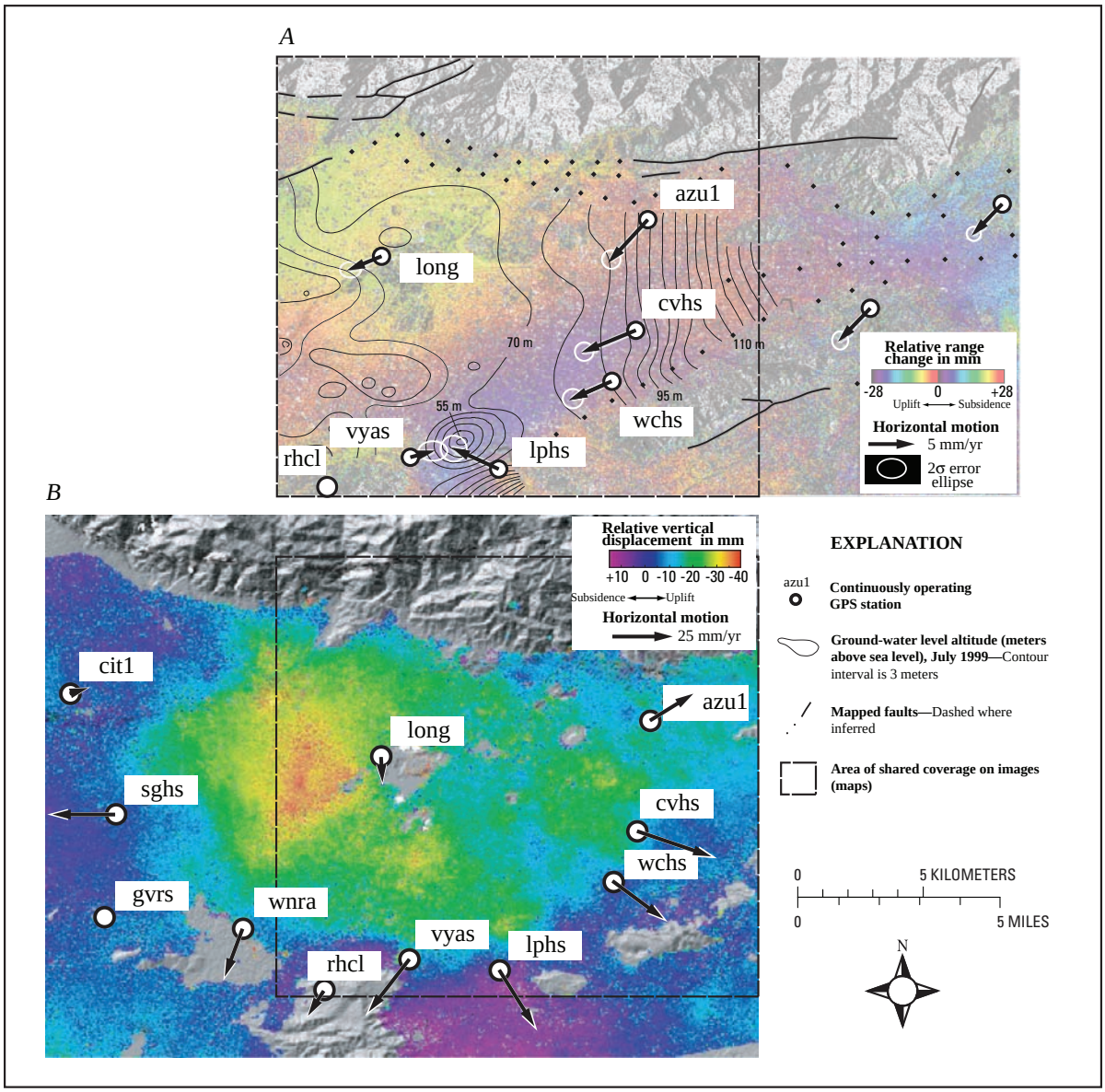

Fig. 2.18

Figure 2.18. Horizontal GPS displacement vectors superimposed on InSAR imagery for the San Gabriel Valley, southern California. *A*. Ground-water levels in the San Gabriel Valley declined about 3.5 m between May and October 1999 corresponding with approximately 12 mm of equivalent (range change) land subsidence measured using InSAR (Bawden, 2002). The neighboring continuous GPS sites (solid white circles) **vyas** and **lphs** are pulled inward towards the zone of maximum subsidence which generally corresponds with the drawdown cone. The generally southwest-trending horizontal motion of the other GPS sites during this period is attributed to regional tectonic processes (Bawden and others, 2001). *B*. Record rainfall in the winter-spring of 2005 produced about 40 mm of uplift measured using InSAR January to July 2005, and radial outward motion of continuous GPS sites **sghs**, **wnra**, **rhcl**, **vyas**, **lphs**, **wchs**, **cvhs**, and **azu1** January through May 2005 (King and others, 2007).

Synthetic Aperture Radar (SAR) Interferometry

Satellite SAR interferometry is ideally suited to measure the spatial extent and magnitude of surface deformation associated with aquifer-system compaction as well as other types of subsidence. SAR interferometry techniques—principally coherent (InSAR) and to a lesser extent, persistent-scatterer (PSI)—frequently are used to map, monitor, and analyze subsidence. By identifying specific areas of deformation within broader regions of interest, SAR interferometry also can be used to site and coordinate local and regional-scale subsidence monitoring (for example, borehole extensometers, GPS networks, and leveling lines; Bawden, 2002). These attributes of SAR interferometry address each of the information needs identified by the National Research Council (1991). Another important attribute of SAR interferometry is the increasing historical SAR data archive. For many areas, a substantial data archive exists for the period from 1992 to the present, enabling measurements of historic surface displacements in this time period. In addition, new acquisitions can be ordered as needed. The detailed procedure and cost depends on the sensor.

InSAR uses radar signals to measure deformation of the Earth's crust in spatial detail and high measurement resolution. InSAR can provide millions of data points in a large region (100 by 100 km/scene) and is often less expensive than obtaining sparse point measurements from labor-intensive spirit-leveling and GPS surveys. Geophysical applications of InSAR take advantage of the phase component of reflected radar signals to measure apparent changes in the range distance of the land surface (Gabriel and others, 1989; Massonnet and Feigl, 1998). The size of a picture element (pixel or posting) on a typical InSAR image (interferogram) made from satellite-borne SAR may be as small as 100 m^2 or as large as 10,000 m^2, depending how the interferogram is processed.

For landscapes with relatively stable radar reflectors (such as buildings or other engineered structures, or undisturbed rocks and ground surfaces) over a period of time, it is possible to make high-precision measurements of the change in the position of the reflectors by subtracting or "interfering" two radar scans made of the same area at different times; the resulting InSAR image is called an interferogram. This is the principle behind InSAR.

Under ideal conditions, it is possible to resolve georeferenced changes in range—the "line-of-sight" distance between the ground and satellite, on the order of 10 mm or less at the scale of 1 pixel. The component of displacement measured using InSAR depends on the look angle of the sensor and for currently available sensor data (for example, for ERS-1 and -2 satellites the look angle for California is about 23° subvertical) is primarily vertical (Galloway and Hoffmann, 2007). InSAR has been used to map spatially-detailed ground-surface deformations associated with earthquakes (for example, Massonnet and others, 1993; Zebker and others, 1994), volcanoes (for example, Massonnet and others, 1995; Rosen and others, 1996; Wicks and others, 1998, 2006), geothermal production (Massonnet and others, 1997; Thatcher and Massonnet, 1997; Vadon and Sigmundsson, 1997; Fialko and Simons, 2000), oil and gas extraction (for example, Fielding and others, 1998), ground-water pumping (for example, Galloway and others, 1998; Amelung and others, 1999; Bawden and others, 2001; Hoffmann and others, 2001; Bell and others, 2002; Hoffmann and others, 2003a; Schmidt and Bürgmann, 2003; Galloway and Hoffmann, 2007), and underground mining (for example, Jarosz and Wanke, 2004; Chang and others, 2005).

Persistent (also known as permanent) scatterer interferometry (PSI) uses a different approach than InSAR for processing SAR imagery, and has been shown to overcome some of the limitations of the InSAR technique. PSI involves the processing of numerous, typically more than 30, interferograms to identify a network of persistent, temporally stable, highly reflective ground features—permanent scatterers (Ferretti and others, 2000, 2001; Werner and others, 2003). These

scatterers typically are cultural features of the developed landscape such as buildings, utility poles, and roadways. The phase history of each scatterer is extracted by estimating a predefined displacement model (typically a linear, constant-rate model) to provide interpolated maps of average annual displacements, or the displacement history, up to the length of a SAR data archive, of each individual scatterer, thus providing a "virtual" GPS network with "instant" history. By focusing on temporally stable targets in the image, temporal decorrelation is avoided or strongly reduced. Furthermore, most of the strong and stable reflectors identified represent small individual scattering elements. For this type of scatterer though, a larger fraction of the reflected energy remains coherent for larger interferometric baselines, allowing a larger set of SAR scenes to be used in the analysis. The large number of observations available in a typical SAR data set used in a PSI analysis supports a statistical analysis of the observed phase histories in space and time, and depending on the characteristics of the displacements, it is often possible to separate the phase differences caused by atmospheric variations and uncompensated topography from those due to surface displacements.

PSI has been applied primarily in urban environments, where the density of stable scatterers typically is quite high (as many as a few hundred per square kilometer). Over natural terrain, the scarcity of stable targets severely limits PSI's successful application. A small number of investigations have demonstrated a successful application of PSI in "rural" terrain (Usai, 2001; Kircher, 2004). However, the investigations in the Netherlands and western Germany, used stable targets such as houses and other man-made features that were present in sufficient numbers. Hooper and others (2004) have proposed a modified algorithm for natural terrain, but this has been demonstrated for relatively dry conditions and it is questionable whether their approach will work over agricultural areas prone to temporal decorrelation owing to variable moisture and crop conditions.

A potentially severe limitation of PSI, particularly where the density of permanent scatterers is small and displacement magnitudes are large, is the necessity to determine a motion model *a priori*, which is used in resolving phase ambiguities. Another limitation of PSI is the difficulty of identifying stable targets in rural and agricultural areas. Consequently, the majority of PSI applications have focused on urban areas—for example, Paris, France (Fruneau and Sarti, 2000); San Francisco Bay area, USA (Ferretti and others, 2004); Bangkok, Thailand (Worawattanamateekul and others, 2004); Phoenix, USA (Beaver and others, 2005); Arno River Basin-Florence, Italy (Canuti and others, 2005); Berlin, Germany (Kampes, 2005) ; London, England (NPA, *http://www.npagroup.com/insar/apps/london_psi.htm*, accessed October 7, 2007) and Las Vegas, USA (Kampes, 2005; Bell and others, 2008).

Analysis and Simulation

The analysis of subsidence-prone areas generally involves evaluation of the material surface- and subsurface-geologic properties, and the potential physical and chemical processes causing land subsidence. The analyses typically include one or more of the following: laboratory and field measurements, and analytical and numerical modeling of subsidence processes. Analytical and numerical models have been used to simulate physical processes governing various types of subsidence. Broadly defined, "A model is a tool designed to represent a simplified version of reality." (Wang and Anderson, 1982). Generally, the more sophisticated models are formulated from basic principles of physics and involve some conceptual coupling of mechanical, hydraulic, and (or) thermal processes. The governing equations used to describe the various coupled processes range from fully decoupled, to weakly coupled, to rigorously coupled. Numerous numerical models have been developed and applied to simulate subsidence owing to aquifer-system compaction

caused by ground-water extractions. Fewer models have been specifically developed to simulate subsidence attributed to other mechanisms. Some general purpose hydraulic-mechanical-thermal models have been used to simulate some of the various other processes.

Calibrated aquifer-system compaction models have been used to forecast subsidence in a number of study areas for specified future ground-water extraction and recharge scenarios. The calibrated models generally are constrained by historical subsidence and ground-water levels and some knowledge of the hydraulic and mechanical parameters governing aquifer-system compaction. The use of models to simulate future conditions is widely applied to manage ground-water resources, and the use of coupled simulation/optimization models (Ahlfeld and Mulligan, 2000; Ahlfeld and others, 2005) is being applied to a limited extent to maximize future beneficial use of the water resource while minimizing deleterious consequences, such as subsidence (for example, Danskin and others, 2003; Phillips and others, 2003).

Subsurface Fluid Withdrawal

The analysis and simulation of regional subsidence caused by the withdrawal of ground water has been addressed primarily using conventional ground-water flow theory (Jacob, 1940) and secondarily using linear poroelastic theory (Biot, 1941). The chief difference between the two theories is the treatment of the deformation of the skeletal-matrix. Conventional ground-water flow theory describes only the vertical deformation of the matrix (assumes no horizontal deformation), and poroelastic theory describes the three-dimensional deformation of the matrix. Both approaches describe a relation between fluid flow and deformation of the aquifer system, but conventional ground-water flow theory essentially decouples fluid flow and matrix deformation, whereas poroelastic theory couples fluid flow and matrix deformation, and is more general and more complex.

It is well known that the extraction of subsurface fluids causes three-dimensional deformation of a pumped aquifer system, and there are several quantitative analyses of the phenomenon (Verrjuit, 1969; Sandhu, 1979; Hsieh, 1996; Burbey and Helm, 1999; Burbey, 2001). As Hsieh (1996) notes, "Analysis of realistic aquifer settings generally requires a numerical poroelascticity model. This type of model is not well-known to most ground-water hydrologists." And, as Burbey (2001) showed, the conventional ground-water theory and the linear poroelasticity approaches yield nearly identical head and volume-strain distributions and therefore, nearly identical volumes of water released from storage owing to subsidence. These factors, coupled with the paucity of regional horizontal-displacement measurements in developed ground-water basins has led to the wide application of analytical and numerical models based on conventional ground-water flow theory to address regional land subsidence problems. This approach is described below.

Almost all the permanent subsidence in aquifer systems is attributable to the compaction of aquitards during the typically slow process of aquitard drainage (Tolman and Poland, 1940). This concept, known as the *aquitard drainage model*, has formed the theoretical basis of many successful subsidence investigations associated with depressuring of porous media (see Helm, 1984; Holzer, 1998). The aquitard drainage model is based on conventional ground-water flow theory and two principles describing the relations between fluid pressure, intergranular stress, and fluid flow.

The relation between changes in ground-water levels and deformation of the aquifer system is based on the *principle of effective stress* first proposed by Terzaghi (1925). According to the Terzaghi relation,

$$\sigma'_{ij} = \sigma_{ij} - \delta_{ij} u \,, \tag{2.1a}$$

where

σ'_{ij} is a component of the effective stress tensor,

σ_{ij} is a component of the geostatic (total) stress tensor,

δ_{ij} is the Kronecker delta function, and

u is the fluid pore pressure or hydrostatic stress.

Equation 2.1a shows that changes in effective stress can result from changes in geostatic stress or changes in pore pressure. The geostatic stress is the load of the overlying saturated and unsaturated sediments and tectonic stresses. Neglecting tectonic stresses, if the aquitards are assumed to be horizontal and laterally extensive with respect to their thickness, changes in pore-pressure gradients within the aquitards will be primarily vertical. Assuming that the resulting strains also are primarily vertical, a one-dimensional form of equation 2.1a can be expressed as

$$\sigma' = \sigma - u \tag{2.1b}$$

where σ' and σ are the vertical components of effective and geostatic stress, respectively.

By this principle, when the support provided by fluid pressure is reduced, such as when ground-water levels are lowered, support previously provided by the pore-fluid pressure is transferred to the skeleton of the aquifer system, which compresses to a degree. Conversely, when the pore-fluid pressure is increased, such as when ground water recharges the aquifer system, support previously provided by the skeleton is transferred to the fluid and the skeleton expands. In this way, the skeleton alternately undergoes compression and expansion as the pore-fluid pressure fluctuates with ground-water discharge and recharge. When the load on the skeleton remains less than any previous maximum load, the fluctuations create only a small elastic deformation of the aquifer system and small displacement of land surface. This fully recoverable deformation occurs in all aquifer systems, commonly resulting in seasonal, reversible displacements in land surface of as much as 1–3 cm or more in susceptible aquifer systems in response to the seasonal changes in ground-water pumpage. The elastic deformation of aquifer systems likely poses little hazard to pipelines except in areas where heterogeneities in the aquifer systems (such as near faults or changes in depositional facies with contrasting hydraulic and mechanical properties) create differential subsidence and amplified lateral deformation.

When the load on the aquitard skeleton exceeds the maximum previous stress on a skeletal element—the preconsolidation stress—the aquitard skeleton may undergo significant, permanent rearrangement, resulting in irreversible compaction. Because the skeleton defines the pore structure of the aquitard, there is a permanent reduction of pore volume as the pore fluid is “squeezed” out of the aquitards into the aquifers. In confined aquifer systems subject to large-scale overdraft, the volume of water derived from irreversible aquitard compaction is essentially equal to the volume of subsidence and typically can range from 5 to 40 percent of the total volume of water pumped. This represents a one-time mining of stored ground water and a small permanent reduction in the storage capacity of the aquifer system. Holzer (1981) showed that alluvial aquifer systems in subsiding areas of Arizona, California, and Texas are naturally overconsolidated by the equivalent of about 16–63 m of water-level decline, and that many values of the natural preconsolidation stress fall in the range from 25 to 40 m.

Because aquitards are by definition much less permeable than aquifers, the vertical drainage of aquitards into adjacent pumped aquifers may proceed very slowly, and thus lag far behind the changing water levels in adjacent aquifers. The duration of a typical irrigation season may allow only a modest fraction of the potential yield from aquitard storage to enter the aquifer system, before pumping ceases for the season and ground-water levels recover in the aquifers. Typically, for thick aquitards, the next cycle of pumping begins before the fluid pressures in the aquitards have equilibrated with the previous cycle. The lagged response within the inner portions of a thick

aquitard may be largely isolated from the higher frequency seasonal fluctuations and more influenced by lower frequency, longer-term trends in ground-water levels. Because the migration of increased internal stress into the aquitard accompanies its drainage, as more fluid is squeezed from the interior of the aquitard, larger and larger internal intergranular stresses (effective stresses) propagate farther into the aquitard.

When the internal effective stresses exceed the preconsolidation stress, the skeletal compressibility increases dramatically, typically by a factor of 20 to 100 times (Riley, 1998), and the resulting compaction is largely nonrecoverable. At stresses greater than the preconsolidation stress, the lag in aquitard drainage increases by comparable factors, and concomitant compaction may require decades or centuries to approach completion. The *theory of hydrodynamic consolidation* (Terzaghi, 1925)—an essential element of the *aquitard drainage model*—describes the delay involved in draining aquitards when heads are lowered in adjacent aquifers, as well as the residual compaction that may continue long after drawdowns in the aquifers have essentially stabilized. Numerical modeling based on Terzaghi's theory has successfully simulated complex histories of compaction observed in response to measured water-level fluctuations (Helm, 1978).

Methods to simulate aquifer-system compaction were developed by Gambolati (1970, 1972a,b), Gambolati and Freeze (1973), Helm (1975, 1976), Narasimhan and Witherspoon (1977), and Neuman and others (1982). The one-dimensional (vertical) model presented by Helm (1975) computes compaction caused by specified ground-water level changes. This approach is used to analyze compaction at borehole extensometer sites for which there are detailed records of compaction and water-level changes (Epstein, 1987; Hanson, 1989; Pope and Burbey, 2003, 2004). Other approaches have focused on incorporating subsidence calculations in widely used two- or three-dimensional models of ground-water flow. Meyer and Carr (1979), Williamson and others (1989), and Morgan and Dettinger (1996) used modified finite-difference models to simulate ground-water flow and subsidence in the area of Houston, Texas; the Central Valley, California; and Las Vegas Valley, Nevada, respectively. Teatini and others (2006) used a finite-element model to simulate historical and future subsidence owing to ground-water pumping in the Emilia-Romagna coastland, Italy.

Leake and Prudic (1991) developed the Interbed Storage Package, version 1 (IBS1), to simulate regional-scale compaction of interbeds within aquifers using the ground-water model program, MODFLOW (McDonald and Harbaugh, 1988). IBS1 also can be used to simulate compaction of confining units if these units can be discretized into one or more model layers (Larson and others, 2001; Nishikawa and others, 2001). MODFLOW and the IBS1 Package also have been used to simulate regional ground-water flow and land subsidence (for example, Hanson and others, 1990; Hanson and Benedict, 1994; Galloway and others, 1998; Nishikawa and others, 2001; Kasmarek and Strom, 2002; Leighton and Phillips, 2003; Hanson and others, 2003, 2004), and one-dimensional ground-water flow and compaction measured at borehole extensometer sites (Sneed and Galloway, 2000; Pavelko, 2003).

The IBS1 formulation assumes that during one model time step, head changes in aquifer material are propagated throughout the entire thickness of compressible interbeds. Thus, the release of water from, or uptake of water into, interbed storage during this time step represents the full volume specified by the interbed storage coefficients (a function of the skeletal compressibility) and the change in aquifer hydraulic head. To relax this assumption, Leake (1990) developed the Interbed Storage Package, version 2 (IBS2). IBS2 allows the user to designate arbitrary systems of interbeds for which delay in release of water will be calculated. Previous studies used this approach to investigate the potential effects of land subsidence in the presence of delay interbeds (for example, Leake, 1990, 1991; Wilson and Gorelick, 1996; Hoffmann and others, 2003a). The SUB Package (Hoffmann and others, 2003b) for MODFLOW-2000 (Harbaugh and others, 2000) documents the IBS2 Package and retains the full functionality of the IBS1 Package.

The SUB Package formulations for delay and no-delay interbeds assume that the total load or geostatic stresses, and the vertical hydraulic conductivities and compressibilities that govern compaction of the deforming aquifer system remain constant. The SUB-WT Package (Leake and Galloway, 2007) for MODFLOW relaxes these assumptions and can be used to simulate changing stresses and compaction in unconfined (water table) and underlying confined aquifers owing to ground-water level variations in the

water table. The SUB-WT Package does not simulate a delay in the release of water from, or uptake of water into, interbed storage during a single model time step, similar to the IBS1 Package.

Simulations of subsidence attributed to oil, gas, and associated water extractions have used techniques based on physical principles similar to those described above for ground-water pumping (for example, Gambolati and Freeze, 1973; Geertsma, 1973; Gambolati and others, 1974a,b; Kosloff and others, 1980a,b; Sharp and Hill, 1995; Gambolati and others, 1999). Models using formulations similar to the Helm model were used to show that subsidence owing to deep petroleum production in the northeast coastal plain of Texas, could explain the additional subsidence that is occurring beyond that attributed to eustasy along the Texas coast (Sharp and Hill, 1995).

The conventional ground-water theory approach to evaluating aquifer-system compaction and land subsidence may be suitable for evaluating regional ground-water resources, but it has limitations in evaluating the hazards associated with ground displacements on local scales. The limiting assumption of purely vertical strain tends to overestimate the amount of vertical displacement (subsidence and uplift) and neglect the lateral displacements that may be important near production wells, and other areas where normally small lateral strains may be amplified such as near the margins of alluvial, basin-fill ground-water basins, and internally to the basins in areas susceptible to earth fissures and near pre-existing surface faults (Burbey, 2001; Burbey, 2002). With respect to evaluating hazards to pipelines, these factors should guide the evaluation and where relevant, the application of poroelastic models should be considered. Burbey (2002) used a granular displacement model (Burbey and Helm, 1999) based on Biot's consolidation theory and found that (1) earth fissures in the vicinity of faults that behave as either flow barriers, or a combination of flow and mechanical barriers, may be significantly influenced by horizontal deformation in aquifers; and (2) fissures in the vicinity of faults that do not behave as horizontal barriers to flow are probably more inclined to be caused by differential subsidence. Therefore, the presence of a surface fault and contrasting aquifer-hydraulic heads on either side of the fault would suggest that horizontal deformation could be important and perhaps should be evaluated prior to pipeline emplacement in these areas of developed ground-water basins.

Drainage of Organic Soils

Widespread drainage of organic soil-wetlands for agriculture has significantly altered the global carbon balance largely through oxidation, facilitated by aerobic microbial activity, of stored carbon and its release to the atmosphere as CO_2. Organic soils subside when they are drained continuously, and the phenomenon is controlled chiefly by the water and organic content, and the temperature of the soil.

Stephens and Stewart (1976) developed an empirical mathematical model to estimate the biochemical subsidence rate for low-moor organic soils:

$$S_T = (a + bD)Q_{10}^{(T-T_0)/10} \tag{2.2}$$

where S_T is the subsidence rate (cm/yr) at temperature T, a and b are constants, D is the depth of the water table, Q_{10} is the change in reaction rate for each 10°C rise in temperature, and T_0 is the threshold soil temperature where biochemical action becomes perceptible. Based on laboratory studies and field data, Stephens and Stewart (1976) found that the subsidence rate at the Everglades Experiment Station S_x could be expressed as

$$S_x = (-0.1035 + 0.0169D)(2)^{(T_x-5)/10}, \tag{2.3}$$

where T_x is the average annual soil temperature (°C) at the 10-cm depth. This relation was developed from organic soils with a mineral content of less than 15 percent, and bulk density of

approximately 0.22 g/cm^3. Muck soils with larger mineral contents and bulk densities would yield smaller subsidence rates under similar conditions.

A simple model for computing subsidence based on the measured CO_2 flux and specific organic soil properties was applied successfully in the Sacramento-San Joaquin Delta (Deverel and Rojstaczer, 1996) and in the Venice Lagoon catchment, Italy (Camporese and others, 2005):

$$\eta = \frac{f_c}{\rho}\frac{p_c}{p_o}, \tag{2.4}$$

where

η is the subsidence rate (LT^{-1}),

f_c is the CO_2 flux (in terms of carbon) resulting from oxidation of organic matter ($ML^{-2}T^{-1}$),

ρ is the soil bulk density (ML^{-3}),

p_c is the percentage of carbon in the soil organic matter, and

p_o is the percentage of organic matter content in the soil.

Van der Linden and others (2005) developed a preliminary numerical method that incorporates soil compaction and oxidation processes to simulate subsidence. This method is useful where the organic soils have significant mineral/clay content and compaction constitutes a significant fraction of the total subsidence.

Sinkholes

Because sinkholes result from a combination of many factors, forecasting their spatial and temporal occurrence is difficult. However, if relations between sinkholes and factors associated with their occurrence can be determined, it is possible to assess geologic hazards associated with pre-existing sinkholes in karst terranes and risks of new sinkhole formation.

Hazards and risk assessment provide a scientific basis for planning the development and construction of transportation and transmission infrastructure. Geologic mapping can identify karst areas and thus areas prone to sinkholes. Aerial photography and airborne LiDAR are useful in identifying specific karst features (such as sinkholes, sinks, and sinkhole lakes/ponds) on the landscape and frequently are used in the design and routing of pipelines through karst. Buried karst features such as paleosinkholes and mantled voids in the mantled karst region of Florida may not have identifiable surface expressions at local scales. Proposed pipeline routes through karst terrane where surface features are evident and where buried, concealed karst features are suspected can be evaluated using a combination of surface geophysical techniques (for example, seismic refraction tomography, seismic shear wave analysis, electrical resistivity, gravimetry, and ground-penetrating radar), test drilling and geotechnical methods (for example, cone penetrometer technology [CPT]). Information gleaned from the geohazards analysis can be used in engineering analyses to determine factors of safety for various pipeline spans and surface-loading conditions. The critical factors are the diameter of the sinkhole or buried cavity and the roof thickness or burial depth of the feature.

In regions prone to sinkholes, one identified and often overlooked risk factor for activating sinkhole formation is ground-water level differences related to the development of ground-water resources. Whitman and others (1999) positively correlated sinkholes with ground-water level differences between surficial aquifers and the underlying Floridan aquifer near Orlando, Florida using remote-sensing data, ground-water levels, and GIS.

In China, in recent decades about 70 percent of the documented sinkhole collapses are anthropogenic, and about 70 percent of those are attributed to ground-water pumping effects (Lei and others, 2002). Hu and others (2001) identified ground-water pumping and earthquakes as

principal risk factors for sinkhole formation in Tangshan, China, and developed a sinkhole risk-assessment model. Based on the results of the risk assessment, the risk of sinkhole formation in Tangshan is serious. High risk areas were identified in important sections of Tangshan, where there exists a serious danger to life and property. To mitigate the hazard, Hu and others (2001) recommended that (1) some high-risk areas be protected or strengthened, and that the northern part of the city should be a focus of future development because of its relatively low risk of sinkholes; (2) ground-water pumping should be limited, generally, and prohibited in specific areas of the city; and (3) further investigations should be carried out to understand the development and distribution of hidden karst features, such as caves and their related disturbed zones, and to develop effective mitigation methods.

Underground Mining

This section focuses on the analysis of subsidence associated with underground coal mining, but applies to underground mining in general. Surface subsidence due to underground coal mining is generally classified as pit subsidence or sag/trough subsidence. Pit subsidence is a circular hole in the ground with essentially vertical to belled-outward sidewalls (fig. 2.19*A*). The diameter of subsidence pits ranges from about 1 to 12 m and generally occurs over shallow mines (depths less than about 50 m) with incompetent bedrock overburden. Sag subsidence is a rectangular depression with gently sloping sides (fig. 2.19*B*) and is typically developed over room-and-pillar mines at greater depths (20 to 100 m or more) and with more competent overburden. Trough subsidence is similar in surface geometry to sag subsidence.

Pit and sag subsidence occurs more or less randomly and unexpectedly when pillars of coal collapse under overburden loading, typically long after an underground mine has been abandoned. Pit subsidence may involve collapse of only a few pillars, while sag subsidence may involve progressive failure of many pillars. Trough subsidence typically occurs in conjunction with longwall mining. The longwall mining technique involves use of moveable hydraulic roof supports, which make it possible to excavate blocks of coal on the order of 300 m wide and about 1,500–3,000 m long. Hydraulic roof supports are advanced behind the excavation so the mine roof and overlying rock fracture and collapse into the void behind the supports. Caving and fracturing propagate up through the overlying rock mass and bulking occurs until the collapsed rock supports the overlying strata (fig. 2.20*A*).

The overlying rock mass subsides and the ground surface ultimately deforms into a trough as shown along the axis of the mined-out panel in figure 2.20*B*. Around the margins of the trough the surface slopes downward over the edges of the longwall panel to a point of maximum subsidence displacement, which is usually about 50 to 80 percent of the mined thickness of coal. As mining continues, the subsidence bowl at the surface elongates in concert with the mined panel beneath the surface, and the transition zone over the advancing face of the longwall panel moves along as a waveform. The sloped zone over the advancing face of the mined panel will tend to flatten as the wave advances. Along the left and right sides of the mined panel, the sloped transitions will remain stationary as the panel extends in length and bounds the width of the subsidence bowl. A measure of the extent of ground surface affected by the mined panel is estimated by the angle of draw shown in figure 2.20.

Sag and trough subsidence takes the form of a reasonably predictable trough depression that will subject a buried pipeline to bending deformation and axial strain (compressive and tensile). Sag subsidence affects a larger area than pit subsidence, but much less than would occur in conjunction with trough subsidence due to longwall mining, and generally with less surface displacement. Surface subsidence and deformation profiles for longwall mining (figs. 2.20 and 2.21) are analogous to a bending beam. The difference in slope between points along a profile is the

curvature. Horizontal displacement is proportional to curvature and, therefore, slope (tilt) by a constant, c, that is analogous to the distance from the neutral axis to the outer fiber of a bending beam. The value of c varies from 0.30 to 0.4 times the ratio of depth (h) to the tangent of angle of influence (β):

$$c = \frac{(-0.35 \pm 0.05)h}{\tan \beta}. \tag{2.5}$$

Limited data on horizontal displacement accompanying subsidence over active mines has been used to constrain simulation of ground movements. Empirical (for example, National Coal Board, 1966; Karmis and others, 1987) and analytical (for example, Ren and others, 1987; Lin and others, 1992) models, and distinct-element models (for example, O'Connor and Dowding, 1992; Exadaktylos and others, 2007) have been used to simulate subsidence. The approach to estimating realistic values of horizontal and vertical ground displacements from subsidence typically requires calibration to case histories in which vertical displacements were monitored, for example, in underground coal mining—over longwall coal mine panels. Horizontal displacements are typically not available from these case histories and need to be estimated based upon analyses using a numerical model capable of computing both vertical and horizontal ground displacement patterns. The computed horizontal ground displacements for a case history are assumed to be those computed with a set of parameters that result in computed vertical displacements consistent with actual measured vertical displacements. Once calibrated in this manner, vertical and horizontal displacements can be determined using the numerical model for any hypothetical pipeline alignment through the subsidence zone.

Prediction of surface subsidence involves the use of mathematical models to compute the subsidence profile. Mathematical models based on the influence function approach assume that extracting a tiny element of an underground seam, for example a coal seam, will cause the ground surface to subside into a predefined shape such as a normal probability distribution. The ground surface directly above the extracted element receives the greatest amount of influence (fig. 2.22*A*). Coal seam elements offset from this location have less influence on that surface point (fig. 2.22*B*). The final subsidence at this point is the summation of the influence of each mined-out element. Explicit techniques that employ finite-element or distinct-element models are capable of accounting for the engineering characteristics of various rock strata as well as the orientation of bedding planes and pre-existing faults. However, the more explicit modeling techniques require much more information than the influence function models, and the numerous input parameters can make it much more difficult to calibrate to case histories.

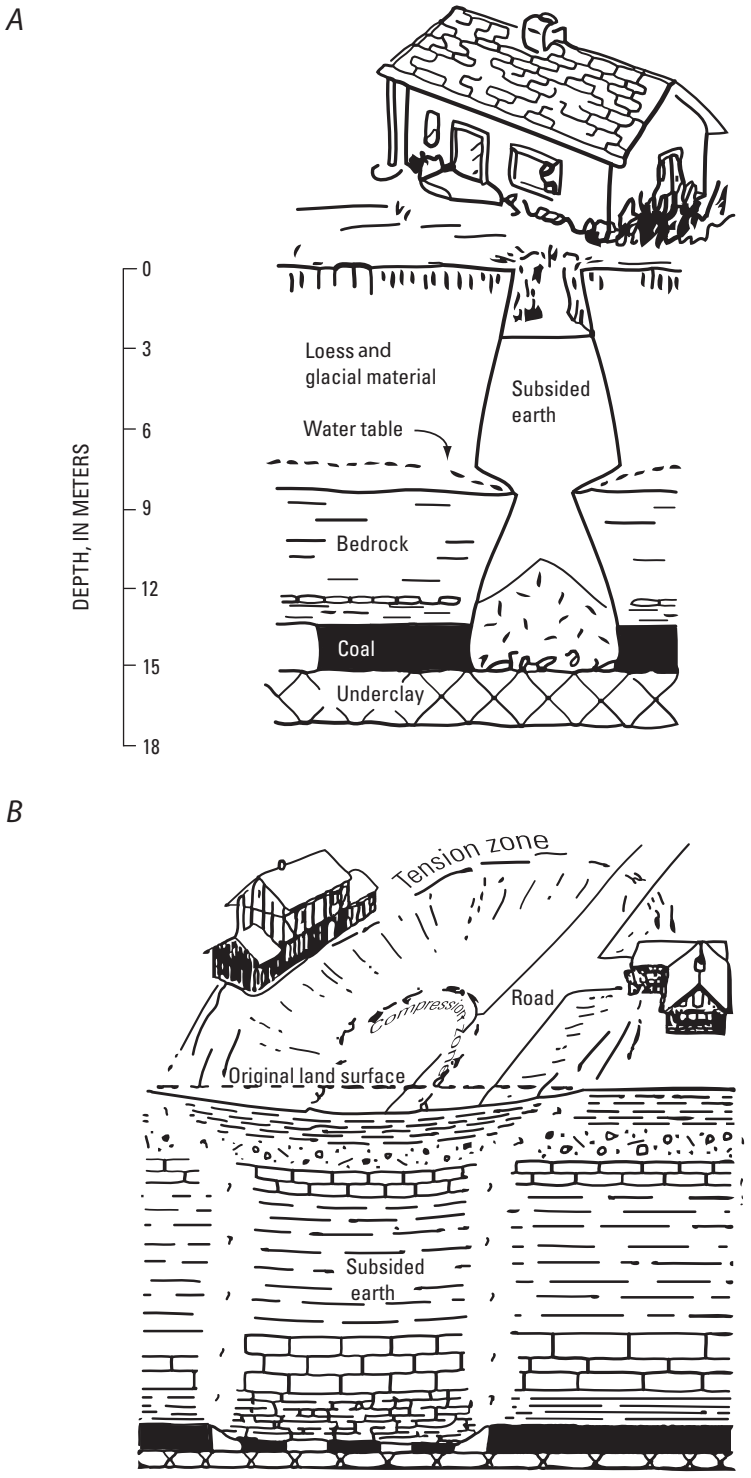

Figure 2.19. Typical types of subsidence associated with underground coal mining: *A.* Pit subsidence, and *B.* Sag subsidence (modified from Bauer and Hunt, 1982).

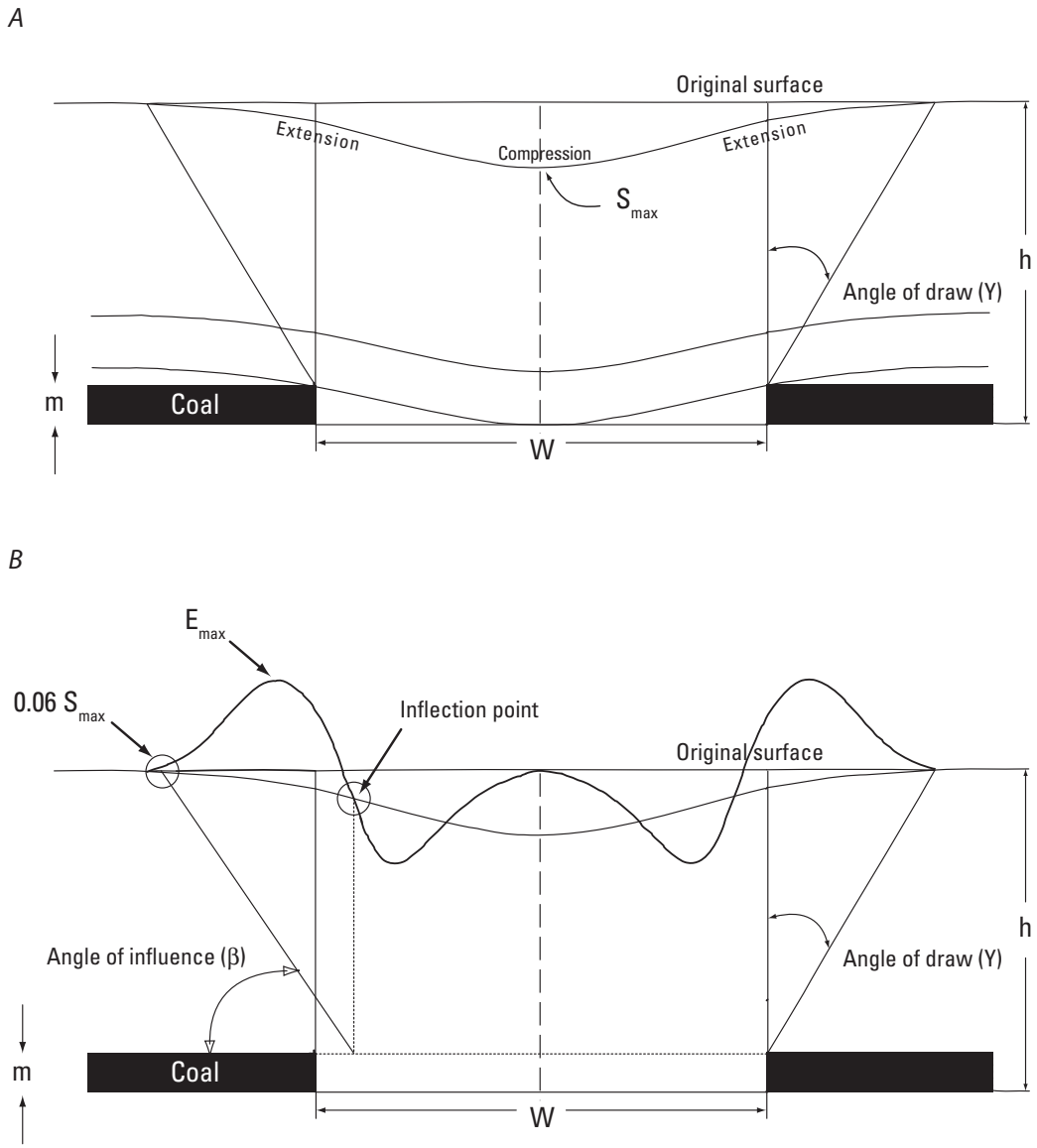

Figure 2.20. Typical profiles and parameters for analyzing deformation associated with underground coal mining: *A.* Subsidence, and *B.* Horizontal strain. (**W** is width of mined-out panel; **h** is depth; $\mathbf{S_{max}}$ is maximum subsidence; $\mathbf{E_{max}}$ is maximum extension)

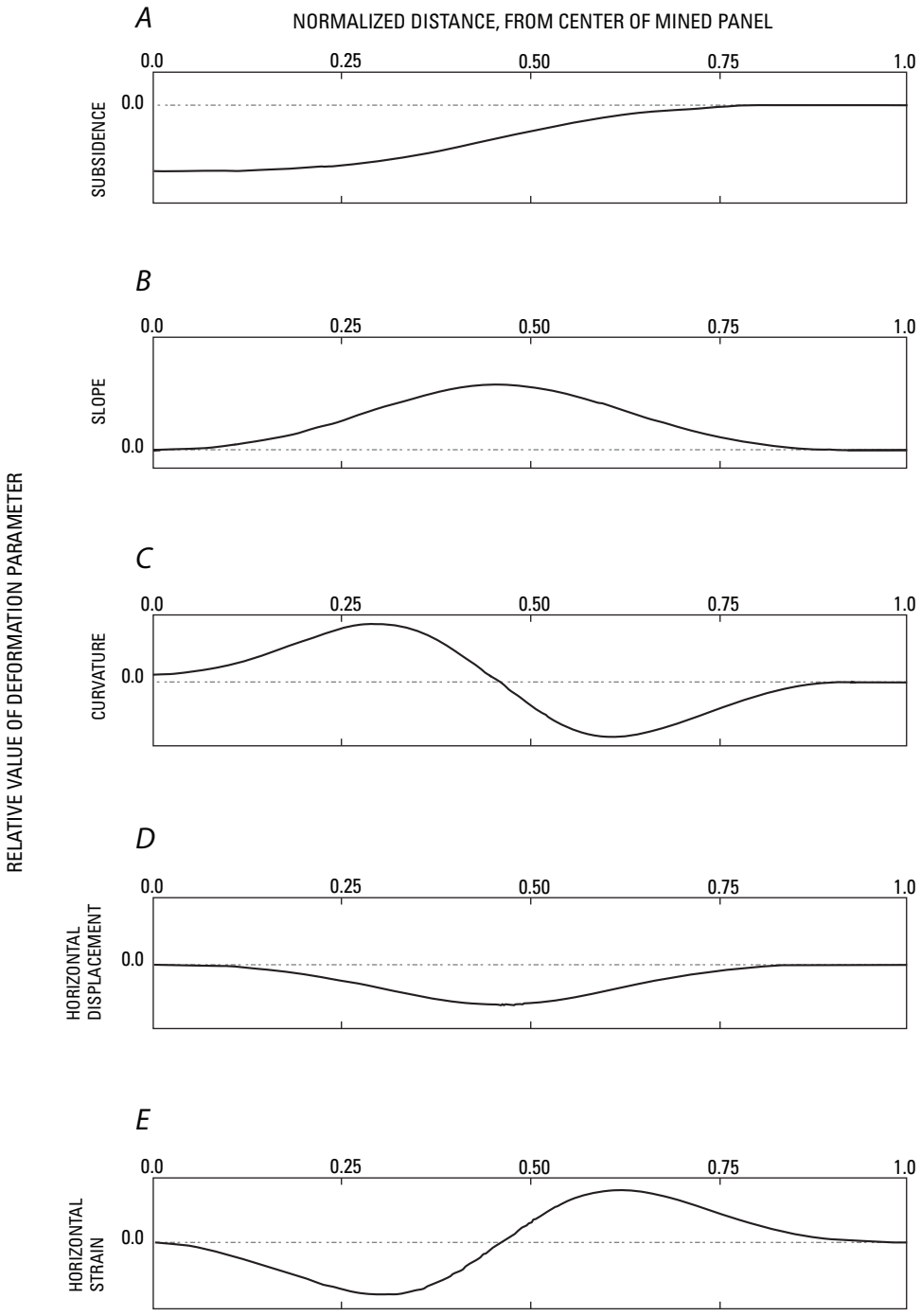

Figure 2.21. Deformation profiles for idealized subsidence feature above underground coal mine: *A.* Subsidence. *B.* Slope. *C.* Curvature. *D.* Horizontal displacement. *E.* Horizontal strain.

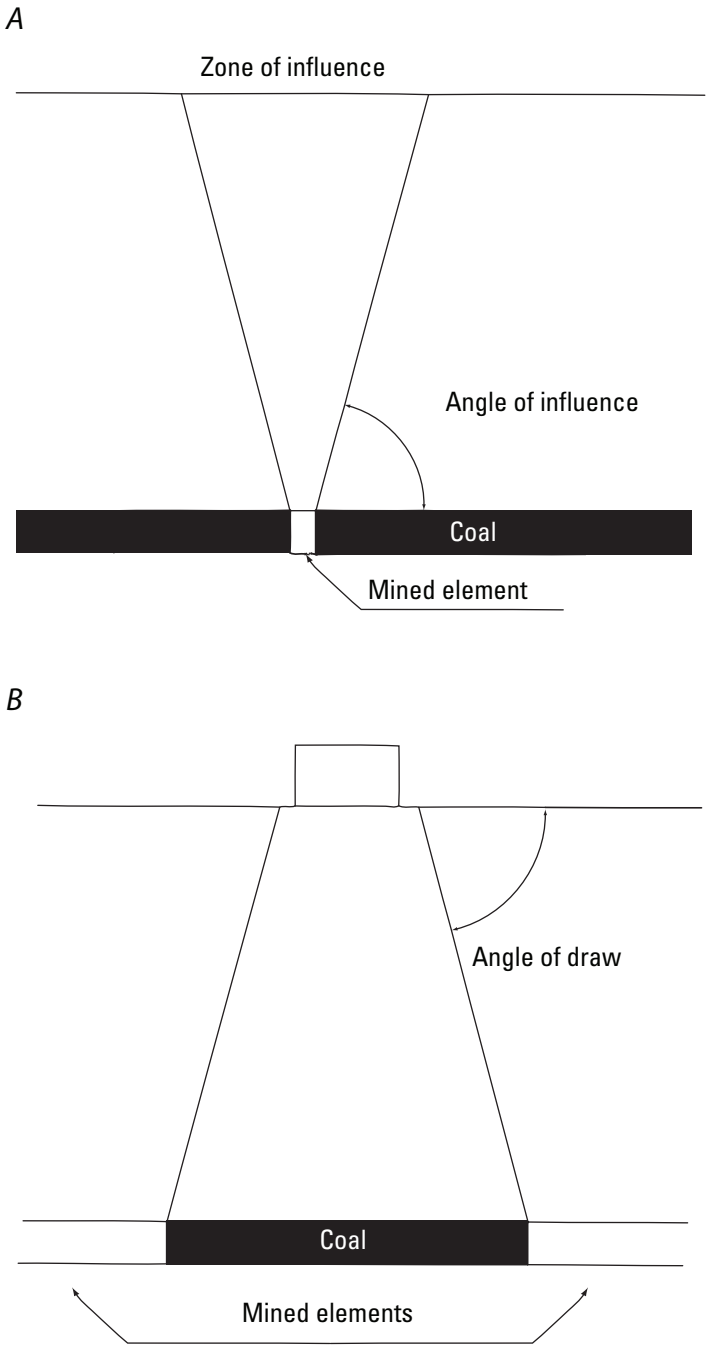

Figure 2.22. Schematic of: *A.* Zone of influence above a mined-out element, and *B.* Subjacent support between two mined-out elements separated by an intact element.

Hydrocompaction

Hydrocompactive or collapsible soils lose a significant amount of volume through reduction of porosity when wetted, and have caused tens of millions of dollars in damage to private and public infrastructure in the USA, including Arizona (Soil Conservation Service, 1975), California (Bull, 1964; Lofgren, 1969), Iowa (Handy, 1973), New Mexico (Love, 2001) and Utah (Kaliser, 1978). For example, on the west side of the San Joaquin Valley, California, hydrocompaction caused $8 million in damage and added an extra $15 million to the cost of constructing canals (National Research Council, 1991).

The susceptibility to subsidence hazards owing to hydrocompaction is difficult to identify and infrequently is incorporated into pipeline-design guidelines. The low-density soils can be detected in boreholes using geophysical density logs, nuclear density gages, or by collecting undisturbed samples and testing for relative density. Hydrocompaction susceptibility largely has been determined by combining soils maps with laboratory data on soil properties to develop maps of "collapse probabilities." Research and geotechnical investigations in New Mexico (for example, Lovelace and others, 1982; Johnpeer and others, 1985; Shaw and Johnpeer, 1985a,b; Haneberg and others, 1992) have produced a large body of information concerning the identification and mitigation of hydrocompactive deposits and associated engineering problems. Experience in British Columbia indicates that soils or fills having in-place densities less than 90 percent of standard Proctor maximum dry density are susceptible to sudden collapse or settlement (Richard Butler, Golder and Associates Ltd., written commun., 2007). Extensive studies of loess or loess-like soils over a period of many years in China, have developed criteria to differentiate the susceptibility of various deposits in differing geographic or climatic regions to sudden collapse or subsidence as a result of wetting (Lin and Liang, 1982).

Reimers (1986) conducted a geotechnical study of hydrocompactive deposits at El Llano, New Mexico, including stepwise multiple regression and discriminant function analyses, in an attempt to delineate index properties that might be used to identify potentially hydrocompactive soils. Most collapsible soils have dry densities ranging from 1.20 to 1.52 gm/cm^3, low Atterberg limits, low moisture content (1–l0 percent), and are poorly graded to silty sands with only minor amounts of clay (1–3 percent). Their soil structure is characterized by delicate grain-point contacts, clay and silt aggregates that bond the larger sand grains together, clay-coated sand grains (cutans), and high porosities, 30–40 percent. Some typical values of geotechnical index properties of collapsible soils near El Llano, New Mexico, are shown in table 2.3.

Table 2.3. Geotechnical index properties of collapsible soils near El Llano, New Mexico (modified from Haneberg and others, 1992).

[Textures are Unified Soil Classification System group symbols: SW—well graded, fine to coarse sand, SP—poorly graded sand, SM—silty sand, and SC—clayey sand]

Index Property	Typical Values
Texture	SW, SP, SM, or SC
Dry Density	1.20-1.52 gm/cm^3
Void Ratio	0.5-1.0
Moisture Content	4-10% by weight
Saturation	<60%
Liquid Limit	0-40
Plastic Limit	0-20
Total Consolidation Upon Wetting	> 5%
Specific Gravity, Granular	2.50-2.65
Clay Mineralogy	smectite, illite, mixed-layer, kaolinite
Blow Count (N value)	<18
P-wave Velocity	<300 m/sec

Thawing Permafrost

During the past two decades, a number of permafrost numerical models have been developed to evaluate spatial and temporal changes in permafrost related to global climate change. Despite the importance of permafrost in the climate-change sciences, modeling of permafrost has remained highly diverse and uncertain regarding appropriate methods, their accuracy, and their applicability to different scales and climatic conditions (Shiklomanov and others, 2004). Typically, permafrost models employ numerical multi-layer one-dimensional models of ground-heat transfer, accounting for phase transitions of moisture as well as snow and vegetation covers. A wide range of numerical models has been developed (Goodrich, 1978; Guymon and others, 1984; Romanovsky and others, 1997; Romanovsky and Osterkamp, 2000; Malevsky-Malevich and others, 2001; Machul'skaya and Lykosov, 2002; Ling and Zhang, 2003; Molkentin and others, 2003; Sergueev and others, 2003). Typical input parameters of a permafrost model include skin temperature at the upper boundary of snow or vegetation cover, the thickness of snow and vegetation covers, and physical properties of soils. At the lower boundary of the domain, the geothermal heat flux generally is prescribed. The principal observational parameters usually are permafrost temperature and the thickness of the active layer or frost zone—the top layer of soil that seasonally freezes and thaws.

Many permafrost-related processes are two- or three-dimensional (such as soil settlement upon thawing, thermokarst development, and differential frost heave). Therefore, even on the local scale, two- and three-dimensional permafrost models are better suited to simulate permafrost dynamics. Prevalent local and regional-scale heterogeneity of permafrost properties raises concerns about the ability of deterministic models, regardless of their dimensionality or scale, to make accurate estimates of the volume of thawed soil. An alternative approach is to consider near-surface permafrost parameters as randomly, spatially distributed variables consisting of both deterministic and stochastic components and to use their probability distribution functions as the metric for evaluation (Anisimov and others, 2002).

Natural Consolidation

Analytical and numerical modeling approaches have been used to simulate overpressures, compaction (porosity reduction), and long-term subsidence rates in geologic basins undergoing natural consolidation. Partially-coupled models using simplifying assumptions (for example, Bredehoeft and Hanshaw, 1968; Bethke, 1989) simulate poroelastic ground-water flow and compaction using formulations for standard ground-water flow with geologic forcing treated as source/sink term (Γ):

$$S_s \frac{\partial h}{\partial t} = \nabla \cdot \bar{K} \nabla h + \Gamma, \tag{2.6}$$

where

S_s is specific storage (L^{-1}),

h is hydraulic head (L),

$\bar{K}$ is the hydraulic conductivity tensor (LT^{-1});

and where compaction, the geologic forcing, is simulated using

$$\Gamma = C_L \frac{\partial l_s}{\partial t}, \tag{2.7}$$

where

C_L is a loading coefficient (dimensionless), and

l_s is the elevation of the sedimentary surface (L).

This approach has been used to demonstrate that compressional strain from loading, and the accompanying subsidence, is capable of generating overpressures in rapidly accreting sedimentary basins (Ingebritsen and others, 2006).

Summary

Land subsidence poses hazards to pipelines. The principal causes of land subsidence in the United States are subsurface fluid withdrawal, drainage of organic soils, sinkholes, underground mining, hydrocompaction, thawing permafrost, and natural consolidation. Many subsidence areas have been identified, mapped, and documented. Most anthropogenic land subsidence in the United States is caused by the withdrawal of subsurface fluids from unconsolidated porous granular media; humans also have caused widespread and significant subsidence by other processes. As measured by area affected, mining of coal and minerals, and drainage of organic soils are the most significant of the other processes.

An area's susceptibility to subsidence can be evaluated through compilation of available geologic, hydrogeologic, and geodetic information as well as other ancillary and anecdotal information such as increased incidences of damaged or protruding wells, a history of adjustments to local geodetic controls, increasing incidences of coastal or riverine flooding, local conveyance and drainage problems, and ground failures—surface faulting and earth fissuring. Measuring, mapping, and monitoring subsidence is needed to adequately assess subsidence hazards. Analysis and simulation of subsidence processes, constrained by the available data, often are used to refine assessments of present and future hazards.

Various ground-based, airborne and space-based methods are used for mapping and measuring spatial gradients and temporal rates of regional and local subsidence and horizontal ground motion. These include conventional geodetic techniques such as spirit leveling and GPS, extensometric methods using horizontal and borehole extensometers, satellite synthetic aperture radar techniques such as interferometric synthetic aperture radar (InSAR) and permanent scatterer interferometry (PSI), and tripod-mounted and airborne LiDAR.

Analyses of subsidence-prone areas typically address material surface- and subsurface-geologic properties, and the potential physical and chemical processes causing land subsidence. The types of analyses generally include laboratory and field measurements, and analytical and numerical modeling of subsidence processes. Numerous numerical models have been developed and applied to simulate subsidence owing to aquifer-system compaction caused by ground-water extractions. Few models have been specifically developed to simulate subsidence attributed to other mechanisms. Some general purpose hydraulic-mechanical-thermal models have been used to simulate some of the various other processes.

Calibrated, numerical aquifer-system compaction models have been used to forecast subsidence in a number of study areas for specified future ground-water extraction and recharge scenarios. Two subsidence-simulation modules, the SUB and SUB-WT Packages, have been developed for the widely used MODFLOW ground-water flow model. The SUB package is used to simulate either the instantaneous or delayed compaction of aquitards under conditions of constant geostatic stress, and is applicable to confined aquifer systems with a static overlying water table. The SUB-WT Package is used to simulate the instantaneous compaction of aquitards under conditions of changing geostatic stresses and stress-dependent hydraulic and mechanical properties. The SUB-WT Package is applicable to confined and unconfined aquifer systems with a dynamic overlying water table.

Empirical and analytical models, and to a limited extent, numerical models are used to simulate subsidence accompanying (1) the extraction of subsurface oil and gas, (2) the drainage and subsequent compaction and oxidation of organic soils, (3) sinkholes in carbonate and evaporite rocks, (4) underground mining, (5) thawing permafrost, and (6) natural consolidation.

References Cited

Ahlfeld, D.P., Barlow, P.M., and Mulligan, A.E., 2005, GWM—A ground-water management process for the U.S. Geological Survey modular ground-water flow model (MODFLOW-2000): U.S. Geological Survey Open-File Report 2005-1072, 124 p., *http://pubs.usgs.gov/of/2005/1072/*, accessed June 11, 2007.

Ahlfeld, D.P., and Mulligan, A.E., 2000, Optimal management of flow in groundwater systems: San Diego, Calif., Academic Press, 185 p.

Amelung, Falk, Galloway, D.L., Bell, J.W., Zebker, H.A., and Laczniak, R.L., 1999, Sensing the ups and downs of Las Vegas—InSAR reveals structural control of land subsidence and aquifer-system deformation: Geology, v. 27, no. 6, p. 483–486.

Anisimov, O.A., Shiklomanov, N.I., and Nelson, F.E., 2002, Variability of seasonal thaw depth in permafrost regions—A stochastic modeling approach: Ecological Modeling, 153(3), p. 217–227.

Barras, J., Beville, S., Britsch, D., Hartley, S., Hawes, S., Johnston, J., Kemp, P., Kinler, Q., Martucci, A., Porthouse, J., Reed, D., Roy, K., Sapkota, S., and Suhayda, J., 2003 (revised January 2004), Historical and projected coastal Louisiana land changes—1978–2050: U. S. Geological Survey Open-File Report 03-334, 39 p., *http://pubs.er.usgs.gov/usgspubs/ofr/ofr03334*, accessed December 3, 2007.

Bauer, R.A., and Hunt, S.R., 1982, Profile, strain and time characteristics of subsidence from coal mining in Illinois, *in* Peng, S.S., and Harthill, M., eds., Proceedings, Workshop on Surface Subsidence due to Underground Mining: West Virginia University, Morgantown, W. Va., Nov. 1981, p. 207–219.

Bawden, G.W., 2002, Optimizing GPS arrays to image both tectonic and anthropogenic deformation: EOS Trans., AGU Fall Meet Suppl 83(52), abstract G22A-11.

Bawden, G.W., 2003, Separating ground-water and hydrocarbon-induced surface deformation from geodetic tectonic contraction measurements across metropolitan Los Angeles, California, *in* Prince, K.R., and Galloway, D.L., eds., U.S. Geological Survey subsidence interest group conference, proceedings of the technical meeting, Galveston, Texas, November 27-29, 2001: U.S. Geological Survey Open-File Report 03-308, p. 81-89, *http://pubs.usgs.gov/of/2003/ofr03-308/*, accessed March 28, 2007.

Bawden, G.W., Thatcher, Wayne, Stein, R.S., Hudnut, K.W., and Peltzer, Gilles, 2001, Tectonic contraction across Los Angeles after removal of groundwater pumping effects: Nature, v. 412, p. 812–815.

Beaver J., Tatlow M., Cohen D., Marra M., 2005, Monitoring subsidence trends in Phoenix with SAR interferometry: EOS Trans., AGU Fall Meet Suppl 86(52), abstract G51C-0852.

Bell, J.W., Amelung, Falk, Ferretti, Alessandro, Bianchi, Marco, and Novali, Fabrizio, 2008, Permanent scatterer InSAR reveals seasonal and long-term aquifer system response to groundwater pumping and artificial recharge: Water Resources Research, v. 44, W02407, doi:10.1029/2007WR006152, 18 p..

Bell, J.W., Amelung, Falk, Ramelli, A.R., and Blewitt, Geoff, 2002, Land subsidence in Las Vegas, Nevada, 1935-2000: New geodetic data show evolution, revised spatial patterns, and reduced rates: Environmental and Engineering Geoscience, v. III, no. 3, p. 155–174.

Bethke, C.M., 1989, Modeling subsurface flow in sedimentary basins: Geologische Rundschau, 78(1), p. 129–154.

Biot, M.A., 1941, General theory of three-dimensional consolidation: Journal of Applied Physics, v. 12, p. 155–164.

Borchers, J.W., Gerber, Martin, Wiley, Jeffrey, and Mitten, H.T., 1998, Using down-well television surveys to evaluate land subsidence damage to water wells in the Sacramento Valley, California, *in* Borchers, J.W., ed., Land subsidence—Case studies and current research, Proceedings of the Dr. Joseph F. Poland Symposium on Land Subsidence: Association of Engineering Geologists Special Publication 8, p. 89–105.

Bredehoeft, J.D., and Hanshaw, B.B., 1968, On the maintenance of anomalous fluid pressures—1, Thick sedimentary sequences: Geological Society of America Bulletin, v. 79, p. 1,097–1,106.

Bull, W.B., 1964, Alluvial fans and near-surface subsidence in western Fresno County California: U.S. Geological Survey Professional Paper 437-A, 71 p., *http://pubs.er.usgs.gov/usgspubs/pp/pp437A*, accessed June 15, 2007.

Burbey, T.J., 2001, Storage coefficient revisited—Is purely vertical strain a good approximation?: Ground Water, v. 39, no. 3, p. 458–464.

_____, 2002, The influence of faults in basin-fill deposits on land subsidence, Las Vegas, Nevada, USA: Hydrogeology Journal, v. 10, no. 5, p. 525–538.

Burbey, T.J., and Helm, D.C., 1999, Modeling three-dimensional deformation in response to pumping of unconsolidated aquifers: Environmental & Engineering Geoscience, 5, p. 199–212.

California Department of Conservation, *undated*, Guidelines for preparing geologic reports for regional-scale environmental and resource management planning: Division of Mines and Geology, Note 52, 8 p., *http://www.consrv.ca.gov/cgs/information/publications/cgs_notes/note_52/note_52.pdf*, accessed June 7, 2007.

California Department of Water Resources, 1964, Design and construction studies of shallow land subsidence for the California Aqueduct in the San Joaquin Valley—Interim report, California Department of Water Resources, 130 p.

Camporese, M., Gambolati, G., Putti, M., Teatini, P., Bonardi, M., Rizzetto, F., Tosi, L., Ferraris, S., Gasparetto Stori, G., Nicoletti, V., Silvestri, S., and Salandin, P., 2005, Monitoring and modeling peat soil subsidence in the Venice Lagoon, *in* Zhang, A., Gong, S., Carbognin, L., and Johnson, A.I., eds., Land subsidence—Proceedings of the Seventh International Symposium on Land Subsidence: Shanghai Scientific and Technical Publishers, v. 2, p. 543–551.

Canadian Geotechnical Society, 2006, Canadian Foundation Engineering Manual (4th ed.): Richmond, B.C., Canada, BiTech Publisher Ltd., 504 p.

Canuti, P., Casagli, N., Farina, P., Marks, F., Ferretti, A., and Menduni, G., 2005, Land subsidence in the Arno River Basin studied through SAR interferometry, *in* Zhang, A., Gong, S., Carbognin, L., and Johnson, A.I., eds., Land subsidence—Proceedings of the Seventh International Symposium on Land Subsidence: Shanghai Scientific and Technical Publishers, v. 1, p 407–416.

Carpenter, M.C., 1993, Earth-fissure movements associated with fluctuations in ground-water levels near the Picacho Mountains, south-central Arizona, 1980–84: U.S. Geological Survey Professional Paper 497-H, 116 p., *http://pubs.er.usgs.gov/usgspubs/pp/pp497H*, accessed March 29, 2007.

Carpenter, M.C., 1999, South-central Arizona—Earth fissures and subsidence complicate development of desert water resources, *in* Galloway, D.L., Jones, D.R., and Ingebritsen, S.E., eds., Land subsidence in the United States: U.S. Geological Survey Circular 1182, p. 65–78, *http://pubs.usgs.gov/circ/circ1182/pdf/09Arizona.pdf*, accessed May 23, 2007.

Chang, Hsing-Chung, Ge, Linlin, and Rizos, C., 2005, DInSAR for mine subsidence monitoring using multi-source satellite SAR images: Proceedings, Geoscience and Remote Sensing Symposium, 2005, IEEE International v3, 25-29 July 2005 p. 1742 – 1745, doi:10.1109/IGARSS.2005.1526339.

Chilingarian, G.V., Donaldson, E.C., and Yen, T.F., eds., 1995, Subsidence due to fluid withdrawal: Amsterdam, Elsevier Science, Developments in Petroleum Science 41, 498 p.
Danskin, W.R., Kasmarek, M.C., and Strom, E.W., 2003, Optimal withdrawal of elastically stored ground water in the Chicot Aquifer, Houston Area, Texas, *in* Prince, K.R., and Galloway, D.L., eds., U.S. Geological Survey Subsidence Interest Group Conference, Proceedings of the Technical Meeting, Galveston, Texas, November 27-29, 2001: U.S. Geological Survey Open-File Report 03-308, p. 39-48, *http://pubs.usgs.gov/of/2003/ofr03-308/*, accessed June 11, 2007.
Darby, H.C., 1956, The draining of the fens (2nd ed.): Oxford, Cambridge University Press, 314 p.
Davies, W.E., and LeGrand, H.E., 1972, Karst of the United States, *in* Herak, M. and Stringfield, V.T., eds., Karst—important karst regions of the northern hemisphere: New York, Elsevier Publishing Co., p. 467–505.
Detournay, E., and Cheng, A.H-D., 1993, Fundamentals of poroelasticity, *in* Fairhurst, C., ed., Volume 2—Analysis and design methods, *in* Hudson, J.A., ed., Comprehensive rock engineering principles, practice and projects: Pergamon Press, chapt. 5, p. 113–117.
Deverel, S.J., and Rojstaczer, S.A., 1996, Subsidence of agricultural lands in the Sacramento-San Joaquin Delta, California: Role of aqueous and gaseous carbon fluxes: Water Resources Research, v. 32, p. 2,359–2,367.
Dunrud, C.R., 1984, Coal mine subsidence—western United States, *in* Holzer, T.L., ed., Man-induced land subsidence: Geological Society of America Reviews in Engineering Geology, v. 6, p. 151–194.
Ege, J.R., 1984, Mechanisms of surface subsidence resulting from solution extraction of salt, *in* Holzer, T.L., ed., Man-induced land subsidence: Geological Society of America Reviews in Engineering Geology, v. 6, p. 203–221.
Epstein, V.J., 1987, Hydrologic and geologic factors affecting land subsidence near Eloy, Arizona: U.S. Geological Survey Water-Resources Investigations Report 87-4143, 28 p., *http://pubs.er.usgs.gov/usgspubs/wri/wri874143*, accessed April 2, 2007.
Exadaktylos, G., Tsouvala, S., Liolios, P., and Barakos, G., 2007, A three-dimensional model of an underground excavation and comparison with *in situ* measurements: International Journal for Numerical and Analytical Methods in Geomechanics, v. 31, no. 3, doi: 10.1002/nag.587, p. 411–433.
Ferretti A., Prati C., and Rocca F., 2000, Nonlinear subsidence rate estimation using permanent scatterers in differential SAR interferometry: IEEE Trans Geosci Remote Sens 38, p. 2,202–2,212.
Ferretti A., Prati C., and Rocca F., 2001, Permanent scatterers in SAR interferometry: IEEE Trans Geosci Remote Sens 39(1), p. 8–20.
Ferretti A., Novali R., Bürgmann R., Hilley G., and Prati C., 2004, InSAR permanent scatterer analysis reveals ups and downs in the San Francisco Bay Area: EOS 85(34), p. 317–324.
Fialko, Yuri, and Simons, Mark, 2000, Deformation and seismicity in the Coso geothermal area, Inyo County, California: Observations and modeling using satellite radar interferometry: Journal of Geophysical Research, v. 25, p. 21, 781–21,794.
Fielding, E.J., Blom, R.G., and Goldstein, R.M., 1998, Rapid subsidence over oil fields measured by SAR interferometry: Geophysical Research Letters, v. 27, p. 3,215–3,218.
Fruneau, B., and Sarti, F., 2000, Detection of ground subsidence in the city of Paris using radar interferometry—Isolation of deformation from atmospheric artifacts using correlation: Geophysical Research Letters, v. 27, no. 24, p. 3,981–3,984, doi: 10.1029/2000GL008489.
Gabriel, A.K., Goldstein, R.M., and Zebker, H.A., 1989, Mapping small elevation changes over large areas—Differential radar interferometry: Journal of Geophysical Research, v. 94, p. 9,183–9,191.

Galloway, D.L., and Hoffmann, Jörn, 2007, The application of satellite differential SAR interferometry-derived ground displacements in hydrogeology: Hydrogeology Journal, v. 15(1), doi: 10.1007/s10040-006-0121-5, p. 133–154.
Galloway, D.L., Hudnut, K.W., Ingebritsen, S.E., Phillips, S.P., Peltzer,G., Rogez, F., and Rosen, P.A., 1998, Detection of aquifer system compaction and land subsidence using interferometric synthetic aperture radar, Antelope Valley, Mojave Desert, California: Water Resources Research, v. 34, no. 10, p. 2,573–2,585.
Galloway, D.L., Jones, D.R., and Ingebritsen, S.E., eds., 1999, Land subsidence in the United States: U.S. Geological Survey Circular 1182, 177 p., *http://pubs.usgs.gov/circ/circ1182/*, accessed March 28, 2007.
Galloway, D.L., Jones, D.R., and Ingebritsen, S.E., 2000, Measuring land subsidence from space: U.S. Geological Survey Fact Sheet 051-00, 4 p., *http://pubs.usgs.gov/fs/fs-051-00/,* accessed March 28, 2007.
Gambolati, G., 1970, A one-dimensional model of the subsoil for computing the surface subsidence: IBM Venice Scientific Center Technical Report CRV002, Venice, Italy, 57 p.
_____, 1972a, Estimate of subsidence in Venice using a one-dimensional model of the subsoil: International Business Machines Journal of Research and Development, v. 16, no 2, p. 130–137.
_____, 1972b, A three-dimensional model to compute land subsidence: Bulletin of the International Association of Hydrological Science, v. 17, no. 2, p. 219–227.
Gambolati, G., Gatto, P., and Freeze, R.A., 1974a, Mathematical simulation of the subsidence of Venice, 2, Results: Water Resources Research, v. 10, p. 563–577.
Gambolati, G., Gatto, P., and Freeze, R.A., 1974b, Predictive simulation of the subsidence of Venice: Science, v. 183, p. 849–851.
Gambolati, G., and Freeze, R.A., 1973, Mathematical simulation of the subsidence of Venice, 1, Theory: Water Resources Research, v. 9, no. 3, p. 721–733.
Gambolati, Giuseppe, Teatini, Pietro, and Tomasi, Lucio, 1999, Stress-strain analysis in productive gas/oil reservoirs: International Journal for Numerical and Analytical Methods in Geomechanics, v. 23(13), doi: 10.1002/(SICI)1096-9853(199911)23:13, p. 1,495–1,519.
Geertsma, J., 1973, Land subsidence above compacting oil and gas reservoirs: Journal of Petroleum Technology, p. 734–744.
Gilluly, J., and Grant, U.S., 1949, Subsidence in the Long Beach Harbor area, California: Geological Society of America Bulletin, v. 60, p. 461–530.
González, J.L., and Törnqvist, T.E., 2006, Coastal Louisiana in crisis—Subsidence or sea level rise?: EOS, Transactions of the American Geophysical Union, v. 87, no. 45, p. 493–498.
Goodrich, L.E., 1978, Efficient numerical technique for one-dimensional thermal problems with phase change: International Journal of Heat and Mass Transfer, 21(5), p.160–163.
Gray, R.E., and Bruhn, R.W., 1984, Coal mine subsidence—eastern United States, *in* Holzer, T.L., ed., Man-induced land subsidence: Geological Society of America Reviews in Engineering Geology, v. 6, p. 123–149.
Guymon, G.L., Hromadka, T.V., and Berg, R.L., 1984, Two-dimensional model of coupled heat and moisture transport in frost-heaving soils: Journal of Energy Resources Technology, 106, p. 336–343.
Hamilton, D.H., and Meehan, R.L., 1971, Ground rupture in the Baldwin Hills: Science, v. 172, p. 333–344.
Handy, R.L., 1973, Collapsible loess in Iowa: Proceedings of the Soil Science Society of America, v. 37, no. 2, p. 281–284.
Haneberg, W., Bauer, P.W., and Chavez, Jr., W.X., 1992, Rio Grande Gorge highway corridor study, Rinconada to Pilar: New Mexico Bureau of Mines and Mineral Resources Open-File

Report 437, 22 p., 2 maps, scale 1:24,000, *http://geoinfo.nmt.edu/publications/openfile/downloads/OFR400-499/426-450/437/ofr_437.pdf*, accessed June 8, 2007.
Hanson, R.T., 1989, Aquifer-system compaction, Tucson Basin and Avra Valley, Arizona: U.S. Geological Survey Water-Resources Investigations Report 88-4172, 69 p., *http://pubs.er.usgs.gov/usgspubs/wri/wri884172*, accessed April 2, 2007.
Hanson, R.T., Anderson, S.R., and Pool, D.R., 1990, Simulation of ground-water flow and potential land subsidence, Avra Valley, Arizona: U.S. Geological Survey Water-Resources Investigations Report 90-4178, 41 p., *http://pubs.er.usgs.gov/usgspubs/wri/wri904178*, accessed April 3, 2007.
Hanson, R.T., and Benedict, J.F., 1994, Simulation of ground-water flow and potential land subsidence, upper Santa Cruz Basin, Arizona: U.S. Geological Survey Water-Resources Investigations Report 93-4196, 47 p., *http://pubs.er.usgs.gov/usgspubs/wri/wri934196* accessed April 3, 2007.
Hanson, R.T., Li, Zhen, and Faunt, C.C., 2004, Documentation of the Santa Clara Valley regional ground-water/surface-water flow model, Santa Clara Valley, California: U.S. Geological Survey Scientific Investigations Report 2004-5231, 85 p., *http://pubs.usgs.gov/sir/2004/5231/*, accessed June 11, 2007.
Hanson, R.T., Martin, Peter, and Koczot, K.M., 2003, Simulation of ground-water/surface-water flow in the Santa Clara—Calleguas ground-water basin, Ventura County, California: U.S. Geological Survey Water–Resources Investigations Report 02-4136, 214 p., *http://pubs.er.usgs.gov/usgspubs/wri/wri024136*, accessed April 3, 2007.
Harbaugh, A.W., Banta, E.R., Hill, M.C., and McDonald, M.G., 2000, MODFLOW-2000, the U.S. Geological Survey modular ground-water model—User guide to modularization concepts and the ground-water flow process: U.S. Geological Survey Open-File Report 2000-92, 121 p., *http://pubs.er.usgs.gov/usgspubs/ofr/ofr0092*, accessed April 3, 2007.
Harris, F.M., and Harlow, E.H., 1947, Subsidence of the Terminal Island-Long Beach area, California: American Society of Civil Engineers Proceedings, v. 73, no. 8, p. 1,197–1,218.
Harrison, W.J., and Summa, L.L., 1991, Paleohydrology of the Gulf of Mexico Basin: American Journal of Science, v. 291, p. 109–176.
Hart, B.S., Flemings, P.B., and Deshpande, A., 1995, Porosity and pressure—Role of compaction disequilibrium in the development of geopressures in a Gulf Coast Pleistocene basin: Geology, 23(1), p. 45–48.
Helm, D.C., 1975, One-dimensional simulation of aquifer system compaction near Pixley, California, 1. constant parameters: Water Resources Research, v. 11, no. 3, p. 465–478.
_____, 1976, One-dimensional simulation of aquifer system compaction near Pixley, California, 2. stress-dependent parameters: Water Resources Research, v. 12, no. 3, p. 375–391.
_____, 1978, Field verification of a one-dimensional mathematical model for transient compaction and expansion of a confined aquifer system: Verification of Mathematical and Physical Models in Hydraulic Engineering, American Society of Civil Engineers Hydraulics Division Specialty Conference, 26th, University of Maryland, College Park, Md., August 9–11, 1978, p. 189–196.
_____, 1984, Field-based computational techniques for predicting subsidence due to fluid withdrawal, *in* Holzer, T.L., ed., Man-induced land subsidence: Geological Society of America Reviews in Engineering Geology, v. 6, p. 1–22.
Hinzman, L.D., Bettez, N.D., Bolton, W.R., Chapin, F.S., Dyurgerov, M.B., Fastie, C.L., Griffith, B., Hollister, R.D., and others, 2005, Evidence and implications of recent climate change in northern Alaska and other Arctic regions: Climate Change, v. 72 (3), doi: 10.1077/s10584-005-5352-2, p. 251–298.

Hoffmann, Jörn, Galloway, D.L., and Zebker, H.A., 2003a, Inverse modeling of interbed storage parameters using land subsidence observations, Antelope Valley, California: Water Resources Research, v. 39 (2), doi: 10.1029/2001WR001252, p. SBH 5-1–5-10.

Hoffman, Jörn, Leake, S.A., Galloway, D.L., and Wilson, A.M., 2003b, MODFLOW-2000 ground-water model—User guide to the subsidence and aquifer-system compaction (SUB) package: U.S. Geological Survey Open-File Report 03-233, 46 p., *http://pubs.usgs.gov/of/2003/ofr03-233/*, accessed March 28, 2007.

Hoffmann, Jörn, Zebker, H.A., Galloway, D.L., and Amelung, F., 2001, Seasonal subsidence and rebound in Las Vegas Valley, Nevada, observed by synthetic aperture radar interferometry: Water Resources Research, v. 37, no. 6, p 1,551–1,566.

Holzer, T.L., 1981, Preconsolidation stress of aquifer systems in areas of induced land subsidence: Water Resources Research, v. 17, no. 3, p. 693–704.

_____, 1984, Ground failure induced by ground-water withdrawal from unconsolidated sediment, *in* Holzer, T.L., ed., Man-induced land subsidence: Geological Society of America Reviews in Engineering Geology, v. 6, p. 67–105.

_____, 1998, History of the aquitard-drainage model in land subsidence case studies and current research, *in* Borchers, J.W., ed., Land subsidence case studies and current research: Proceedings of the Dr. Joseph F. Poland symposium on land subsidence, Association of Engineering Geologists Special Publication No. 8, p. 7–12.

Holzer, T.L., and Gabrysch, R.K., 1987, Effect of water-level recoveries on fault creep, Houston, Texas: Ground Water, v. 25, no. 4, p. 392–397.

Holzer, T.L., and Galloway, D.L., 2005, Impacts of land subsidence caused by withdrawal of underground fluids in the United States, *in* Ehlen, J., Haneberg, W.C., and Larson, R.A., eds., Humans as geologic agents: Geological Society of America Reviews in Engineering Geology, v. 16, p. 87–99, doi: 10.1130/2005.4016(08).

Hooper A., Zebker, H.A., Segall, P., Kampes, B., 2004, A new method for measuring deformation on volcanoes and other natural terrains using InSAR persistent scatterers: Geophysical Research Letters 31:L23611. doi: 10.1029/2004GL021737.

HRB Singer, Inc., 1977, Nature and distribution of subsidence problems affecting HUD and urban areas: U.S. Department of Housing and Urban Development, 113 p. (Available from NTIS, PB 80172778).

Hsieh, P.A., 1996, Deformation-induced changes in hydraulic head during ground-water withdrawal: Ground Water, v. 36, no. 6, p. 1,082–1,089.

Hu, R., Yeung, M., Lee, C., Wang, S., and Xiang, J., 2001, Regional risk assessment of karst collapse in Tangshan, China: Environmental Geology, v. 40(11-12), doi: 10.1007/s002540100319, p. 1,377–1,389.

Ikehara, M.E., and Phillips, S.P., 1994, Determination of land subsidence related to ground-water level declines using global positioning system and leveling surveys in Antelope Valley, Los Angeles and Kern Counties, California, 1992: U.S. Geological Survey Water-Resources Investigations Report 94-4184, 101 p., *http://pubs.er.usgs.gov/usgspubs/wri/wri944184*, accessed March 29, 2007.

Ingebritsen, S.E., Sanford, W.E., and Neuzil, C.E., 2006, Groundwater in geologic processes, 2nd edition: New York, Cambridge Univ. Press, 536 p.

Ingerson, I. M., 1941, The hydrology of the southern San Joaquin Valley, California, and its relation to imported water supplies: Transactions American Geophysical Union, v. 22, p. 20–45.

IPCC, 2001, Climate change 2001—The scientific basis, Contribution of Working Group I to the Third Assessment Report of the Intergovernmental Panel on Climate Change, Houghton, J.T.,

Ding, Y., Griggs, D.J., Noguer, M., van der Linden, P.J., Dai, X., Maskell, K., and Johnson, C.A., eds.: Cambridge, United Kingdom and New York, NY, USA, Cambridge University Press, 881 p.
Jachens, R.C., and Holzer, T.L., 1982, Differential compaction mechanism for earth fissures near Casa Grande, Arizona: Geological Society of America Bulletin, v. 93, no. 10, p. 998–1,012.
Jacob, C.E., 1940, On the flow of water in an elastic artesian aquifer: American Geophysical Union Transactions, v. 21, p. 574–586.
Jarosz, A., and Wanke, D.D., 2004, Use of InSAR for monitoring of mining deformations, *in* Lacoste, H., ed., Proceedings of the FRINGE 2003 Workshop, Frascatti, Italy, 1-5 December 2003: ESA Special Publication 550, [CDROM] p. 44.1.
Johnpeer, G.D., Love D.W., Hawley, J.W., Bobrow, D., Hemingway, M., and Reimers, R.F., 1985, El Llano and vicinity geotechnical study—final report: Socorro, New Mexico Bureau of Mines and Mineral Resources, Open-File Report 226, variously paginated, *ftp://geoinfo.nmt.edu/Open-files/OFR200-299/226-250/226/ofr_226.pdf*, accessed June 14, 2007.
Johnson, K.S., 2005, Salt dissolution and subsidence or collapse caused by human activities, *in* Ehlen, J., Haneberg, W.C., and Larson, R.A., eds., Humans as geologic agents: Geological Society of America Reviews in Engineering Geology, v. 16, p. 101–110, doi: 10.1130/2005.4016(09).
Johnson, W., and Miller, G.C., 1979, Abandoned coal-mined lands; nature, extent, and cost of reclamation: U.S. Department of the Interior, Bureau of Mines, 20 p.
Kaliser, B.N., 1978, Relative hydrocompaction susceptibility map, Cedar City, Utah: Utah Geological Survey Map No. 44.
Kampes, D., 2005, Displacement parameter estimation using permanent scatterer interferometry: DLR-Forschungsberichte 16.
Karmis, M., Jarosz, A. and Schilizzi, P., 1987, Monitoring and prediction of ground movements above underground mines in the Eastern United States, *in* Peng, S., ed., Proceedings of the 6th International Conference on Ground Control in Mining: Department of Mining Engineering, West Virginia University, p. 184–194.
Kasmarek, M.C., and Strom, E.W., 2002, Hydrogeology and simulation of ground-water flow and land-surface subsidence in the Chicot and Evangeline aquifers, Houston-Galveston region, Texas: U.S. Geological Survey Water-Resources Investigations Report 02-4022, 68 p., *http://pubs.er.usgs.gov/usgspubs/wri/wri024022*, accessed April 3, 2007.
King, N.E., Argus, D., Langbein, J., Agnew, D.C., Bawden, G.W., Dollar, R.S., Liu, Z., Galloway, D., Reichard, E., Yong, A., Webb, F.H., Bock, Y., Stark, K., and Barseghian, D., 2007, Space geodetic observation of expansion of the San Gabriel Valley, California, aquifer system, during heavy rainfall in winter 2004–2005: Journal of Geophysical Research, v. 112, B03409, doi:10.1029/2006JB004448.
Kircher, M., 2004, Analyse flächenhafter Senkungserscheinungen in sedimentären Gebieten mit den neuen Techniken der Radarfernerkundung am Beispiel der Niederrheinischen Bucht [Analysis of extensive subsidence in sedimentary areas with the new techniques of radar remote sensing using the example of the lower Rhine basin]: Universität Bonn, Germany, PhD Thesis, 109 p.
Kosloff, D., Scott, R.F., and Scranton, J., 1980a, Finite element simulation of Wilmington oil field subsidence, I—Linear modeling: Tectonophysics, v. 65, p. 339–368.
Kosloff, D., Scott, R.F., and Scranton, J., 1980b, Finite element simulation of Wilmington oil field subsidence, II—Nonlinear modeling: Tectonophysics, v. 70, p. 159–183.
Larson, K.J., Basagaolu, H., and Mario, M., 2001, Numerical simulation of land subsidence in the Los Banos-Kettleman City area, California: University of California Davis Water Resources Center Technical Completion Report Contribution no. 207, 83 p.

Leake, S.A., 1990, Interbed storage changes and compaction in models of regional ground-water flow: Water Resources Research, v. 26, no. 9, p. 1,939–1,950.

_____, 1991, Simulation of vertical compaction in models of regional ground-water flow, *in* Johnson, A.I., ed., Land subsidence—Proceedings of the Fourth International Symposium on Land Subsidence, May 12–17, 1991: Houston, Texas, International Association of Hydrological Sciences Publication, 200, p. 565–574, *http://www.cig.ensmp.fr/~iahs/redbooks/a200/iahs_200_0565.pdf*, accessed December 3, 2007.

Leake, S.A., and Galloway, D.L., 2007, MODFLOW ground-water model—User guide to the Subsidence and Aquifer-System Compaction Package (SUB-WT) for water-table aquifers: U.S. Geological Survey Techniques and Methods Report 6–A23, 42 p., *http://pubs.usgs.gov/tm/2007/06A23/*, accessed December 3, 2007.

Leake, S.A., and Prudic, D.E., 1991, Documentation of a computer program to simulate aquifer-system compaction using the modular finite-difference ground-water flow model: U.S. Geological Survey Techniques of Water-Resources Investigations, book 6, chap. A2, 68 p., *http://pubs.usgs.gov/twri/twri6a2/*, accessed March 28, 2007.

Lei, Mingtang, Jiang, Xiaozhen, Yu, Li, 2002, New advances in karst collapse research in China: Environmental Geology, v. 42, doi: 10.1007/s00254-001-0506-7, p. 462–468.

Leighton, D.A., and Phillips, S.P., 2003, Simulation of ground-water flow and land subsidence in the Antelope Valley ground-water basin, California: U.S. Geological Survey Water-Resources Investigations Report 03-4016, 118 p., *http://pubs.er.usgs.gov/usgspubs/wri/wri034016*, accessed April 3, 2007.

Lin, Shumin, Reddish, D.J., and Whittaker, B.N., 1992, An integrated analytical model of subsidence induced by level seam extractions: Geotechnical and Geological Engineering, v. 10, p. 203–221.

Lin, Z., and Liang, W., 1982, Engineering properties and zoning of loess and loess-like soils in China: Canadian Geotechnical Journal, Issue 19, p. 76–91.

Ling, F., and Zhang, T., 2003, Impact of the timing and duration of seasonal snow cover on the active layer and permafrost in the Alaskan Arctic: Permafrost and Periglacial Processes, 14, p. 141–150.

Lofgren, B.E., 1969, Land subsidence due to the application of water, *in* Varnes, D.J., and Kiersch, G.A., eds., Reviews in Engineering Geology, v. 2, p. 271–303.

Love, D.W., 2001, What decision makers should know about collapsible soils in New Mexico, *in* Johnson, P.S., ed., Water, watersheds, and land use in New Mexico—Impacts of population growth on natural resources, Santa Fe region 2001: New Mexico Bureau of Mines and Mineral Resources, New Mexico Decision-Makers Field Guide No. 1, p. 61–62, *http://geoinfo.nmt.edu/publications/decisionmakers/2001/dmfg2001_complete.pdf*, accessed June 14, 2007.

Lovelace, A.D., Bennett, W.D., and Lueck, R.D., 1982, Test section for the stabilization of collapsible soils on Interstate 25, Project 1-025-4(58) 243, Algodones, New Mexico: Santa Fe, Geotechnical Section, Materials Laboratory Bureau, New Mexico State Highway Department Report MB-RR-83-1, 27 p.

Lucas, R.E., 1982, Organic soils (Histosols)—Formation, distribution, physical and chemical properties and management for crop production: Michigan State University Farm Science Research Report 435, 77 p.

MacFarlane, I. C., 1969, Engineering characteristics of peat, *in* MacFarlane, I.C., ed., Muskeg engineering handbook: Toronto, University of Toronto Press, p. 78–126.

Machul'skaya, E.E., and Lykosov, V.N., 2002, Simulation of the thermodynamic response of permafrost to seasonal and interannual variations in atmospheric parameters: Izvestiya. Atmosph. Ocean Physics, 38, p. 20–33.
Magara, Kinji, 1978, Compaction and fluid migration: New York, Elsevier Scientific Publishing Co., 319 p.
Malevsky-Malevich, S.P., Molkentin, E.K., Nadyozhina, T.D., and Shklyarevich, O.B., 2001, Numerical simulation of permafrost parameters distribution: Cold. Reg. Sci. andTech., no. 32, p. 1–11.
Martin, J.C., and Serdengecti, S., 1984, Subsidence over oil and gas fields, *in* Holzer, T.L., ed., Man-induced land subsidence: Geological Society of America Reviews in Engineering Geology, v. 6, p. 23–34.
Martinez, J.D., Johnson, K.S., and Neal, J.T., 1998, Sinkholes in evaporite rocks: American Scientist, v. 86, p. 38–51.
Massonnet, D., Briole, P., and Arnaud, A., 1995, Deflation of Mount Etna monitored by spaceborne radar interferometry: Nature, v. 375, p. 567–570.
Massonnet, D., and Feigl, K.L., 1998, Radar interferometry and its application to changes in the earth's surface: Reviews of Geophysics, v. 36, p. 441–500.
Massonnet, D., Holzer, T., and Vadon, H., 1997, Land subsidence caused by the East Mesa geothermal field, California, observed using SAR interferometry: Geophysical Research Letters, v. 24, p. 901–904.
Massonnet, D., Rossi, M., Carmona, C., Adragna, F., Peltzer, G., Feigl, K., and Rabaute, T., 1993, The displacement field of the Landers earthquake mapped by radar interferometry: Nature, v. 364, p. 138–142.
Maxey, G.B., and Jameson, C.H., 1948, Geology and water resources of Las Vegas, Pahrump, and Indian Springs Valleys, Clark and Nye Counties, Nevada: Nevada State Engineer Water Resources Bulletin 5, 121 p.
Mayuga, M.N., and Allen, D.R., 1969, Subsidence in the Wilmington oil field, Long Beach, California, U.S.A., *in* Tison, L.J., ed., Land subsidence, Volume 1: International Association of Scientific Hydrology Publication 88, p. 66–79, *http://www.cig.ensmp.fr/~iahs/redbooks/a088/088013.pdf*, accessed December 2, 2007.
McDonald, M.G., and Harbaugh, A.W., 1988, A modular three-dimensional finite-difference ground-water flow model: U.S. Geological Survey Techniques of Water-Resources Investigations, book 6, chap. A1, 586 p., *http://pubs.er.usgs.gov/usgspubs/twri/twri06A1*, accessed April 3, 2007.
McMillan, J.F., 1973, Land subsidence—Antelope Valley area of Los Angeles County: County of Los Angeles, Department of County Engineer, Survey Division, variously paginated, and Survey Division File Map No. 65-58.
Meyer, W.R., and Carr, J.E., 1979, A digital model for simulation of ground-water hydrology in the Houston area, Texas: U.S. Geological Survey Open-File Report 79-677, 143 p., [currently not available on line].
Molkentin E.K., Nadyozhina, E.D., and Shklyarevich, O.B., 2003, Model estimates of vegetation impact on permafrost degradation in the warming climate: Russian Meteorology and Hydrology, no. 3, p. 87–95.
Morgan, D.S., and Dettinger, M.D., 1996, Ground-water conditions in Las Vegas Valley, Clark County, Nevada, Part 2. Hydrogeology and simulation of ground-water flow: U.S. Geological Survey Water-Supply Paper 2320-B, 124 p., 2 plates, *http://pubs.er.usgs.gov/usgspubs/wsp/wsp2320B*, accessed April 3, 2007.

Morton, R.A., Bernier, J.C., and Barras, J.A., 2006, Evidence of regional subsidence and associated interior wetland loss induced by hydrocarbon production, Gulf Coast region, USA: Environmental Geology, v. 50, doi 10.1007/s00254-006-0207-3, p. 261–274.
Nagel, N.B., 2001, Compaction and subsidence issues within the petroleum industry—From Wilmington to Ekofisk and beyond: Physics and Chemistry of the Earth, v. 26, p. 3–14.
Narasimhan, T.N., and Witherspoon, P.A., 1977, Numerical model for saturated-unsaturated flow in deformable porous media, 1. Theory: Water Resources Research, v. 13, p. 657–664.
National Coal Board, 1966 (rev. 1975), Subsidence engineers' handbook: London, Hobart House, NCB Publications, 111 p.
National Research Council, 1991, Mitigating losses from land subsidence in the United States: Washington, D.C., National Academy Press, 58 p.
Neuendorf, K.K.E., Mehl, J.P., Jr., and Jackson, J.A., 2005, Glossary of Geology, 5th edition: Alexandria, VA, American Geological Institute, 779 p.
Neuman, S.P., Preller, C., and Narasimhan, T.N., 1982, Adaptive explicit-implicit quasi three-dimensional finite element model of flow and subsidence in multiaquifer systems: Water Resources Research, v. 18, no. 5, p. 1,551–1,561.
Nieuwenhuis, H.S., and Schokking, F., 1997, Land subsidence in drained peat areas of the Province of Friesland, the Netherlands: Quarterly Journal of Engineering Geology, v. 30, p. 37–48.
Nishikawa, Tracy, Rewis, D.L., and Martin, Peter, 2001, Numerical simulation of ground-water flow and land subsidence at Edwards Air Force Base, Antelope Valley, California: U.S. Geological Survey Water-Resources Investigations Report 01-4038, 111 p., [currently not on line].
O'Connor, K.M., and Dowding, Ch. H., 1992, Distinct element modeling and analysis of mining-induced subsidence: Rock Mechanics and Rock Engineering, v. 25, p. 1–25.
Osterkamp, T.E., and Romanovsky, V.E., 1996, Characteristics of changing permafrost temperatures in the Alaskan Arctic, U.S.A.: Arctic and Alpine Research 28 (3), p. 267–273.
Paine, J.G., 1993, Subsidence of the Texas coast—Inferences from historical and late Pleistocene sea levels: Tectonophysics, v. 222, p. 445–458.
Parson E.A, Carter, Lynne, Anderson, Patricia, Wang, Bronwen, and Weller, Gunter, 2001, Potential consequences of climate variability and change for Alaska, *in* National Assessment Synthesis Team, Climate change impacts on the United States—The potential consequences of climate variability and change: Cambridge, U.K., Cambridge Univ. Press, Report for the U.S. Global Change Research Program, chapt. 10, p. 283–312, *http://www.usgcrp.gov/usgcrp/Library/nationalassessment/10Alaska.pdf* accessed April 30, 2007.
Pavelko, M.T., 2003, Estimates of hydraulic properties from a one-dimensional numerical model of vertical aquifer-system deformation, Lorenzi Site, Las Vegas, Nevada: U.S. Geological Survey Water-Resources Investigations Report 03-4083, 35 p., *http://pubs.usgs.gov/wri/wri034083/index.html,* accessed April 2, 2007.
Penland, S., and Ramsey, K.E., 1990, Relative sea-level rise in Louisiana and the Gulf of Mexico—1908–1988: Journal of Coastal Research, v. 6, p. 323–342.
Penland S., Ramsey, K.E., McBride, R.A., Mestayer, J.T., and Westphal, K.A., 1988, Relative sea-level rise and delta-plain development in the Terrebonne Parish region: Louisiana Geological Survey Coastal Geology Tech Report 4.
Phillips, S.P., Carlson, C.S., Metzger, L.F., Howle, J.F., Galloway, D.L., Sneed, M., Ikehara, M.E., Hudnut, K.W., and King, N.E., 2003, Analysis of tests of subsurface injection, storage, and recovery of freshwater in Lancaster, Antelope Valley, California: U.S. Geological Survey Water-Resources Investigations Report 03-4061, 122 p., *http://ca.water.usgs.gov/pubs/wrir_03-4061.html*, accessed June 11, 2007.

Poland, J.F., and Davis, G.H., 1969, Land subsidence due to withdrawal of fluids, *in* Varnes, D.J., and Kiersch, G., eds.: Geological Society of America Reviews in Engineering Geology, v. 2, p. 187–269.

Pope, J.P., and Burbey, T.J., 2003, Characterization and modeling of land subsidence due to ground-water withdrawals from the confined aquifers of the Virginia Coastal Plain, *in* Prince, K.R., and Galloway, D.L., eds., U.S. Geological Survey Subsidence Interest Group Conference, Proceedings of the Technical Meeting, Galveston, Texas, November 27-29, 2001: U.S. Geological Survey Open-File Report 03-308, p. 49–56, *http://pubs.usgs.gov/of/2003/ofr03-308/*, accessed June 11, 2007.

Pope J.P., and Burbey T.J., 2004, Multiple-aquifer characterization from single borehole extensometer records: Ground Water, v 42, no. 1, p. 45–58.

Pratt, W.E., and Johnson, D.W., 1926, Local subsidence of the Goose Creek oil field: Journal of Geology, v. 34, p. 577–590.

Reimers, R.F., 1986, Geology, collapse mechanisms, and prediction of collapsible soil in El Llano, New Mexico: Socorro, New Mexico Bureau of Mines and Mineral Resources, Open-File Report 239, 249 p., *ftp://geoinfo.nmt.edu/Open-files/OFR200-299/226-250/239/ofr_239.pdf*, accessed June 14, 2007.

Ren, G., Reddish, D.J., and Whittaker, B.N. 1987, Mining subsidence and displacement prediction using influence function methods: Mining Science and Technology, v. 5, p. 89–104.

Riley, F.S., 1969, Analysis of borehole extensometer data from central California, *in* Tison, L.J., ed., Land subsidence, Volume 2: International Association of Scientific Hydrology Publication 89, p. 423–431, *http://www.cig.ensmp.fr/~iahs/redbooks/a088/088047.pdf*, accessed July 11, 2007.

_____, 1986, Developments in borehole extensometry, *in* Johnson, I.A., Carborgnin, Laura, and Ubertini, L., eds., Land subsidence: International Association of Scientific Hydrology Publication 151, p. 169–186, *http://www.cig.ensmp.fr/~iahs/redbooks/a151/iahs_151_0169.pdf*, accessed November 27, 2007.

_____, 1998, Mechanics of aquifer systems—The scientific legacy of Joseph F. Poland, *in* Borchers, J.W., ed., Land Subsidence—Case studies and current research, Proceedings of the Dr. Joseph F. Poland Symposium on Land Subsidence: Association of Engineering Geologists Special Publication 8, p. 13–27.

Roberts, H.H., Bailey A., and Kuecher, G.J., 1994, Subsidence in the Mississippi River delta—important influences of valley filling by cyclic deposition, primary consolidation phenomena, and early diagenesis: Transactions of the Gulf Coast Association of Geological Societies, v. 44, p. 619–629.

Robinson, G.M., and Peterson, D.E., 1962, Notes on earth fissures in southern Arizona: U.S. Geological Survey Circular 466, 7 p., *http://pubs.er.usgs.gov/usgspubs/cir/cir466*, accessed April 27, 2007.

Rojstaczer, S.A., and Deverel, S.J., 1993, Time dependence of atmospheric carbon inputs from drainage of organic soils: Geophysical Research Letters, v. 20, p. 1,383–1,386.

Romanovsky, V.E., and Osterkamp, T.E., 2000, Effects of unfrozen water on heat and mass transport processes in the active layer and permafrost: Permafrost and Periglacial Processes, 11, p. 219–239.

Romanovsky, V.E., Osterkamp, T.E., and Duxbury, N., 1997, An evaluation of three numerical models used in simulations of the active layer and permafrost temperature regimes: Cold Regions Science and Technology, 26, p. 195–203.

Rosen, P., Hensley, S., Zebker, H., and Webb, F., 1996, Surface deformation and coherence measurements of Kilauea Volcano, Hawaii, from SIR-C radar interferometry: Journal of Geophysical Research, v. 101(B10), p. 23,109–23,125.
Sandhu, R.S., 1979, Modeling land subsidence, *in* Saxena, S.K., ed., Evaluation and prediction of subsidence: American Society of Civil Engineers, p. 565–579.
Schmidt, D.A., and Bürgmann, R., 2003, Time dependent land uplift and subsidence in the Santa Clara Valley, California, from a large InSAR data set: Journal of Geophysical Research, 108(B9), 2416, doi:10.1029/2002JB002267.
Schothorst, C.J., 1977, Subsidence of low moor peat soils in the western Netherlands: Geoderma, v. 17, p. 265–291.
Schumann, H.H., 1995, Land subsidence and earth-fissure hazards near Luke Air Force Base, Arizona, *in* Prince, K.R., Galloway, D.L., and Leake, S.A., eds., U.S. Geological Survey Subsidence Interest Group Conference, Edwards Air Force Base, Antelope Valley, California, November 18–19, 1992: Abstracts and summary: U.S. Geological Survey Open-File Report 94-532, p. 18–21, *http://pubs.usgs.gov/of/1994/ofr94-532/*, accessed December 3, 2007.
Sergueev, D., Tipenko, G., Romanovsky, V., and Romanovskii, N., 2003, Mountain permafrost thickness evolution under influence of long-term climate fluctuations (results of numerical simulation): Proceedings of the VIII International Permafrost Conference, Switzerland, July 21–25, p. 1,017–1,021.
Sharp, J.M., Jr., and Domenico, P.A., 1976, Energy transport in thick sequences of compacting sediment: Geological Society of America Bulletin, v. 87, p. 390–400.
Sharp, J.M., Jr., and Hill, D.W., 1995, Land subsidence along the northeastern Texas Gulf coast—Effects of deep hydrocarbon production: Environ. Geol., v. 25, p. 181–191.
Shaw, D., and Johnpeer, G., 1985a, Ground subsidence near Espanola, New Mexico: New Mexico Geology, v. 7, p. 32–34.
Shaw, D., and Johnpeer, G., 1985b, Ground-subsidence study near Espanola and recommendations for construction on collapsible soils: New Mexico Geology, v. 7, p. 59–62.
Shih, S.F., Glaz, B., and Barnes, Jr., R.E., 1998, Subsidence of organic soils in the Everglades Agricultural Area during the past 19 years: Soil and Crop Science Society of Florida Proceedings 57:20–29.
Shiklomanov, N.I., Anisomov, O.A., Romanovsky, V.E., and Zhang, T., 2004, Spatially distributed permafrost models—Current status, problems and needs: EOS, Transactions American Geophysical Union, 85(47), Fall Meet. Suppl., Abstract C12A-01.
Sneed, Michelle, and Galloway, D.L., 2000, Aquifer-system compaction and land subsidence: measurements, analyses, and simulations—the Holly site, Edwards Air Force Base, Antelope Valley, California: U.S. Geological Survey Water-Resources Investigations Report 00-4015, 65 p., *http://ca.water.usgs.gov/archive/reports/wrir004015/*, accessed April 3, 2007.
Soil Conservation Service, 1975, Selected soil features and interpretations for major soils of Arizona: Tucson, Arizona Agricultural Experiment Station, 22 p.
Stephens, J.C., Allen, L.H., Jr., and Chen, Ellen, 1984, Organic soil subsidence, *in* Holzer, T.L., ed., Man-induced land subsidence: Geological Society of America Reviews in Engineering Geology, v. 6, p. 107–122.
Stephens, J.C., and Stewart, E.H., 1976, Effect of climate on organic soil subsidence, *in* Johnson, A.I., ed., Land subsidence: International Association of Scientific Hydrology Publication 121, p. 647–655, *http://www.cig.ensmp.fr/~iahs/redbooks/a121/iahs_121_0647.pdf*, accessed December 3, 2007.
Swanson, A.A., 1998, Land subsidence in the San Joaquin Valley, updated to 1995, *in* Borchers, J.W., ed., Land subsidence—Case studies and current research, Proceedings of the Dr. Joseph F.

Poland Symposium on Land Subsidence: Association of Engineering Geologists Special Publication 8, p. 75–79.
Teatini, P., Ferronato, M., Gambolati, G., and Gonella, M., 2006, Groundwater pumping and land subsidence in the Emilia-Romagna coastland, Italy—Modeling the past occurrence and the future trend: Water Resources Research, v. 42(1), W01406, doi:10.1029/2005WR004242.
Terzaghi, K., 1925, Erdbaumechanik auf bodenphysikalisher Grundlage [Earthworks mechanics based on soil physics]: Vienna, Austria, Deuticke, 399 p.
Thatcher, W., and Massonnet, D., 1997, Crustal deformation at Long Valley caldera, eastern California, 1992–1996 inferred from satellite radar interferometry: Geophysical Research Letters, v. 24, no. 20, p. 2,519–2,522.
Tolman, C.F., and Poland, J.F., 1940, Ground-water infiltration, and ground-surface recession in Santa Clara Valley, Santa Clara County, California: American Geophysical Union Transactions, v. 21, part 1, p. 23–34.
Usai, S., 2001, A new approach for long term monitoring of deformations by differential SAR interferometry: the Netherlands, Technische Universiteit Delft, PhD Thesis, 165 p.
U.S. Department of the Navy, 1982 [revalidated by change (1), Sept. 1986], Design Manual 7.01—Soil Mechanics: Alexandria, Va., Naval Facilities Engineering Command, NAVFAC DM-7.01, 348 p.
U.S. Geological Survey, 1996, Permafrost map of Alaska: Eros Alaska field office, map metadata, scale 1:2,500,000, *http://agdc.usgs.gov/data/projects/fhm/*, accessed May 10, 2007.
_____, 2003, Principal aquifers of the 48 conterminous United States, Hawaii, Puerto Rico, and the U.S. Virgin Islands (ver. 1.0): *http://nationalatlas.gov/atlasftp.html*, accessed September 27, 2007.
Vadon, H., and Sigmundsson, F., 1997, 1992–1995 crustal deformation at Mid-Atlantic ridge, SW Iceland, mapped by radar interferometry: Science, v. 275, p. 193–197.
Van Der Linden, Wim, De Lange, Ger, Veling, E.J.M., and Leake, S.A., 2005, A method for simulating compaction, time-dependent creep, and oxidation of shallow soils, *in* Zhang, A., Gong, S., Carbognin, L., and Johnson, A.I., eds., Land subsidence—Proceedings of the Seventh International Symposium on Land Subsidence: Shanghai Scientific and Technical Publishers, v. 2, p. 552–559.
Van Hasselt, J.P., 1992, Reservoir compaction and surface subsidence resulting from oil and gas production: Geologie en Mijnbouw, v. 71, p. 107–118.
Verbeek, E.R., Ratzlaff, K.W., and Clanton, U.S., 1979, Faults in parts of north-central and western Houston metropolitan area, Texas: U.S. Geological Survey Miscellaneous Field Studies Map MF-1136, 1 sheet, scale 1:24,000, *http://pubs.usgs.gov/mf-maps/mf1136/mf1136/*, accessed May 16, 2007.
Verruijt, A., 1969, Elastic storage of aquifers, *in* De Wiest, R.J.M., ed., Flow through porous media: New York, Academic Press, p. 331–376.
Waksman, S.A., and Purvis, E.R., 1932, The influence of moisture upon the rapidity of decomposition of lowmoor peat: Soil Science, v. 34, p. 323–336.
Waksman, S.A., and Stevens, K.R., 1929, Contribution to the chemical composition of peat, part 5. The role of microorganisms in peat formation and decomposition: Soil Science, v. 28, p. 315–340.
Wang, H.F., 2000, Theory of linear poroelasticity with applications to geomechanics and hydrogeology: Princeton, NJ, Princeton University Press, 287 p.
Wang, H.F., and Anderson, M.P., 1982, Introduction to groundwater modeling: San Francisco, W.H. Freeman and Co., 237 p.

Werner, C., Wegmüller, U., Strozzi, T., and Wiesmann, A., 2003, Interferometric point target analysis for deformation mapping: Proceedings, IEEE International, Geoscience and Remote Sensing Symposium, IGARSS'03, v. 7, p. 4,362–4,364.
White, W.B., Culver, D.C., Herman, J.S., Kane, T.C., and Mylroie, J.E., 1995, Karst lands: American Scientist, v. 83, p. 450–459.
Whitman, D., Gubbels, T., and Powell, L., 1999, Spatial interrelationships between lake elevations, water tables, and sinkhole occurrence in central Florida—A GIS approach: Photogrammetric Engineering and Remote Sensing, v. 65(10), p. 1,169–1,178.
Wicks, C., Thatcher, W., and Dzurisin, D., 1998, Migration of fluids beneath Yellowstone caldera inferred from satellite radar interferometry: Science, v. 282, p. 458–462.
Wicks, C., Thatcher, W., Dzurisin, D., and Svarc, J., 2006, Uplift, thermal unrest, and magma intrusion at Yellowstone caldera: Nature, v. 440, p. 72–75.
Williamson, A.K., Prudic, D.E., and Swain, L.A., 1989, Ground-water flow in the Central Valley, California: U.S. Geological Survey Professional Paper 1401-D, 127 p., *http://pubs.er.usgs.gov/usgspubs/pp/pp1401D*, accessed April 3, 2007.
Wilson, A.M., and Gorelick, Stephen, 1996, The effects of pulsed pumping on land subsidence in the Santa Clara Valley, California: Journal of Hydrology, v. 174, p. 375–396.
Worawattanamateekul, J., Hoffmann, J., Adam, N., Kampers, B., and Altermann, W., 2004, Radar interferometry technique for urban subsidence monitoring: a case study in Bangkok and its vicinity: ENVISAT Symposium 2004, Salzburg, Austria, 6–10 Sept 2004.
Wosten, J.H.M., Ismail, A.B., and van Wijk, A.L.M., 1997, Peat subsidence and its practical implications: A case study in Malaysia: Geoderma, v. 78, p. 25–36.
Yerkes, R.F., and Castle, R.O., 1969, Surface deformation associated with oil and gas field operation in the United States, *in* Tison, L.J., ed., Land subsidence: International Association of Scientific Hydrology Publication 88, v. 1, p. 55–64, *http://www.cig.ensmp.fr/~iahs/redbooks/a088/088012.pdf*, accessed December 2, 2007.
Zebker, H.A., Rosen, P.A., Goldstein, R.M., Gabriel, A., Werner, C.L., 1994, On the derivation of coseismic displacement fields using differential radar interferometry—The Landers earthquake: Journal of Geophysical Research, v. 99, no. B10, p. 19,617–19,635.
Zilkoski, D.B., D'Onofrio, J.D., and Frakes, S.J., 1997, Guidelines for establishing GPS-derived ellipsoid heights (Standards: 2 cm and 5 cm), ver. 4.3: National Oceanic and Atmospheric Administration Technical Memorandum NOS NGS-58, [20+] p., *http://geodesy.noaa.gov/PUBS_LIB/NGS-58.pdf*, accessed November 29, 2007.

Prepared in cooperation with the U.S. Department of Transportation, Pipeline Research Council International, and DGH Consulting Inc.

Landslide Investigation Methods

By Rex L. Baum and Gerald F. Wieczorek

Chapter 3 of
Landslide and Land Subsidence Hazards to Pipelines

Open-File Report 2008–1164

U.S. Department of the Interior
U.S. Geological Survey

Contents

Figures

Tables

Conversion Factors

Inch/Pound to SI

Multiply	By	To obtain
	Length	
inch (in.)	2.54	centimeter (cm)
inch (in.)	25.4	millimeter (mm)
foot (ft)	0.3048	meter (m)
mile (mi)	1.609	kilometer (km)
yard (yd)	0.9144	meter (m)
	Area	
square foot (ft^2)	929.0	square centimeter (cm^2)
square foot (ft^2)	0.09290	square meter (m^2)
square inch (in^2)	6.452	square centimeter (cm^2)
	Volume	
cubic inch (in^3)	16.39	cubic centimeter (cm^3)
cubic foot (ft^3)	0.02832	cubic meter (m^3)
cubic yard (yd^3)	0.7646	cubic meter (m^3)
	Flow rate	
foot per second (ft/s)	0.3048	meter per second (m/s)
cubic foot per second (ft^3/s)	0.02832	cubic meter per second (m^3/s)

inch per hour (in/h)	0 .0254	meter per hour (m/h)
mile per hour (mi/h)	1.609	kilometer per hour (km/h)
	Mass	
pound, avoirdupois (lb)	0.4536	kilogram (kg)
	Pressure	
pound per square foot (lb/ft^2)	0.04788	kilopascal (kPa)
pound per square inch (lb/in^2)	6.895	kilopascal (kPa)
	Density	
pound per cubic foot (lb/ft^3)	16.02	kilogram per cubic meter (kg/m^3)

Temperature in degrees Celsius (°C) may be converted to degrees Fahrenheit (°F) as follows:
$°F=(1.8×°C)+32$
Temperature in degrees Fahrenheit (°F) may be converted to degrees Celsius (°C) as follows:
$°C=(°F-32)/1.8$

SI to Inch/Pound

Multiply	By	To obtain
	Length	
centimeter (cm)	0.3937	inch (in.)
millimeter (mm)	0.03937	inch (in.)
meter (m)	3.281	foot (ft)
meter (m)	1.094	yard (yd)
	Area	
square centimeter (cm^2)	0.001076	square foot (ft^2)
square meter (m^2)	10.76	square foot (ft^2)
square centimeter (cm^2)	0.1550	square inch (ft^2)
	Volume	
cubic centimeter (cm^3)	0.06102	cubic inch (in^3)
cubic meter (m^3)	35.31	cubic foot (ft^3)
cubic meter (m^3)	1.308	cubic yard (yd^3)
	Flow rate	
meter per second (m/s)	3.281	foot per second (ft/s)
cubic meter per second (m^3/s)	35.31	cubic foot per second (ft^3/s)
kilometer per hour (km/h)	0.6214	mile per hour (mi/h)
	Mass	
gram (g)	0.03527	ounce, avoirdupois (oz)
kilogram (kg)	2.205	pound avoirdupois (lb)
	Pressure	
kilopascal (kPa)	20.88	pound per square foot (lb/ft^2)
kilopascal (kPa)	0.1450	pound per square inch (lb/ft^2)
	Density	
kilogram per cubic meter (kg/m^3)	0.06242	pound per cubic foot (lb/ft^3)

Temperature in degrees Celsius (°C) may be converted to degrees Fahrenheit (°F) as follows:
°F=(1.8×°C)+32
Temperature in degrees Fahrenheit (°F) may be converted to degrees Celsius (°C) as follows:
°C=(°F-32)/1.8

Landslide Investigation Methods

By Rex L. Baum and Gerald F. Wieczorek

Abstract

As land development increases, more and more pipelines are being forced onto hillsides with the result that avoidance of landslide areas is becoming increasingly difficult. Once regional studies have identified landslides or potential landslides along the path of a proposed pipeline or pipeline corridor, detailed investigations may be needed in locations where landslides cannot be avoided. Width, depth, level of activity or potential for reactivation, and expected displacement are some of the primary objectives of landslide investigations for pipelines. Future landslide displacement (rate, amount, and direction) is one of the most important considerations in planning pipelines across landslide-prone areas. However, estimating the rate and amount of displacement is one of the most difficult aspects of landslide investigation, because long-term prediction of precipitation, ground-water levels, and other factors that affect slope stability is highly uncertain. Heterogeneity, anisotropy, discontinuities, and other natural subsurface features of bedrock and surficial deposits further complicate the problem.

Rates of landslide movement range from imperceptibly slow (millimeters per year) to extremely rapid (many meters per second). Real or potential pipeline damage resulting from rapidly moving landslides is serious and must be avoided, but is much less common than damage resulting from slow landslides and reactivation (whether slow or rapid) of landslide deposits. Even though movement of many slow landslides appears to be relatively steady, detailed monitoring has shown that movement may be episodic or that movement rates may vary greatly over timescales ranging from hours to years. Empirical correlations have been made between movement rate and either rainfall or pore pressure. Movement rates vary nonlinearly with changes in pore pressure. Periods of relatively rapid movement, known as surges, have been observed in many slow landslides. Surges result from pore-pressure increases, accumulating strain, and rapid external loading acting together or separately. The surges may last several hours or days, and commonly result in displacements of several decimeters to several meters. Instrumental monitoring is the most reliable way to detect the onset of surges.

Many techniques are available for landslide investigation, including mapping, subsurface exploration, monitoring, and analysis. Methods of engineering geologic mapping are highly developed and make it possible to define the boundaries and major internal structures of existing landslides, estimate past displacement, and reconstruct history of movement. Engineering geologic mapping also aids the detailed characterization of potential landslide areas. Recently laser scanners have become available to accelerate and improve the accuracy of detailed geologic mapping. Traditional methods of drilling and sampling can be used to estimate the probable depth and identify the range of materials within a landslide. Recent innovations show promise for improved sample recovery during drilling. Field and laboratory tests are available for determining the deformation, strength, and hydraulic properties of landslide materials. Improved computer control of test apparatus makes it possible to simulate realistic stress paths during testing, which represents a major advancement over traditional strain-controlled testing.

A large variety of instrumentation is available for monitoring landslide movement, deformation, and subsurface water pressures, and for defining the depth of landslide movement. Most landslide monitoring projects rely on a combination of campaign-style surveys (a connected series of measurements to characterize a landslide at discrete points in time) and continuous or real-time monitoring of electronic instruments. Recent advances in surveying equipment and methods such as GPS, laser scanning, and radar methods have improved remote measurement of landslide movement and deformation. Synthetic aperture radar is capable of detecting and measuring small displacements and has recently been applied to landslide monitoring. Real-time landslide monitoring is becoming more common and makes it possible to track changes in rate of displacement at remote locations.

Available methods for numerical modeling of slope stability and landslides can provide time-independent estimates of likelihood of failure, and analyze stress, deformation, and mode of failure. Limit-equilibrium slope-stability analyses provide an estimate of the factor of safety against failure and are useful for evaluating how changes in slope geometry, loading, or pore pressure may affect slope stability. Probabilistic and/or reliability analyses help quantify the amount of uncertainty in factor-of-safety calculations; however, they typically do not estimate the annual probability of failure. In addition to factor-of-safety, finite-element and finite-difference analyses compute deformation, which aids in confirming or predicting failure mechanisms and eliminates the need to guess the depth and mode of failure in potential landslides as required for limit-equilibrium slope-stability analyses. Computed deformation has approximately reproduced observed amount and direction of displacement for a few specific case studies. Discrete-element methods have been developed to account for the discontinuous nature of rock slopes and some soil slopes. Discrete-element methods have been used to study landslide mechanisms, including simulation of historical rock avalanches and to estimate displacement (runout) of potential rock avalanches. Recent advances in continuum and discrete-element modeling include the ability to combine ground-water flow and slope deformation as coupled processes. The accuracy of stress and deformation computed by numerical methods depends on how accurately the landslide and its material properties have been characterized during the field and laboratory investigations. Modeling technique, choice of constitutive equations, and other details also affect the accuracy of model results.

Computing annual probability of landslide movement or slope failure requires information about landslide recurrence obtained either by historical or geochronological methods. Historical observations of landslide displacement in the same region that have similar materials and geometries may provide the best estimates of future displacements. However, even among landslides occurring in the same geologic materials, levels of activity and rates of movement commonly differ.

Introduction

Although avoidance remains the preferred method for reducing or eliminating landslide damage to pipelines, occasionally existing landslides or landslide-prone areas may be unavoidable in planning and constructing new pipelines. Damage to pipelines caused by landslide movement is costly and disruptive. Notable examples include repeated rupturing of a 66-cm-diameter natural gas pipeline that crosses the Cascades landslide complex in the Columbia River Gorge (Braun and others, 1998). In February 1999 movement of a small landslide in the complex resulted in an explosion that dug a 60-m-wide crater (Schuster and Pringle, 2002). Reactivation of the Manti, Utah, landslide during the spring of 1974 destroyed a 20-cm-diameter water supply line, thereby disrupting the municipal water supply and hydroelectric power system of the city of Manti

(Fleming and others, 1988). Reactivation of a deep-seated landslide in the spring of 1998 destroyed two gas lines that supply the city of Santa Cruz, California, leaving 60,000 customers without gas for several days (fig. 3-1; Schuster and others, 1998).

Methods and techniques described in this chapter are applicable where landslides pose a significant threat to pipelines or related facilities. Estimates of amount and rate of potential displacement and assessments of the likelihood of movement are needed where pipelines must cross known landslide areas or highly suspect (potential landslide) areas. Field investigations attempt to provide these estimates and assessments as well as information that might be used in remedial works to reduce potential landslide movement. Landslide investigations usually start with a review of existing literature for the area and desk study of existing geologic maps, aerial photographs, and similar information. Landslide field investigations generally begin with surface exploration, including mapping of landslide structures and features as well as geologic materials involved in the landslide. Subsurface exploration of existing landslides helps define the depth of the slip surface, ground-water levels, and subsurface materials. Soil and rock samples collected from landslides may be tested in the laboratory or the field to determine strength and hydraulic properties. Instrumental monitoring is commonly used to observe variation in ground-water levels and the rate, amount, and direction of landslide movement. Various numerical models are used to estimate the likelihood of landslide movement or to determine how an existing or potential landslide will respond to external forces or changes such as grading or drainage. Sometimes historical studies are used to estimate the age of landslide deposits, recurrence of landslide movement, or the amount of movement that might occur during a future episode.

This chapter provides a summary review of available methods for investigating individual landslides and landslide-prone sites. Because of the importance of characterizing displacement where pipelines cross landslides, we also provide a summary discussion of landslide rates and displacements as background for describing existing approaches to and the difficulty of predicting rates and net displacements. A companion chapter in this report describes applicable methods for identifying regional landslide hazard to pipelines (Harp, 2007). Once regional methods have identified specific landslides or landslide-prone areas that pose a major threat to facilities, site-specific methods outlined in this report can be used to further characterize the hazard. A thorough review of site-specific methods available up through 1996 is provided in Turner and Schuster (1996). Due to the large volume of material already available there and the quality of treatment of the subject, emphasis here is on methods that have advanced significantly since that publication. However for completeness, we have also provided a brief description and discussion of older techniques that are particularly relevant to pipelines. Seismic hazards were beyond the scope of this project; therefore, methods specific to seismically induced landslides have not been included in this report.

Landslide Movement Rates

Rates of landslide movement range from imperceptibly slow (millimeters per year) to extremely rapid (many meters per second). Based on previous work by Varnes (1978), Cruden and Varnes (1996) proposed a landslide velocity scale, as illustrated in figure 3-2. The scale is divided into seven velocity classes, and the divisions increase by multiples of 100. Rapidly moving landslides (velocity classes 5, 6, and 7, figure 3-2) include rock and debris avalanches, debris flows, rapid earth flows in sensitive clays, rock falls, and some rockslides. Although small rock falls and shallow debris flows are unlikely to damage buried pipelines, avoiding large rapidly moving landslides and their effects is critical in preventing damage to pipelines. Nearly all types of landslides may display long-lasting slow movements. However, slow landslides (velocity classes

1, 2, and 3) most commonly include translational landslides in stiff clays and other fine-grained deposits (earth slides and earth flows) as well as many deep-seated landslides and spreads, complex movements in rock masses, and some slides in granular soils (Picarelli and Russo, 2004).

Slow movements deserve further attention because of their potential to damage pipelines over time as cumulative displacement gradually increases. Even though movement of many slow landslides appears to be relatively steady, detailed monitoring has shown that movement may be episodic or that movement rates may vary greatly over timescales ranging from hours to years (Keefer and Johnson, 1983; Kalaugher and others, 2000; Coe, Ellis, and others, 2003; Petley, 2004; Picarelli and Russo, 2004). These changes in rate of movement result from external factors such as precipitation and erosion as well as internal changes in the landslide mass that result from deformation. Various workers have made empirical correlations between movement rate and either rainfall (Grivas and others, 1996, 1998; O'Neil and others, 1996) or pore pressure. Movement rates vary nonlinearly with changes in pore pressure (Picarelli and Russo, 2004). The net long-term effect of this variation in the instantaneous rate of movement is that cumulative displacement usually varies from season to season and year to year, thus making it difficult to forecast long-term displacements based on data from a brief (1–2 year) period of observation.

In new landslides (first time failures), a period of slow but gradually accelerating movements typically precedes failure. Once failure occurs, movement accelerates rapidly, and the newly released landslide mass moves abruptly (Picarelli and Russo, 2004). Subsequent movements tend to be slow, but periods of relatively rapid movement, known as surges, have been observed in many slow landslides. Pore-pressure increases and changes in external loading acting together or separately have been identified as causing surges (Keefer and Johnson, 1983; Kalaugher and others, 2000). The surges may last several hours or days, and commonly result in displacements of several decimeters to several meters. Major shear distortions have been observed during the early stages of displacement surges (Kalaugher and others, 2000). Instrumental monitoring of strain and pore pressure is the most reliable way to detect the onset of surges.

Reactivated landslides commonly follow a similar pattern. An example is the spring 1974 reactivation of the Manti, Utah, landslide that resulted from loading at the head by debris flows (Fleming and others, 1988). The landslide had moved small amounts during the previous 35 years and began accelerating soon after deposition of the debris flows. Movement slowed or stopped following winter and began again in the spring of 1975. Displacements of many meters occurred during 1975 and the 3-km-long landslide was fully developed by November 1975. Movement stopped during the winter and began again in spring 1976; however movements were much smaller than during 1974 and 1975. The average slope of this landslide was only 8°, yet it moved many tens of meters during 1974 and 1975 and destroyed a water pipeline that supplied the city of Manti, as noted previously.

Duration of movement episodes is another factor (besides variable rates) that determines net displacement of a landslide. For example, annual displacements at a landslide in central Utah varied over a 4-year period (1983–1986) in response to varying amounts of water, derived mainly from snowmelt (Baum and others, 1993). Daily rates following spring snowmelt were variable and the cumulative displacement at one particular point ranged from 58 cm in 1983 to 280 cm in 1984 (250 cm in 1985 and 95 cm in 1986). The number of days the slide was active ranged from about 45 days in 1984 to 116 days in 1986. Similarly, landslides in the US Highway 50 corridor east of Sacramento, California, move longer and farther in years when a wet winter season is followed by a wet spring than in years when a wet winter season is followed by a dry spring (Mark Reid, USGS, oral commun., 2007).

Inferring Probable Rate of Movement

Differentiating between potentially slow and rapid landslides is a key consideration for pipelines as it is more critical that large, rapid landslides, or their impacts, need to be avoided than slow landslides. Where pipelines must cross a slow landslide, the probable rate of movement may determine the preferred approach for avoiding pipeline damage.

Form and nature of the deposits provide a general indication of rate of movement of past landslides. In other words, it is often (but not always) possible to distinguish deposits of debris flows, debris avalanches, and other rapidly moving landslides from deposits of slow landslides or other processes. Debris flows usually have lateral levees and the main deposits have characteristic fan-shaped morphology; the deposits typically have large clasts supported by fine-grained matrix (Cruden and Varnes, 1996; Pierson, 2005). Slope and materials also give some indication of potential rate of movement. For example, most landslides in high-plasticity clay on slopes flatter than 12°–15° usually move at slow to moderate rates (velocity classes 1, 2, 3, and 4); however as noted previously, even slow earth flows in plastic soils are noted for occasional surges to rates of several meters per minute (Keefer and Johnson, 1983; Baum, 2003) or reactivation with sustained slow movement that results in many meters of displacement (Fleming and others, 1988). On the other hand, quick-clay landslides usually move rapidly and enlarge retrogressively a distance that is many times the slope height. Landslides on steep slopes (>25°–30°) always have the potential for rapid movement.

Despite some general dependence of potential rate on slope, morphology, and earth materials, experience also indicates that rate of movement of landslides can be quite unpredictable. A recent tragic example is the La Conchita landslide in Southern California, which moved at rates of meters per day when it was active in 1995 and moved catastrophically at rates of meters or tens of meters per second in 2005 (Jibson, 2005). It has also been observed that debris flows commonly form on the toes of large landslide deposits (Mark Reid, USGS, oral commun., 2003). Thus, material from a large slow-moving landslide may become part of a smaller rapidly moving landslide. A classic example of the difficulty of predicting rate of movement is the 1963 Vaiont landslide, which moved catastrophically after creeping slowly for about 3 years (Kiersch, 1964). Although such catastrophic movements may be relatively uncommon, nearly all slow landslides have the potential for abrupt or sustained relatively rapid movements ranging from a few decimeters to several meters or more. We are unaware of any set of circumstances, conditions, or characteristics that positively ensure that a slow-moving or inactive landslide will not undergo future displacements large and rapid enough to damage or rupture a pipeline.

Engineering Geologic Mapping and Related Field Studies

The purpose of engineering geologic mapping in landslide investigations is to determine the dimensions and to identify and locate boundaries and other surface features (fig. 3-3) and geologic materials of the landslide. Mapping and related field studies also help to unravel the geological history of landslide, which may result in estimates of magnitude and frequency of past movements. Engineering geologic mapping at various scales serves different purposes. Large-scale (1:50–1:1,000) mapping shows the geologic (lithology, structure, geomorphology) and hydrologic (springs, sag ponds) details needed for study of individual landslides and landslide-prone sites. Mapping at small (1:25,000–1:100,000) and intermediate scales show landslides and landslide-prone areas in the context of the regional and local geology and terrain.

Small-Scale Mapping

Small-scale regional mapping was discussed in the companion paper by Harp (2008, chapter 1 of this report), but some of the data collected in connection with regional mapping can contribute to an understanding of specific landslides. Although showing existing landslides on a map does not necessarily represent exactly where future landslides may occur, such mapping does help bound the ranges of several landslide characteristics for a particular area. For example, ranges in size and travel distance of landslides in a pipeline corridor can be determined from small-to-medium-scale mapping (landslide inventory maps, figure 3-4A). The observed size ranges provide some constraints or guidance for estimating the potential widths of future landslides.

Detailed geologic maps showing a history of different periods of previous and recent landslides, sometimes referred to as multitemporal maps because they show landslides from multiple events spread over a period of years or decades, have been prepared within several areas of California, for example, Brabb and Pampeyan (1972), Campbell (1975), Wieczorek (1982, 1984) Wieczorek and others (1999), and Coe, Godt, and others (2004). Similar maps exist for other areas, but coverage tends to be spotty. Carrara and others (1995), using GIS technology in mapping landslides, include landslide typology, degree of activity, relative age, estimated depth, estimated or observed velocity, and degree of certainty in mapping and classification. Information needed to ascertain landslide hazard can be obtained from analysis of a multitemporal landslide-inventory map that portrays the distribution, type, and pattern of landslides and their changes in time. The multitemporal map may be compiled from landslide-inventory maps prepared through the analysis of stereoscopic aerial photographs of different ages and by use of field surveys (Reichenbach and others, 2004). Although uncommon prior to about the 1960s, series of relatively high-quality, medium-scale (1:10,000–1:25,000) stereo air photographs taken at 5- to 10-year periods, or more frequently, can be utilized to obtain information on the extent, progression, and annual probability of occurrence of landslides along or adjacent to pipeline corridors. An estimate of the annual probability of landslide occurrence, even if approximate, can provide valuable input in the selection of alternative pipeline alignments, as well as in decision making with respect to acceptance of existing risks or the need for, and extent of, mitigative measures. Depiction of prehistoric, historical, and recent landslides on detailed maps can depict the regional potential future landslide hazard (Wieczorek and others, 1999).

Recent applications of Light Detection and Ranging (LIDAR) to landslide mapping are also very useful. LIDAR is a technique based on airborne scanning with a laser rangefinder and GPS ground control to produce high-resolution topographic data. Using algorithms for virtual deforestation (Haugerud and others, 2003), LIDAR data acquired during the leaf-off season are capable of producing detailed bare-earth digital-elevation models. The quality of LIDAR mapping has steadily improved over the last several years as point densities of LIDAR surveys have steadily increased and postprocessing has become more sophisticated. LIDAR topographic data are becoming available for more and more areas of the United States as public and private entities commission increasing numbers of LIDAR surveys. In some areas these data are in the public domain and freely available; in areas where LIDAR has been acquired with private funding, the data may be available for purchase from a vendor.

Use of LIDAR-derived topography is particularly effective where pipeline alignments and adjacent landforms, including landslide features, are masked by extensive tree or vegetation cover or where excessively steep and/or otherwise inaccessible or dangerous terrain limits or precludes effective ground-based mapping. LIDAR topography has been utilized extensively along the Vancouver to Whistler highway, British Columbia, and utility corridor to map steep rock bluffs and slopes, and to establish accurate topography and assess potential slide features within heavily tree

covered slopes elsewhere within coastal British Columbia (Richard Butler, written commun., 2007). Schulz (2004, 2005) used LIDAR-derived imagery to map landforms in Seattle, Washington, that were created primarily by landslides. These landforms included landslide deposits, head scarps, and denuded slopes that were created by prehistoric landslides that have occurred since the retreat of the last glacier. Over 93 percent of about 1,300 reported historical landslides are located within the LIDAR-mapped landform boundaries. The spatial densities of reported historical landslides within the LIDAR-mapped landforms provide the relative susceptibilities of the landforms (particularly landslide head scarps and deposits) to landslide activity in the recent past. The spatial densities also provide reasonable estimates of future landslide susceptibility. The mapped landforms and susceptibilities provide useful tools for landslide hazard reduction in Seattle.

Although buried pipelines are not usually subject to damage by rock fall, aboveground facilities such as pumping stations and valves may be exposed to rock falls. Techniques of engineering geologic mapping and related field studies characterize the potential for rock fall in these areas (fig. 3-4B, Coe and others, 2005). Three-dimensional analysis of rock-slope stability has been developed using joint directions, slope orientations, and friction angles with a stereo net to create Markland plots (Markland, 1972). A rock-slope stability analysis in Navajo National Monument, Arizona, was used to assess the potential for planar or wedge sliding along discontinuities at various stations along a steep rocky trail (Wieczorek and Harp, 2000). Using Markland plots shows the discontinuities (bedding and joints) in relation to potential wedge and planar sliding surfaces on a lower hemisphere stereonet projection in the rock-slide region (Wieczorek and Harp, 2000, their figs. 4 and 5). The slope face is shown as a great circle and friction is represented by an interior circle.

Large-Scale Mapping

Detailed observation of bedrock, field-developed cross sections, classes of slope stability, and surface-water features are useful for surface observation and geologic mapping of landslides and landslide-prone areas (Keaton and DeGraff, 1996). Details to be included in a large-scale engineering geologic map of a landslide depend somewhat on the landslide types and processes involved. Several landslide classification schemes are used worldwide; one of the most widely used is the Varnes classification, which is based on material and process (Varnes, 1978; Cruden and Varnes, 1996). The different types have different three-dimensional forms, but the types that most commonly damage pipelines have features similar to those depicted in figure 3-3.

Complex landslides can be depicted on detailed scale maps (Bogaard and others, 2000; Chelli and others, 2005). Fleming and Johnson (1989) described, mapped, and interpreted the various structures that commonly occur on the surface of landslides. Their methodology for detailed mapping of large individual landslides is useful for constructing conceptual and physical models and forms a basis for analyzing landslide movement (fig. 3-4C). Major structures and features of the landslide emerge from mapping individual cracks, scarps, lateral shear zones, and other deformational features. Examples include the Slumgullion, Colorado, landslide (Baum and Fleming, 1996; Fleming and others, 1999) and the Alani-Paty, Hawaii, landslide (Baum and Reid, 1995; Baum and others, 1998). Areas of active or potential enlargement are identified by mapping small fractures outside the main body of the active landslide.

Similar levels of detail can be portrayed in engineering-geologic mapping of a potential landslide area. Although landslide features may not be present, detailed mapping can be used to show geologic structures (faults, folds, joints, foliation, and other discontinuities), variations in lithology, zones of weathering or alteration, depth to bedrock, seepage zones, and other features

relevant to slope stability, most notably any evidence of recent or ongoing ground deformation. Locations of boreholes, trenches, test pits, measurements, geophysical surveys, and instruments can also be shown on large-scale engineering geologic maps of landslide and potential landslide areas.

Methods of Estimating Displacement

When mapping landslides, it is usually desirable to estimate total past displacement. Such estimates often provide an upper bound on possible future displacements (Skempton and others, 1989). Major reactivations of large old landslide deposits, such as the Manti, Utah, landslide (Fleming and others 1988) and the Thistle, Utah, landslide (Schuster and Fleming, 1986), which have resulted in major movement and enlargement beyond the previous boundaries of these landslides, are notable exceptions. The most direct method is to measure offsets at the boundaries. For example, where a fence or road crosses a landslide, the offset across the boundary gives an estimate of the total displacement. Displacement varies from point to point; so, where possible, multiple measurements of offset should be gathered. Measurements of displaced volume usually do not provide reliable estimates of net displacement, because they are based on vertical changes and do not track material points on the surface. Point-tracking methods (Smith, 1996; Coe, Ellis, and others, 2003) are described in the section on monitoring.

Landslide History

Information on landslide history or recurrence of movement constitutes the basis for most estimates of temporal landslide probability. Absolute or relative ages of landslides (or rather, the ages of their last movements) are also used to make a preliminary assessment of their stability. Landslides that have not moved in hundreds or thousands of years are commonly assumed to be more stable than those that have moved more recently. However, this approach must be used with caution because climate extremes, increased erosion rates, and human activities such as irrigation, grading, excavation, or other changes to the land surface can invalidate this assumption.

Several techniques are available for partially reconstructing history of movement in landslide areas. These include use of crosscutting relationships and features (such as scarps and hummocks), scarp degradation to define relative ages of deposits (McCalpin, 1984), as well as methods for obtaining "absolute" ages. Radiometric ages of buried soils (Madole, 1996) and datable materials (wood, bone, or charcoal) embedded in landslide deposits (Chleborad, 1996) provide approximate ages of past movement. Ages of organic-rich deposits that have accumulated in sag ponds and depressions that have formed on the surface of a landslide (Alexandrowicz and Alexandrowicz, 1999) or in the lacustrine sediments that have accumulated upstream of a landslide that has dammed a valley (Schuster and Pringle, 2002) can also be determined by radiometric techniques. Dendrochronology (Stoffel, 2006), lichenometry (Bull and others, 1994), pollen analysis (Adam, 1975; Baron and others, 2004), and similar techniques have also been used for estimating ages of landslides. Dendrochronology is capable of giving more precise ages than other methods, but corrections are needed when determining ages of young surfaces (Pierson, 2007). It should be kept in mind that ages determined by any of these methods are approximate and subject to various limitations. Selection of sites for collecting datable materials requires a clear understanding of the morphology and internal structure of a particular landslide, as well as an understanding of which locations will give minimum ages and an awareness of other potential difficulties (Van Den Eeckhaut and others, 2007). The cost of obtaining radiocarbon ages is about $300–$600 (U.S. dollars, 2007) per sample, depending on sample size. In areas where historical data on landslide occurrence is unavailable, the value of a landslide history constrained by radiocarbon or other ages may far exceed the cost.

Historical records are also useful for identifying major episodes of past movement, particularly in areas that have been occupied for long periods of time (Bisci and others, 1996; Castelli and others, 2004; Coe, Michael, and others, 2004). Unfortunately long historical records of landslide activity are relatively rare.

Regardless of the techniques used for determining ages of landslides, an important question is how wide an area should be studied to develop a landslide history. At a minimum, a landslide history would be needed for the entire length of the pipeline transect or corridor. A more conservative approach would be to develop the history for all drainage basins that contribute directly to hazard along the pipeline. For example, Coe, Godt, and others (2003) used the basin approach in assessing debris flow probability for a major transportation corridor in central Colorado. This approach results in a study area that has variable width along the pipeline, but it ensures that potential landslide sources are not overlooked by setting an arbitrary fixed width for the study area. As noted previously in the case of the Manti landslide, natural processes occurring within the drainage basin, but hundreds of meters away from the actual pipeline, can affect slope stability. The same can be said for human activities (excavation, grading, irrigation) occurring upslope or downslope of a pipeline.

Subsurface Exploration

Drilling and trenching are the most commonly used methods for subsurface exploration of landslides. Geophysical techniques are sometimes used where drilling is not feasible or to aid extrapolating measurements from a single borehole or between boreholes. The most commonly used geophysical techniques include seismic reflection, seismic refraction, ground-penetrating radar, and methods based on electrical resistivity. In this section, we provide a brief summary of commonly used techniques and highlight recent developments. McGuffey and others (1996) provide a complete detailed description of subsurface exploration techniques and methods of data presentation.

Drilling of deep-seated landslides is the most useful and most widely applicable method for subsurface exploration of landslides. Boring logs for existing water wells or oil and gas wells on or near the landslide can be useful sources of supplemental information. At many sites, drilling is necessary to determine the depth of the slip surface and the geometry of the landslide mass. For documenting landslides, drilling and sampling can determine types of subsurface geologic materials, locations, and orientations of joints, landslide shear zones, and ground-water levels. Although boring methods have changed little from those described by McGuffey and others (1996), a few new techniques and improvements to old ones are worth noting. For example, new types of drilling fluid have been developed for use with diamond drilling to help reduce sample disturbance and improve sample recovery. Nakamura (2004) described a new technique known as Jet Foam Boring that uses stiff foam to help protect the core.

For major projects, such as a large landslide affecting an important pipeline corridor, large-diameter (60–90 cm) boreholes can also be used by geologists or engineers in the same way as test pits and trenches to make detailed subsurface logs (maps of borehole walls) and photography for documentation deep within the landslide mass and to collect relatively undisturbed samples of the basal shear surface. Deep drilling of landslides has often revealed the detailed mechanisms of movement, such as that of the October 2, 1978, Bluebird Canyon Landslide in Laguna Beach, California, that destroyed 24 homes (Sydnor, 1979). In April 2005, another large, translational landslide about 60 m east of the Bluebird Canyon landslide moved destroying 19 homes and resulting in evacuation of more than 345 homes. Detailed geologic logs of large-diameter boreholes in this landslide revealed details including the presence of ancient landslide debris, the

depth, thickness, and orientation of shear zones, fractures, and bedding as well as presence or absence of seepage zones to depths of nearly 30 m (Gary Stoney, Stoney-Miller Consultants, Inc., written commun., 2007).

Borehole logging methods including electric and nuclear logging have been described by McGuffey and others (1996, fig. 10-2). These logging techniques help to characterize lithology and rock or soil density throughout the depth of borehole. Large diameter boreholes and downhole logging methods have been proved to be valuable in landslide investigations, for example, in Napa County, California, by Johnson and Cole (2001). Borehole televiewers have recently been developed to help with logging of smaller diameter boreholes (Borchers, 1994; Nakamura, 2004).

For landslides involving rock masses, rock-strength properties, including friction angle of rock surfaces, the roughness of natural rock surfaces, fracture infilling, and recently displaced fractures, are significant (Wyllie and Norrish, 1996). Much of this information can be obtained from boreholes. For example, detailed subsurface geologic drilling and examination using geophysical logging and borehole television revealed details of the morphology and structure of granitic bedrock near Wawona within Yosemite National Park, California (Borchers, 1994; 1996). Use of oriented-core sampling methods, with or without complementary borehole video or photographic examination provides high-quality information on orientation of rock structure or bedding.

Direct-push (Geoprobe®) techniques have been developed for advancing small-diameter holes (up to 75 mm) in soil and soft rock by direct push or driving a sampler into the ground. This method returns high-quality samples for logging and some types of testing. Probing can reach depths of 30 m, which is adequate for many landslide investigations. Probing can be used as a primary method for subsurface exploration on smaller landslides or as a rapid method of creating additional holes for installing piezometers or other instruments (Bianchi and Farrington, 2001). At steep or difficult sites, probing can be performed by a two-or-three-man crew using a gas- or electric-powered breaker hammer; a manual jack can be used to extract the sampler. Hydraulic probing rigs that mount on the back of a pickup truck as well as self-contained track-mounted rigs are also available. Tools for cone-penetration testing (CPT) as well as electrical and hydraulic logging are available for these rigs.

CPT has been available for some time on larger truck- and track-mounted rigs and has evolved into a highly developed technique for geotechnical subsurface exploration, with many variants as described by McGuffey and others (1996). A steel rod with a conical tip is forced into the ground while the required force is recorded continuously. Within soft-to-stiff or loose-to-compact soils, electronic Cone Penetration Test probes can be used to obtain continuous profiles of subsurface characteristics to depths of 30 m or more within a short time period. Since CPT methods typically record variations in subsurface conditions over penetration distances of 50 mm or less, CPT profiling is effective in detecting the presence of weak or sheared zones that need further investigation by more direct methods, as well as the boundaries between or within various soil strata. Cone penetrometers can be equipped for geophysical and piezometric measurements. Thus, electronic CPT equipment is also typically capable of determining the variations in transient pore-water pressures with depth, as well as pore-water-pressure dissipation properties. It can also be utilized to determine uphole or downhole shear wave measurements, or electrical resistivity profiles. CPT is invaluable as a supplemental exploration technique for landslides.

Trenches and test pits permit direct observation and sample collection in relatively inactive landslides to depths of 3–6 m with adequate shoring or stepped excavation in the case of trenches. Consequently, trenches and pits are useful in landslides of moderate depth, and near the edges of deep landslides. Trenches can be excavated in a few hours by backhoe at relatively low cost and provide a three-dimensional view that is unachievable by any other method (James P. McCalpin,

oral commun., 2007). Information obtained by careful logging of trenches can aid in accurate interpretation of samples and cuttings from boreholes. Trenches near the toes of landslides commonly expose the basal shear zone, which may be quite different in composition and appearance from most of the landslide debris, so that the shear-zone materials can be adequately sampled and tested (fig. 3-5).

Use of test pits or test trenches and large-diameter boreholes is often limited by the presence of seepage or ground-water levels, or materials having minimal stand-up time close to the ground surface. Use of sonic drilling techniques can be used to obtain near continuous, although disturbed cores of soils, ranging from fine sands and silts or clays to cobbles and boulders, and weak-to-moderate-strength rock. Recent investigations in British Columbia indicate that such soils and rock can be penetrated to depths of the order of 40 m and possibly more (Richard Butler, written commun., 2007). Sonic drilling methods can also be used as a relatively rapid means to permit installation of slope inclinometers and conventional or rapid-response piezometers.

The use of geophysical techniques in subsurface exploration is based on attempts to relate changes in physical properties, such as the elastic modulus or electrical resistivity, to changes in lithology, the location of the water table, or other subsurface features of interest in landslide investigations. Ground-penetrating radar (GPR) can be used to detect the soil or rock strata and bedding features, and, in particular, zones of disturbance to depths of the order of 5 to 15 m in granular soils or rock, although it may have limited penetration within fine-grained soils. Use of these indirect methods requires considerable skill in interpretation of the results. Example applications include locating the base of a landslide deposit by seismic reflection and refraction methods (Williams and Pratt, 1996; Corsini and others, 2006), or by a combination of seismic and electrical methods (Bogaard and others, 2000; Chelli and others, 2005). Electrical methods have also been used to investigate ground-water distribution in landslides (Hiura and others, 2000). Geophysical techniques are often best combined with direct investigation methods to permit correlation and corrections to the inferred depths and properties of soil or rock strata while assisting in interpreting the variations in conditions between the direct investigation sites.

Sampling

Samples obtained from the ground surface or from subsurface exploration can be used to determine the types and strengths of the geologic materials involved in landslides. In some cases, samples can be used to determine the geologic age of the materials and possibly the previous age of landslide movement. For example as noted previously, radiometric analysis of wood or charcoal fragments found beneath a landslide can be used to determine the approximate age of previous historic/prehistoric landslide movement. Regardless of the specific test(s) or analysis(es) planned for a particular sample or suite of samples, the object of sampling is to obtain materials that represent the properties or range of properties relevant to understanding past, present, and future behavior of the landslide. The heterogeneous nature and complex history of most landslides and landslide-prone areas make it imperative that the relationship of samples and sample locations to the overall geometry and structure of the landslide or potential landslide be well understood. Without adequate understanding it is very likely that irrelevant materials will be sampled and tested. For example, it has been observed in many relatively slow-moving landslides of the type that are common in areas crossed by pipelines that the basal and lateral shear zones consist of much weaker materials than those that make up the main body of the landslide (Baum and Reid, 2000).

Drilling can be used to obtain detailed samples of landslide materials at many different depths. McGuffey and others (1996) describe in detail the various types and applications of sampling available with modern drill rigs. We are unaware of any major advances in sampling

technique in the last decade. Sample recovery is typically less than 100 percent but careful examination of recovered samples makes it possible to approximately reconstruct the distribution of materials in the subsurface. In cohesive clay soils, it is sometimes possible to recover materials from the basal shear zone for shear-strength testing; however it is usually necessary to use inclinometer observations to confirm the depth of sliding. In cases where the basal shear zone can be sampled directly, either in a trench or large-diameter borehole, it is possible to obtain relatively undisturbed block samples for oriented (shearing parallel to the movement direction) direct-shear tests of the slip surface. Again, we refer the reader to McGuffey and others (1996) for a detailed discussion of sampling methods.

Testing

The main purpose of testing landslide materials is to determine strength and hydraulic properties (Wu, 1996; Lambe and Whitman, 1969). Determination of shear strength of materials at the landslide slip surface is relevant to stability analysis, estimates of landslide movement and understanding failure mechanisms of slopes (Leroueil, 2001). Landslide materials are often inhomogeneous, and the strength parameters can vary over an order of magnitude between different materials. Therefore correctly identifying slip-surface material is critical to obtaining representative test results. In the case of potential landslide areas, a detailed exploration sampling program is needed to identify and sample materials from potential slip surfaces. Hydraulic properties are used in predicting effects of rainfall, subsurface drainage and other factors on subsurface water pressures (Baum and Reid, 1995; Iverson, 2000; Hungr and others 2005). Field tests usually provide the most meaningful values of hydraulic properties for landslide modeling purposes. Methods that have been used effectively to determine the ground-water and piezometric conditions, including "perched" or nonhydrostatic conditions, at depth within soil and rock include multi-port piezometers, CPT dissipation testing, and conventional falling-/rising-head testing (Richard Butler, written communication, 2007; McGuffey and others, 1996).

Shear Strength

Once relevant materials have been obtained for testing, consideration must be given to the type of test. Strength testing attempts to duplicate field conditions as closely as possible. These conditions include the stress state, stress path, rate of shear, drainage, whether the material has previously been sheared, and whether displacement is concentrated along a discrete plane or distributed. A complete understanding of soil behavior in the context of slopes is needed to plan a soil-testing program and interpret test results (Lerouiel, 2001). The stress-strain and strength properties of soils are typically determined in the laboratory by direct-shear and triaxial tests. Some soils, such as coarse granular materials, sensitive silty or organic soils present at depths of 10 m or more below the ground surface, and fractured or friable rocks may be difficult or impossible to sample without excessive disturbance. In such cases, use of field testing methods, such as the Menard Pressuremeter, dilatometer, and strain-controlled field-vane methods, may be desirable or necessary to permit determination of strength values (McGuffey and others, 1996; Wu, 1996).

Wu (1996) provides a complete description of laboratory and field test procedures; the following paragraphs contain a brief summary of laboratory test procedures. Figures 6A and 6B respectively show the general configurations of a laboratory direct-shear test apparatus and a triaxial test apparatus.

In a direct-shear test, the soil is placed in a steel or bronze box that is split along the line of the shear plane as depicted in figure 3-6A. A normal force, F_n, is applied along the top of the box

and a shear force, F_s, is applied to the side of the upper, moveable block to cause shearing in the enclosed soil. Shear and normal stress magnitudes are obtained by dividing the shear and normal force by the original horizontal cross-sectional area of the soil sample. These stresses and the displacements of the upper block are recorded and the results are given in terms of shear and normal stress on the shear plane and the horizontal and vertical displacements of the upper, moveable block. In addition, changes in pore-water pressure in partially saturated or saturated soils can be recorded. A ring-shear or torsional-shear device is similar to direct shear in that it forces shear to occur on a plane, but the ring-shaped sample is sheared about its central axis, allowing large displacements to occur.

In the triaxial test apparatus shown in figure 3-6B, the soil sample, enclosed in a flexible membrane, is placed between a moveable upper platen and a fixed lower platen and confining pressure is applied. This is followed by application of an axial load. The axial load is converted to axial stress by dividing the axial load by the original horizontal cross-sectional area of the soil sample. The axial stress is the major (most compressive) principal stress and the confining pressure is the minor (least compressive) principal stress in a compression test. A porous stone disc connected to an outlet tube allows drainage of fluid from the bottom of the sample. The valve on the outlet tube is left open in a drained test. An undrained test, considered relevant to rapid loading, is achieved by shutting the valve on the outlet tube. The stresses and the displacements of the upper platen are recorded and, in addition, changes in water pressure in an undrained test for wet or saturated soils are usually recorded. Further details on direct shear and triaxial tests on soils are found in Lambe and Whitman (1969), Bishop and Henkel (1957), and Wu (1996).

Depending on their initial porosity relative to the applied normal stress, soils initially exhibit either contractive or dilatant behavior during shearing deformation. Loose soils tend to compact or contract as they deform under load. Dense soils tend to dilate or expand as they deform under a normal load. Both tend toward a “steady” or “critical” state as deformation increases under constant normal load (Lambe and Whitman, 1969). Soil particles deform very little at the low normal stresses present in shallow soils on steep slopes. Rather, soil deformation at low normal stresses mainly involves rearrangement of soil particles and changes in pore space.

Figure 3-7 shows the results of triaxial tests on granular soil in loose and dense states. The dense soil failed in a relatively brittle manner, as indicated by the steep slope of the initial (rising) part of the force-displacement curve. It reached its peak strength after an axial strain of a few percent. After reaching the peak, the strength of the dense soil gradually declined toward the ultimate or residual shear strength. As shown by the change in void ratio, the dense soil began dilating after a very small axial strain and continued dilating throughout most of the test (fig. 3-7).

The initial slope of the force-displacement curve of the loose, contractive soil is much flatter than that of the dense soil, indicating ductile failure (fig. 3-7). The shearing resistance of the loose soil gradually builds to its ultimate strength, which is attained after significant axial strain. Change in void ratio indicates that the soil compacted slightly at the beginning of the test and then dilated to approximately its original void ratio. After large axial strain (about 30 percent), the “critical state” is reached where the shear strength and void ratio of the dense and loose specimens are approximately equal.

Shear strength varies with displacement and soil porosity. Dense and cemented soils display a peak strength that is developed within the first few millimeters of displacement. Upon further shearing, the soil weakens toward the so-called residual strength (fig. 3-7). Peak strength is usually considered relevant to first-time slides in natural normally consolidated clay and intact rock. The fully softened strength is relevant to first-time failure of stiff-fissured clays and claystones (Skempton, 1985; Wu, 1996). Residual strength is generally considered relevant to reactivation of landslides (Skempton, 1985), but desiccation or precipitation of minerals from pore

water can cause strength to regain between episodes of movement (Bromhead, 2004). In some cases, residual strength also appears to be relevant to analyzing progressive failure (Dixon and Bromhead, 2002).

The results of direct shear and triaxial tests of soil show that at the point of incipient shear failure there can occur planes along which the shear stress is given by

$$\tau = c + \sigma \tan \phi \tag{1}$$

where τ is the shear stress on a potential failure plane, σ is the normal stress at failure on this plane, c is cohesion, and ϕ is the angle of internal friction of the soil. Equation 1, first proposed by Coulomb in 1773, is known as the Coulomb failure criterion. Although other failure criteria have been proposed and used in some modeling exercises, the Coulomb criterion remains the most widely used and easily understood failure criterion for soils. It plots as a straight line in two-dimensional Mohr stress space (Terzaghi, 1943) as shown in figure 3-8A. This line separates the Mohr stress space into stable and unstable parts. If a Mohr circle constructed from the major and minor principal stresses, σ_1 and σ_3, lies below the Coulomb failure line, the soil behaves elastically. If, however, a Mohr circle becomes tangent to these lines, failure will ensue. No Mohr circle can lie beyond this limiting line because the shear stress cannot exceed the yield strength of the soil.

The strength parameters, cohesion, c, and the angle of internal friction, ϕ, of a soil are determined as illustrated in figures 8A and 8B. Mohr's circles representing the state of stress at failure for three different tests are plotted and a line tangent to the circles is constructed (fig. 3-8B). This line is the failure envelope. Commonly, the failure envelope can be treated as a linear, two-parameter model, the Mohr-Coulomb failure criterion (Equation 1), over the range of stresses that apply in shallow landslides. Figure 3-8C shows Mohr-Coulomb strength parameters determined by drained direct-shear testing of two soils from the Alani-Paty landslide in Hawaii (Baum and Reid, 1995). The expansive clay is similar to material from the basal failure surface of the landslide and the sandy clay represents some of the material in the body of the landslide above the failure surface. Primes indicate that the strength parameters were determined under effective-stress conditions, conditions that we now review.

For water-saturated soils, effective stress is defined by subtracting pore-water pressure (interstitial fluid pressure), p, from the total normal-stress components (Terzaghi, 1943). In Cartesian *xyz* coordinates the total normal-stress components are σ_x, σ_y, and σ_z and the effective stresses are given by $\sigma'_x = \sigma_x - p$, $\sigma'_y = \sigma_y - p$, and $\sigma'_z = \sigma_z - p$. Static pore pressure does not affect shear stress; however, ground-water flow fields can affect shear stresses as well as normal stresses (Iverson and Reid, 1992). When pore pressure is present, the Mohr-Coulomb failure criterion becomes

$$\tau = c' + (\sigma - p) \tan \phi' \tag{2}$$

where c' and ϕ' are, respectively, the cohesion and the angle of internal friction measured under effective-stress conditions. Thus pore pressure reduces the normal stress on potential failure planes and, in effect, reduces the internal friction that resists failure on these planes. Thus increasing pore pressure reduces the shear strength of a soil mass. This effect is illustrated in figure 3-8D, where we see that the addition of positive pore pressure shifts the Mohr circle to the left toward tangency with the failure envelope.

Recent Improvements in Test Procedures

The main advancements in laboratory testing during the last decade have been development and improvement in stress-controlled testing and improved methods for unsaturated soils (Jotisankasa and others, 2007), whereas most traditional methods were strain-controlled and restricted to saturated soils. Standardized procedures for tests based on direct shear, torsional shear, and triaxial methods have long been codified in standards of the American Society for Testing and Materials (ASTM) and national institutes of standards of other countries. Perhaps the most notable recent improvement in these procedures is that automated equipment for conducting these tests is readily available from commercial sources; however, the tests themselves have changed little over the years. Systems for static, dynamic, and controlled stress triaxial tests are also available commercially. Recently Sassa and others (2004) developed a new torsional-shear testing device that allows stress or strain control for static and dynamic testing. The primary advantage of stress-controlled tests is their ability to mimic stress conditions within different parts of the landslide. For example, in the traditional strain-controlled direct-shear test, normal stress is held constant, and the sample is sheared at a constant rate, which results in variable shear stress throughout the test. In a modern stress-controlled direct-shear or ring-shear test, normal stress can be varied to represent changing pore pressures and shear stress can be held constant to represent the static gravity loading on a hillside (Bromhead, 2004). More sophisticated stress-controlled tests can simulate earthquake loading or other field situations (Sassa and others, 2004). Research has also continued to develop true triaxial test systems in which stresses on all three principal axes differ independently (Alshibli and Williams, 2005; AnhDan and others, 2006), unlike traditional triaxial systems in which only the lateral confining stress and axial stress can differ.

Improvements for testing unsaturated soils include methods for determining soilwater characteristics that are more relevant to landslides than the traditional agricultural tests, improved methods for testing the shear strength of unsaturated soils, and a new framework for applying the effective stress concept to unsaturated soils. The soil-water-characteristic curves define the relationships between water content, hydraulic conductivity, and matric suction. Recently, capillary-rise experiments have been used to define the soil-water characteristics for wetting, which is relevant to characterizing the effects of rainfall infiltration on landslides (Godt, 2004; Lu and Likos, 2004). Research and development have continued on ways to improve laboratory systems for measuring shear strengths of unsaturated soils (Jotisankasa and others, 2007; Miller and Hamid, 2007). Recently Lu and Likos (2006) introduced the suction-stress characteristic curve as a framework for extending the effective-stress concept to unsaturated soils. This framework overcomes many of the limitations of previous attempts to describe the mechanical behavior of unsaturated soils (Bishop, 1959; Fredlund and Rahardjo, 1993).

Monitoring and Instrumentation of Landslides

Monitoring and instrumentation have several applications in the assessment of deep-seated landslides: (1) to obtain parameters and dimensions for stability and deformation analysis, (2) to observe the performance or stability of a slope, (3) to help identify the extent of movement (for example, what are the limits of the area that is moving?), and (4) to provide notification of renewed or accelerated movement. The cost and complexity of instrumentation limits the practical use of long-term monitoring and instrumentation to investigations of large, complex landslides that pose a serious threat to facilities. In this section we describe three different monitoring styles and various measurements, techniques, and kinds of instruments available for each.

Kinds of Measurements to Be Made

The applications of monitoring and instrumentation mentioned above rely on several kinds of measurements. Instrumentation to obtain parameters needed for slope stability analysis and numerical modeling is concerned primarily with determination of landslide depth or thickness and pore-water pressure in the landslide, particularly at its basal slip surface when the landslide is active. Most other instrumental monitoring of landslides is concerned with observing and characterizing the displacement and deformation of the landslide mass. Precipitation is commonly recorded as well to observe any connection between precipitation and landslide movement (Mikkelsen, 1996; Baum and Reid, 1995).

Styles and Techniques of Monitoring

For the purposes of this report, landslide monitoring can be classified into three different styles or types based on the frequency and mode of measurement: (1) campaign, (2) continuous, and (3) real-time. Campaign-style monitoring consists of a series of repeated surveys and measurements at established monitoring points or repeated acquisition of remotely sensed imagery. Consequently, this style of monitoring is generally the least frequent and is amenable to simple measuring devices as well as sophisticated instruments. Campaign monitoring shows progressive changes in a landslide and is best suited to slow-moving landslides. With the exception of remote sensing methods, campaign-style monitoring requires regular visits to the field site. Continuous monitoring relies on instruments and equipment to record measurements continuously or at regular closely spaced intervals and to save the measurements at the site for later retrieval. Real-time (more correctly, near-real-time) monitoring combines continuous monitoring with some form of automated telemetry and data processing so that monitoring results from a remote site are available to project engineers, emergency-response personnel, or others within a short time after the actual measurements occur. Real-time data processing may occur on site or at the project office. Continuous and real-time monitoring both require periodic visits to the field site for instrument maintenance or repairs; continuous monitoring also requires regular visits to collect the stored data.

Different landslide-monitoring techniques provide measurements of rate and amount of movement or deformation, landslide depth, landslide extent (plan-view dimensions), subsurface water conditions, and earth pressures. Each of the three monitoring styles includes a range of available techniques for making different kinds of measurements. Most landslide-monitoring projects require a combination of different styles of monitoring to adequately characterize movement and conditions that induce landslide movement. For completeness, brief reference is made in the following sections to long-established (pre-1996) monitoring techniques. Techniques that have appeared since the publication of Transportation Research Board Special Report 247 (Turner and Schuster, 1996) are described briefly. Olalla (2004) provides additional descriptions of some of the more recent monitoring techniques.

Campaign Monitoring

Campaign monitoring includes the classical methods of landslide monitoring such as repeated surveys for landslide movement, depth, and water levels and new methods that use laser scanners or satellite remote sensing. The primary strength of campaign monitoring is its ability to determine the spatial variability of conditions, such as movement or water level, in landslides.

Displacement and Deformation

Several styles of campaign monitoring exist for determining displacement and deformation as described briefly in the following paragraphs. Tables 1 and 2 provide additional description and comparison of the methods.

Point and Line Surveys

Time-lapse surveys for displacement or deformation continue to serve an important function in characterizing the spatial distribution of movement and have been applied along pipelines that cross landslides (Braun and others, 1998). Regardless of technique, these surveys attempt to determine the change in position of points on the ground surface of the landslide. Originally these surveys were performed using a steel measuring tape, tape extensometer, or conventional surveying instruments to determine the positions of known points on the landslide relative to fixed points on stationary ground (Keaton and DeGraff, 1996). More recently the surveys have been performed using total station or Global Positioning System (GPS) survey equipment (Bogaard and others, 2000; Coe, Ellis, and others, 2003; Tagliavini and others, 2007). Table 3-1 summarizes techniques used for these surveys. Keaton and DeGraff (1996) have compiled a more detailed evaluation of various conventional and modern surveying techniques for use in geologic mapping and monitoring of landslides.

Terrestrial Laser Scanning

The recent advent of laser scanning, also referred to as terrestrial LiDAR or tripod LiDAR, opens new avenues for time-lapse surveys (Galloway and others, 2008, Chapter 2 this report). Laser scanners are capable of rapidly measuring and recording locations of millions of closely spaced points on the ground surface. Laser scans make it possible to image the surfaces of landslides and unstable hillsides (Rowlands and others, 2003; Jones, 2006; Collins and others, 2007). Differencing scans taken on different dates reveals changes that result from landslide deformation and redistribution of materials (fig. 3-9). Displacement can also be computed for features or markers that are identifiable in imagery from successive scans. Distance accuracy ranges from ±1–5 cm for rapid, long-range scanners that are suited to topographic surveying to a few millimeters for slower, short-range scanners that are designed for detailed scanning. Despite the exciting possibilities offered by laser scanning, certain disadvantages hinder widespread application to routine landslide monitoring. These are high equipment and software costs, a steep learning curve, and the large amount of time required to process data after acquisition. Equipment costs are likely to decline as these systems become more widely adopted in the construction industry. Processing time is likely to decrease in the near future as personal-computer (PC) operating systems and software become capable of accessing larger amounts of memory and of parallel processing as computers with multiple processors/cores become more widely available. Application of laser scanning to continuous or real-time monitoring is limited to repeatedly scanning a small area of several square meters from a fixed point (G. Bawden, oral commun., 2007). Although this might be adequate for a small landslide or small area of particular concern, repeated scanning of selected more widely scattered points using a robotic (automated) total station might be more effective on a larger landslide. A robotic total station can be programmed to automatically re-survey a series of targets using either standard prism reflectors or reflectorless technology.

Aerial and Satellite Remote Sensing

Much recent work has been devoted to detecting landslides and determining landslide displacement from remotely sensed data (Van Westen, 2004; Farina and others, 2006;). High-resolution aerial photography and Synthetic-Aperture-Radar (SAR) imagery have been the most widely used for determining displacement (table 3-2). Use of remotely sensed imagery for mapping landslides was discussed previously in the section on engineering-geologic mapping and in the companion report by Harp. All of these techniques use imagery acquired on different dates to determine landslide displacement.

Displacement measurements based on high-resolution aerial photography use analytical photogrammetric techniques to determine x-y-z coordinates of photo-identifiable points (fig. 3-10). Differencing these coordinates determines the net three-dimensional displacement of points on the surface of the landslide (Fraser and Gruendig, 1985). Accuracy and reliability of photogrammetric displacement measurements is mainly a function of image scale and quality and the use of precise targets on the landslide surface and adjacent non-moving ground (Fraser and Gruendig, 1985). Photo-identifiable points, such as boulders, shrubs, and urban features (such as corners, manhole covers) usually provide less-precise measurements than targets. However, when using archival photography, such points are often the only basis for controlling the photography and determining displacement (Baum and others, 1998; Bruckl and others, 2006). Despite these limitations, analysis of photogrammetrically derived displacements and changes in elevation yielded information on surface geometry and depth (Baum and others, 1998; Casson and others, 2005). The development and increasing availability of digital photogrammetric equipment and software, as well as image-processing software, are making these techniques more readily available, but reliable identification of points still requires operator judgment (Kääb, 2002; Brückl and others, 2006).

Satellite Synthetic Aperture Radar interferometry (InSAR) uses two satellite images taken from roughly the same point in space on different dates to determine displacement (Van Westen, 2004; Froese and others, 2005; Colesanti and Wasowski, 2006; Galloway and others, 2008, Chapter 2 of this report). Wavelengths of radar satellite signals are about 5–6 cm, and displacement is determined from the phase shift in the radar signal between the two measurements when compared to a reference signal. Consequently, displacement of less than one wavelength can be determined. The angle of incidence for radar signals is usually very steep, and so the observed displacement (parallel to that line of sight from the radar satellite to the Earth's surface) is mainly the vertical component, except on very steep slopes. As a result of these characteristics of radar imagery from currently available radar satellites, InSAR is only capable of reliably detecting and measuring very slow ground-surface displacements. Farina and others (2006) found that the use of InSAR for the monitoring of single slow landslides threatening built-up areas provided satisfactory results, allowing the measurement of superficial deformations with high accuracy on landslide sectors characterized by good radar reflectivity and coherence. Vegetation and ground disruption, due to grading or landslide deformation, degrade image coherence and prevent accurate measurements (Froese and others, 2005). Recent analysis of archival L-band radar data, which is planned for some future satellites, showed that the L-band radar is capable of detecting higher rates of movement and is less affected by vegetation than currently available radar bands (Strozzi and others, 2005).

A technique known as persistent or permanent scatterers (PS) has been developed to overcome several limitations of conventional SAR differential-interferometry (DInSAR) applications in landslide studies (Van Westen, 2004; Colesanti and Wasowski, 2006). PS makes use of stable reflectors to help identify pixels on radar images and uses long time series of interferometric data. However, it has the drawbacks that it requires a large number of SAR scenes and measurements can be made for only a limited number of points (Van Westen, 2004). Colesanti

and Wasowski (2006) report that, under favorable environmental conditions, PS is suitable for monitoring slope deformations with millimeter precision. Environmental conditions that limit the application of PS include atmospheric effects, vegetation or ground disruption that degrades image coherence, and inadequate distribution of natural permanent scatterers. The PS technique combines the wide-area coverage typical of satellite imagery with the capability of providing displacement data relative to individual image pixels. However, PS is subject to the same reliability limitations mentioned previously for InSAR. Future satellites with new sensors and different acquisition geometries, combined with the improvements to radar data processing, are expected to allow a full 3D reconstruction of deformation data and help to further reduce the current limitations of the PS and similar DInSAR approaches (Colesanti and Wasowski, 2006). Froese and others (2005) and Farina and others (2006) reported detecting previously unknown landslides using differential and PS InSAR techniques; however, independent ground checking is required to determine whether the observed deformation is due to a landslide, subsidence, or other process.

Landslide Depth

Determination of landslide depth is critical to conducting stability analysis on existing landslides or other numerical modeling of a landslide and to planning remedial measures. Hutchinson (1983) described a number of techniques for determining or estimating landslide depth and emphasized that multiple techniques ought to be used, starting first with the more readily accessible observations. Multiple slip surfaces often exist and it is important to find the deepest. The more reliable methods depend on direct observation of offset in a borehole following landslide movement. The simplest and least expensive of these is the borehole probe pipe, usually a 25-mm-diameter semi-rigid plastic tube (commonly the riser pipe of a piezometer or observation well) that is inserted into a borehole. Metal rods of increasing length can be lowered down the tube in turn and the rod length that is unable to pass a certain point indicates an increased curvature of the pipe at that depth. A section of rod can be hung on a thin wire and left at the bottom of the tube; after movement has occurred, the rod can be raised to determine the lower limit of movement. The practical application of this technique in landslide investigations is to provide landslide depth information from deep piezometers that are located some distance away from the nearest inclinometer hole (Baum and Reid, 1995).

Probe inclinometers, first developed in the 1950s, continue to be the preferred method to determine landslide depth (Mikkelsen, 1996). An inclinometer casing, consisting of an internally grooved, round, rigid plastic or metal pipe, is inserted into a vertical borehole and grouted into place to provide an oriented track for the probe to travel down the boring. Alternately some inclinometer probes use a casing of square cross section (Mikkelsen, 1996). Repeated measurements of biaxial borehole inclination at fixed depth increments reveal depth, amount, and plan-view directions of borehole tilt, which are integrated to determine displacement. If the casing is correctly installed, probe inclinometers provide millimeter resolution of displacement amount. Landslide depth can be determined to within about one probe length, usually about 0.5 m (fig. 3-11).

Pore Pressure and Water Level

Wells and open-tube piezometers have long been used to determine water-table depth and pore pressure in landslides (Mikkelsen, 1996). Measurements can be made by manually probing the well or electronically by installing a pressure transducer. Pore pressure at the basal slip surface is needed for slope-stability analysis. In the absence of more detailed data about subsurface water, water-table depth indicates the approximate pore pressure for stability analysis. A well that is screened or has a slotted casing over its entire depth indicates water-table depth if the landslide

behaves like an unconfined aquifer. Open-tube piezometers, which consist of semi-rigid plastic pipe with a porous tip, measure pore pressure at a specific depth (Lambe and Whitman, 1969). The height of the column of water in an open-tube piezometer provides an accurate indication of static or slowly changing water pressure surrounding the piezometer tip, but the time lag required for water levels to respond to changing pressures prevents wells and open-tube piezometers from accurately indicating transient changes in pore pressure in response to intense rainfall, earthquakes, or landslide movement (Mikkelsen, 1996). Pneumatic piezometers use a mechanical pressure transducer that consists of a chamber filled with nitrogen and a small diaphragm that senses pressure changes. Small-diameter pneumatic tubes connect the piezometer to the ground surface, where the pressure is read by a pneumatic gage. Although these gages are more accurate than open-tube piezometers (practically no time lag) due to the small amount of water displaced, they are not easily automated (Mikkelsen, 1996). Various types of electronic pressure transducers used in continuous and real-time monitoring can also be used for campaign-style monitoring.

Continuous and Real-Time Monitoring

Continuous and real-time monitoring both have the advantage of providing time-series measurements, but the cost of instrument acquisition and installation often limits continuous measurements to relatively few discrete points. Continuous monitoring is used mainly in larger projects and in performance monitoring of major engineered works for landslide remediation. Real-time monitoring is effective when continuous monitoring is needed at remote sites and in cases where construction of engineered works is either in progress or considered too costly or dangerous and monitoring would provide adequate warning to take the actions needed to prevent loss (Fukuoka and others, 2005; Read and others, 2005). Techniques and measurements performed by continuous and real-time monitoring are essentially the same, because both rely on electronic sensors and digital recording devices (dataloggers, fig. 3-12).

Displacement and Deformation

A large range of instruments and techniques exist for making time-series measurements of landslide displacement and deformation (table 3-3). Although the majority of these techniques are designed for monitoring points on the ground surface, at least one remote-sensing technique for monitoring changes over an area is adapted to continuous monitoring, and several subsurface techniques of strain and displacement monitoring are available as well. Each technique listed in table 3-3 has certain advantages and drawbacks. For example, wire extensometers are relatively inexpensive and reliable, but wind, animals, and other environmental factors can cause false readings unless the extensometer cable is adequately protected. Most devices for continuous displacement monitoring must occasionally be reset or realigned after an amount of movement that varies with the nature and measurement range of the instrument and the rate of movement of the landslide. Others, such as borehole inclinometers and coaxial cables for TDR, are destroyed when displacement exceeds the range of the instrument. Most available techniques have been described and evaluated elsewhere (Mikkelsen, 1996; Keaton and DeGraff, 1996). However a few new techniques are worth describing further.

Real-Time GPS

"Real-time" GPS has the advantage of being able to measure three-dimensional landslide displacement without the constraints of cables or targets required by many other forms of displacement monitoring. LaHusen and Reid (2000) developed and tested an automated real-time GPS system for monitoring landslide displacement. The modular design uses a low-power

controller to store and forward raw data from a variety of single- or dual-frequency GPS receivers to a Windows-based PC that controls the remote stations and intermittently calculates fixed static solutions. Application of real-time GPS using a short baseline (<10 km) were configured using single-channel receivers. Individual solutions obtained twice per hour from 5–20 minutes of 10-second data showed repeatability of 1 cm horizontal and 2 cm vertical. LaHusen and Reid were able to filter noise and clearly discriminate sub-centimeter movements by using the median of 5 successive solutions to observe changes over 2-hour intervals and 48 successive solutions to observe changes over 24-hour intervals. By installing multiple field stations on an active landslide, it is possible to monitor displacement at several critical locations on a landslide. Recently such a system was installed at the Ferguson rock slide near Yosemite National Park, California. Due to the dangerous nature of this slide, the field stations were installed as "spiders," self-contained, self-leveling instrument enclosures that can be transported and lowered to the site by helicopter (Mark Reid, oral commun., 2006). Continuous GPS systems have also been tested in France (Bogaard and others, 2000).

Terrestrial Radar Interferometry

Radar interferometry implemented using ground-based instrumentation has been tested in Europe for monitoring landslides (Tarchi and others, 2003; Luzi and others, 2004; Duranthon, 2004; Tarchi and others, 2005). Researchers have used the technique to derive accurate, high-resolution, multitemporal surface-deformation maps of the entire depletion zone of a landslide (Tarchi and others, 2003). The portable device used by Tarchi and others (2003) is known as Linear SAR (LISA), and it uses radar waves in various frequency ranges with a synthetic aperture of up to 2.8 m. The recorded pixel displacements compared closely with independent measurements carried out by a motorized theodolite and Electronic Distance Meter (EDM) on two benchmarks. Tarchi and others (2003) reported measuring displacement rates up to about 1 m/day with millimeter accuracy and a pixel resolution of approximately 2×2 m on the ground. Scans can be made at intervals of about 15 minutes. A contractor working for the California Department of Transportation has recently deployed such a system for real-time monitoring of the Ferguson rock slide, just west of Yosemite National Park, California (Mark Reid, oral commun., 2007). Although terrestrial radar overcomes many of the challenges of satellite radar techniques, factors that degrade image coherence (quality), such as atmospheric effects, vegetation, and ground disruption, remain a challenge.

Pore Pressure, Matric Suction, and Water Content

Several types of sensors exist for observing subsurface water conditions (table 3-4). Figure 3-13 shows a time-series plot of pore pressure near the base of a landslide. Measurement of positive pore pressure is the most common requirement for deep-seated landslides (Mikkelsen, 1996), but measurements of negative pore pressure (suction) or soil-water content may be needed in the tropics (Beneveli and others, 2004) and for shallow landslides in temperate regions (Baum and others, 2005; Tan and others, 2007). The main differences in types of instruments for measuring pore pressure involve barometric correction, response times, and the ability to measure only positive pressure or a combination of positive and negative pressure. Vibrating-wire piezometers are the most commonly used type in geotechnical applications, especially where long-term monitoring is planned. As their name suggests, vibrating-wire sensors are based on measuring the frequency of a tensioned wire that is attached to a diaphragm. The diaphragm is in contact with the pore water; changes in water pressure move the diaphragm, which changes the frequency of the wire. Vibrating-wire sensors tend to be stable, accurate, and reliable, and they can be read at

intervals as short as 5 seconds. Long-term landslide monitoring usually requires readings at intervals of 10–60 minutes. Electrical-resistance pressure transducers have rapid response times allowing multiple readings per second for dynamic applications in seismically active areas, but most commercially available models have a shorter lifespan than vibrating wire sensors.

Landslide Depth

Remote measurement of landslide depth has some definite advantages and offers cost savings over regular field visits to make instrument readings. For this reason, time-domain reflectometry (TDR) is gaining wider acceptance as an alternative to using probe inclinometers for determining landslide depth (Mikkelsen, 1996). A length of coaxial cable may be fastened to the outside of an inclinometer casing or other rigid tubing before installing the casing in a borehole, which is then filled with grout. As movement occurs, the coaxial cable kinks and may eventually break. A cable tester can determine the location and amount of strain or location of a break in the cable (Kane and Beck, 1994). The time delay after a transmitted pulse and the reflection from a cable deformity determines its location. Unlike probe inclinometers, time-domain reflectometry can be readily automated for continuous or real-time monitoring. As with other instruments that are monitored in real time, the data-collection system can be programmed to issue an alarm when critical amount of strain is detected. Landslide depths determined by TDR are comparable to those determined by inclinometers.

Internal Forces and Pressures

Vibrating-wire earth-pressure cells and load cells have been available since the 1980s or perhaps earlier for monitoring lateral pressures in landslides or forces applied by a landslide mass on a wall or on tieback systems. We found few published papers on use of these instruments in landslides; most applications seem to be for monitoring dams, embankments, and other earth works. Li and others (2004) installed earth-pressure sensors in a landslide, but published no results related to the earth-pressure measurement. Load cells have been used to monitor tension in tie-backs (Nichol and Graham, 2001), and increasing load was related to landslide movement at one end of a tie-back wall, but could not be explained at the opposite end.

The distribution of forces within a landslide is related to its stability. Internal forces are likely to change in response to progressive and retrogressive failure, movement, and external changes (applied loads, major erosion). One potential application of earth-pressure measurements to landslides would be for comparing lateral earth pressures in zones of longitudinal shortening or extension with results of limit-equilibrium and finite-difference or finite-element slope-stability analyses (Baum and Fleming, 1991; Picarelli and Russo, 2004). Application of earth-pressure measurements to landslide investigation or warning seems to be an area ripe for additional research. However, practical use of earth-pressure measurements in landslide monitoring and investigation appears to be quite limited at present.

Seismoacoustic Emissions

Since the 1960s, a small body of research has been conducted on detecting landslide movement using microseismicity (Goodman and Blake, 1965; Kolesnikov and others, 2003). Fracturing of rocks or soil during the formation, reactivation, and movement of landslides emits distinctive acoustic and seismic signals that can be detected by seismic monitoring at the site. Microseismic monitoring has potential application to detection and early warning of movement, rather than monitoring the amount of displacement. Although microseismicity has found application in other fields such as hydraulic fracturing and structural monitoring, very few

applications have been made to landslides (Gomberg and others, 1996; Gaertner and others, 2000; Amitrano and others, 2007).

Environmental Factors

Precipitation is the most commonly measured environmental variable in landslide investigations and monitoring. Tipping-bucket rain gages are commonly used in these studies. The gages can be calibrated for millimeter or inch measurements with reported accuracy of ±1 mm or ±0.01 inch. Strong correlation usually exists between precipitation and pore pressure at depth, even in landslides that are many meters deep (Iversen, 2000; Lollino and others, 2006). Measurements of barometric pressure at the site are needed to make corrections to measurements by sealed piezometers. Barometer measurements should occur on the same schedule as piezometer measurements. Evidence also exists that changes in barometric pressure may affect pore pressure in low-permeability clays and thereby induce landslide movement (Köhler and Schulze, 2000). Various types of recording barometers are available; however, the corrections can also be made by monitoring a pressure transducer of the same type as used for measuring subsurface water pressures. Soil temperature can also be measured to observe time and depth of soil freezing. Most pressure transducers used in electronic piezometers and tensiometers are temperature-compensated and have built in temperature sensors that can be used to make soil-temperature observations.

Measurement Locations

Obtaining meaningful or representative results from subsurface exploration and monitoring depends on placing boreholes and instruments in optimal locations (table 3-5). Mapping a landslide in enough detail to identify its main features (fig. 3-3) and distinguish shallow surficial movements from the main body of the landslide is the first step in defining those locations. Landslides tend to be thinner and generally move more slowly near the edges than in the central part of the main body. The critical parameters to be observed for an existing landslide include depth and shape of the basal failure surface, pore-water pressure, shear strength, and displacement or deformation. Similar observations need to be made for potential landslides, but finding the optimal locations for these observations is much more difficult because the boundaries of a potential landslide may be difficult or impossible to define. In either case, observations of the depth and shape of the basal slip surface should concentrate on the main body of the slide (or potential landslide), initially near the central axis that is parallel to the direction of downslope movement (table 3-5). The basal slip surface often intersects the ground surface at the main scarp and at the contact between the toe and undisturbed ground beneath the toe (fig. 3-3). For example, a line of boreholes like those in figure 3-14 makes it possible to construct a representative cross section of the landslide. In the case of more complicated landslide shapes (in plan view), or other complicating factors, a different arrangement of boreholes may be appropriate (Corsini and others, 2006).

Landslide investigations commonly proceed in stages. Information gathered during the early stages of exploration and instrumentation usually guide more detailed exploration and instrumentation in the later stages (Baum and Reid, 1995; Chelli and others, 2005; Read and others, 2005). Once the depth of the basal slip surface has been determined by inclinometer or time-domain reflectometry observations, piezometers can be installed in adjacent boreholes as close as possible to the depth of the basal slip surface. If the budget allows, additional piezometers can be installed at lesser depths (higher levels) within the slide. Assuming adequate sample recovery, geotechnical testing (especially shear-strength measurements) should concentrate on materials from the depth of the observed slip surface.

Optimal locations of displacement measurements are usually in the same locations as depth and pore-pressure observations. For application to pipelines, observations should, at a minimum, be made at several points across the landslide along the pipeline alignment (table 3-5). Additional observations of displacement at points in the main body upslope and downslope of the alignment can help in recognizing waves of more rapid movement that are propagating either upslope or downslope toward the pipeline (Iverson, 1986).

Costs and Reliability

Available technology offers a wide range of possibilities for monitoring landslides depending on field conditions, expected style and potential consequences of movement, and the goals and budget of the monitoring program. Field data collection and monitoring, whether manual or automated, are labor intensive and therefore costly activities. Design of a monitoring program for an individual landslide or a group of landslides along a pipeline corridor requires substantial field work and analysis to determine the locations and types of measurements needed (Angeli and others, 2000). As a result of rapidly changing technologies, background research must be conducted to identify the most suitable components for a monitoring system. A common pitfall in this phase of landslide investigation is underestimating the true costs of instrumental monitoring programs. Estimating the cost of the initial investment in equipment and installation is relatively straightforward. However, in addition to the initial, one-time costs of background fieldwork and research, and equipment acquisition and installation, the costs of data collection, surveillance (monitoring system performance and data flow), repairs, maintenance, and data processing continue for the life of the project. Depending on the duration of the project, the continuing costs can approach or, in some cases, exceed the initial investment.

Costs

We estimated relative costs of various measurement and monitoring techniques applicable to landslides as an aid in comparing methods for obtaining similar kinds of measurements. These costs have been averaged over 5 years to balance acquisition costs against operating costs. Although the service life of instruments varies considerably, 5 years seems like a reasonable average based on our experience. To compute labor costs, we estimated amount of labor from USGS experience in installing, operating, or maintaining similar equipment, multiplied by an annual labor cost of $100,000. We did not include any costs for overnight travel associated with fieldwork. Tables 1 and 2 list techniques for campaign-style measurements and assume a low annual measurement frequency (one or two per year). Tables 3 and 4 list techniques for continuous measurement and assume high measurement frequencies (multiple measurements per day or per hour), with data analysis occurring four times per year. Continuous measurement techniques are automated and have much lower cost per data point than most campaign-style measurement techniques. Campaign-style measurements are labor-intensive and their cost rapidly escalates with increasing frequency of measurement. For example, measurements using tape or tape extensometer rise from low to intermediate cost as frequency increases to quarterly or monthly.

Tables 3 and 4 compare the costs of operating individual instruments for various kinds of measurements. A more likely scenario is to operate a suite of instruments at a site. To provide a representative example, we computed the cost of a real-time monitoring system that includes a rain gage, three borehole tilt meters, and three piezometers (each in a separate borehole), data logger, solar power, radio telemetry, and a PC with software to receive and analyze data. As might be expected, the cost is in the "high" range ($22,500 annually for 5 years). Taken individually, however, the cost of each of the seven sensors drops into the "low" range and the quantity and

quality of data that can be collected by such a system far exceeds what can be done for the same cost using manual techniques.

Reliability

Reliability of monitoring results generally increases with the spatial distribution and density, and the frequency of measurements. Instrument accuracy and reliability aside, measurement of displacement, pore pressure, or any other quantity at a single point on a landslide has a high degree of uncertainty. Rates of movement, water levels, and other characteristics of landslides are known to be highly variable in space and time (Baum and Reid, 1995). Understanding the structure and geometry of a landslide helps ensure that measurements are made in areas that represent movement of the main parts of a landslide. Making frequent measurements at multiple locations is key to characterizing a landslide adequately to make any forecasts about future movements. Considerable thought and analysis of all available data must go into planning of a landslide instrumentation project (Mikkelsen, 1996; Angeli and others, 2000).

A combination of technologies is generally needed to adequately monitor and characterize ground movements that potentially affect a pipeline or another linear facility. Most monitoring technologies offer adequate accuracy and precision (tables 1–4); their limiting factors tend to be high cost (for some techniques), mode of deployment, and their technical characteristics. For example, wire extensometers are capable of providing detailed continuous records of movement, but they provide no directional information and their range of motion is somewhat limited. Periodic surveys (total-station or GPS) are needed to provide a complete record of movement at an extensometer. Surveys to show the spatial distribution of movement are needed to detect changing patterns of movement and possible acceleration in locations where continuous monitoring is considered to be unnecessary or impractical.

The need for redundant measurements is another factor that must be emphasized. Despite efforts to engineer sensors for harsh environmental conditions, instrumental measurements routinely fail, often at critical times. Lightening strikes, battery failure, vandalism, animals, and other adverse events can and do render monitoring equipment inoperable. Even when instruments are working correctly, measurement errors occur as a result of animals, weather, and other factors. A back-up system of measurements is needed to assure that measurements can continue during critical times and to maintain a continuous record. One advantage of real-time monitoring over continuous monitoring without telemetry is that instrument or measurement failure can be detected soon after it occurs. Another advantage is that the data can be integrated easily with a geographic information system (GIS) to facilitate interpretation and decision making (Hutchinson and others, 2004).

The choice between automated and campaign-style data collection depends on economics, safety, and remoteness of the landslide(s) as well as technical factors. In developing countries, where a pipeline crosses a populated area of slow landslides on gentle to moderate slopes, campaign-style monitoring using local labor and simple, inexpensive technology might prove effective and adequate. In areas where a pipeline crosses steep terrain and rapid movements are possible, automated monitoring may be the safest and most practical choice. However, in most areas, some combination of automated and campaign monitoring (either by site visit or remote sensing) will be needed to satisfy technical and budgetary requirements of the project. The demands of continuous or real-time data collection commonly preclude monitoring a large number of points, therefore campaign-style measurements and remote sensing techniques provide the spatial distribution of observations that cannot be observed by a few continuous monitoring stations alone (Coe, Ellis, and others, 2003).

Measurement priorities for landslides that affect or potentially affect pipelines are generally driven by the need to protect the pipeline from damage or rupture. Thus, displacement where the pipeline crosses the landslide boundaries (head scarp, toe, lateral shear zones, or internal shears) is generally the first priority. Next is displacement at points upslope and downslope of the pipeline to observe progressive or retrogressive movements that might soon affect the pipeline. At landslides where remedial measures are considered, measurements of landslide depth and pore-water pressure at the basal shear surface are needed as input for slope-stability analysis. Monitoring of pore-water pressure can also identify threshold pore pressure needed to induce movement and provide early warning of impending movement (Picarelli and Russo, 2004; Ellis and others, 2007).

Areas for further research include use of strain gages or load cells along a pipeline where it crosses a landslide to provide early warning of distress before significant damage can occur. Use of horizontal coaxial cable encased in grout and buried in the trench alongside the pipeline might provide a means to monitor differential movements and locate them using time-domain reflectometry. TDR technology appears promising based on a similar application to a railway (Kane, 2007). The development of wireless networks based on low-cost sensors and wireless servers is an area of active research based on USGS contacts with universities (Sheth and others, 2005; Kevin Moore, Colorado School of Mines, written commun., 2006). However, application of these technologies to landslide monitoring awaits advances to reduce power consumption to acceptable levels for remote applications and greatly improved locational accuracy of the wireless-sensor technology.

Methods of Stability, Stress, and Deformation Analysis

Mathematical analysis of landslides is used to understand their individual mechanisms and make predictions about their responses to natural or human-induced changes in their geometry, external loading, ground-water levels, and other factors. Simple empirical methods of analysis use observational data to make predictions about time to failure, travel distance for debris flows, or threshold pore-pressure levels or rainfall amounts to induce landslide movement. Limit-equilibrium slope-stability analysis (LE) is very useful in determining the factors that affect stability of a landslide mass, hillside, or earthwork as well as planning and evaluating potential remedial works for landslides. LE methods have some important limitations because, as their name implies, LE methods attempt to solve only the equations of equilibrium. Analytical solutions have been obtained for a few boundary- and initial-value problems that describe important landslide processes in one or two dimensions; however, their value is primarily for understanding the process rather than application to particular landslides (Savage and Wasowski, 2006). Numerical methods of stress and deformation analysis solve the equations of motion (or equilibrium) and continuity for different material constitutive models to provide estimates of deformation as well as internal forces/stresses (Savage and others, 2003; Smith and Griffiths, 2004). Some recent methods are even capable of analyzing the dynamics of large deformations associated with movement of rock slides and debris avalanches (Crosta and others, 2003; Denlinger and Iverson, 2004).

In the following paragraphs, we review the capabilities, data requirements, recent developments and trends, and pitfalls of the various types of mechanical analysis available for landslides. The discussion focuses on groups and classes of methods used in these analyses, rather than details of specific methods and software, which are constantly changing. Nevertheless, the capabilities and limitations of various methods are illustrated with a few specific examples from the literature.

Methods and Capabilities

Empirical and Statistical Methods

Prediction of Time to Failure

In several case studies of creeping slopes that subsequently failed, post-failure empirical analysis of accelerating displacements has been relatively successful in predicting the observed time of failure. Small but measurable displacements commonly occur prior to initial failure of a slope or reactivation of landslide deposit. Saito (1965) observed an accelerating trend in these displacements and proposed using this trend in forecasting time to failure. Fukuzono (1990) found that plotting inverse velocity (v^{-1}) versus time yields a straight line that can be used to predict the time of failure. Other workers have used Saito's observation or further developed the related theory (Varnes, 1982; Voight, 1988; Kilburn, and Petley, 2003). Recent work indicates that linearity probably is associated with crack growth and would be expected where brittle failure is the primary process occurring at depth. An asymptotic trend in the plot of inverse velocity versus time is expected where ductile failure or sliding on existing surfaces is occurring at depth (Kilburn and Petley, 2003). Using displacement observations at multiple points on the surface of the developing landslide or reactivation makes it possible to observe the spatial progression of the failure and greatly aids interpretation of the failure process (Petley, 2004).

Movement Thresholds

Landslide movement thresholds, based on either rainfall or pore pressure/water level, have been determined by comparison between measurements of rainfall or pore pressure and displacement. Such models are useful for making predictions and have modest data requirements, such as several years of displacement and rainfall observations. However, they are unable to predict changes in displacement by other factors, such as loading at the head of the landslide by debris flows or rock falls or erosion at the toe. Grivas and others (1996, 1998) and O'Neil and others (1996) developed empirical models for predicting movement of a slow landslide based on monthly rainfall. These authors also explored application of time-series analysis to the development of rainfall-displacement models. For the case studied, the models provided reasonably accurate predictions of long-term (10-year) cumulative displacement. Hong and others (2005) developed rainfall intensity and duration thresholds for movement of deep-seated rockslides. Dixon and Brook (2007) used predicted climate change with empirical precipitation thresholds for movement of the Mam Tor landslide in Derbyshire, UK, to analyze future reactivation potential and showed that damaging movements may become more frequent by the latter part of the 21st century. Rainfall thresholds have been developed for debris-flow initiation for many areas of the world as summarized by Wieczorek and Glade (2005). Pore-pressure thresholds have been developed for individual landslides, such as the Johnson Creek landslide on the Oregon coast (Ellis and others, 2007).

Travel Distance

Several empirical and semianalytic approaches have been developed for predicting travel distance or potential travel distance of debris flows and rapidly moving landslides. For application to pipelines, these methods have application to identifying areas where above-ground pipeline facilities might be subject to damage or inundation by debris flows as well as identifying where debris flows might impact existing deep-seated landslides and increase their potential for reactivation. Hungr and others (2005) summarize most of the available methods, including their

advantages and limitations. The majority of these methods requires some type of observational data relating travel distance to one or more other parameters such as slope height, slope angle, or landslide volume.

Limit-Equilibrium Analysis

Despite considerable advances in numerical methods of stress and deformation analysis, review of recent literature reveals that LE methods continue to be used routinely in engineering investigations of landslides (Sharma, 2007). Research to improve the efficiency of LE methods also continues (Das, 2005; Zhu and others, 2005). LE methods require the analyst to make certain assumptions about the failure mechanism and provide no information about potential landslide deformation because these methods attempt to solve only the equations of equilibrium.

Limit-equilibrium methods use the balance of forces acting on a landslide or potential landslide to compute what is called a factor of safety (also known as safety factor). In simplest terms, the factor of safety is the ratio of resisting forces that tend to keep the mass in stable equilibrium (shear strength of soil and/or rock, tree roots, retaining structures) to the driving forces (gravity and external loads) tending to cause the mass to slide downhill. This is based on a classical approach used in designing engineering structures which considers the relationship between the capacity C (strength or resisting force) of the element and the demand D (stress or disturbing force). The factor of safety of the structure can be simply defined as $F = C/D$ and failure is assumed to occur when F is less than 1. Methods of slope-stability analysis assess the ratio of the shear strength to the shear stress required for equilibrium using soil cohesion, angle of internal friction, and normal stress on the basal slip surface, which depends on pore-water pressures, soil unit weight and landslide geometry (Morgenstern and Sangrey, 1978; Duncan, 1996). Many limit-equilibrium methods subdivide the landslide into vertical slices (Morgenstern and Price, 1969; Duncan, 1996; Sharma, 2007), as shown in figure 3-15.

The factor of safety is complex because landslides can begin in several different modes, including sliding, toppling, and a combination of sliding and toppling. An example of more complex slope-stability analysis using methods of slices within landslides is shown by Wu (1969, p. 248–250). Many factors contribute to slope-stability analysis, including distribution and physical properties of geologic materials, slope configuration, external loading conditions, ground-water infiltration and levels, types and depths of vegetation, and daily and seasonal precipitation affected by temperature. Different approaches to and methods of stability analysis are relevant to different types and depths of landslides, such as, shallow debris flows and deep rock slides, depending on their geometry, internal structure, mode of failure, and other factors. Dynamic loads may be treated as static loads (pseudo-static); equivalence between pseudo-static loading and gravity loading greatly simplify analysis (Shukha and others, 2005).

Methods of static slope-stability investigations using available limit-equilibrium analyses, including an assessment of their accuracy were presented in Duncan (1996) and Chapter 9 of Blake and others (2002). The primary differences between methods are how interslice forces are treated and whether the method satisfies all equations of moment and force equilibrium. Methods that satisfy all equations of equilibrium are considered more accurate than those that satisfy only some of the equations (Duncan, 1996; Sharma, 2007).

Performing slope-stability analysis using physical evaluation and depth measurements can be very difficult because of unknown information, as described by Duncan (1996). Errors in stability analysis arise more from choice of strength parameters, pore pressures and external loading than from the method of analysis used. Physically determining the detailed orientation of the geologic materials and variability of the strength and moisture at different depths of materials

can affect the accuracy of slope-stability analysis. Fracturing, ground-water movement, and other changes at a landslide site make it difficult or impossible to determine pre-failure slope-stability conditions, even though landslide boundaries and depth can be determined precisely. Conversely, although the materials can be measured and ground water can be monitored before a landslide failure initiates, it generally is impossible to determine, in advance, the exact location, shape, and depth of the movement.

Unless the shape of the slip surface is known in advance, LE methods must search for the so-called "critical" slip surface, which has the lowest factor of safety. Most search routines are limited to circular slip surfaces, but new methods based on optimization techniques of variational calculus (Baker, 2005), genetic algorithms (Das, 2005), and neural networks (Samui and Kumar, 2006) as well as an approach using "stress acceptability criteria" (Sarma and Tan, 2006) have been devised to find the critical slip surface and overcome the limitations of previous methods. These new methods can search for circular and noncircular critical slip surfaces in homogeneous and non-homogeneous materials, and their success is not limited by user assumptions about the shape or general location of the slip surface. However, these new methods have not yet been extensively applied; so their accuracy and reliability are not fully known.

Three-Dimensional Methods

Use of three-dimensional slope-stability analysis is still rare, but is becoming more common (Bromhead, 2004). Three-dimensional methods began to appear in the late 1970s and 1980s (Hovland, 1977; Chen and Chameau, 1982; Xing, 1987; Hungr and others, 1989; Casamichele and others, 2004). These methods involve subdividing the landslide or potential landslide into vertical columns and solving depth-averaged equations of equilibrium to obtain a factor of safety. Three-dimensional methods differ from one another in the assumptions made about intercolumn forces and each is based on a corresponding 2-D method. Two-dimensional analyses continue to be the most widely used methods of slope-stability analysis, in part because they are widely considered to yield lower factors of safety than 3-D methods and in part because data and computational requirements of 3-D analysis are much greater than for corresponding 2-D analysis. However, recent work has shown that for certain landslides, 2-D factors of safety on the principal cross section are actually higher than 3-D factors of safety (Bromhead, 2004).

Bromhead and others (2002) and Bromhead (2004) reviewed circumstances where three-dimensional analysis is required; these include landslides of irregular shape, localized loading, weak zones, localized pore-water or pore-pressure concentration, and landslides with bedding-controlled basal shear surfaces. In one recent application of 3-D methods, a digital-elevation model (DEM) is searched for the most critical slip surface centered at each grid cell to identify the areas most prone to rotational or other deep-seated failure (Brien and Reid, 2001; Brien and Reid, 2007). Bromhead (2004) described a numerically integrated "wide-column" approach that uses concepts from finite-element analysis to adapt methods of columns to landslides of general shape.

Authors of different methods of 3-D slope-stability analysis have tested and verified their methods against corresponding 2-D methods and some simple 3-D cases (Chen and Chameau, 1982; Hungr and others, 1989). The method of Hovland (1977) neglects intercolumn forces and computes lower factors of safety than other 3-D methods. Based on these analyses, 3-D methods appear to give accurate results; however, we are unaware of any rigorous evaluations of 3-D limit-equilibrium methods.

Ground-Water Flow Modeling

Ground-water flow modeling is a broad field that continues to experience rapid advancements; in this section, we briefly review some recent applications of ground-water flow models to landslide analysis. Iverson (2000) analyzed the effects of transient rainfall infiltration on landslide initiation and movement. His analysis included an explanation of how rainfall infiltration affects movement rates of translational landslides. Malet and others (2005) used a depth-averaged three-dimensional model of ground-water flow to analyze long-term hydrologic effects and climate change on a large deep-seated landslide. Tacher and others (2005) used a three-dimensional ground-water model to analyze long-term ground-water levels in large deep-seated landslides considering effects of infiltration, heterogeneity lateral in flow, and artificial drainage. Their model demonstrated that a proposed drainage scheme could significantly reduce water pressures and the potential for future surges.

Continuum Stress and Deformation Analysis

Many landslides and hillsides can be modeled using a continuum approach. Numerical continuum methods currently available for slope-stability and deformation analysis make it possible to compute a full solution of the stress and deformation equations in two and three dimensions (Hungr and others, 2005; Griffiths and Marquez, in press). Some models are specifically designed for modeling stress and deformation of coherent landslides and can also compute a factor of safety just as computed by LE methods (Savage and others, 2003; Smith and Griffiths, 2004). In a recent development (Cala and others, 2004), the shear-strength-reduction technique used for computing the factor of safety has been extended to analyze several potential failure modes/slip surfaces. Besides computing factor of safety, some numerical codes are designed for modeling the movement of large, long-runout landslides, flows, and avalanches once initial failure has occurred (Crosta and others, 2003; Denlinger and Iverson, 2004; Hungr and others, 2005). Despite recent advances in software and methods, stress and deformation analyses of landslides still are not routine. They require more time and effort than limit-equilibrium analyses and require considerable expertise to achieve accurate and meaningful results.

Numerical analyses currently available are based on finite-element, boundary-element, and finite-difference formulations and are capable of handling a wide variety of constitutive models. This includes the ability to introduce strain-softening properties for the various materials, without the need to pre-define or “average” strength reductions. Strain softening has been implemented in various 2-D and 3-D continuum codes. For example, Puebla and others (2006) modeled progressive/retrogressive strain softening and resulting moderate to large (1 m or more) deformations in good agreement with observed ground movements. Troncone (2005) used a strain-softening constitutive model to analyze the progressive failure mechanism of the slope and obtained good agreement between the observed and predicted failure geometry and mechanism. Some codes offer the possibility of coupled analyses of ground-water flow and slope deformation (Hungr and others, 2005). For example, Konietzky and others (2004) modeled ground-water flow and slope stability in response to rainfall and changes in reservoir level. Most methods, including traditional finite-element analyses use Lagrangian (material or moving) coordinates and are able to model slope deformation so long as it does not drastically distort the mesh (Hungr and others, 2005). Some recent efforts have used combined Lagrangian and Eulerian (fixed-in-space) coordinates to enable them to model large deformations without distorting the finite-element mesh (Crosta and others, 2003). Other recent advances include zero-thickness elements for representing joints (Hürlimann and others, 2004) and fracture-mechanics elements to represent growth of fractures or slip surfaces (Zi and Belytschko, 2003).

One of the advantages of continuum methods over LE methods is that the model automatically or "naturally" determines the critical failure surface as part of the solution (Griffiths and Lane, 1999). Strain localization and development of a displacement or velocity discontinuity clearly delimits the depth of the failure zone (fig. 3-16). Numerical analysis of some complex landslides has predicted shear zones that are in close agreement with observed ones (Savage and others, 2000; Savage and others, 2003; Baron and others, 2005; Marcato and others, 2006; Chugh and others, 2007). Another advantage of these methods over the LE methods is that no assumptions need to be made about interslice or intercolumn forces to compute the factor of safety.

Displacement Predictions

Computation of displacements is of interest in application to pipelines, because expected displacement determines the potential for slope movement to damage a pipeline. Accuracy of displacement predictions depends on many factors, including material properties, geological details, and modeling details. Further, it is necessary to calibrate continuum models against reasonably well known landslide or ground-movement records prior to using them to make predictions about displacements under various pore-pressure or loading scenarios. Otherwise application of the models to conditions for which there is no or limited comparable existing landslide data is open to question. Model results are sensitive to variation in geotechnical parameters, ground-water conditions, and geometric factors (location and inclination of weak zones, material contacts, and so on). Natural soils and rock tend to be nonuniform and have more complex stress-deformation behavior than engineered materials (Duncan, 1996). Therefore, model construction, calibration, and analysis require considerable time and effort. Reliability of calculated movements for natural slopes is not as great as for engineered embankments (Duncan, 1996).

Recent work by various authors (cited below) using calibrated models has provided displacement estimates within a factor of two or three of observed displacements. Although displacements of some points in the models were well within ±10 percent of the observed values, and the overall patterns and directions of displacement agreed well, the least accurate points or rates differed by roughly a factor of two (-50 percent/+100 percent) or three (-67 percent/+200 percent). Vulliet and Hutter (1988) obtained fair to good agreement between observed and predicted displacements using 3-D equations and viscous sliding laws to model the La Frasse landslide, Switzerland. Subsequently, Tacher and others (2005) used coupled ground-water flow and stress-deformation finite-element models to investigate the effects of the proposed drainage scheme on future landslide movement. Model results for a past episode of relatively rapid movement showed fair agreement between observed (2.6 m) and calculated (4.6 m) displacement. Konietzky and others (2004) used a Lagrangian finite-difference method to predict displacements within a factor of two of observed displacements for rain-induced slip events of a slope. Chugh and others (2007) obtained a similar level of accuracy in an analysis of a landfill failure. Amatruda and others (2004) used an indirect boundary-element method to compute mean-annual displacements of a large landslide. Deng and others (2007) obtained fair to good agreement between observed and computed displacement directions for a complex landslide. Corominas and others (2005) solved a one-dimensional version of the momentum equation using finite differences in a viscoplastic analysis and obtained fair to good agreement between model results and observations. Monitoring and modeling have contributed to greater understanding of how pore-pressure fluctuations, erosion, and stress relief drive the movement of slow active landslides (Picarelli and Russo, 2004). In addition to modeling deformation from static or quasi-static loading, continuum methods can also analyze stability during dynamic loadings such as earthquake shaking or sudden failure; however, temporal predictions are rarely attempted because of the complexity and detailed data requirements

(Hungr and others, 2005). Various workers have been successful in modeling large displacements of debris avalanches and debris flows using either the equivalent-fluid approach in depth-averaged 2-D (Hungr, 1995; Kwan and Sun, 2006) and 3-D models (Denlinger and Iverson, 2004; McDougall and Hungr, 2004; McDougall and others, 2006) or 2-D finite-element methods (Crosta and others, 2003).

Discrete-Element Analysis

Rather than treating a hillside as a continuum, the discrete- or distinct-element method subdivides it into independent, disconnected pieces or elements. This method is well suited to slopes where discontinuities, such as faults, joints, bedding planes, or foliation control the mechanism of instability. Thus, discrete-element analysis has obvious applications to modeling the stability of rock slopes, including failure as rock fall, rock slides, and debris avalanches, but it can also be applied to more coherent landslides (Hungr and others, 2005). A physical analogy for a 2-D discrete-element model is a stack of rods (of any desired cross-sectional shape) with their long axes parallel to one another. In three dimensions, the discrete elements represent a pile of balls or blocks. The elements can be either rigid or deformable, but most methods allow the blocks to deform. Discrete-element models apply the laws of dynamics to each individual element and its interactions with its neighbors and the surroundings to compute the forces acting on and within the mass, as well as computing movement of the individual parts.

Rock-fall-simulation models are one of the simplest examples of discrete-element analysis. For example, the extent of the areas potentially subject to rock-fall hazards in the Yosemite Valley were obtained using STONE (Guzzetti and others, 2002), a physically-based rock-fall-simulation computer program. The software computes 3-D rock-fall trajectories starting from a digital-elevation model (DEM), the location of rock-fall release points, and maps of the dynamic rolling-friction coefficient and of the coefficients of normal and tangential energy restitution. For the Yosemite Valley, a DEM with a ground resolution of 10×10 m was prepared using topographic contour lines from U.S. Geological Survey 1:24,000-scale maps (Guzzetti and others, 2003). For each DEM cell, the software calculates the number of rock falls passing through the cell, the maximum rock-fall velocity and the maximum flying height. However, the modeling software STONE is unable to consider the volume and mass of the falling boulder, the shape of the block, or the tendency of rock falls to split during successive impacts.

Although generally used when more detailed topography or profiles, with slope breaks, are available, the Colorado Rockfall Simulation Program (CRSP) (Jones and others, 2000) and a probabilistic rock-fall program, based on the work of Stevens (1998), incorporate shape and mass (CRSP) or mass (Stevens, 1998) and provide data on both the velocity and impact energy of the rock fragment considered. The program by Stevens (1998) also provides estimates of rock-fall runout for the various sizes (masses) considered.

In a survey of recent literature, Hungr and others (2005) found that distinct-element analysis has been used to investigate a wide variety of rock-slope failure mechanisms including planar sliding, complex deep-seated sliding, rotation, toppling, and buckling. Konietzky and others (2004) used particle modeling to investigate creeping rock-/debris-slide deposits on the slope of a reservoir and were able to decipher the failure mechanism and estimate the volume of material that would flow into the reservoir under worst-case conditions. Discrete-element models have also been used to analyze effects of rock fall on covered galleries (Shiu and others, 2006). Stead and others (2004) used a hybrid finite-/discrete-element method to model a complex rock-slope failure mechanism. Coupled hydromechanical, distinct-element modeling has been used to analyze the effects of drainage on landslide movement (Hungr and others, 2005).

Data Requirements

All types of landslide analysis have several basic data requirements in common. Table 3-6 summarizes the data requirements for different methods of analysis. At a minimum, data requirements include geometry of the landslide or potential landslide mass (surface topography, stratigraphy, structure and discontinuities, and geometry of the basal slip surface), relevant strength properties, and subsurface water pressures. Stress and deformation analysis require some additional types of data beyond that required for LE methods (observed displacements, rates of movement, and elastic properties), but this addition is fairly modest. However, determining representative deformation moduli beyond the elastic range, necessary for continuum analyses of permanent ground movements and failures, is extremely difficult using normal laboratory or even field testing. The dimensionality and complexity of a slope or landslide have a great impact on the amount of data required to perform a satisfactory analysis regardless of the chosen method of analysis.

Challenges, Dilemmas, and Reliability

During the last decade, several advances have been made in numerical modeling techniques for landslides. These include some incremental improvements to application of limit-equilibrium analyses, major advances in continuum and discrete-element methods and increased use of probabilistic or reliability (Duncan, 2000) methods to define the degree of uncertainty in the results of numerical analyses of all types. These advances allow models to better represent and predict failure modes and mechanisms, slip-surface geometry, displacement, and interaction between subsurface water and hillslope materials (Hungr and others, 2005).

Software for nearly all of the numerical modeling techniques described here (except new or experimental techniques) is available in ready-to-use commercial packages, but some is also available in the form of published source code (such as, Smith and Griffiths, 2004). The majority of the published analyses in recent years (including most of those cited in this report) have used commercial software packages to conduct sophisticated numerical analyses. Commercial packages generally offer technical support and software maintenance, but users are not able to view or modify the source code; thus the details of how the software handles certain situations or computations may not be well documented. Open-source software on the other hand is open to scrutiny and modification by the user, but generally little or no technical support is offered.

A wide variety of methods is now available for modeling landslides and slope stability and the widespread availability of powerful personal computers and modeling software make modeling adaptable to diverse project requirements and relatively easy and accessible. However, this abundance of user-friendly modeling tools opens the possibility of modeling without having any real physical understanding of the processes and factors involved (Bromhead, 2004). Modeling efforts must be closely tied to field mapping and monitoring as well as to laboratory and in-place testing and measurements to ensure that meaningful results are obtained (Hungr and others, 2005). Modeling is a useful tool, but it must not be substituted for critical thinking and sound judgment.

A series of questions may help define some of the challenges and limitations of modeling.

- What are the objectives of modeling?
- What tools and how much modeling effort are needed to achieve the objectives?
- How much data of what quality is needed to produce the desired results?
- How far can the problem be simplified and how does one recognize adequate conceptual models?
- Are the modeling results consistent with field observations and measurements?

The first question although obvious, is an important one, because modeling objectives must be clearly defined at the outset, and the objectives must determine the answers to the remaining questions. Modeling intended to make a prediction of landslide displacement over some given period of time requires different techniques, significantly more effort, and higher-quality data than modeling to determine a factor of safety. This translates into significantly higher costs, not only for the actual analysis, but also for the field investigation, monitoring, and material-properties testing. In many cases the quality of the data available is only adequate to model present conditions and to obtain some qualitative understanding of the failure mechanism and factors that influence stability. The question of simplification, although dependent on data quality, usually requires judgment and some experimentation to determine how much complexity must be included to enable the model to reproduce observed behavior of a landslide. Forward modeling to make predictions about potential movements or responses to various changes requires much additional high-quality data (Hungr and others, 2005).

Cost

The cost of modeling is another factor to be considered. The cost of field-data acquisition needed to support modeling is usually substantial; some of these costs have been described briefly in the section on monitoring and instrumentation. Costs specific to modeling include computer hardware and software and staff time needed to develop, parameterize, calibrate, and run the model. Using the cost scheme developed for monitoring, the cost of empirical modeling and 2-D LE modeling, is usually in the low to moderate range. As a model becomes more complicated, its cost increases by adding the third spatial dimension, time dependence, heterogeneity, or other special model features. As a result, the cost of using 2-D or 3-D, time-dependent continuum models to analyze displacements for complex landslides is usually in the high to very high cost range.

Reliability

The question of reliability in modeling landslides is challenging. Previous authors have shown that numerical modeling is capable of producing results that are in reasonable agreement with observation for factor of safety (Duncan, 1996; Bromhead, 2004; Chugh and others, 2007), slip -surface/shear-zone location and shape (Baron and others, 2005; Hungr and others, 2005; Chugh and others, 2007), and displacement amount (Crosta and others, 2003; Konietzky and others, 2004; Chugh and others, 2007). However, uncertainty remains in any model results, and the input data are usually sources of much greater uncertainty than the method of computation (Bromhead, 2004).

Nadim and others (2005) discussed uncertainty in terms of a probabilistic approach. Among other notable findings, they report that in some cases a potential slip surface with a higher factor of safety may also have a higher probability of failure than a slip surface with a low factor of safety (fig. 3-17). This can result from greater uncertainty in pore pressure, strength parameters, and other factors. Most probabilistic analyses lack the necessary data to compute an actual annual probability of failure; rather they provide a measure of the uncertainty in the input data and the computed factor of safety or displacement. Computing an annual probability of landslide movement or slope failure requires information about landslide recurrence obtained either by historical (Coe, Michael, and others, 2004) or geochronological methods described previously. Probabilistic analyses require additional effort and some additional data (probability or frequency distribution of strength parameters, range of uncertainty on pore pressures, slip surface geometry, and so forth), but they complement conventional deterministic analyses (Nadim and others, 2005).

Interpreting computed displacements in a probabilistic sense has special challenges. Several sources of error contribute to the differences between computed and observed displacements. First is measurement error in the observed displacements, which in most cases is relatively small. Other sources of error affect the computed displacements and include uncertainty in model parameters, uncertainty in the geometry of zones that have similar geotechnical properties and geologic structures, uncertainty in ground-water levels and pore pressures, and uncertainty or inaccuracy in the actual computational models. In cases like some reported in the literature where extreme values of the difference between observed and computed displacement exceed 100 percent, the difference has a skewed (non-normal) distribution. However, few data are available to define the expected form and parameters of the distribution, which may vary considerably depending on the modeling approach and quality of the input data. Computing displacement for different scenarios of changing pore pressure, erosion, or changes in external loading is usually necessary to define the range of probable slope responses to future events. The task of defining the most probable displacement during the design life of a pipeline becomes an exercise in combining model uncertainty with the computed slope responses of the different scenarios and their likelihoods.

Conclusions

A wide variety of techniques is available for investigating specific landslides and potential landslide areas to define the hazard they pose to pipelines. Many of these have advanced considerably during the last decade, making it possible to characterize and monitor landslides in considerable detail. Methods of numerical modeling have also greatly improved. However, predicting future ground displacements remains extremely challenging. Difficulties in adequately characterizing the subsurface and in foreseeing future changes in climate, weather, ground-water levels, and natural or man-made changes to the loading and configuration of existing slopes and landslide deposits remain the primary sources of uncertainty in such predictions. These uncertainties affect empirical and numerical techniques. A probabilistic approach that considers various scenarios and their likelihoods during the expected lifespan of a pipeline may be needed to determine the most probable displacement amounts for use in pipeline design. In addition to geotechnical investigation and analysis, geologic studies of landslide history are needed to define the annual probability of ground movement.

Acknowledgments

Partial funding for this report was provided by Pipeline Research Council International (PRCI) and the U.S. Department of Transportation through a Cooperative Research and Development Agreement (CRADA) with D.G. Honegger Consulting. William L. Ellis (USGS) made useful suggestions about computing and presenting cost data. D. Vaughan Griffiths (Colorado School of Mines) provided a stimulating discussion of numerical models. Mark E. Reid (USGS) shared insights about the challenges of predicting landslide movement. James P. McCalpin (GEO-HAZ Consulting, Inc.) provided an informative tour of his exploratory trenches at Snodgrass Mountain depicted in figure 3-5. Douglas G. Honegger (D.G. Honegger Consulting), Ray Boivin (Plateau Geotechnical, Ltd.), Moness Rizkalla (Visitless Integrity Assessment, Ltd.), and Richard Butler (Golder Associates, Ltd.) provided constructive reviews of an early draft of this report. Robert L. Schuster and William Z. Savage (both USGS, emeritus) provided constructive reviews of a revised version of this report.

References Cited

Adam, D.P., 1975, A late Holocene pollen record from Pearson's Pond, Weeks Creek landslide, San Francisco Peninsula, California: U.S. Geological Survey Journal of Research, v. 3, no. 6, p. 721–731.

Alexandrowicz, S.W., and Alexandrowicz, Z., 1999, Recurrent Holocene landslides—A case study of the Krynica landslide in the Polish Carpathians: The Holocene, v. 9, p. 91–99.

Alshibli, K., and Williams, H., 2005, A true triaxial apparatus for soil testing with mixed boundary conditions: Geotechnical Testing Journal, v. 28, Issue 6, Paper ID: GTJ12679, doi: 10.1520/GTJ12679

Amatruda, G., Castelli, M., Scavia, C., Mallen, L., and Forlati, F., 2004, A 3D numerical model for the simulation of the average annual displacement of a large landslide movement, *in* Lacerda, W.A., Erlich, M., Fontoura, S.A.B., and Sayao, A.S.F., eds., Landslides—Evaluation and stabilization, Proceedings of the 9th International Symposium on Landslides: London, A.A. Balkema Publishers, v. 2, p. 1,061–1,066.

Amitrano, David, Gaffet, Stephane, Malet, Jean-Philippe, Maquaire, Olivier, 2007, Understanding mudslides through micro-seismic monitoring: the Super-Sauze (South-East French Alps) case study: Bulletin de la Societe Geologique de France, v. 178: p. 149–157.

AnhDan, L., Koseki, J., and Sato, T., 2006, Evaluation of quasi-elastic properties of gravel using a large-scale true triaxial apparatus: Geotechnical Testing Journal, v. 29, Issue 5, Paper ID: GTJ100221, doi: 10.1520/GTJ100221.

Angeli, M.-G., Pasuto, Alessandro, and Silvano, Sandro, 2000, A critical review of landslide monitoring experiences: Engineering Geology, v. 55, no. 3, p. 133–147.

Baek, Y., Koo, H.B., and Bae, G.J., 2004, Study on development monitoring system of slope using the optical fiber sensor, *in* Lacerda, W.A., Erlich, M., Fontoura, S.A.B., and Sayao, A.S.F., eds., Landslides—Evaluation and stabilization, Proceedings of the 9th International Symposium on Landslides: London, A.A. Balkema Publishers, v. 1, p. 755–758

Baker, Rafael, 2005, Variational slope stability analysis of materials with nonlinear failure criterion: The Electronic Journal of Geotechnical Engineering, v. 10, bundle A, on-line at *http://www.ejge.com/2005/Ppr0514/Ppr0514.htm* (accessed 3/2/2007).

Baron, I., Agliardi, F., Ambrosi, C., and Crosta, G.B., 2005, Numerical analysis of deep-seated mass movements in the Magura Nappe; Flysch belt of the western Carpathians (Czech Republic): Natural Hazards and Earth System Sciences, v. 5, p. 367–374.

Baron, I., Krejci, O., Cilek, V., Hubatka, F., 2004, Holocene history and paleo-geomorphic reconstruction of deep-seated landslides in the Raca Unit (flysch belt of the western Carpathians, Czech Republic): Geophysical Research Abstracts, v. 6, 06156.

Baum, R.L., 2000, Computer programs for limit-equilibrium slope stability analysis—FelleniusGS, BishopGS, and JanbuGS: U.S. Geological Survey Open-File Report 00-107.

Baum, R.L., 2003, Earth flows, *in* Middleton, G.V., Church, M.J., Coniglio, M., Hardie, L.A., and Longstaffe, F.J., eds., Encyclopedia of sediments and sedimentary rocks: Dordrect, Netherlands, Kluwer Academic Publishers, p. 247–248.

Baum, R.L., and Fleming, R.W., 1991, Use of longitudinal strain in identifying driving and resisting elements of landslides: Geological Society of America Bulletin, v. 103, p. 1,121–1,132 and supplemental data.

Baum, R.L., and Fleming, R.W., 1996, Kinematic studies of the Slumgullion landslide *in* Varnes, D.J., and Savage, W.Z., eds., The Slumgullion earth flow—A large-scale natural laboratory: U.S. Geological Survey Bulletin 2130, ch. 2, p. 9–12.

Baum, R.L., Fleming, R.W., and Johnson, A.M., 1993, Kinematics of the Aspen Grove landslide, Ephraim Canyon, central Utah, chap. F *of* Landslide processes in Utah—Observation and theory: U.S. Geological Survey Bulletin 1842, p. F1–F34.

Baum, R.L., Harp, E.L., and Hultman, W.A., 2000, Map showing recent and historic landslide activity on coastal bluffs of Puget Sound between Shilshole Bay and Everett, Washington: U.S. Geological Survey Miscellaneous Field Studies Map, MF 2346, 1 sheet, scale 1:24,000.

Baum, R.L., Johnson, A.M., and Fleming, R.W., 1988, Measurement of slope deformation using quadrilaterals, chap. B *of* Landslide processes in Utah—Observation and theory: U.S. Geological Survey Bulletin 1842, p. B1–B23.

Baum, R.L., McKenna, J.P., Godt, J.W., Harp, E.L., and McMullen, S.R., 2005, Hydrologic monitoring of landslide-prone coastal bluffs near Edmonds and Everett, Washington, 2001–2004: U.S. Geological Survey Open-File Report 2005-1063, 42 p.

Baum, R.L., Messerich, James, and Fleming, R.W., 1998, Surface deformation of slow-moving, clay-rich landslides, Honolulu, Hawaii: Environmental & Engineering Geoscience, v.4, no. 3, p. 283–306.

Baum, R.L., and Reid, M.E., 1995, Geology, hydrology, and mechanics of a slow-moving, clay-rich landslide, Honolulu, Hawaii, *in* Haneberg, W.C., and Anderson, S.A., eds., Clay and shale slope instability: GSA Reviews in Engineering Geology X, p. 79–105.

Baum, R.L., and Reid, M.E., 2000, Groundwater isolation by low-permeability clays in landslide shear zones, *in* Bromhead, E., Dixon, N, and Ibsen, M., eds., Landslides in research, theory and practice, Proceedings of the 8th International Symposium on Landslides: London, Thomas Telford, p. 139–144.

Baum, R.L., Reid, M.E., Wilburn, C.A., and Torikai, J.D., 1991, Summary of geotechnical and hydrologic data collected from May 1, 1990 through April 30, 1991, for the Alani-Paty landslide, Manoa Valley, Honolulu, Hawaii: U.S. Geological Survey Open-File Report 91-598, 102 p.

Beneveli, R.M., Carvalho, M.O.M., and Carvalho, J.C., 2004, Using a thermal sensor to determine the soil matric suction of a gully slope, *in* Lacerda, W.A., Erlich, M., Fontoura, S.A.B., and Sayao, A.S.F., eds., Landslides—Evaluation and stabilization, Proceedings of the 9th International Symposium on Landslides: London, A.A. Balkema Publishers, v. 1, p. 767–772.

Bianchi, J.C., and Farrington, S.P., 2001, Direct push monitoring point assessment: Air Force Research Laboratory Report AFRL-ML-TY-TP-2000-4535, 715 p.

Bisci, Carlo; Burattini, Fausto; Dramis, Francesco; Leoperdi, Stefano; Pontoni, Fabrizio; Pontoni, Franco, 1996, The Sant'Agata Feltria landslide (Marche region, central Italy); a case of recurrent earthflow evolving from a deep-seated gravitational slope deformation: Geomorphology, v.15, no. 3–4, p. 351–361.

Bishop, A.W., and Henkel, D.J., 1957, The triaxial test: London, Edward Arnold, 228 p.

Bishop, A.W., 1959, The principle of effective stress: Teknisk Ukeblad, v. 39, p. 859–863.

Blake, T.F., Hollingsworth, R.A., and Stewart, J.P., 2002, Recommended procedures for implementation of DMG Special Publication 117 guidelines for analyzing and mitigating landslide hazards in California: South California Earthquake Center, 120 p.

Bogaard, T.A., Antoine, P., Desvarreux, P., Giraud, A., and van Asch, Th. W. J., 2000, The slope movements within the Mondores graben (Drome, France); the interaction between geology, hydrology and typology: Engineering Geology, v. 55, no. 4, p. 297–312.

Borchers, J. W., 1994, Characterization of fractures in granitic rocks at Wawona, Yosemite National Park, California; a comparison of borehole geophysical and downhole visualization tools, *in* Lawson, C.A., and Bennett, P.C., eds., Scientific visualization workshop: U.S. Geological Survey Open-File Report 94-134, 33 p.

Borchers, J.W., 1996, Ground-water resources and water-supply alternatives in the Wawona area of Yosemite National Park, California: U.S. Geological Survey Water Resources Investigation Report 95-4229, 77 p.
Brabb, E.E., and Pampeyan, E.H., 1972, Preliminary map of landslide deposits in San Mateo County, California: U.S. Geological Survey Miscellaneous Field Studies Map MF-344, scale 1: 62,500.
Braun, Jill, Major, Graeme, West, D.O., Bukovansky, Michal, 1998, Geologic hazards evaluation boosts risk management program for Western U.S. pipeline: Oil and Gas Journal, November 9, p. 73–79.
Brien D.L., Reid, M.E., 2001, 3-D slope stability of coastal bluffs incorporating 3-D pore pressures, Seattle, Washington: Transactions of the American Geophysical Union, v. 82, no. 47, p. F410.
Brien, D.L., and Reid, M.E., 2007, Modeling 3-D slope stability of coastal bluffs using 3-D ground-water flow, southwestern Seattle, Washington: U.S. Geological Survey Scientific Investigations Report 2007-5092, 54 p.
Bromhead, E.N., Ibsen, M-L., Papanastassiou, X., and Zemichael, A.A., 2002, Three-dimensional stability analysis of a coastal landslide at Hanover Point, Isle of Wight: Quarterly Journal of Engineering Geology and Hydrogeology, v. 35, p. 79–88.
Bromhead, E.N., 2004, Landslide slip surfaces—Their origins, behaviour and geometry, *in* Lacerda, W.A., Erlich, M., Fontoura, S.A.B., and Sayao, A.S.F., eds., Landslides—Evaluation and stabilization, Proceedings of the 9th International Symposium on Landslides: London, A.A. Balkema Publishers, v. 1, p. 3–22.
Brückl, E., Brunner, F.K., and Kraus, K., 2006, Kinematics of a deep-seated landslide derived from photogrammetric, GPS and geophysical data: Engineering Geology, v. 88, no. 3–4, p. 149–159.
Bull, W.B., King, J., Kong, F., Moutoux, T., Phillips, W.M., 1994, Lichen dating of co-seismic landslide hazards in alpine mountains: Geomorphology, v. 10, p. 253–264.
Cala, M., Flisiak, J, and Tajdus, A., 2004, Slope stability analysis with modified shear strength reduction technique, *in* Lacerda, W.A., Erlich, M., Fontoura, S.A.B., and Sayao, A.S.F., eds., Landslides—Evaluation and stabilization, Proceedings of the 9th International Symposium on Landslides: London, A.A. Balkema Publishers, v. 2, p. 1,085–1,089.
Campbell, R.H., 1975, Soil slips, debris flows, and rainstorms in the Santa Monica Mountains and vicinity, southern California: U.S. Geological Survey Professional Paper 851, 51 p.
Campbell Scientific, 2007, Time-domain reflectometry, *http://www.campbellsci.com/time-domain-reflectometry* (accessed March, 2007).
Carrara, Alberto; Cardinali, Mauro; Guzzetti, Fausto; and Reichenbach, Paola, 1995, GIS technology in mapping landslide hazard, *in* Carrara, A., and Guzzetti, F., eds., Geographical information systems in assessing natural hazards: Netherlands, Kluwer Academic Publishers, p. 135–175.
Casamichele, P., Maugeri, M., Motta, E., 2004, New approach for a three-dimensional analysis of slope stability, *in* Lacerda, W.A., Erlich, M., Fontoura, S.A.B., and Sayao, A.S.F., eds., Landslides—Evaluation and stabilization, Proceedings of the 9th International Symposium on Landslides: London, A.A. Balkema Publishers, v. 2, p. 1,617–1,623
Casson, B., Delacourt, C., and Allemand, P., 2005, Contribution of multi-temporal remote sensing images to characterize landslide slip surface—Application to the La Clapière landslide (France): Natural Hazards and Earth System Sciences, v. 5, p. 425–437.
Castelli, M., Amatruda, G., Scavia, C., Paro, L., and Forlati, F., 2004, The IMIRILAND methodology—A proposal for a multidisciplinary risk assessment procedure with respect to large landslide, *in* Lacerda, W.A., Erlich, M., Fontoura, S.A.B., and Sayao, A.S.F., eds., Landslides—

Evaluation and stabilization, Proceedings of the 9th International Symposium on Landslides: London, A.A. Balkema Publishers, v. 1, p. 229–235.
Chelli, A., Mandrone, G., Ruffini, A., and Truffelli, G., 2005, Dynamics and conceptual model of the Rossena castle landslide (Northern Apennines, Italy): Natural Hazards and Earth System Sciences, v. 5, p. 903–909.
Chen, R.H., and Chameau, J.-L., 1982, Three-dimensional limit equilibrium analysis of slopes: Geotechnique, v. 32, no 1., p. 31–40.
Chleborad, A.F., 1996, Radiocarbon age of a newly identified Slumgullion landslide deposit, *in* Varnes, D.J., and Savage, W.Z., eds., The Slumgullion earth flow—A large-scale natural laboratory: U.S. Geological Survey Bulletin 2130, ch. 5, p. 29–33.
Chugh, A.K., Stark, T.D., and DeJong, K.A., 2007, Reanalysis of a municipal landfill slope failure near Cincinnati, Ohio, USA: Canadian Geotechnical Journal, v. 44, p. 33–53, doi: 10.1139/T06-089.
Coe, J.A., Ellis, W.L., Godt, J.W., Savage, W.Z., Savage, J.E., Michael, J.A., Kibler, J.D., Powers, P.S., Lidke D.J., and Debray, S., 2003, Seasonal movement of the Slumgullion landslide determined from Global Positioning System surveys and field instrumentation, July 1998-March 2002: Engineering Geology, v. 68, no. 1–2, p. 67–101.
Coe, J.A., Godt, J.W., Parise, M, and Moscariello, A., 2003, Estimating debris-flow probability using debris-fan stratigraphy, historic records, and drainage-basin morphology, Interstate 70 Highway corridor, central Colorado, *in* Rickenmann, D., and Chen, C., eds., Debris flow hazards mitigation: Mechanics, prediction, and assessment: Proceedings of the Third International Conference on Debris-Flow Hazards Mitigation, Millpress, Rotterdam, p. 1,085–1,096.
Coe, J.A., Godt, J.W., and Tachker, Pierre, 2004, Map showing recent (1997–98 El Niño) and historical landslides, Crow Creek and vicinity, Alameda and Contra Costa Counties, California; U.S. Geological Survey Scientific Investigations Map 2859, *http://pubs.usgs.gov/sim/2004/2859/*.
Coe, J.A., Harp, E.L., Tarr, A.C., Michael, J.A., 2005, Rock-fall hazard assessment of Little Mill Campground, American Fork Canyon, Uinta National Forest, Utah: U.S. Geological Survey Open-File Report 2005-1229, 48 p., 2 pls., 1: 3,000-scale.
Coe, J.A., Michael, J.A., Crovelli, R.A., Savage, W.Z., Laprade, W.T., and Nashem, W.D., 2004, Probabilistic assessment of precipitation-triggered landslides using historical records of landslide occurrence, Seattle, Washington: Environmental & Engineering Geoscience, v. 10, no. 2, p. 103–122.
Colesanti, Carlo, and Wasowski, Janusz, 2006, Investigating landslides with space-borne synthetic aperture radar (SAR) interferometry: Engineering Geology, v. 88, no. 3–4, p. 173–199.
Collins, B.D., Kayen, Robert, Reiss, Thomas, and Sitar, Nicholas, 2007, Terrestrial LIDAR investigation of the December 2003 and January 2007 activations of the Northridge Bluff landslide, Daly City, California: U.S. Geological Survey Open-File Report 2007-1079, 32 p.
Corominas, J., Moya, J., Lloret, A., Gili, J.A., Angeli, M.G., Pasuto A., and Silvano, S., 2000, Measurement of landslide displacements using a wire extensometer: Engineering Geology, v. 55, no. 3, p. 149–166.
Corominas, Jordi, Moya, José, Ledesma, Alberto, Lloret, Antonio, Gili, J.A., 2005, Prediction of ground displacements and velocities from groundwater level changes at the Vallcebre landslide (Eastern Pyrenees, Spain): Landslides, v. 2, p. 83–96.
Corsini, A., Borgatti, L., Caputo, G., De Simone, N., Sartini, G., and Truffelli, G., 2006, Investigation and monitoring in support of the structural mitigation of large slow moving landslides: an example from Ca' Lita (Northern Apennines, Reggio Emilia, Italy): Natural Hazards and Earth System Sciences, v. 6, p. 55–61.

Crosta, G.B., Imposimato, S., and Roddeman, D.G., 2003, Numerical modeling of large landslides stability and runout: Natural Hazards and Earth System Sciences v. 3 p. 523–538.
Cruden, David, M., and Varnes, David J., 1996, Landslide types and processes: Chapter 3, *in* Turner, A.K., and Schuster, R.L. eds., Landslides—Investigation and mitigation: Transportation Research Board, Special Report 247, p. 36–75.
Das, S.K., 2005, Slope stability analysis using genetic algorithm: The Electronic Journal of Geotechnical Engineering, v. 10, bundle A, on-line at *http://www.ejge.com/2005/Ppr0504/Ppr0504.htm* (accessed 3/2/2007).
Denlinger, R.P., and Iverson R.M., 2004, Granular avalanches across irregular three-dimensional terrain—1. Theory and computation: Journal of Geophysical Research, v. 109, F01014.
Deng, J.H., Tham, L.G., Lee, C.F., and Yang, Z.Y., 2007, Three-dimensional stability evaluation of a preexisting landslide with multiple sliding directions by the strength-reduction technique: Canadian Geotechnical Journal 44(3): 343–354, doi:10.1139/T06-115.
Dixon, N., and Bromhead, E.N., 2002, Landsliding in London clay coastal cliffs: Quarterly Journal of Engineering Geology and Hydrogeology, v. 35 p. 327–343.
Dixon, N., and Brook, E., 2007, Impact of predicted climate change on landslide reactivation—case study of Mam Tor, UK: Landslides, v. 4, no. 2, p. 137–147.
Dowding, C.H., Su, M.B., and O'Connor, K., 1989, Measurement of rock mass deformation with grouted coaxial cables: Rock Mechanics and Engineering, v. 22, p. 1–22.
Duncan, J.M., 1996, Soil slope stability analysis, Chapter 13, *in* Turner, A.K., and Schuster, R.L. eds., Landslides— Investigation and mitigation: Transportation Research Board, Special Report 247, p. 337–371.
Duncan, J.M., 2000, Factors of safety and reliability in geotechnical engineering: Journal of Geotechnical and Geoenvironmental Engineering, April 2000, p. 307–316; Discussions and Closure, August 2001, p. 700–721.
Duranthon, J.P., 2004, The landslide of "Ruines de Séchilienne" ground radar for monitoring of landslides, *in* Lacerda, W.A., Erlich, M., Fontoura, S.A.B., and Sayao, A.S.F., eds., Landslides—Evaluation and stabilization, Proceedings of the 9th International Symposium on Landslides: London, A.A. Balkema Publishers, v. 1, p. 635–641.
Ellis, W.L., Priest, G.R., and Schulz, W.H., 2007, Precipitation, pore pressure, and landslide movement—Detailed observations at the Johnson Creek landslide, coastal Oregon, *in* Schafer, V.R., Schuster, R.L., and Turner, A.K., eds., Conference presentations, 1st North America landslide conference, Vail, Colorado: Association of Environmental and Engineering Geologists Special Publication 23, CD-ROM.
Farina, Paolo; Colombo, Davide; Fumagalli, Alfio; Marks, Florian; and Moretti, Sandro, 2006, Permanent scatterers for landslide investigations: outcomes from the ESA-SLAM project: Engineering Geology, v. 88, no. 3–4, p. 200–217.
Fleming, R.W., Baum, R.L., and Giardino, Marco, 1999, Map and description of the active part of the Slumgullion landslide, Hinsdale County, Colorado; U.S. Geological Survey Geologic Investigations Series Map I-2672, *http://pubs.usgs.gov/imap/i-2672/i-2672pm.pdf*.
Fleming, R.W., and Johnson, A.M., 1989, Structures associated with strike slip faults that bound landslide elements: Engineering Geology, 27, p. 39–114.
Fleming, R.W., Johnson, R.B., and Schuster, R.L., 1988, The reactivation of the Manti landslide, Utah, Chapter A *in* The Manti, Utah, landslide: U.S. Geological Survey Professional Paper 1311, p. 1–22.
Fraser, C.S., and Gruendig, L., 1985, The analysis of photogrammetric deformation measurements on Turtle Mountain: Photogrammetric Engineering and Remote Sensing, v. 51, no. 2, p. 207–216.

Fredlund, D.G., and Rahardjo, H., 1993, Soil mechanics for unsaturated soils: New York, Wiley, 517 p.
Froese, C.R., Keegan, T.R., Cavers, D.S., and van der Kooij, M., 2005, Detection and monitoring of complex landslides along the Ashcroft rail corridor using spaceborne InSAR, *in* Hungr, O., Fell, R., Couture, R., and Bernhard, E., eds., Landslide risk management, Proceedings of the 2005 International Conference on Landslide Risk Management: New York, A.A. Balkema, p. 565–570.
Fukuoka, Hiroshi; Sassa, Kyoji; Wang, Gonghui; Wang, Fawu; Wang, Yong; and Tian, Yongjin, 2005, Landslide risk assessment and disaster management in the Imperial Resort Palace of Lishan, Xian, China (C101-4), Chapter 9, *in* Sassa, K., Fukuoka, H., Wang, F. and Wang, G., eds., Landslides—Risk analysis and sustainable disaster management: Berlin, Springer, p. 81–89.
Fukuzono, T., 1990, Recent studies on time prediction of slope failure: Landslide News, v. 4, p. 9–12.
Gaertner, G., Pohl,W., Lindner, H., 2000, Monitoring and modeling of post-failure behavior of a large overburden slide in the lignite mine of Zwenkau (Saxony, Germany), *in* Bromhead, Eddie; Dixon, Neil; and Ibsen, Maia-Laura, eds., Landslides in research, theory and practice, v. 2, Proceedings of the Eighth International Symposium on Landslides: London, Thomas Telford, p. 603–608.
Galloway, D.L., Bawden, G.W., Leake, S.A., and Honegger, D.G., 2008, Land subsidence hazards, Chapter 2, *of* Baum, R.L., Landslide and land subsidence hazards to pipelines: U.S. Geological Survey Open-File Report 2008-1164, p. 32–105.
Gili, J.A., Corominas, Jordi, and Rius, Joan, 2000, Using Global Positioning System techniques in landslide monitoring: Engineering Geology, v. 55, no. 3, February 2000, p. 167–192.
Godt, J.W., 2004, Observed and modeled conditions for shallow landsliding in the Seattle, Washington, area: Boulder, University of Colorado, Ph.D. dissertation, 151 p.
Gomberg, J.S., Bodin, P.W., Savage, W.Z., Jackson, M.E., 1996, Slidequakes and fault creep at the Slumgullion landslide—An analog to crustal tectonics, *in* Varnes, D.J., and Savage, W.Z., eds., The Slumgullion earth flow—A large-scale natural laboratory: U.S. Geological Survey Bulletin 2130, ch. 14, p. 85–91.
Goodman, R., and Blake, W., 1965, An investigation of rock noise in landslides and cut slopes: Rock Mechanics and Engineering Geology, v. 21, p. 88–93.
Greif, V., Sassa, K., and Fukuoka, H., 2004, Monitoring of rock displacements at Bitchu-Matsuyama rock slope in Japan using Linear Variable Differential Transformer (LVDT) Sensors, *in* Lacerda, W.A., Erlich, M., Fontoura, S.A.B., and Sayao, A.S.F., eds., Landslides—Evaluation and stabilization, Proceedings of the 9th International Symposium on Landslides: London, A.A. Balkema Publishers, v. 1, p. 773–779.
Griffiths, D.V., and Lane, P.A., 1999, Slope stability analysis by finite elements: Géotechnique v. 49, no. 3, p. 387–403.
Griffiths, D.V., and Marquez, R.M., in press, Three-dimensional slope stability analysis by elasto-plastic finite elements: Géotechnique.
Grivas, D.A., Schultz, B.A., O'Neil, G.D., and Simmonds, G.R., 1996, Phenomenological models to predict rainfall-induced ground movements, *in* Proceedings of the 15th International Conference on Offshore Mechanics and Arctic Engineering, Florence, Italy, June: New York, American Society of Mechanical Engineers, p. 355–362.
Grivas, D.A., Schultz, B.C., Cuscuna, Sergio, Brambati, E., 1998, Regional models for ground movement hazard to pipelines: preliminary site classification procedure, *in* Proceedings of the International Conference on Offshore Mechanics and Arctic Engineering: Fairfield, New Jersey, American Society of Mechanical Engineers, 9 p.

Guzzetti, F., Carrara, A., Cardinali, M., and Reichenbach, P., 1999, Landslide hazard evaluation: a review of current techniques and their application in a multi-scale study, central Italy: Geomorphology, v. 31, no. 1, December 1999, p. 181–216.
Guzzetti, F., Crosta, G., Detti, R., and Agliardi, F., 2002, STONE: a computer program for the three-dimensional simulation of rock-falls: Computers and Geosciences, v. 28, no. 9, 1,079–1,093.
Guzzetti, F., Reichenbach, P., and Wieczorek, G.F., 2003, Rockfall hazard and risk assessment in the Yosemite Valley, California, USA: Natural Hazards and Earth System Sciences, v. 3, p. 491–503, *http://www.copernicus.org/EGU/nhess/3/2003/6/nhs-3-491.pdf*.
Harp, E.L., 2008, Landslide hazards to pipelines—Regional hazard mapping, chap. 1 *of* Baum, R.L., Landslide and land subsidence hazards to pipelines: U.S. Geological Survey Open-File Report 2008-1164, p. vi–31.
Haugerud, R.A., Harding, D.J., Johnson, S.Y., Harless, J.L., Weaver, C.S., and Sherrod, B.L., 2003, High-resolution LIDAR topography of the Puget lowland, Washington: GSA Today 13, (6) (Jun): 4-10, http://www.gsajournals.org (accessed August 7, 2007).
Highland, L.M., 2004, Landslide types and processes: U.S. Geological Survey Fact Sheet 2004-3072, 4 p.
Hillel, Daniel, 1982, Introduction to soil physics: San Diego, Academic Press, 364 p.
Hiura, H., Furuya, G, Fukuoka, H., and Sassa, K., 2000, Investigation of the groundwater distribution in crystalline schist landslide Zentoku, Shikoku Island, Japan, *in* Bromhead, Eddie, Dixon, Neil, and Ibsen, Maia-Laura, eds., Landslides in research, theory and practice, v. 2, Proceedings of the Eighth International Symposium on Landslides: London, Thomas Telford, p. 719–724.
Hong, Yong; Hiura, Hiromasa; Shino, Kazuo; Sassa, Kyoji; and Fukuoka, Hiroshi, 2005, Quantitative assessment on the influence of heavy rainfall on the crystalline schist landslide by monitoring system—Case study on Zentoku landslide, Japan: Landslides, v. 2, no. 1, p. 31–41, doi: 10.1007/s10346-005-0044-6.
Hovland, H.J., 1977, Three-dimensional slope stability analysis method: American Society of Civil Engineers Journal of the Geotechnical Engineering Division, v. 103, no. GT9, p. 971–986.
Hungr, O., 1995, A model for the runout analysis of rapid flow slides, debris flows and avalanches: Canadian Geotechnical Journal, v. 32, p. 610–623.
Hungr, O., Salgado, F.M., and Byrne, P.M., 1989, Evaluation of a three-dimensional method of slope-stability analysis: Canadian Geotechnical Journal, v. 26, p. 679–686.
Hungr, O., Corominas, J., and Eberhardt, E., 2005, Estimating landslide motion mechanism, travel distance, and velocity, *in* Hungr, O., Fell, R., Couture, R., and Bernhard, E., eds., Landslide risk management, Proceedings of the 2005 International Conference on Landslide Risk Management: New York, A.A. Balkema, p. 99–128.
Hürlimann, M., Ledesma, A., Corominas, J., and Prat, P., 2004, Numerical modeling of a large, deep-seated slope deformation at Encampadana, Andorra, *in* Lacerda, W.A., Erlich, M., Fontoura, S.A.B., and Sayao, A.S.F., eds., Landslides—Evaluation and stabilization, Proceedings of the 9th International Symposium on Landslides: London, A.A. Balkema Publishers, v. 2, p. 1073–1078.
Husaini, Omar, and Ratnasamy, M., 2001, An early warning system for active landslides: Quarterly Journal of Engineering Geology and Hydrogeology, v. 34, p. 299–305.
Hutchinson, J.N., 1983, Methods of locating slip surfaces in landslides: Bulletin of the Association of Engineering Geologists, v. 20, no. 3, p. 235–252.
Hutchinson, D.J., Harrap, R., Ball, D., Diederichs, M., and Kjelland, N., 2004, Development of geotechnical sensor network analysis capabilities for slope stability monitoring, within a GIS

based decision support system, *in* Lacerda, W.A., Erlich, M., Fontoura, S.A.B., and Sayao, A.S.F., eds., Landslides—Evaluation and stabilization, Proceedings of the 9th International Symposium on Landslides: London, A.A. Balkema Publishers, v. 1, p. 759–765.
Iverson R.M., 1986, Unsteady, nonuniform landslide motion—2. Linearized theory and the kinematics of transient response: Journal of Geology, v. 94, p. 349–364.
Iverson R.M., 2000, Landslide triggering by rain infiltration: Water Resources Research, v. 36, no. 7, p. 1,897–1,910.
Iverson R.M., and Reid, M.E., 1992, Gravity-driven groundwater flow and slope failure potential 1. Elastic effective-stress model: Water Resources Research, v. 28, p. 925–938.
Jibson, R.W., 2005, Landslide hazards at La Conchita, California: U.S. Geological Survey Open-File Report 2005-1067, 13 p.
Johnson, P.L., and Cole, W.F., 2001, The use of large-diameter boreholes and downhole logging methods in landslide investigations, *in* Ferriz, Horacio, and Anderson, Robert, eds., Engineering geology practice in northern California: Denver, Colo., Association of Engineering Geologists, p. 95–106.
Jones, C.L., Higgins, J.D., and Andrew, R.D., 2000, Colorado rockfall simulation program (CRSP), version 4.0, March 2000: Colorado Geological Survey Report MI 66.
Jones, L.D., 2006, Monitoring landslides in hazardous terrain using terrestrial LiDAR: an example from Montserrat: Quarterly Journal of Engineering Geology and Hydrogeology 39, p. 371–373.
Jotisankasa, A., Coop, M., Ridley, A., 2007, The development of a suction control system for a triaxial apparatus: Geotechnical Testing Journal, v. 30, issue 1, paper ID: GTJ100026, doi: 10.1520/GTJ100026.
Kääb, A., 2002, Monitoring high-mountain terrain deformation from repeated air-and spaceborne-optical data—Examples using digital aerial imagery and ASTER data: ISPRS Journal of Photogrammetry and Remote Sensing 57 (2002), p. 39–52.
Kalaugher, P.G., Hodgson, R.L.P., Grainger, P., 2000, Pre-failure strains as precursors of sliding in a coastal mudslide: Quarterly Journal of Engineering Geology and Hydrogeology, v. 33, p. 325–334.
Kane, W.F., and Beck, T.J., 1994, Development of a time domain reflectometry system to monitor landslide activity: Proceedings of the 45th Highway Geology Symposium, p. 163–173.
Kane, W.F., 2007, Railway alert system: The Campbell update, Campbell Scientific Inc., Logan, Utah, v. 18, no. 1, p. 5–6.
Keaton, J.R., and DeGraff, J.V., 1996, Surface observation and geologic mapping, Chapter 9, *in* Turner, A.K., and Schuster, R.L. eds., Landslides—Investigation and mitigation: Transportation Research Board, Special Report 247, p. 179–230.
Keefer, D.K., and Johnson, A.M., 1983, Earth flows–Morphology, mobilization and movement: U.S. Geological Survey Professional Paper 1264, 56 p.
Kilburn, C.R.J. and Petley, D.N., 2003, Forecasting giant, catastrophic slope collapse—Lessons from Vaiont, northern Italy: Geomorphology, v. 54, p. 49–62.
Kiersch, G.A., 1964, Vaiont reservoir disaster: Civil Engineering, v. 34 no. 3, p. 32–39.
Köhler, H.-J., Schulze, R., 2000, Landslides triggered in clay soils—Geotechnical measurements and calculations, *in* Bromhead, Eddie, Dixon, Neil, and Ibsen, Maia-Laura, eds., Landslides in research, theory and practice, v. 2, Proceedings of the Eighth International Symposium on Landslides: London, Thomas Telford, p. 837–842.
Kolesnikov, Yu.I., Nemirovich-Danchenko, M.M., Goldin, S.V., and Seleznev, V.S., 2003, Slope stability monitoring from microseismic field using polarization methodology: Natural Hazards and Earth System Sciences, v. 3, p. 515–521.

Konietzky, H., Lorenz, K., and Witter, W., 2004, Complex 3D landslide simulation, *in* Lacerda, W.A., Erlich, M., Fontoura, S.A.B., and Sayao, A.S.F., eds., Landslides—Evaluation and stabilization, Proceedings of the 9th International Symposium on Landslides: London, A.A. Balkema Publishers, v. 2, p. 1,053–1,059.

Kwan, J.S.H., and Sun, H.W., 2006, An improved landslide mobility model: Canadian Geotechnical Journal 43(5): 531–539, doi:10.1139/T06-010.

LaHusen, R.G., and Reid, M.E., 2000, A versatile GPS System for monitoring deformation of active landslides and volcanoes: Transactions of the American Geophysical Union, v. 81, no. 48, p. F320.

Lambe, T.W., and Whitman, R.V., 1969, Soil Mechanics, New York, John Wiley, 553 p.

Leroueil, S., 2001, Natural slopes and cuts—Movement and failure mechanisms: Geotechnique, v. 51, no. 3, p. 197–243.

Li, A.G., Tham, L.G., Lee, C.F., Yue, Q.Z., Law, K.T., and Deng, J.H., 2004, Field instrumentation for a saprolite cut slope, *in* Lacerda, W.A., Erlich, M., Fontoura, S.A.B., and Sayao, A.S.F., eds., Landslides—Evaluation and stabilization, Proceedings of the 9th International Symposium on Landslides: London, A.A. Balkema Publishers, v. 1, p. 759–765.

Lollino, G., Arattano, M., Allasia, P., and Giordan, D., 2006, Time response of a landslide to meteorological events: Natural Hazards and Earth System Sciences, v. 6, p. 179–184.

Lu, N., and Likos, W.J., 2004, Unsaturated soil mechanics: New York, John Wiley & Sons Inc., 556 p.

Lu, N., and Likos, W.J., 2006, Suction stress characteristic curve for unsaturated soil: American Society of Civil Engineers Journal of Geotechnical and Geoenvironmental Engineering, v. 132, no. 2, p. 131–142.

Luzi, G.; Pieraccini, M.; Mecatti, D.; Noferini, L.; Guidi, G.; Moia, F.; Atzeni, C., 2004, Ground-based radar interferometry for landslides monitoring: atmospheric and instrumental decorrelation sources on experimental data: IEEE Transactions on Geoscience and Remote Sensing, v. 42, no. 11, p. 2,454–2,466, doi: 10.1109/TGRS.2004.836792.

Madole, R.F., 1996, Preliminary chronology of the Slumgullion landslide, Hillsdale County, Colorado, *in* Varnes, D.J., and Savage, W.Z., eds., The Slumgullion earth flow—A large-scale natural laboratory: U.S. Geological Survey Bulletin 2130, Chapter 1, p. 5–7.

Malet, J.-P., van Asch, Th.W.J., van Beek, R., and Maquaire, O., 2005, Forecasting the behaviour of complex landslides with a spatially distributed hydrological model: Natural Hazards and Earth System Sciences, v. 5, p. 71–85.

Marcato, G., Mantovani, M., Pasuto, A., Silvano, S., Tagliavini, F., Zabuski, L., and Zannoni A., 2006, Site investigation and modelling at “La Maina” landslide (Carnian Alps, Italy): Natural Hazards and Earth System Sciences, v. 6, p. 33–39.

Markland, J.T., 1972, A useful technique for estimating the stability of rock slopes when the rigid wedge slide type of failure is expected: Imperial College Rock Mechanics Research Reprints, no. 19.

McCalpin, J.P., 1984, Preliminary age classification of landslides for inventory mapping: Proceedings of the 1984 Symposium on Engineering Geology and Soils Engineering, Boise Idaho, p. 99–111.

McDougall, Scott, Boultbee, Nicole, Hungr, Oldrich, Stead, Doug, and Schwab, J.W., 2006, The Zymoetz River landslide, British Columbia, Canada: description and dynamic analysis of a rock slide–debris flow: Landslides, v. 3, no. 3, p. 195–204, doi: 10.1007/s10346-006-0042-3.

McDougall S., and Hungr, O., 2004, A model for the analysis of rapid landslide motion across three-dimensional terrain: Canadian Geotechnical Journal, v. 41, no. 6, p. 1,084–1,097.

McGuffey, V.C., Modeer, V.A., Jr., and Turner, K.A., 1996, Subsurface exploration, Chapter 10, *in* Turner, A.K., and Schuster, R.L. eds., Landslides—Investigation and mitigation: Transportation Research Board, Special Report 247, p. 231–277.
Mikkelsen, P.E., 1996, Field instrumentation, Chapter 11, *in* Turner, A.K., and Schuster, R.L. eds., Landslides—Investigation and mitigation: Transportation Research Board, Special Report 247, p. 278–316.
Mikkelsen, P.E., 2002, Cement-bentonite grout backfill for borehole instruments: Geotechnical Instrumentation News, December, p. 38–42.
Miller, G.A., and Hamid, T.B., 2007, Interface direct shear testing of unsaturated soil: Geotechnical Testing Journal, v. 30, issue 3, paper ID: GTJ13301, doi: 10.1520/GTJ13301.
Morgenstern, N.R., and Price, V.E., 1965, The analysis of the stability of general slip surfaces: Geotechnique, v. 15, no. 1, p. 79–93.
Morgenstern, N.R., and Sangrey, Dwight A., 1978, Methods of stability analysis: Chapter 7, *in* Schuster, R.L., and Krizek, R.J., eds., Landslides Analysis and Control, Special Report 176: Washington, D.C., Transportation Research Board and National Academy of Sciences, p. 155–171.
Nadim, F., Einstein, H., Roberds, W., 2005, Probabilistic stability analysis for individual slopes in soil and rock, *in* Hungr, O., Fell, R., Couture, R., and Bernhard, E., eds., Landslide risk management, Proceedings of the 2005 International Conference on Landslide Risk Management: New York, A.A. Balkema, p. 63–98.
Nakamura, H., 2004, Field instrumentation and laboratory investigation, *in* Lacerda, W.A., Erlich, M., Fontoura, S.A.B., and Sayao, A.S.F., eds., Landslides—Evaluation and stabilization, Proceedings of the 9th International Symposium on Landslides: London, A.A. Balkema Publishers, v. 1, p. 541–548.
Nichol, D., and Graham, J.R., 2001, Remediation and monitoring of a highway across an active landslide at Trevor, North Wales: Engineering Geology, v. 59, no. 3–4, p. 337–348.
Olalla, C., 2004, Recent developments in landslide monitoring, *in* Lacerda, W.A., Erlich, M., Fontoura, S.A.B., and Sayao, A.S.F., eds., Landslides—Evaluation and stabilization, Proceedings of the 9th International Symposium on Landslides: London, A.A. Balkema Publishers, v. 1, p. 549–555.
O'Neil, G.D., Simmonds, G.R., Grivas, D.A., and Schultz, B.A., 1996, Rainfall-ground movement modeling for natural gas pipelines through landslide terrain, *in* Proceedings of the 1st International Pipeline Conference: Calgary, Alberta, IPC, September, v. 2, p. 1,307–1,314.
Petley, D.N., 2004, The evolution of slope failures—mechanisms of rupture propagation: Natural Hazards and Earth System Sciences, v. 4, p. 147–152.
Picarelli, L., and Russo, C., 2004, Remarks on the mechanics of slow active landslides and the interaction with man-made works, *in* Lacerda, W.A., Erlich, M., Fontoura, S.A.B., and Sayao, A.S.F., eds., Landslides—Evaluation and stabilization, Proceedings of the 9th International Symposium on Landslides: London, A.A. Balkema Publishers, v. 2, p. 1,141–1,176.
Pierson, T.C., 2007, Dating young geomorphic surfaces using age of colonizing Douglas Fir in southwestern Washington and northwestern Oregon, USA: Earth Surface Processes and Landforms, v. 32, p. 811–831, doi:10.1002/esp.1445.
Pierson, T.C., 2005, Distinguishing between debris flows and floods from field evidence in small watersheds: U.S. Geological Survey Fact Sheet 2004-3142, 2 p.
Puebla, H., Butler, R.C., O'Neill, E.S., Williams, R.R., 2006, Static and seismic stress-deformation analyses of a deep soil mix wall, *in* Proceedings of the 4th International FLAC Symposium on Numercial Modelling in Geomechanics, Paper 04-05: Itasca Consulting Group, Inc., ISBN 0-9767577-0-2.

Read, R.S., Langenberg, W., Cruden, D.M., and 23 others, 2005, Frank slide a century later—the Turtle Mountain monitoring project, *in* Hungr, O., Fell, R., Couture, R., and Bernhard, E., eds., Landslide risk management, Proceedings of the 2005 International Conference on Landslide Risk Management: New York, A.A. Balkema, p. 713–723.

Reichenbach, Paola; Galli, Mirco; Cardinalli, Mauro; Guzzetti, Fausto; and Ardizzone, Francesca, 2004, Geomorphologic mapping to assess landslide risk: concepts, methods and applications in the Umbria Region of central Italy, *in* Glade, Thomas, Anderson, Malcolm, and Crozier, M.J., eds., Landslide hazard and risk: New York, John Wiley and Sons, Ltd., p. 429–468.

Rowlands, K.A., Jones, L.D., Whitworth, M., 2003, Landslide laser scanning: a new look at an old problem: Quarterly Journal of Engineering Geology and Hydrogeology, v. 36, p. 155–157.

Saito, M., 1965, Forecasting the time of occurrence of slope failure, *in* Proceedings of the Sixth International Conference on Soil Mechanics and Foundation Engineering: Montréal, Canada, v. 2, p. 537–541.

Samui, Pijush, and Kumar, Bimlesh, 2006 Artificial neural network prediction of stability numbers for two-layered slopes with associated flow rule: The Electronic Journal of Geotechnical Engineering, v. 11, bundle A, on-line at http://www.ejge.com/2006/Ppr0626/Ppr0626.htm (accessed 11/26/2007).

Sarma, S.K., and Tan, D., 2006, Determination of critical slip surface in slope analysis: Géotechnique, v. 56, no. 8, p. 539–550, doi: 10.1680/geot.2006.56.8.539.

Sassa, Kyoji; Fukuoka, Hiroshi; Wang, Gonghui; and Ishikawa, Naohide, 2004, Undrained dynamic-loading ring-shear apparatus and its application to landslide dynamics: Landslides v. 1, no. 1, p. 7–19, doi: 10.1007/s10346-003-0004-y.

Savage, J.E., Savage, W.Z., and Huntoon, P.W., 2003, Development of deep-seated landslides in the Grand Canyon: Proceedings of the 39th U.S. rock mechanics symposium, v. 2, p. 2,471–2,475.

Savage, W.Z., Baum, R.L., Morrissey, M.M., and Arndt, B.P., 2000, Finite element analysis of the Woodway landslide, Washington: U.S. Geological Survey Bulletin 2180, 9 p.

Savage, W.Z., and Baum, R.L., 2005, Instability of steep slopes, Chapter 4 *in* Jacob, M. and Hungr, O., eds., Debris flow hazards and related phenomena: Chichester, U.K., Praxis Publishing House and Springer-Verlag, p. 53–79.

Savage, W., and Wasowski, J., 2006, A plastic flow model for the Acquara-Vadoncello landslide in Senerchia, southern Italy: Engineering Geology, v. 83, p. 4–21.

Schulz, W.H., 2004, Landslide mapping using LIDAR imagery, Seattle, Washington: U.S. Geological Survey Open-File Report 2004-1396, 11 p., http://pubs.usgs.gov/of/2004/1396/OF2004-1396_508.pdf.

Schulz, W.H., 2005, Landslide Susceptibility Estimated From Mapping Using Light Detection and Ranging (LIDAR) Imagery and Historical Landslide Records, Seattle, Washington: U.S. Geological Survey Open File Report 05-1405, 13 p., http://pubs.usgs.gov/of/2005/1405/.

Schuster, R.L., and Fleming, R.W., 1986, Economic losses and fatalities due to landslides: Bulletin of the Association of Engineering Geologists, v. 23, no. 1, p. 11–28.

Schuster, R.L., Baum, R.L., and Highland, L.M., 1998, The April 1998 El Niño-triggered Anzar Road landslide, San Benito County, California: AEG News v. 41, no. 4, p. 5–7.

Schuster, R.L., and Pringle, P.T., 2002, Engineering history and impacts of the Bonneville landslide, Columbia River gorge, Washington-Oregon, USA, *in* Rybar, Jan, Stemberk, Josef, Wagner, Peter, eds., Landslides, Proceedings of the first European conference on landslides, Prague, Czech Republic, July 22–24: Lisse, Netherlands, A.A. Balkema Publishers, p. 689–699.

Sharma, Sunil, 2007, Slope stability assessment using limit equilibrium methods, *in* Turner, A.K., and Schuster, R.L., eds., Landslides and society: Keynote and invited presentations at the First

North America Landslide Conference in Vail, Colorado, June 3–8: Association of Engineering Geologists Special Publication no. 22, p. 239–260.
Sheth, A.N., Tejaswi, K., Mehta, P., Parekh, C., Bansal, R., Merchant, S., Singh, T.N., Desai, U.B., Thekkath, C.A., and Toyama, K., 2005, SenSlide—A sensor network based landslide prediction system [abs.]: Proceedings of SenSys 2005, November 2–4.
Shiu, Wen-Ji, Donzé, F.V., and Magnier, S.-A., 2006, Numerical study of rock falls on covered galleries by the discrete element method: The Electronic Journal of Geotechnical Engineering, v. 11, bundle D, on-line at *http://www.ejge.com/2006/Ppr0669/Ppr0669.htm* (accessed 3/2/2007).
Shukha, Robert, Baker, Rafael, and Leshchinsky, Dov, 2005, Engineering implications of the relation between static and pseudo-static slope stability analysis: The Electronic Journal of Geotechnical Engineering, v. 10, bundle G, on-line at *http://www.ejge.com/2005/Ppr0616/Ppr0616.htm* (accessed 3/2/2007).
Skempton, A.W., 1985, Residual strength of clays in landslides, folded strata, and the laboratory: Geotechnique, v. 35, p. 3–18.
Skempton, A.W., Leadbeater, A.D., and Chandler, R.J., 1989, The Mam Tor landslide, North Derbyshire: Philosophical Transactions of the Royal Society of London, v. A329, p. 503–547.
Smith, I.M., and Griffiths, D.V., 2004, Programming the finite element method, 4th ed.: Wiley, 628 p.
Smith, W.K., 1996, Photogrammetric determination of slope movements on the Slumgullion landslide, *in* Varnes, D.J., and Savage, W.Z., eds., The Slumgullion earth flow—A large-scale natural laboratory: U.S. Geological Survey Bulletin 2130, ch. 9, p. 57–60.
Stead, D., Coggan, J.S., and Eberhardt, E., 2004, Modeling of complex rock slope failure mechanisms using a hybrid finite-/discrete element code, *in* Lacerda, W.A., Erlich, M., Fontoura, S.A.B., and Sayao, A.S.F., eds., Landslides—Evaluation and stabilization, Proceedings of the 9th International Symposium on Landslides: London, A.A. Balkema Publishers, v. 2, p. 1,067–1,072.
Stevens, W.D., 1998, ROCFALL—A tool for probabilistic analysis, design of remedial measures and prediction of rockfalls: Toronto, University of Toronto, Master of Applied Science thesis, 28 p., 2 appendixes, (http://www.rocscience.com/downloads/rocfall/wds98.zip, accessed August 22, 2007).
Stoffel, M., 2006, A review of studies dealing with tree rings and rock fall activity—The role of dendrogeomorphology in natural hazard research: Natural Hazards, v. 51-70, doi: 10.1007/s11069-005-2961-z.
Strozzi, Tazio; Farina, Paolo; Corsini, Alessandro; Ambrosi, Christian; Thüring, Manfred; Zilger, Johannes; Wiesmann, Andreas; Wegmüller, Urs; and Werner, Charles, 2005, Survey and monitoring of landslide displacements by means of L-band satellite SAR interferometry: Landslides, v. 2 no. 3 p. 193–201.
Sydnor, Robert H., 1979, Bluebird Canyon landslide, Laguna Beach, California, *in* Fife, D.L, ed., Geologic guide of San Onofre nuclear generating station and adjacent regions of southern California: American Association of Petroleum Geologists, Pacific Section Guidebook no. 46, p. 25–37.
Tacher, Laurent; Bonnard, Christophe; Laloui, Lyesse; and Parriaux, Aurèle, 2005, Modelling the behaviour of a large landslide with respect to hydrogeological and geomechanical parameter heterogeneity: Landslides, v. 2, no. 1, p. 3–14, doi: 10.1007/s10346-004-0038-9.
Tagliavini, F., Mantovani, M., Marcato, G., Pasuto, A., and Silvano, S., 2007, Validation of landslide hazard assessment by means of GPS monitoring technique—a case study in the Dolomites (Eastern Alps, Italy): Natural Hazards and Earth System Sciences, v. 7, p. 185–193.

Tan, Elsa, Fredlund, D.G., and Marjerison, Brent, 2007, Installation procedure for thermal conductivity matric suction sensors and analysis of their long-term readings: Canadian Geotechnical Journal v. 44 no. 2, p. 113–125, doi:10.1139/T06-098.

Tarchi, Dario; Casagli, Nicola; Fanti, Riccardo; Leva, D.D.; Luzi, Guido; Pasuto, Alessandro; Pieraccini, Massimiliano; and Silvano, Sandro, 2003, Landslide monitoring by using ground-based SAR interferometry—An example of application to the Tessina landslide in Italy: Engineering Geology, v. 68, no. 1–2, p. 15–30.

Tarchi, Dario; Antonello, Giuseppe; Casagli, Nicola; Farina, Paolo; Fortuny-Guasch, Joachim; Guerri, Letizia; and Leva, Davide, 2005, On the use of ground-based SAR interferometry for slope failure early warning—the Cortenova rockslide (Italy): Chapter 43, *in* Sassa, K., Fukuoka, H., Wang, F. and Wang, G., eds., Landslides—Risk analysis and sustainable disaster management: Berlin, Springer, p. 337–342.

Terzaghi, K., 1943, Theoretical soil mechanics: New York, John Wiley, 510 p.

Troncone, A., 2005, Numerical analysis of a landslide in soils with a strained softening behavior: Geotechnique, v. 55, no. 8, p. 585–596.

Turner, A.K., and Schuster, R.L. eds., 1996, Landslides—Investigation and mitigation: Transportation Research Board Special Report 247, 673 p.

Van Den Eeckhaut, M., Verstraeten, G., Poesen, J., 2007, Morphology and internal structure of a dormant landslide in a hilly area—the Collinabos landslide (Belgium): Geomorphology, v. 89, no. 3–4, p. 258–273, doi:10.1016/j.geomorph.2006.12.005.

Van Westen, C.J., 2004, Geo-information tools for landslide risk assessment—an overview of recent developments, *in* Lacerda, W.A., Erlich, M., Fontoura, S.A.B., and Sayao, A.S.F., eds., Landslides—Evaluation and stabilization, Proceedings of the 9th International Symposium on Landslides: London, A.A. Balkema Publishers, v. 1, p. 759–765.

Varnes, D.J., 1982, Time-deformation relations in creep to failure of Earth materials: Proceedings of the 7th Southeast Asian Geotechnical Conference, v. 2, p. 107–130.

Varnes, D.J., 1978, Slope movement types and processes, *in* Schuster, R.L., and Krizek, R.J., eds., Landslides Analysis and Control, Special Report 176: Washington, D.C., Transportation Research Board and National Academy of Sciences, p.11–33.

Voight, B., 1988, A relation to describe rate-dependent material failure: Science, v. 243, p. 200–203.

Vulliet, L., and Hutter, K., 1988, Continuum model for natural slopes in slow movement: Geotechnique, v. 38, no. 2, p. 199–217.

Wieczorek, G.F., 1982, Map showing recently active and dormant landslides near La Honda, central Santa Cruz Mountains, California: U.S. Geological Survey Miscellaneous Field Studies Map 1422, scale 1:4,800.

Wieczorek, G.F., 1984, Preparing a detailed landslide-inventory map for hazard evaluation and reduction: Association of Engineering Geologists Bulletin, v. 21, no. 3, p. 337–342.

Wieczorek, G.F., Morrissey, M.M., Iovine, G., and Godt, J., 1999, Rock-fall potential in the Yosemite Valley, California: U.S. Geological Survey Open-File Report 99-578, 1 pl. 1:12,000, 7 p. *http://greenwood.cr.usgs.gov/pub/open-file-reports/ofr-99-0578/*.

Wieczorek, G.F., and Harp, E.L., 2000, Rock-fall hazard assessment of the Aspen Forest Trail, Navajo National Monument, Arizona: U.S. Geological Survey Open-File Report 00-305, 11p., *http://greenwood.cr.usgs.gov/pub/open-file-reports/ofr-00-0305/*.

Wieczorek, G.F., and Glade, T., 2005, Climatic factors influencing occurrence of debris flows, *in* Jakob, M., and Hungr, O., eds., Debris-flow hazards and related phenomena: Berlin Heidelberg, Praxis Springer, p. 325–362.

Williams, R.A., and Pratt, T.L., 1996, Detection of the base of Slumgullion landslide by seismic reflection and refraction methods, *in* Varnes, D.J., and Savage, W.Z., eds., The Slumgullion earth flow—A large-scale natural laboratory: U.S. Geological Survey Bulletin 2130, ch. 13, p. 77–83.
Wu, Tien Hsing, 1969, Soil mechanics: Boston, Allyn and Bacon, Inc., 431 p.
Wu, T. H., 1996, Soil strength properties and their measurement, Chapter 12, *in* Turner, A.K., and Schuster, R.L. eds., Landslides—Investigation and mitigation: Transportation Research Board, Special Report 247, p. 319–336.
Wyllie, D.C., and Norrish, N.I., 1996, Rock strength properties and their measurement, Chapter 14, *in* Turner, A.K., and Schuster, R.L. eds., Landslides—Investigation and mitigation: Transportation Research Board, Special Report 247, p. 372–390.
Xing, Z., 1987, Three-dimensional stability analysis of concave slopes in plan view: American Society of Civil Engineers Journal of the Geotechnical Engineering Division, v. 114, p. 658–671.
Zhu, D.Y., Lee, C.F., Qian, Q.H., and Chen, G. R., 2005, A concise algorithm for computing the factor of safety using the Morgenstern–Price method: Canadian Geotechnical Journal 42(1): 272–278, doi:10.1139/t04-072.
Zi, G., and Belytschko, T., 2003, New crack-tip elements for XFEM and applications to cohesive cracks: International Journal of Numerical Methods in Engineering, v. 57, p. 2,221–2,240.

Figure 3-1. Toe of the Anzar Road landslide, San Benito County, Califorina, that severed two 25-cm-diameter gas pipelines on April 22, 1998. The pipelines served approximately 60,000 residential and business customers in Santa Cruz County. The white pipe is a temporary bypass pipe that was placed across the toe soon after the landslide occurred (photograph by Lynn Highland, USGS; Schuster and others, 1998).

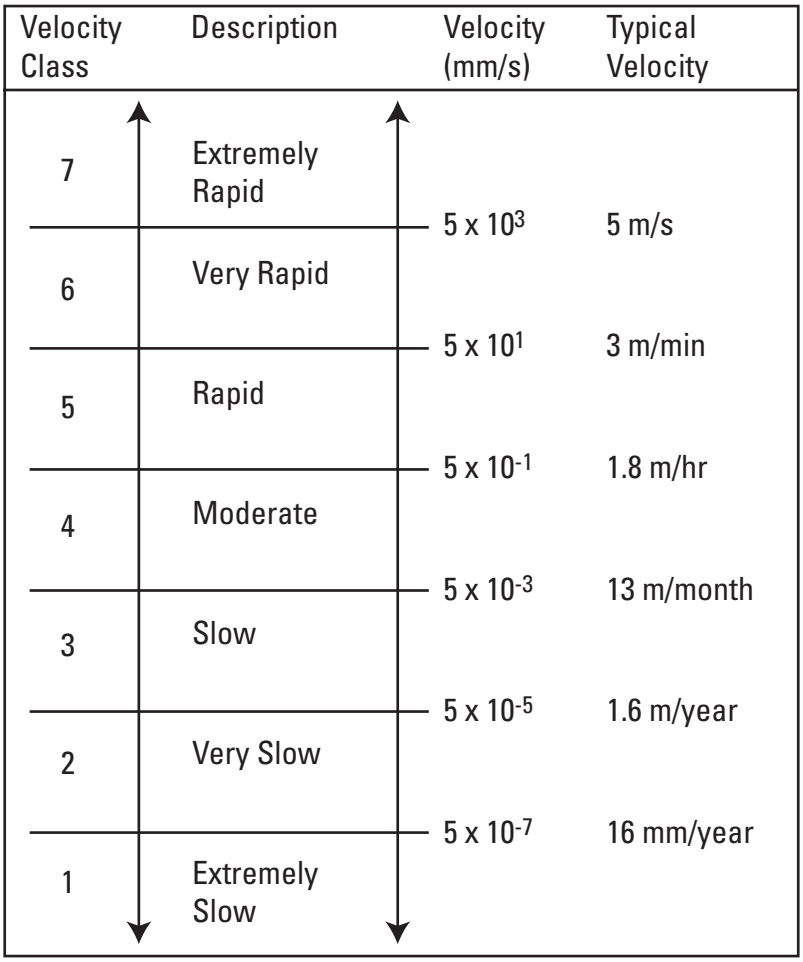

Figure 3-2. Landslide velocity scale (after Cruden and Varnes, 1996).

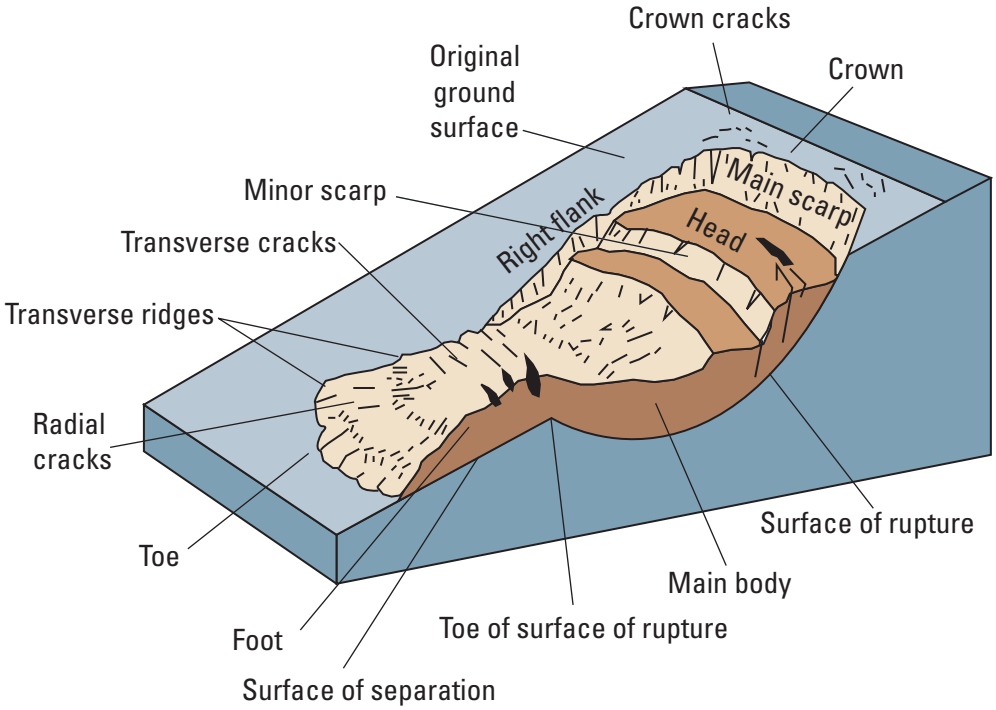

Figure 3-3. Block diagram showing the main parts of a landslide (after Varnes, 1978; Highland, 2004).

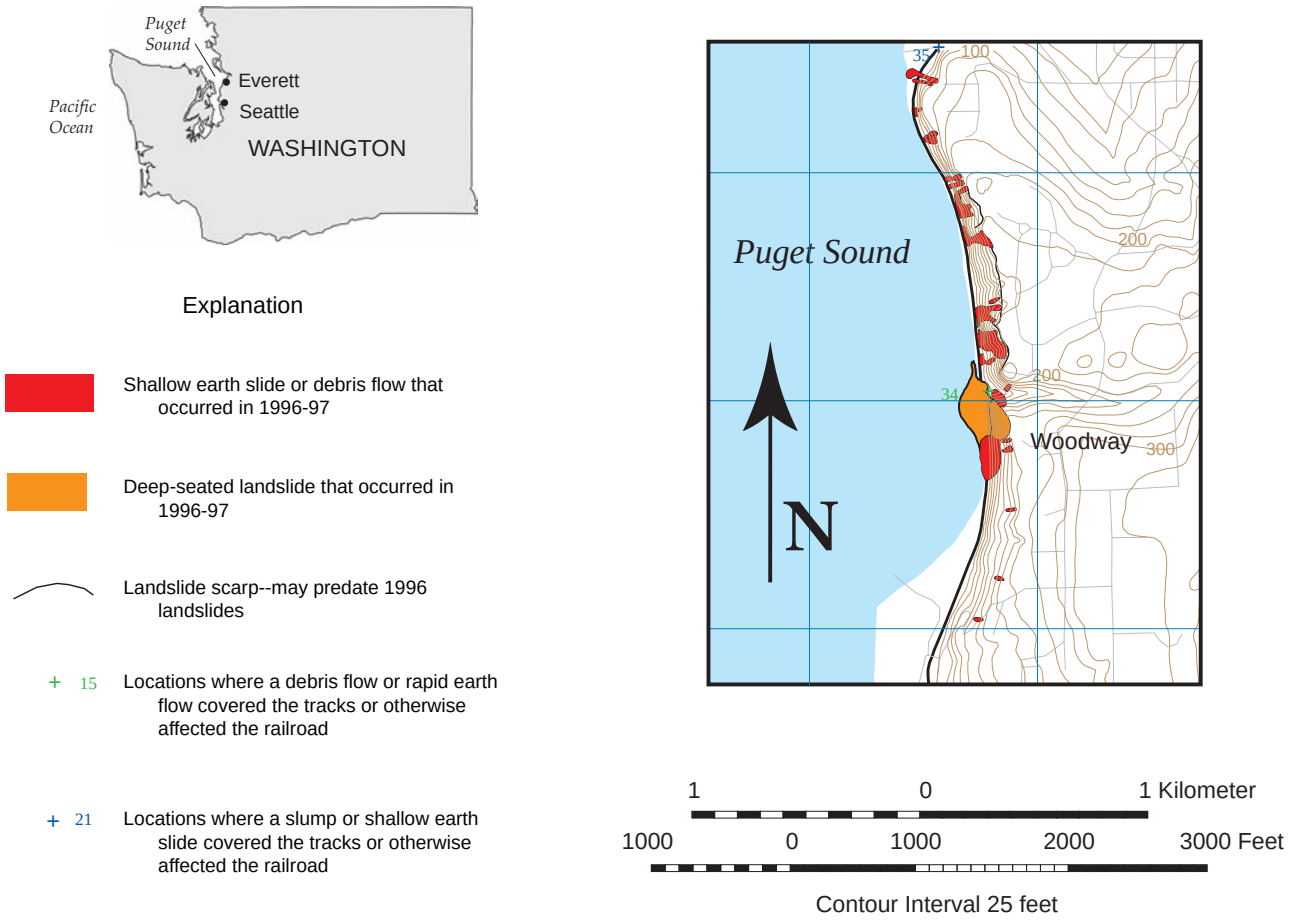

Figure 3-4. Examples of engineering geologic maps showing: (A) landslides from a major storm event near Seattle, Washington; red polygons represent shallow debris flows and earth slides, orange polygon represents a large deep-seated landslide (Baum and others, 2000);

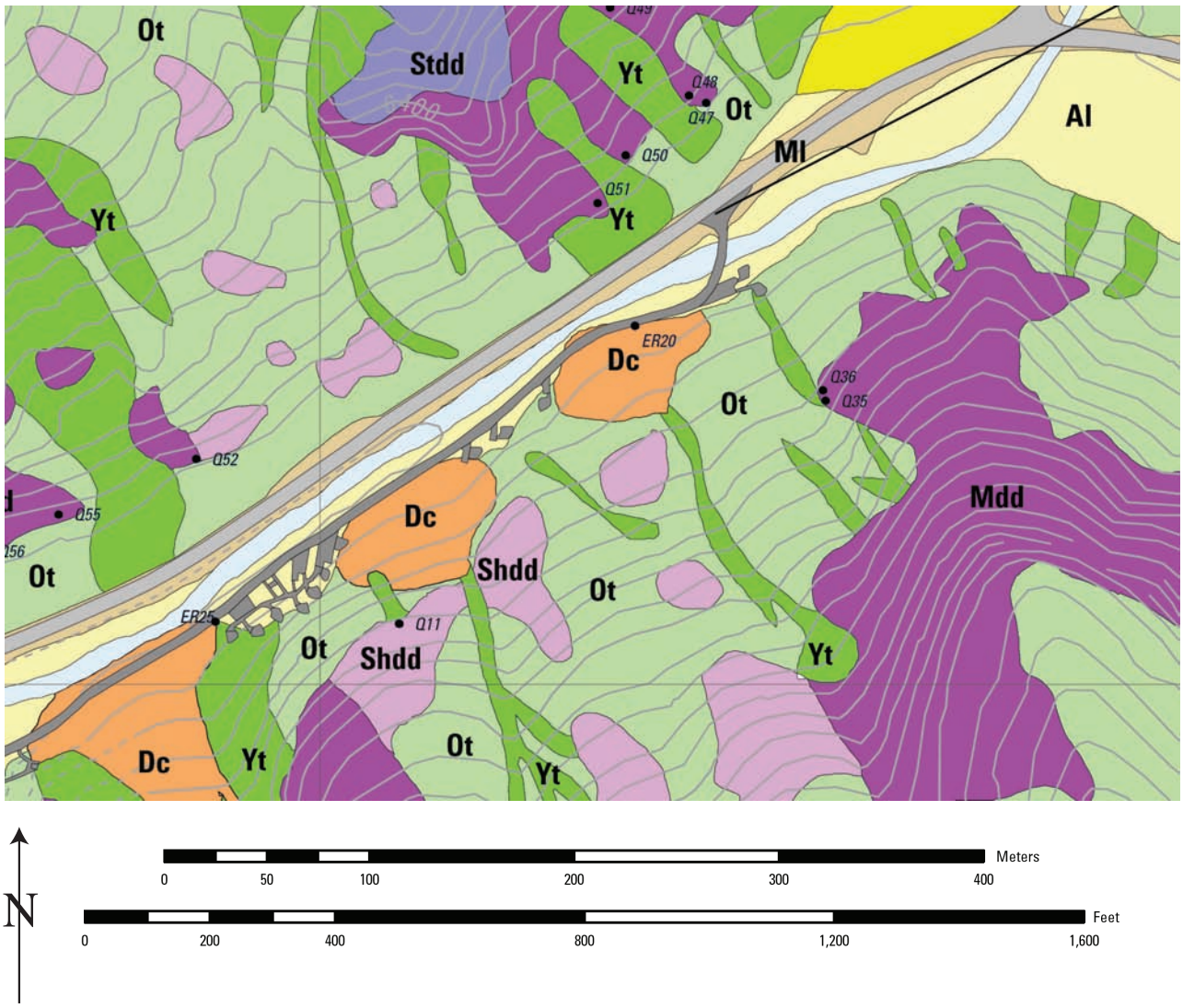

Figure 3-4, Continued. (B) Engineering geology of a rock-fall-prone area (Coe and others, 2005, plate 1); Al, alluvium mixed with rock-fall debris; Ot, older talus, colluvium, soil; Yt, young talus; Stdd, steeply dipping limestone; Mdd, moderately dipping limestone and/or fold axial zone; Shdd, shallow dipping limestone; Dc, debris cone; Df, debris fan; Ml, modified land; Q50, measurement of rock-mass quality; ER 20, measurement of extreme rock-fall runout;

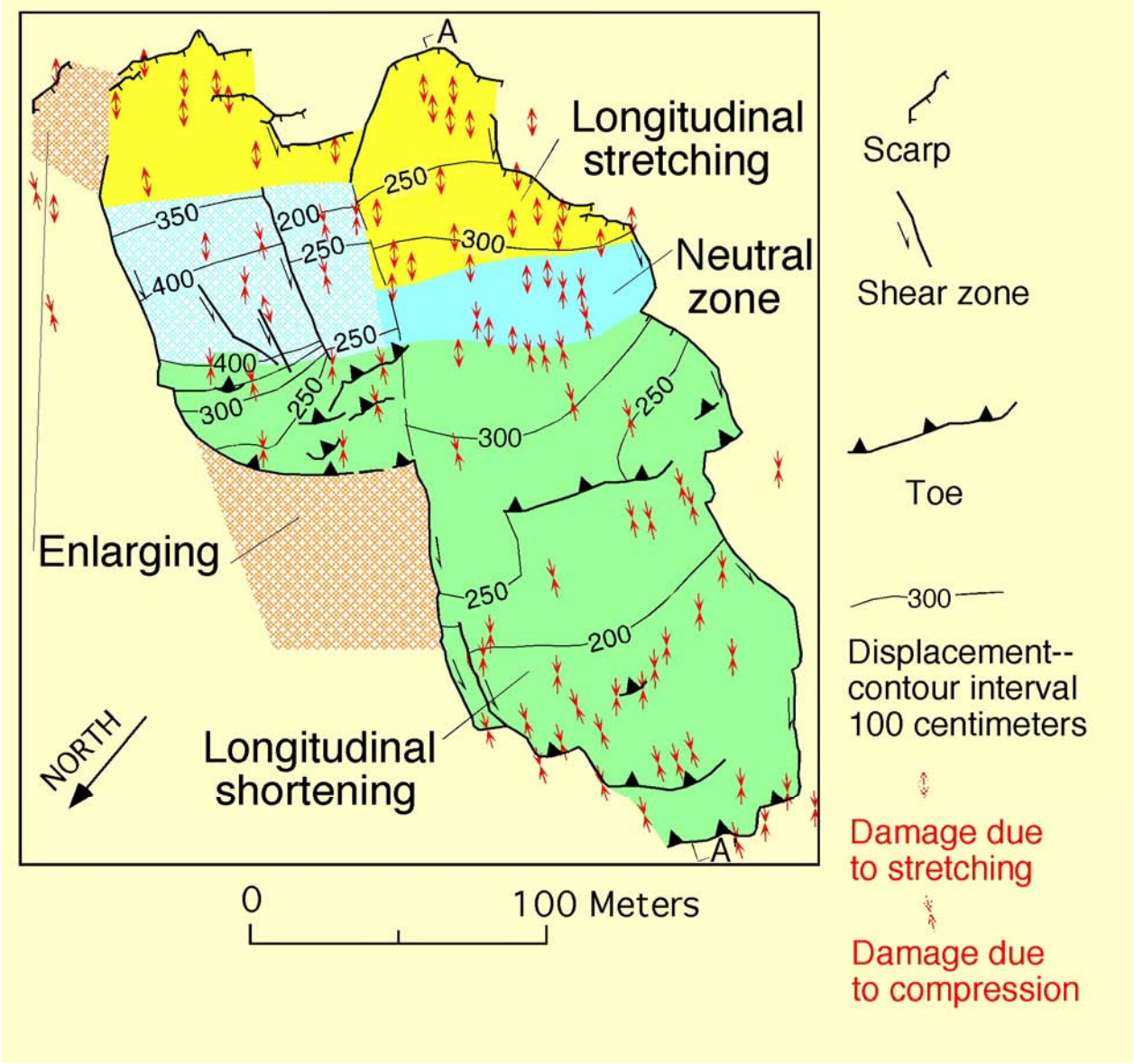

Figure 3-4, Continued. (C) Major structures and features of a landslide (Baum and others, 1998).

Figure 3-5. Use of trenches in landslide subsurface exploration: (A) Location of exploratory trenches in a landslide deposit on the southeast side of Snodgrass Mountain, near Crested Butte, Colorado;

Figure 3-5, Continued. (B) Landslide basal shear zone exposed in lower trench. Red paint spots added to highlight contact between gray crushed-shale landslide debris and yellow-brown sandy clay of shear-zone material.

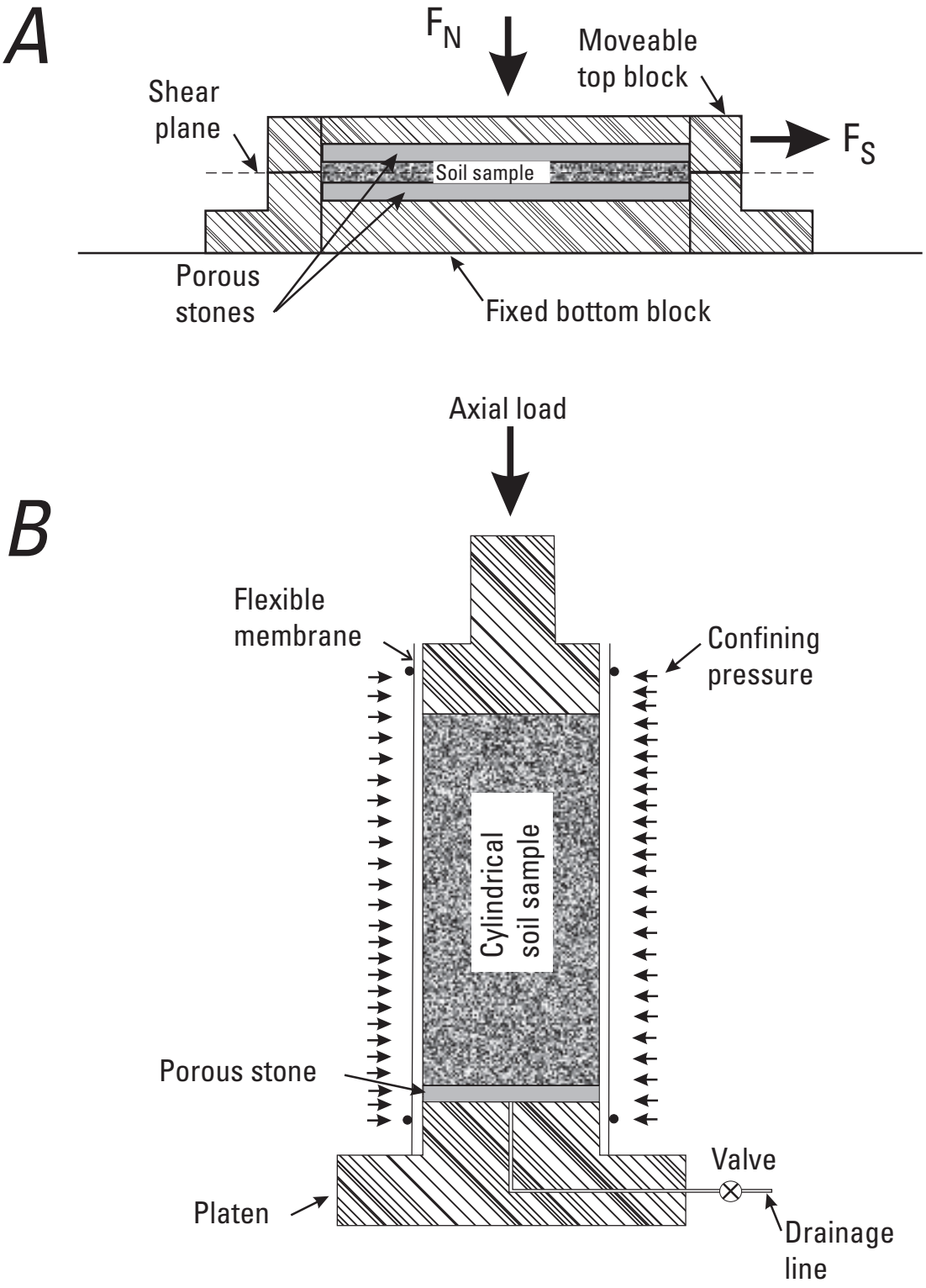

Figure 3-6. Sketches of soil test apparatus (modified from Savage and Baum, 2005): (A) Cross-sectional sketch of a direct-shear apparatus. The shear box encloses the soil sample and may be rectangular or circular in plan view. (B). Cross-sectional sketch of a triaxial test apparatus. This apparatus is usually circular in plan view.

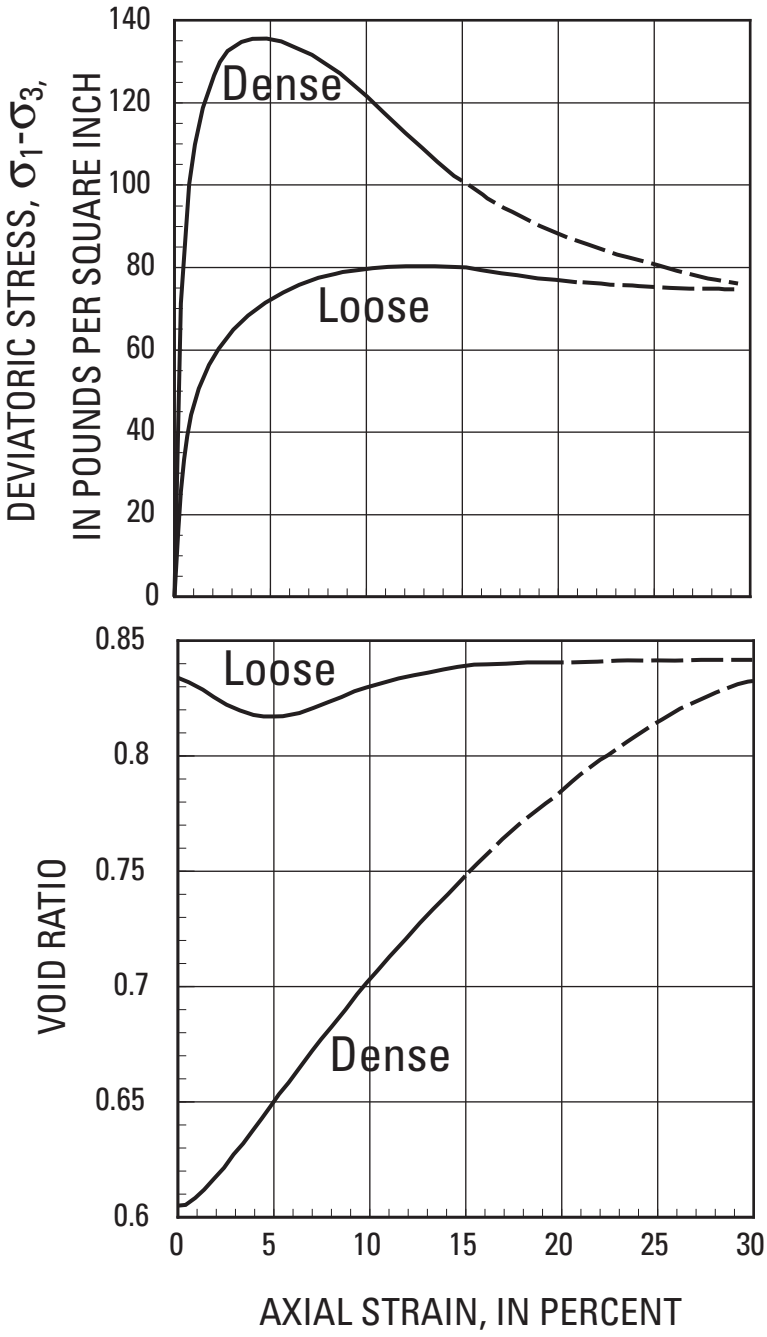

Figure 3-7. Stress-strain curves for drained triaxial tests on loose (contractive) and dense (dilatant) medium-fine sand (modified from Lambe and Whitman, 1969, p. 131). Solid lines, actual test data; dashed lines, extrapolations based on results of other tests. The dense soil reached its peak strength after small axial strain, but continued to dilate, as axial strain increased. The loose soil began contracting early in the test and reached its ultimate strength after a relatively large axial strain.

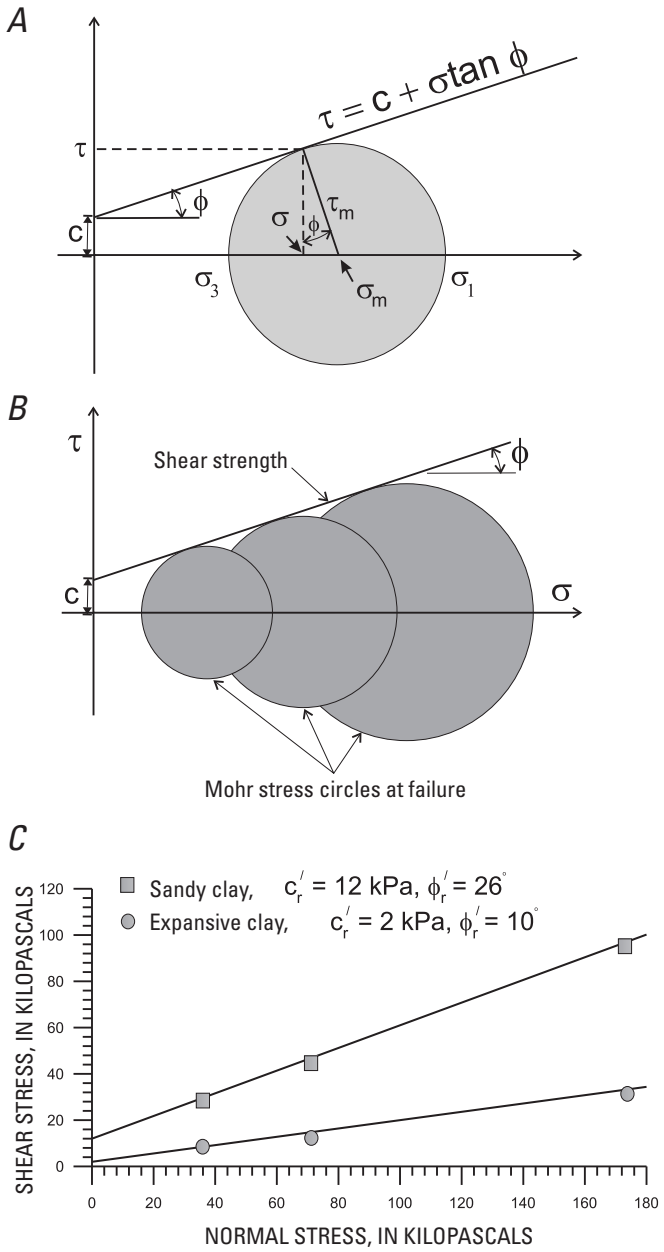

Figure 3-8. The Mohr-Coulomb failure criterion and effective stress: (A) Sketch showing Mohr-Coulomb failure criterion. Here, $\tau_m = (\sigma_1 - \sigma_3)/2$ is the maximum shear stress and $\sigma_m = (\sigma_1 + \sigma_3)/2$ is the mean stress, where σ_1 is the major (most compressive) principal stress and σ_3 is the minor (least compressive) principal stress in a triaxial test. The stresses τ and σ, are, respectively, the shear and normal stresses on planes undergoing shear failure, c is cohesion, and ϕ is the angle of internal friction of the soil. (B) Construction of a Mohr-Coulomb failure envelope for a soil. (C) Mohr-Coulomb strength parameters determined by direct-shear testing of two soils from the Alani-Paty landslide in Hawaii. Primes indicate that the strength parameters are determined under effective-stress conditions and the subscript r indicates that the strength parameters are residual values.

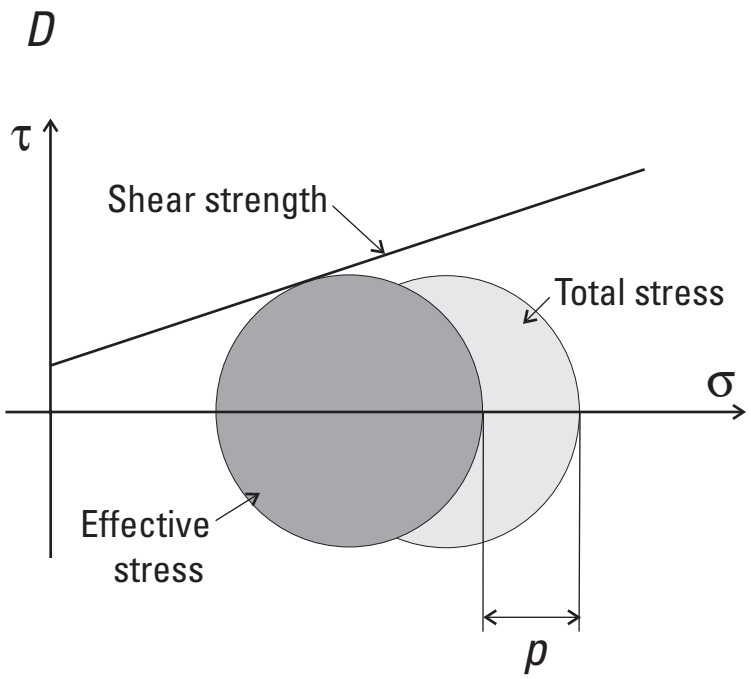

Figure 3-8, Continued. (D). Function of effective stress in reducing the shear strength of soil (after Savage and Baum, 2005).

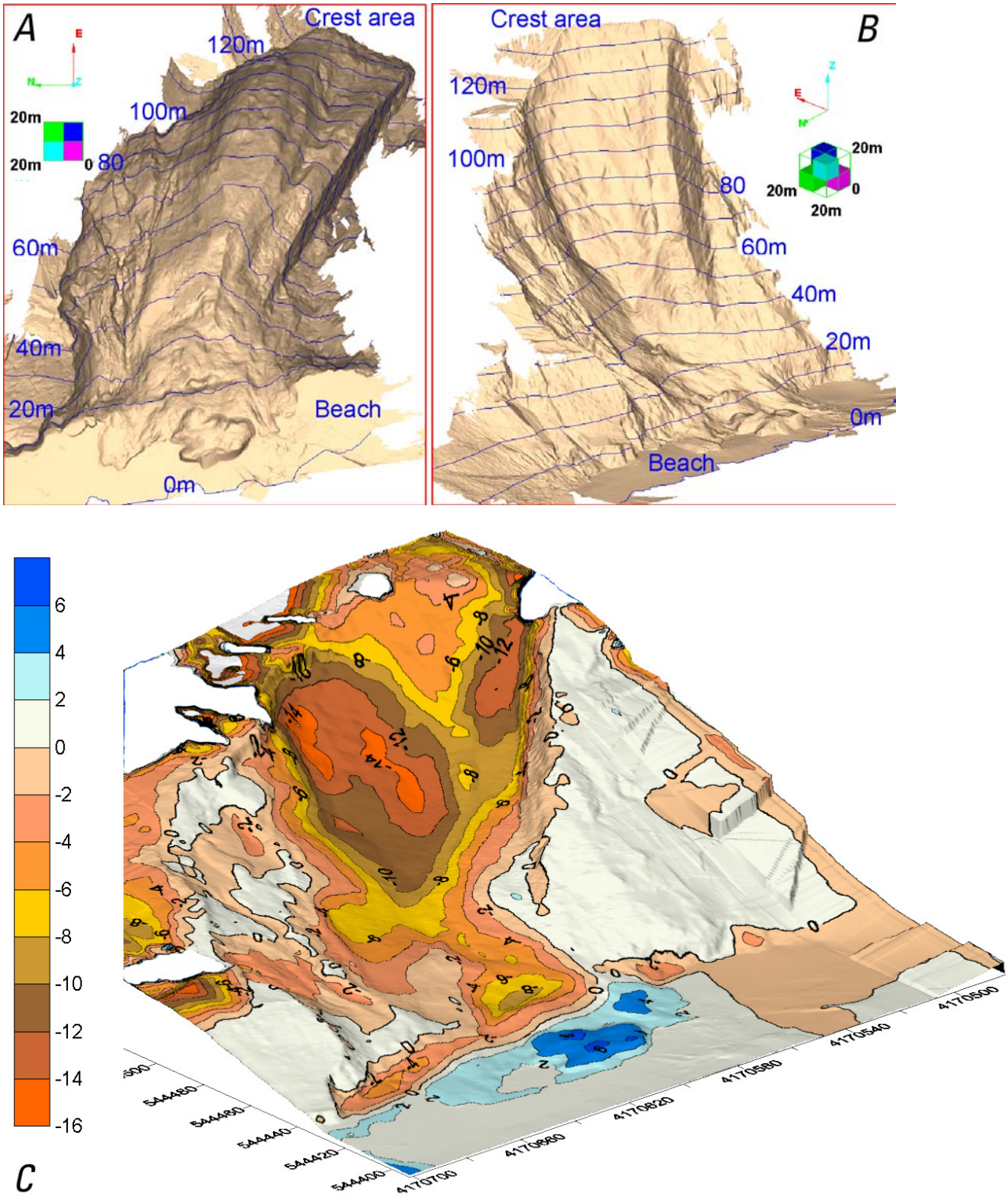

Figure 3-9. Example images of landslide area obtained by laser scanning: (A) shaded relief and contour map, plan view, (B) oblique view, (C) difference plot showing changes in elevation that resulted from landslide movement (Collins and others, 2007).

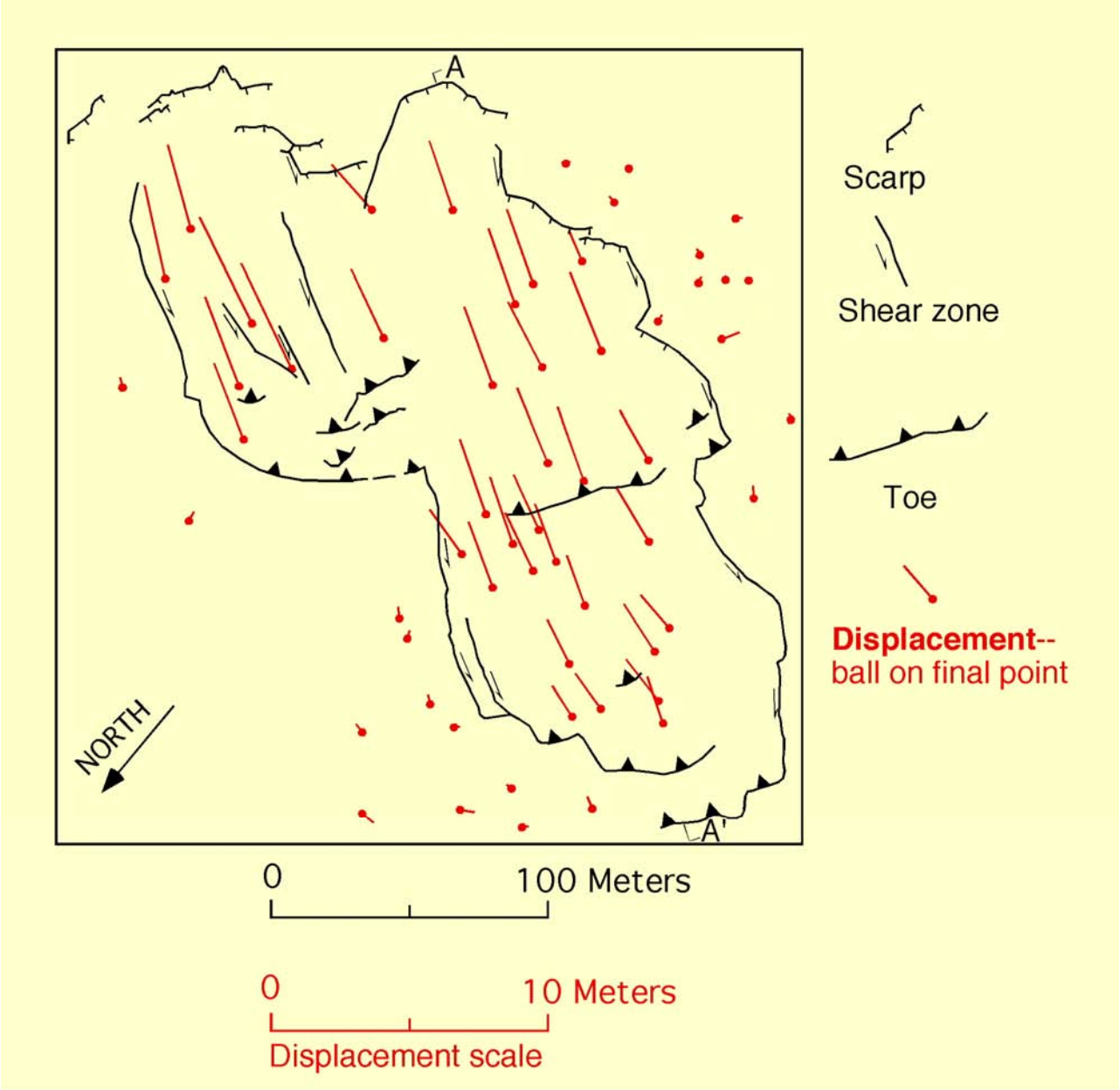

Figure 3-10. Map of landslide displacements obtained using aerial photogrammetry (modified from Baum and others, 1998).

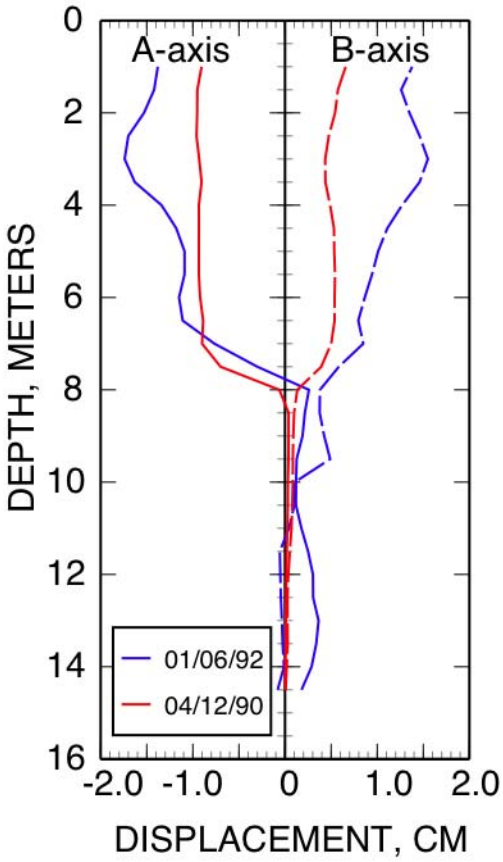

Figure 3-11. Plot of displacements since initial measurement (Nov. 28, 1989) versus depth obtained using a slope inclinometer: A-axis is the primary (roughly downslope) axis, and B-axis (dashed line) is the secondary axis, 90° from primary (modified from Baum and others, 1991).

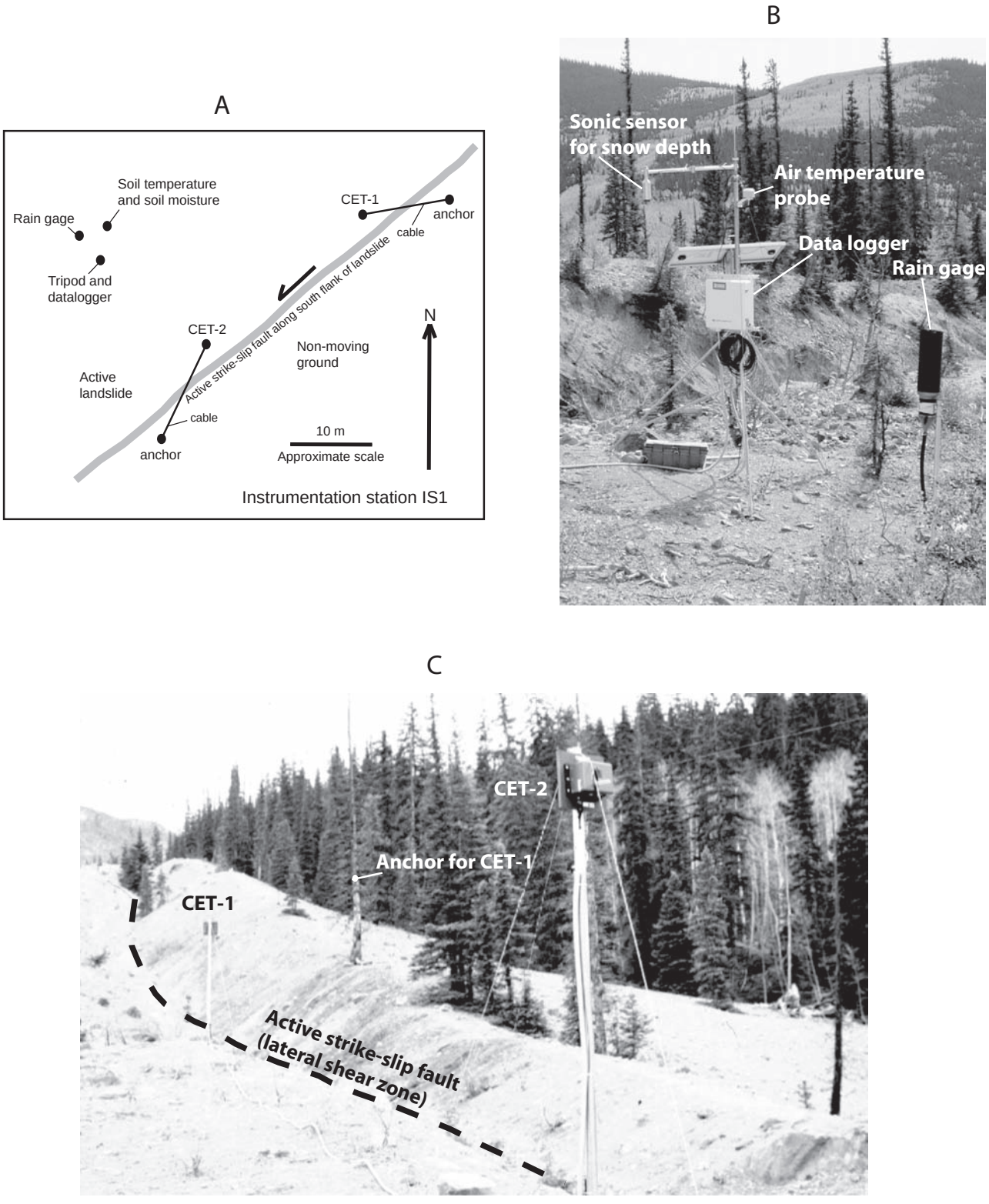

Figure 3-12. Typical monitoring installation showing: (A) Base station with data collection hardware, (B) Wire extensometer (modified from Coe, Ellis, and others, 2003).

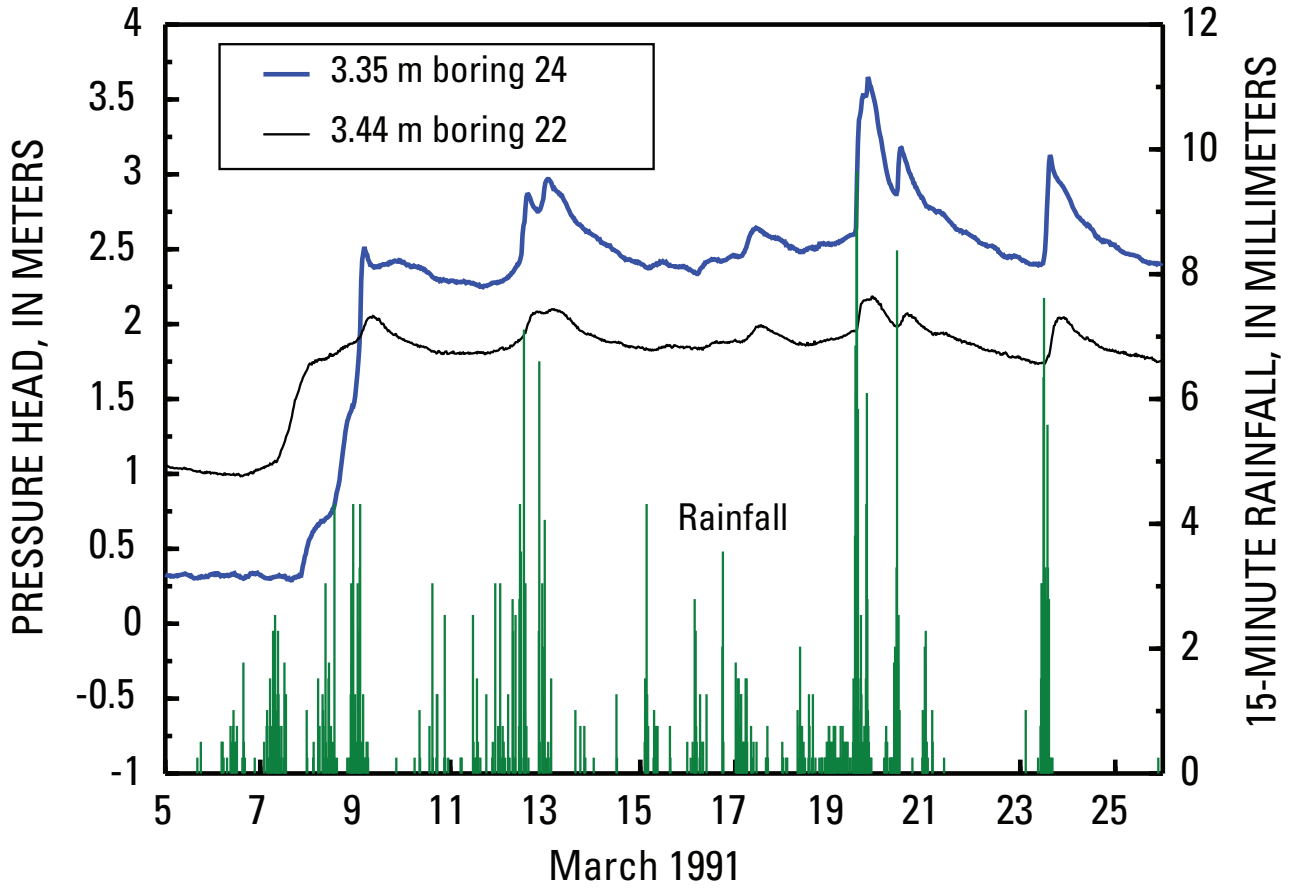

Figure 3-13. Plot of rainfall measured at 15-minute intervals by a tipping-bucket rain gage and subsurface pore-pressure variation obtained using vibrating-wire piezometers (Baum and Reid, 1995).

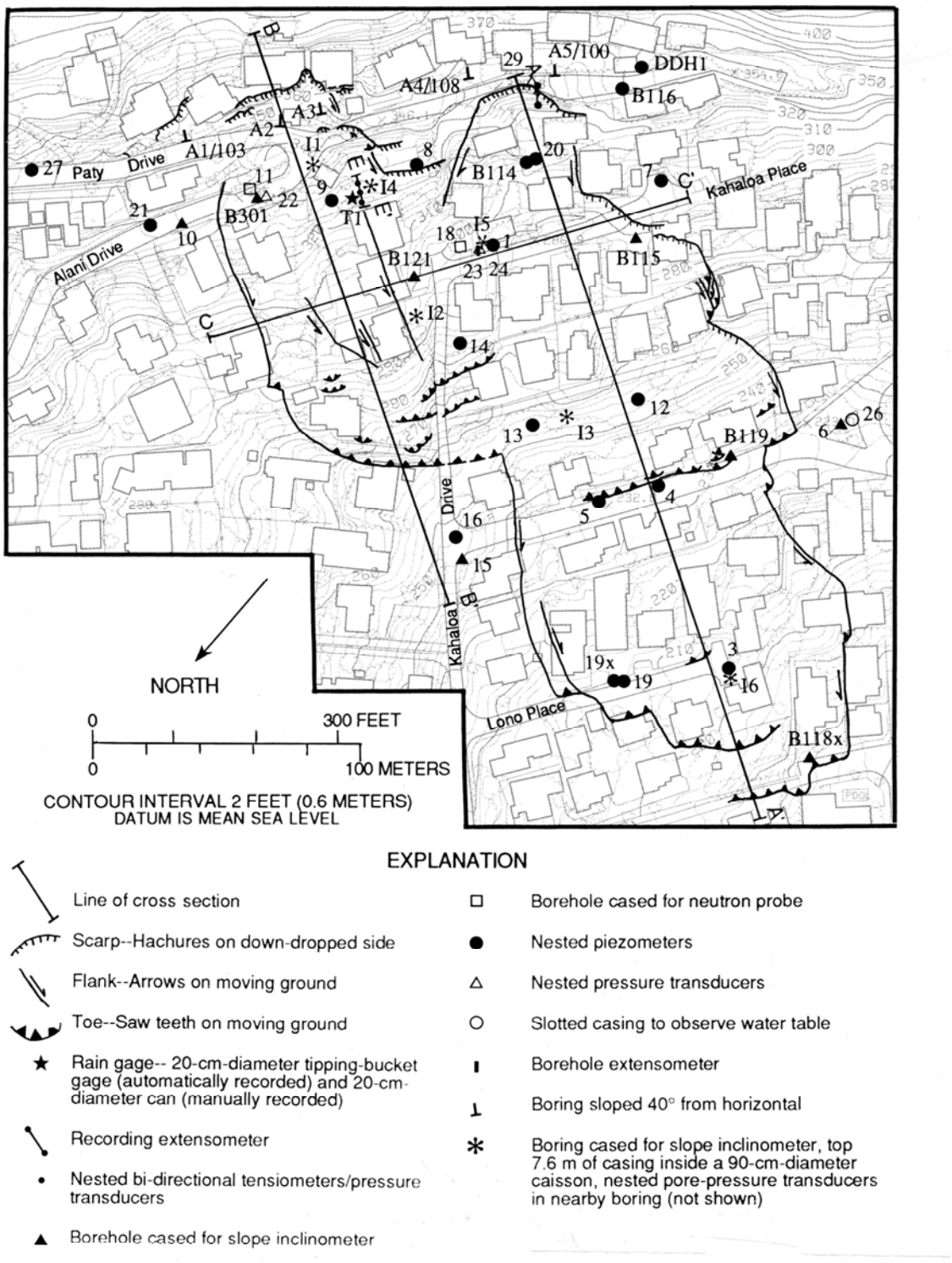

Figure 3-14. Map showing the location of boreholes and instrumentation in the Alani-Paty landslide, Honolulu, Hawaii (Baum and Reid, 1995).

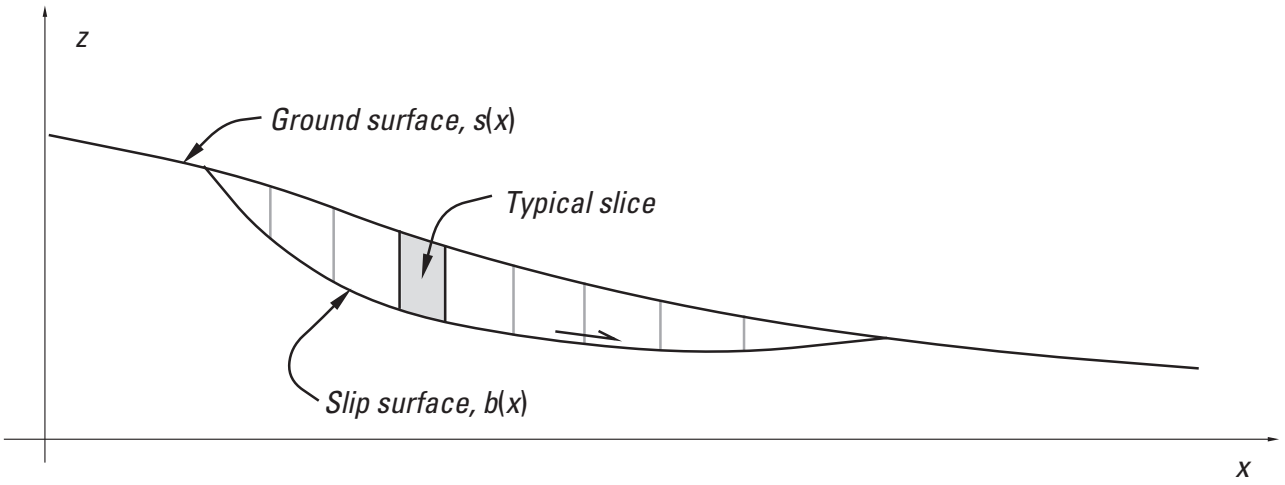

A

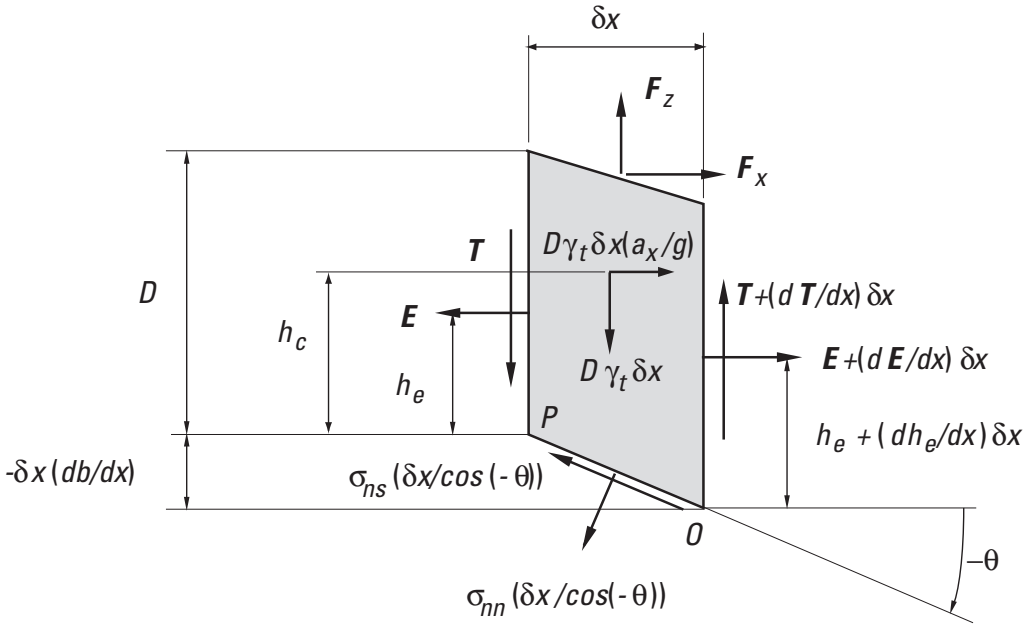

B

Figure 3-15. The method of slices used in limit-equilibrium slope-stability analysis: (A) Diagrammatic cross section through landslide, (B) Detail showing slice dimensions and the forces and stresses acting on a slice (Baum, 2000).

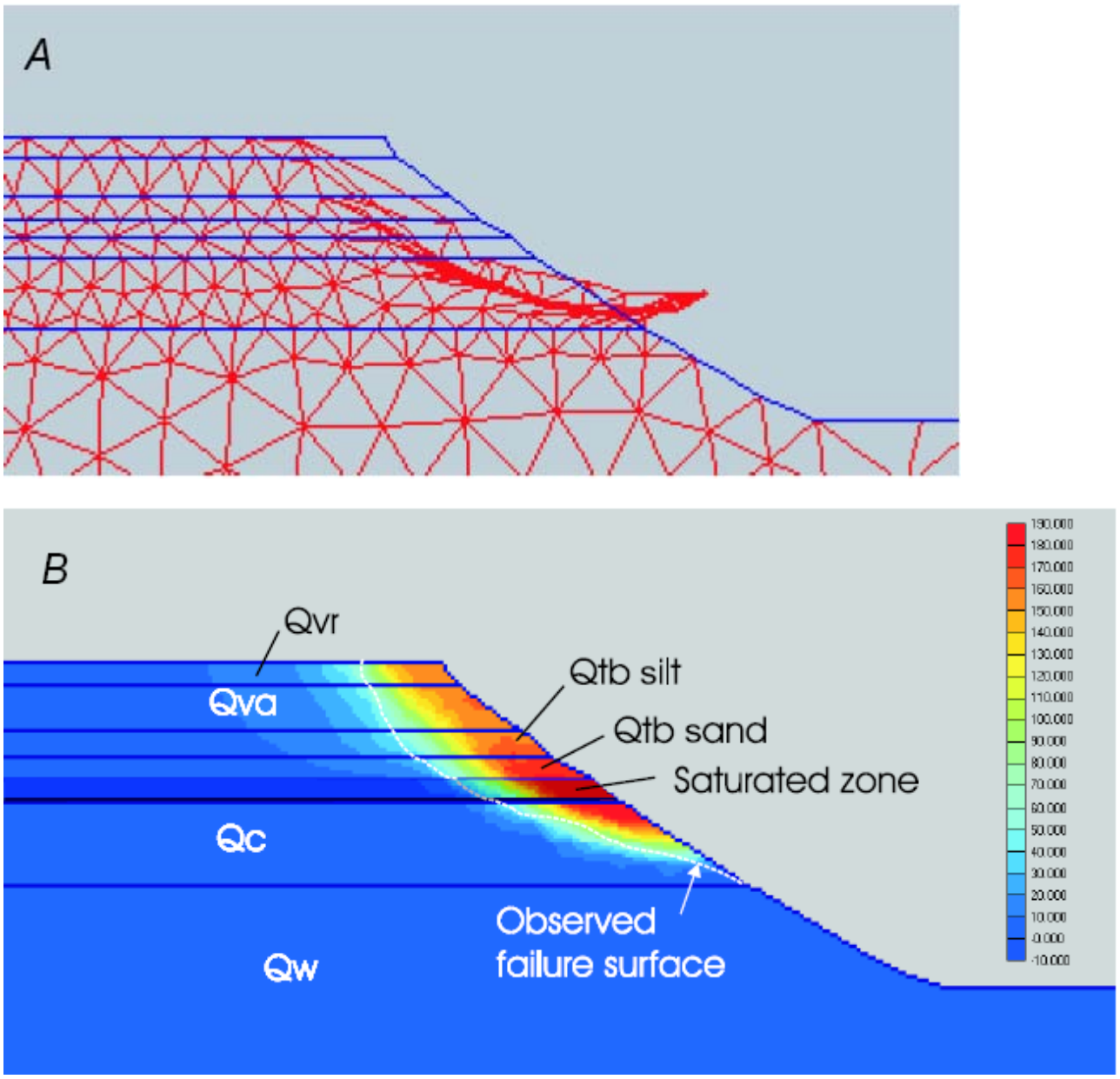

Figure 3-16. Example of results from finite-element analysis (Savage and others, 2000): (A) deformed finite-element mesh showing computed displacements, (B) contour diagram comparing displacements to actual failure-surface profile; warm colors correspond to larger displacements. Geologic units are identified by the following symbols: Qvr, recessional outwash; Qva, advance outwash; Qtb, transitional beds; Qc, Lawton Clay; Qw, Whidbey Formation.

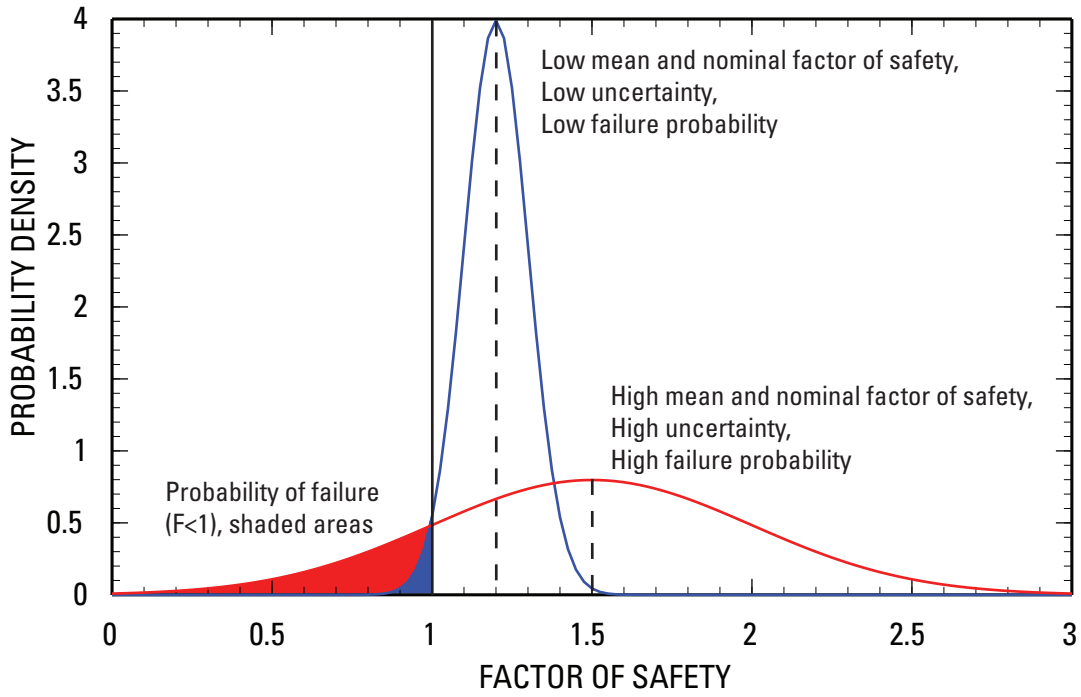

Figure 3-17. Probability chart for factor of safety, illustrating the relationship between data uncertainty, factor of safety, and likelihood of failure (after Nadim and others, 2005). The blue line represents a case where the computed factor of safety is low, but there is little uncertainty in the input data or failure mechanism so there is a low probability (blue shaded area) of failure. The red line represents a case where the computed factor of safety is high, but there is much uncertainty in the input data or failure mechanism, so there is a high probability (red plus blue shaded areas) of failure.

Table 3-1. Comparison of equipment and resolution for repeat ground surveys to determine surface displacement.

[Annual cost averaged over 5 years, including acquisition and maintenance, data collection and analysis assuming two measurement campaigns per year; low, less than $5,000; intermediate, $5,000–$15,000; high, $15,000–$25,000; very high, greater than $25,000]

Technique	Description	Resolution	Advantages and drawbacks	Cost	Reference
Tape	Measure distances between stakes arranged in grids, quadrilaterals, or other configurations to determine displacement.	Sub-decimeter to centimeter resolution, depending on distance, ground-surface irregularities, and other factors.	Simple, reliable, inexpensive technology Stakes subject to tilting or other disturbance, provides only 1-D displacement, manual readings contribute to increased frequency of errors.	Low	Baum and others, 1989; Keaton and DeGraff, 1996
Tape extensometer	Measure distances between fixed points.	Millimeter	Simple, reliable technology Requires specialized monuments	Low	Mikkelsen, 1996
Total station	By means of standard surveying techniques, establish 3-D locations of points on the ground surface.	Centimeter to sub-centimeter, depending on environmental conditions and skill of operator.	Provides accurate 3-D displacement of discrete points. Some units capable of measuring hard-to-reach points without a prism.	Intermediate	Keaton and DeGraff, 1996
Differential GPS	Uses fixed GPS base station and roving receivers to acquire position data at selected points.	Sub-centimeter horizontal, sub-decimeter vertical if stations occupied at least 20 minutes each.	Rapidly provides accurate georeferenced positions of discrete points. Vertical position is less accurate than other methods.	Intermediate-High	Keaton and DeGraff, 1996; Gili and others, 2000; Coe, Ellis, and others, 2003; Brückl and others, 2006
Terrestrial Laser Scanner (Tripod LiDAR)	Measures distance from instrument to millions of points on the ground surface, capable of producing detailed images or digital elevation models of the surface.	Sub-decimeter to millimeter, depending on set-up, field and atmospheric conditions, instrument, and other factors.	Can monitor displacement of discrete areas on a slope face, rather than a few single points. Equipment and software are very expensive and post-processing is complex.	Very high	Rowlands and others, 2003; Jones, 2006; Collins and others, 2007; Bawden, oral commun., 2007

Table 3-2. Aerial and satellite remote sensing methods for landslide displacement.

[Annual cost averaged over 5 years, including acquisition and maintenance, data collection and analysis assuming one measurement campaign per year; low, less than $5,000; intermediate, $5,000–$15,000; high, $15,000–$25,000; very high, greater than $25,000]

Technique	Description & Resolution	Advantages and drawbacks	Cost	Reference
High-resolution aerial photogrammetry	Uses an analytical plotter or digital photogrammetry to measure displacement of photo-identifiable points on time-lapse, stereoscopic, aerial photography. Resolution depends on quality and scale of photography and ground control. Sub-centimeter accuracy has been reported from 1:2000-scale photography.	Capable of providing accurate 3-D displacement. Requires ground-control survey and permanent photo-identifiable targets for most-accurate results.	Intermediate	Fraser and Gruendig, 1985; Baum and others, 1998; Brückl and others, 2006
INSAR	Uses synoptic, time-lapse satellite radar images to measure landslide displacement; applicable only to slow movement and small deformations; millimeter accuracy.	Applicable over large areas. Provides only 1-D displacement, which is either vertical or a combination of vertical and horizontal, depending on the angle of incidence of radar beam.	Intermediate	Van Westen, 2004; Colesanti and Wasowski, 2006

Table 3-3. Techniques and sensors for continuous measurement of landslide displacement and deformation.

[Annual cost averaged over 5 years, including acquisition, installation, and maintenance; continuous measurement assuming data collection from data loggers and analysis four times per year; low, less than $5,000; intermediate, $5,000–$15,000; high, $15,000–$25,000; very high, greater than $25,000. Acquisition cost includes purchase price of sensor, data logger, cable, and accessories]

Observation	Technique or sensor	Description, Comments and resolution	Advantages and drawbacks	Cost	Reference
Surface or subsurface displacement	Extensometer	Can be installed across a landslide boundary or in a borehole. Resolution increases as measurement range decreases. Borehole extensometers tend to measure smaller displacement than surface displacement. 1-D, centimeter to sub-millimeter accuracy.	Provides highly detailed time series record of landslide movement. Cable subject to disturbance by wind and animals.	Intermediate	Corominas, and others, 2000; Ellis and others, 2007
Surface displacement	Theodolites	Motorized, computer-controlled theodolites or total stations observe position of monitoring points. 3-D, sub-centimeter accuracy.	Accurate, non-contact measurement of selected points. Requires shelter and stable base for long-term measurements.	High	Angeli and others, 2000
Surface displacement	Laser and ultrasonic sensors	Laser or ultrasonic beam aimed at target across landslide boundary. Return time determines distance, 1-D, sub-decimeter to centimeter accuracy, depending on distance from target.	Non-contact measurement Limited by short range of sensors (about 15 m) and potential for landslide movement to cause misalignment between sensor and target.	Intermediate	W.L. Ellis, USGS, 2007, oral commun.
Surface displacement and deformation	Terrestrial radar interfereometry	A portable synthetic aperture radar scans landslide surface at frequent intervals. Interferometric techniques reveal surface changes. Reported accuracy ranges from millimeters to centimeters.	Interferogram reveals spatial distribution of displacement. Measured displacements are 1-D; apparatus not yet commercially available.	High	Tarchi and others 2003; Duranthon, 2004;

Observation	Technique or sensor	Description, Comments and resolution	Advantages and drawbacks	Cost	Reference
Surface displacement	Wireless transceiver	Wireless networks. Other applications using wireless sensor networks are under development, 3-D, meter to sub-meter accuracy.	Non-contact measurement Information available so far indicates that the spatial resolution of these networks is not yet adequate for landslide monitoring.	High	Kevin Moore, Colorado School of Mines, oral commun., 2006; Sheth, and others, 2005
Displacement	LVDT	The Linear Variable Differential Transformer (LVDT) consists of a mobile armature and outer transformer windings. LVDTs are capable of high precision (2-5 x 10^{-4} mm) measurements over a small range of displacement (±5-±75 mm). Application is mainly to rock slopes where small displacements can be expected. 3-D displacements are possible by using three mutually perpendicular LVDTs.	Provides highly accurate measurements across cracks. Limited to use in areas of small displacement.	Intermediate	Greif and others, 2004
Subsurface soil strain	Soil strain meter	Measures soil strain over a distance of 2-5 m, if ground is cracked, strainmeter is installed perpendicular to cracks. 1-D, displacement range of a few centimeters, capable of detecting unit strains of 0.0001.	Useful in detecting distributed strain in the soil prior to cracking or other visible evidence of deformation.	Intermediate	Mikkelsen, 1996; Husaini and Ratnasamy, 2001

Observation	Technique or sensor	Description, Comments and resolution	Advantages and drawbacks	Cost	Reference
Subsurface strain or displacement	Coaxial cable using time-domain reflectometry	A length of coaxial cable, grouted into a borehole, serves as the system's sensor. Electronic pulses are sent down the cable; reflected pulses are related to deformation of the cable or to pre-established reference points (crimps). Areas of offset in the resulting trace depict zones of extension or shear along the cable. Crimps, at measured intervals along the cable, partially reflect the transmitted signal and provide a more accurate scale for correlation of deformational zones to depth. Crimps appear as small negative polarity events along the trace of the waveform. Events that offset the waveform indicate deformational zones; the polarity of the offset indicates whether a zone is experiencing tensile or shear deformation. 1-D, decimeter to sub-decimeter accuracy for depth of deformation.	An alternative to inclinometers that allows for remote or continuous monitoring to establish landslide depth.	Intermediate	Dowding, and others, 1989; Kane and Beck, 1994; Campbell Scientific, Inc., 2007
Surface displacement	Real-time GPS	Measurements on approximately 30-minute cycle reveal displacement at point(s) on landslide relative to base station, sub-centimeter resolution, location of measurement stations can be anywhere on the landslide surface. 3-D, sub-centimeter accuracy.	Capable of making displacement measurements anywhere on the surface of a landslide. Can be deployed in remote locations. Requires high-bandwidth communications. Commercial applications tend to be high to very high cost.	Intermediate-high	LaHusen and Reid, 2000

Observation	Technique or sensor	Description, Comments and resolution	Advantages and drawbacks	Cost	Reference
Tilt of ground surface or borehole inclination	Borehole tiltmeters	Repeated or continuous measurements of tilt reveal surface or shallow subsurface deformation. 1-D or 2-D, 5 nanoradian to 1 microradian resolution.	Sensitive to very small changes. Interpretation sometimes difficult without aid of displacement measurements.	Intermediate	Mikkelsen, 1996
Landslide movement at discrete depths	Borehole inclinometers	Internally grooved plastic or metal pipe grouted into vertical borehole. Repeat measurements of biaxial borehole inclination at fixed depth increments reveal depth, amount, and plan-view directions of displacement. Millimeter resolution of displacement if correctly installed and carefully measured. 2-D displacement, millimeter accuracy.	Capable of providing detailed time series record of deformation at various depths. Instrument destroyed or becomes ineffective after displacement exceeds a few decimeters.	Intermediate	Mikkelsen, 1996
Surface or subsurface strain or displacement	Optical time-domain reflectometry	An optical fiber is used as a sensor. The optical time-domain reflectometer (OTDR) measures variations in intensity of light reflections. Experimental device used in laboratory, but Baek and others (2004) claim it could be adapted to field use. 1-D displacement	Not commercially available	Intermediate	Baek and others, 2004

Table 3-4. Subsurface water measurement techniques.

[Annual cost averaged over 5 years, including acquisition, installation, and maintenance, continuous measurement assuming data collection from data loggers and analysis four times per year; low, less than $5,000; intermediate, $5,000–$15,000; high, $15,000–$25,000; very high, greater than $25,000. Acquisition cost includes purchase price of sensor, data logger, cable, and accessories. For observation well, open-tube piezometer, and direct-burial piezometer, acquisition cost includes $5,000 for drilling and well construction.]

Measurement	Technique or sensor	Description and comments	Advantages and drawbacks	Cost	Reference
Water-table depth	Water-level indicator or pressure transducer in observation well	Screened or slotted casing for entire depth of well allows measurement of depth of water table. Measurements can be taken manually or automatically.	Damaged instrument can be easily removed and replaced. Oversimplifies pore-pressure distribution unless used in combination with piezometers.	Intermediate	Mikkelsen, 1996
Pore pressure	Pressure transducer in open-tube piezometer	Usually constructed from PVC pipe terminated with a porous tip. The piezometer tip is installed at the desired depth in the borehole and covered with coarse backfill. Layers of bentonite or grout above and below the piezometer tip prevent the flow of water between different horizons intersected by the borehole. Response time increases with decreasing diameter.	Damaged instrument can be easily removed and replaced. Pore pressures can be observed at depths relevant to landslide movement. Response time may be too slow to accurately indicate pore pressures associated with rainfall and snowmelt events.	Intermediate	Lambe and Whitman, 1969; Mikkelsen, 1996
Pore pressure and matric suction below depth range of tensiometers	Pressure transducer (direct burial piezometer)	Intallation in cement-bentonite grout or use of high-air-entry porous tip allows measurement of matric suction of soils subject to seasonal drying.	Response time faster than in open-tube piezometer. Replacement of damaged instrument requires new boring.	Intermediate	Mikkelsen, 1996, 2002
Matric suction	Tensiometer	Depth range is surface to about 2 m. Useful for monitoring rainfall infiltration. Conventional tensiometers require regular maintenance of fluid level; newer designs require only annual maintenance.	Rapid accurate measurements of pore pressure above water table. Subject to damage by freezing.	Intermediate	Hillel, 1982; Baum and Reid, 1995; Baum and others, 2005

Measurement	Technique or sensor	Description and comments	Advantages and drawbacks	Cost	Reference
Matric suction	Thermal sensor	Experimental design, uses moisture-induced variation in thermal properties of porous ceramic tip to estimate soil-matric suction.	Does not require a water reservoir like tensiometers. Provides fast and accurate measurements. Not commercially available.	Intermediate	Beneveli and others, 2004; Tan and others, 2007
Soil volumetric water content	Time-domain reflectometry	Depth range is surface to about 2 m for profilers; certain probe designs can be buried to depths of several meters in boreholes. Relies on changes in the soil dielectric constant to observe water content.	Capable of fast accurate measurements of soil water content. For accurate measurements, must be calibrated to site soils.	Intermediate	Campbell Scientfic, 2007
Soil volumetric water content	Soil moisture profilers and probes	Depth range is surface to about 2 m for profilers; certain probe designs can be buried to depths of several meters in boreholes. For accurate measurements, must be calibrated to site soils; relies on soil capacitance to observe water content.	Provides accurate measurements of soil-water content for as many as eight different depths in a vertical profile. For accurate measurements, must be calibrated to site soils.	Intermediate	Baum and others, 2005

Table 3-5. Preferred locations for landslide exploration and instrumentation.

Observation or measurement	Primary location	Secondary locations	Comments
Landslide depth	Central part of main body	Upslope and downslope of central area first along main axis and then off the axis	At least three points between the head and the toe to control cross section
Pore pressure	Central part of main body	Upslope and downslope of central area first along main axis and then off main axis	Install piezometers as close as possible to basal slip surface. Additional piezometers above or below the basal slip surface help determine ground-water flow directions.
Shear strength	Basal slip surface	Other weak layers discovered during subsurface exploration	See earlier section on soil testing and Wu (1996) for guidance on selecting appropriate test procedures depending on soil type. Wyllie and Norrish (1996) describe procedures for determining appropriate rock strength parameters.
Displacement	Main body along pipeline alignment	Upslope and downslope of alignment	A line of points adjacent to the pipeline will show how displacement varies across the landslide. Additional points may be needed to detect differential movement on internal structures such as lateral shear zones.

Table 3-6. Data types used in various numerical and analytical methods of landslide analysis.

[LE, limit-equilibrium methods; FE/FD, finite-element and finite-difference methods; DE, discrete-element methods; A, data used to perform analysis; V, data used to validate analysis results; N, not used by these methods]

Data type	Source and purpose	LE	FE/FD	DE
Surface topography and landslide features	Detailed site survey (profiles or map) to define free surface of landslide as well as any surcharge loads, detailed geologic mapping define plan-view shape of landslide and any shear zones or other features that subdivide the landslide into mechanically distinct parts.	A	A	A
Site stratigraphy	Geologic mapping and subsurface exploration (drilling, trenching) define internal geometry of hillside or landslide, with attention to details that affect variation in material properties.	A	A	A
Discontinuities and structure	Geologic mapping and subsurface exploration define internal geometry of hillside or landslide, with attention to details that affect bulk material properties and identify potential surfaces of shear or separation.	A	A	A
Slip-surface geometry	Subsurface exploration and inclinometer or TDR monitoring define the basal boundary of the landslide for accurate computation of the factor of safety by limit-equilibrium methods or validation of predicted basal shear zone for other methods.	A	V	V
Shear-strength parameters	Subsurface sampling and in-place or laboratory testing of landslide materials determines internal shearing resistance as well as shearing resistance along the basal slip surface.	A	A	A
Stress-strain properties	Subsurface sampling and in-place or laboratory testing of landslide materials to determine stress-strain properties allow numerical models to predict landslide movement/deformation in response to changes in pore pressure, external loading, or other factors.	N	A	A
Displacements and rates	Time-series monitoring data of movement and pore pressure allow definition of minimum pore pressures needed to initiate or sustain movement. Spatial distribution of displacement amounts or rates provides check on model predictions.	A/V	V	V
Subsurface water pressures	Pore pressure at the basal slip surface and within the landslide as determined by monitoring (possibly supplemented by numerical modeling of ground-water flow) allows computation of the effective stress, which in turn affects strength and deformation of landslide materials.	A	A	A